Biodegradable polymeric prodrugs
for the delivery of antimalarial combination therapy

Lisa Fortuin

Dissertation presented in partial fulfilment of the requirements

for the degree of PhD (Polymer Science)

Stellenbosch University

Supervisor: Prof. Bert Klumperman

Co-supervisor: Dr Rueben Pfukwa

Department of Chemistry and Polymer Science

Faculty of Science

December 2019

Declaration

By submitting this dissertation electronically, I declare that the entirety of the work contained therein is my own, that I am the sole author thereof (save to the extent explicitly otherwise stated), that reproduction and publication thereof by Stellenbosch University will not infringe any third party rights and that I have not previously in its entirety or in part submitted it for obtaining any qualification.

Abstract

The design and synthesis of a novel polymeric prodrug was achieved for the synergistic antimalarial drug combination of artemether and lumefantrine. To this end, a lumefantrine-conjugated amphiphilic block copolymer (BCP) was self-assembled into micelles with artemether entrapped within the hydrophobic core of the micelles. To develop this, different acid-labile linkages were investigated for their ability to selectively cleave under the low pH conditions of the parasitophorous food vacuole within a *Plasmodium*-infected red blood cell and remain stable in the neutral pH conditions of serum. The β-thiopropionate ester, amide and maleimide linkages as well as the acetal linkage were studied using ^{1}H NMR spectroscopy-based kinetic analysis, by synthesising seven model drug compounds, where the model drug (aromatic group) was linked to RAFT-made poly(*N*-vinylpyrrolidone) (PVP). The model system based on the acetal linkage had a $t_{1/2}$ of 107 h at pH 5.0, and remained stable at pH 7.4, providing the impetus for its use in the synthesis of the antimalarial polymeric prodrug.

The parent BCP of PVP-*block*-poly(δ-valerolactone) (PVP-*b*-PVL) was explored and the synthesis optimised to aid in the development of PVP-*block*-poly(α-allylvalerolactone) (PVP-*b*-PAVL), used as the polymer carrier in the drug delivery system. To achieve this, hydroxy-functional PVP was applied as the macroinitiator in the ring-opening polymerisation of δ-valerolactone or its allylated derivative, where triazabicyclodecene was found to be the more effective organocatalyst compared with diazabicycloundecene and cocatalyst thiourea. The crystallisation-driven self-assembly (CDSA) behaviour of PVP-*b*-PVL was studied in detail where spherical micelles, cylindrical micelles and lamellar micelles were observed using TEM analysis. A novel method to induce micellar morphological transitions was developed in the form of the freeze-thaw process.

Lumefantrine was conjugated to the BCP in a 'click'-type reaction via an acetal linkage, after PVP-*b*-PAVL was carboxylated and functionalised with EGVE. Artemether was physically entrapped within the core of spherical micelles (114 nm in diameter from DLS) using the cosolvent technique with THF as the non-selective solvent and water as the selective solvent for the hydrophilic block, PVP. The targeting ligand, a low molecular weight peptide with sequence 'GSRSKGT' was modified to bear thiol groups using succinimidyl 3-(2-pyridyldithio)propionate (SPDP) modification (quantitative) and it was bioconjugated to the BCP prodrug micelles using disulfide exchange (12 ± 3 mol%). The prodrug micelles had a drug loading content of 20.5 wt.%, a critical micelle concentration of 2.0×10^{-3} mg·mL^{-1} indicating thermodynamic stability, and remained stable in a simulated physiological environment for up to four days. Negligible haemolysis to RBCs and non-cytotoxicity to HepG2 cells were found. The prodrug micelles can be classified as having good activity towards *P. falciparum* parasites; however, they exhibit a higher IC$_{50}$ value of 1021.8 ± 270.9 nM compared with the free drug combination. The developed drug delivery system is robust, tuneable and non-toxic to healthy cells, indicating that it holds potential for its application and further development in therapeutic nanosystems.

Opsomming

Die ontwerp en sintese van 'n nuwe polimeriese pro-middel is bewerkstellig vir die sinergistiese antimalariële middelkombinasie van artemether en lumefantrine. Ten einde hierdie resultaat te bereik is 'n lumefantrine-gekonjugeerde amfifiliese blokkopolimeer self-saamgestel in miselle met artemether vasgevang binne die hidrofobiese kern van die miselle. Om dit te ontwikkel was verskillende suur-labiele verbindings ondersoek vir hul vermoë om selektief skeiding te ondergaan onder die lae pH-toestande van die parasitoforiese voedselvakuool binne 'n *Plasmodium*-besmette rooibloedsel (pH 5.0) en stabiel te bly in die pH-toestande van bloedserum (pH 7.4). Die β-tiopropionaat-ester-, amied- en maleimiedverbindings, sowel as die asetale verbinding is bestudeer deur gebruik te maak van ¹H KMR kinetiese analise deur die sintese van sewe model-entmiddelsamestellings, waar die model-entmiddel (aromatiese groep) verbind is tot RAFT gepolimiseerde poli(*N*-vinielpyrrolidoon) (PVP). Die modelsisteem gebaseer op die asetaalverbinding het 'n $t_{1/2}$ van 107 uur teen pH 5.0 gehad en het stabiel gebly by pH 7.4, en het derhalwe die impetus verskaf vir die gebruik daarvan in die sintese van die antimalariële polimeerpro-middel.

Die blokkopolimeer van PVP-*blok*-poli(δ-valerolaktoon) (PVP-*b*-PVL) is ondersoek en die sintese geoptimiseer om die ontwikkeling van PVP-*blok*-poli(α-allielvalerolaktoon) (PVP-*b*-PAVL) te fasiliteer, wat gebruik is as die polimeerdraer in die middel afleweringsisteem. Om dit te bereik is hidroksiefunksionele PVP gebruik as die makro-inisieerder in die ring-openingspolimerisasie van valerolaktoon of die alliel-afgeleide daarvan, waar daar bevind is dat triazabisiklodekeen die doeltreffender organokatalisator is in vergelyking met diazabisikloundekeen en kokatalisator thio-ureum. Die kristalisasie-gedrewe self-samestelling gedrag van PVP-*b*-PVL is in detail bestudeer en deur middel van TEM analise, is sferiese miselle, staafagtige miselle, silindriese miselle en lamella miselle waargeneem. 'n Nuwe metode om molekulêre morfologiese oorgange te bewerkstellig, is ontwikkel in die vorm van die vries-ontdooiingsproses.

Lumefantrine is gekonjugeer met die blokkopolimeer in 'n 'kliek'-tipe reaksie via 'n asetaalverbinding, nadat PVP-*b*-PAVL gekarboksileer en met EGVE gefunksionaliseer is. Artemether was fisies vasgevang binne die kern van sferiese miselle (114 nm in deursnee van DLS) deur gebruik te maak van die mede-oplosmiddelstegniek met THF as die nie-selektiewe oplosmiddel en water as die selektiewe oplosmiddel vir die hidrofobiese blok, PVL. Die teikenligand, 'n lae molekulêre gewig peptied met volgorde 'GSRSKGT' is verander om tiolgroepe te dra deur gebruik te maak van SPDP verandering (kwantitatief) en dit was biogekonjugeer met die blokkopolimeer miselle deur disulfied-uitruiling (12 ± 3 mol%). Die pro-middel miselle het 'n middelladingsinhoud van 20.5 gew.%, 'n kritieke miselkonsentrasie van 2.0×10^{-3} mg·mL⁻¹ wat termodinamiese stabiliteit aandui, en het tot vier dae binne 'n gesimuleerde fisiologiese omgewing stabiel gebly. Onbeduidende hemolise vir rooibloedsele en nie-sitotoksisiteit vir HepG2 selle is gevind. Die pro-middel miselle kan geklassifiseer word as synde goeie aktiwiteit te toon teenoor *P. falciparum* parasiete, alhoewel hulle 'n hoër IC₅₀-waarde van 1021.8 ± 270.9 nM toon in vergelyking met die vrye entmiddel kombinasie. Die onwikkelde middel afleweringsisteem is robuust, verstelbaar en nie-toksies vir gesonde selle, wat daarop dui dat dit potensiaal het vir die toepassing en verdere ontwikkeling in terapeutiese nanosisteme.

Acknowledgements

Thank you to all of the free radical group members and lab-mates who made this journey all the more memorable and for making these past few years such a joyful time. Thank you to all of my close friends for the coffees, laughs and dates. Thank you all for supporting me through this journey. Thank you to the Jooste family, now my family too, I truly appreciate all of the love and support. Thank you to the best sisters in the world, the sunshine girls. Thank you to my incredible husband who has been on this journey with me from the start and who has been my rock. Thank you to my grandparents and parents, everything I am is because of your love, sacrifice and care. I can't put into words how grateful I am to have had such steadfast support and encouragement in my life.

Table of Contents

Chapter 5 | Polymeric prodrug assembly and application

List of Figures

List of Schemes

List of Tables

List of Equations

List of Abbreviations

ABC	Accelerated blood clearance
ACT	Artemisinin-based combination therapy
ADME	Absorption, (bio)distribution, metabolism and elimination
AIBN	4,4'-Azobisisobutyronitrile
AL	Artemether-lumefantrine (combination drug therapy)
AM	Artemether (drug)
ATR-FTIR	Attenuated total reflectance Fourier transform infrared spectroscopy
ATRP	Transition-metal-catalysed atom transfer radical polymerisation
AVL	α-Allylvalerolactone
BCP(s)	Block copolymer(s)
BPPLED	Bipolar pulse longitudinal eddy current delay pulse sequence
CDSA	Crystallisation-driven self-assembly
CL	ε-Caprolactone
CMC	Critical micelle concentration
CPT	Camptothecin (drug)
CTA	Chain transfer agent
DLS	Dynamic light scattering
DOSY	Diffusion ordered spectroscopy
DOX	Doxorubicin (drug)
DRI	Differential refractive index
DSC	Differential scanning calorimetry
EPR	Enhanced permeability and retention
ESI	Electron spray ionisation
FBS	Fetal bovine serum
FDA (US)	Food and Drug Administration (United States)
FV	Food vacuole (parasitophorous)
HepG2	Human liver carcinoma cells
ITP	Iodine transfer polymerisation
KAHRP	Knob-associated histidine-rich protein
LAMs	Less activated monomers

LC-MS	Liquid chromatography-mass spectroscopy
LUM	Lumefantrine (drug)
MAMs	More activated monomers
MD	Molecular dynamics
MESA	Mature parasite-infected erythrocyte surface antigen
MRT	Mean residence time
MW	Molecular weight
NMP	Nitroxide-mediated polymerisation
NMR	Nuclear magnetic resonance
NPPs	New permeability pathways
NRF (SA)	National Research Foundation (South Africa)
NSF	National Science Foundation
NVP	*N*-Vinylpyrrolidone
OCRP	Organocobalt-mediated radical polymerisation
OHRP	Organoheteroatom-mediated polymerisation
P. berghei	*Plasmodium berghei*
P. falciparum	*Plasmodium falciparum*
P. knowlesi	*Plasmodium knowlesi*
P. vivax	*Plasmodium vivax*
PAA	Poly(acrylic acid)
PAM	Polyacrylamide
PAVL	Poly(α-allylvalerolactone)
PBS	Phosphate buffered saline
PCL	Poly(ϵ-caprolactone)
PDMA	Poly(*N*,*N*-dimethylacrylamide)
PDO	Poly(ρ-dioxanone)
PEG	Poly(ethylene glycol)
PEO	Poly(ethylene oxide)
PEO-*b*-PCL	Poly(ethylene oxide)-*block*-poly(ϵ-caprolactone)
PfEMP1	*P. falciparum* erythrocyte membrane protein 1
PGA	Poly(glycolide)

PHPMA	Poly(*N*-(2-hydroxypropyl)methacrylamide)
PLA	Poly(L-lactide)
PLGA	Poly(D,L-lactide-*co*-glycolide)
PMMA	Poly(methyl methacrylate)
Polymeric prodrug	Polymer-conjugated drug
PSS	Polymer Standard Service
PV	Parasitophorous vacuole
PVA	Poly(vinyl alcohol)
PVL	Poly(δ-valerolactone)
PVM	Parasitophorous vacuole membrane
PVP	Poly(*N*-vinylpyrrolidone)
PVP-*b*-PAVL	Poly*(N*-vinylpyrrolidone)-*block*-poly(α-allylvalerolactone)
PVP-*b*-PVL	Poly*(N*-vinylpyrrolidone)-*block*-poly(δ-valerolactone)
RAFT	Reversible addition-fragmentation chain transfer
RAFT/MADIX	RAFT / macromolecular design by interchange of xanthate
RBC(s)	Red blood cell(s)
RDRP	Reversible deactivation radical polymerisation
RES	Reticuloendothelial system
ROP	Ring-opening polymerisation
SEC	Size exclusion chromatography
SFRP	Stable free radical polymerisation
SMA	Poly(styrene-*co*-maleic acid/anhydride)
SE	Standard error of the mean
SPDP	Succinimidyl 3-(2-pyridyldithio)propionate
TEM	Transmission electron microscopy
TGA	Thermogravimetric analysis
TVN	Tubulovesicular network
UV	Ultraviolet
WHO	World Health organisation

Chapter One

Prologue

1.1 Introduction

Malaria is the most fatal human parasitic infection and alarmingly, the *Plasmodium falciparum* parasite has developed resistance to most antimalarial drugs currently in use.[1] Recently, the combination of two synergistic antimalarial drugs, with different modes of action, has been used as a strategy to inhibit the development of resistance to either component. Among the artemisinin-based therapies, artemether and lumefantrine in combination is the first-line treatment for uncomplicated malaria.[2] Despite the combination's high success rate, there are major complications associated with the oral dosage form such as the requirement to take these drugs along with fat-supplemented food to avoid low and/or erratic absorption, the requirement of drug administration twice per day and the degradation of the drugs in the gastric fluid.[3]

These challenges can be overcome through the use of biodegradable, targeted polymeric prodrugs to effectively improve the therapeutic profile of the loaded drugs. Polymer-conjugated drugs generally exhibit prolonged half-lives, higher stability, increased aqueous solubility, lower immunogenicity and antigenicity as well as the ability to specifically target tissues or cells.[4] The ability of amphiphilic block copolymers to undergo spontaneous self-assembly by solvophobic forces has been skilfully applied in the field of drug delivery, where nanosized carriers protect the toxic payload until the diseased site of delivery has been detected. Controlled pharmaceutical dosage forms resulting from nanocarriers may also serve to limit drug resistance by malaria parasites.

Of particular interest are the polymers poly(*N*-vinylpyrrolidone) (PVP) and poly(δ-valerolactone) (PVL) which can be constructed to create an amphiphilic block copolymer able to undergo spontaneous self-assembly into micelles. Peptidic homing devices can be tethered to the hydrophilic PVP periphery of nanosized micelles via reducible disulfide bonds, making it possible to target *Plasmodium*-infected RBCs. The *Plasmodium*-infected red blood cell is composed of various compartments with a pH gradient reaching its nadir within the parasitophorous food vacuole. Here, the low pH can act as a trigger to cause the cleavage of a covalently conjugated antimalarial drug from the block copolymer micelles, leading to the ultimate destabilisation of the micelles. This destabilisation would be the primary cause for the release of the second antimalarial drug, which had been physically entrapped within the hydrophobic cores of the self-assembled antimalarial polymeric prodrug micelles. In this way, antimalarial combination therapy within a polymeric prodrug can be achieved.

1.2 Objectives

The purpose of this study was to design and synthesise a novel drug delivery system for the synergistic antimalarial combination therapy of artemether and lumefantrine. The fundamental objectives can be summarised as follows:

1. The investigation of seven acid-degradable linkages as applied in RAFT-polymerised PVP-based model drug systems. The acetal and the β-thiopropionate ester acid-degradable linkages are compared with lesser known derivatives of the latter, where the ester group is substituted for an amide and a maleimide group and where the effects of a supplementary methylene unit in each is determined.

2. The synthesis of hydroxy-functional PVP (PVP-OH) through RAFT/MADIX polymerisation and subsequent ring-opening polymerisation (ROP) of δ-valerolactone (VL) to create the block copolymer (BCP), PVP-*b*-PVL.

3. The study of the crystallisation-driven self-assembly of PVP-*b*-PVL.

4. The synthesis of the functional cyclic ester monomer, α-allylvalerolactone (AVL) and the ROP of this monomer using PVP-OH as the macroinitiator to render PVP-*b*-PAVL; as well as the carboxylation of this BCP, its functionalisation with EGVE and conjugation with lumefantrine.

5. The physical entrapment of artemether within the hydrophobic core of the micelles self-assembled from the lumefantrine-conjugated BCP and the investigation of the various characteristics of the prodrug micelles related to drug delivery applications.

6. The evaluation of the haemolytic toxicity against RBCs and cytotoxicity against HepG2 cells of the prodrug micelles and their activity against *P. falciparum* NF54 parasites.

1.3 Thesis layout

Chapter 1 | Prologue

A brief introduction is given relating to the challenges within malaria therapy, specifically regarding drug resistance and the shortcomings of free drug formulations *in vivo*, and how polymer-based nanotechnology is promising in addressing some of these challenges. The objectives of the research project are presented.

Chapter 2 | Historical and theoretical background

A comprehensive literature review is presented where the historical significance of malaria therapy is outlined as well as the theoretical foundations of the nanotherapeutic tools that will be key in combating malaria and drug resistance to it. The role of polymers in nanomedicine, such as drug delivery, is also highlighted, particularly with regard to PVP and aliphatic polyesters. Various key concepts regarding

drug delivery systems are also discussed, such as stimuli-responsive linkers, drug release, targeting, cellar uptake, self-assembly into nanovessels as well as the size and morphology of those vessels.

Chapter 3 | Acid-degradable linkages

This chapter delves into possible acid-degradable linkages which could be applied to drug delivery systems. To achieve this, seven PVP-based, acid-degradable model drug systems are formulated and assessed. In this way, two primary synthesis routes are outlined to incorporate these linkages in RAFT polymerised systems.

Chapter 4 | Block copolymer synthesis and self-assembly

In this chapter, the synthesis of the block copolymer carrier, PVP-*b*-PAVL, used for the antimalarial prodrug, is optimised with special focus on ROP organocatalysts. PVP-*b*-PVL is used as the model system to achieve this, and CDSA is used as a strategy to create a range of nanomorphologies using the crystallisable parent block copolymer.

Chapter 5 | Polymeric prodrug assembly and application

In this chapter, the assembly of the final antimalarial prodrug is detailed, where PVP-*b*-PAVL undergoes the post-polymerisation synthesis steps needed to attach lumefantrine to the block copolymer. The physical entrapment of artemether through spontaneous self-assembly is also conducted. The drug delivery system undergoes a series of experiments to determine its suitability *in vivo*. The haemolytic toxicity against red blood cells and cytotoxicity against liver carcinoma cells is determined, as well as the activity against *P. falciparum* NF54 parasites.

Chapter 6 | Epilogue

The final chapter provides a summary of the work described in this dissertation. Suggestions are also presented for future studies.

1.4 References

(1)   *World Malaria Report*; World Health Organization: Geneva, 2017.

(2)   Nosten, F.; White, N, J. *Am. J. Trop. Med. Hyg.* **2007**, *77* (1), 181.

(3)   Bhandari, S.; Rana, V.; Tiwary, A. K. *Ther. Deliv.* **2017**, *8* (4), 201.

(4)   Rohini, N. A.; Anupam, J.; Alok, M. *J. Antivir. Antiretrovir.* **2013**, *15* (1), 12.

Chapter Two

Historical and Theoretical Background

2.1 Malaria

2.1.1 An overview

From as far back as 2700 BC,[1] ancient script has documented what was very likely incidences of malaria. These texts detailed symptoms of poor health, periodic fevers and the enlarged spleens of people living in wetland areas. Hippocrates, now fondly regarded as the 'father of medicine', was first to describe the manifestations of the disease and relate them to the time of year and where the patients lived.[2]

For many years, the cause of this disease was thought to be due to miasma (μίασμα, ancient Greek: pollution, defilement) which rose from these marshy areas. Although this was disproven in subsequent years, the Italian name *mal'aria* persevered which loosely translates to 'bad air'. The connotation with stagnant waters led to the construction of drainage strategies by the Romans, which is the first noted intervention against malaria. The First World War was also met with an unlikely rival in the form of malaria, where it is estimated that around 1.5 million solders were infected with the disease. Historians believe it was thought to have a bigger impact on the Eastern Front including the Russian, Romanian and Albanian troops compared with the Western Front in north-eastern France, Belgium, Luxembourg and western Germany.[3] Figure 2.1 shows a couple of the advertisements used to urge soldiers to protect themselves from mosquitoes.
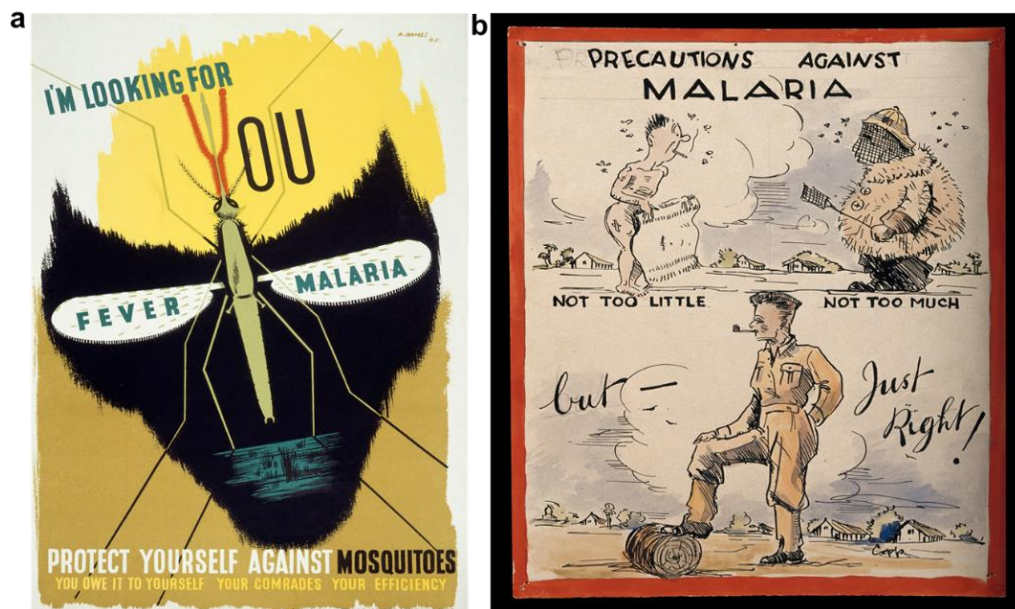
Figure 2.1 a) The malaria mosquito forming the eye-sockets of a skull, representing death from malaria. Colour lithograph, A. Games, 1941. b) Advice to British soldiers about malaria. Colour pen drawing by C. Copp, 1944.[4,5]

Alphonse Lavern discovered the cause of malaria in 1880. Lavern noted his observations, "…on the edges of a pigmented spherical body, filiform elements which move with great vivacity, displacing the neighbouring red blood cells..." From his microscope he observed crescent-shaped forms having frenzied motion, which he identified as living parasites moving energetically within fresh blood specimens. Although many before him had theorised this cause, they had not succeeded in identifying the parasite.

A succeeding factor in Lavern's discovery was his use of wet blood films, as thankfully, he was unaware of Paul Ehrlich's popular blood fixing and staining invention developed in the previous year.[6,7] In 1897, Ronald Ross was able to prove the role of *Anopheles* mosquitoes in the transmission of malaria parasites in birds. These findings earned each a Nobel prize in physiology in 1902 (Ross) and 1907 (Lavern).[8–10] The Italian scientists Giovanni Battista Grassi, Amico Bignami, Giuseppe Bastianelli, Angelo Celli, Camillo Golgi and Ettore Marchiafava also contributed significantly by resonating Ross's findings and delving further into the intricacies of human malaria between the years of 1898 to 1900.[1]

In the present day, the *World malaria report 2017* stated that in 2016, 91 countries reported a total of 216 million cases of malaria, an increase of 5 million cases from 2015. The global tally of malaria deaths rose to 445 000. Though malaria case incidence has dropped worldwide since 2010, a worrying trend has emerged in that the rate of decline has halted and even reversed in some regions since 2014. Mortality rates have followed suit. A major reason for this decline is the malaria parasite's varying degree of resistance to all antimalarials used to date.[11] The African region continues to account for 90% of malaria cases and deaths worldwide. Fifteen countries, of which only one is not in sub-Saharan Africa, bear 80% of the global malaria burden.[12] In South Africa it was reported that in December 2017, high numbers of malaria cases were being registered in malaria transmission areas in Limpopo and Mpumalanga provinces.[13] With this in mind, we should feel urgently impelled to take responsibility in updating our response to age-old diseases such a malaria, by using new tools that have become available through advanced nanotechnology and experience. The parasite is ever-evolving, and so too should our approach be to drug resistance and the eradication of this disease.

2.1.2 The nature of the disease

It is now known that malaria is a vector-borne disease caused by the apicomplex of the protozoan parasite of the genus *Plasmodium*, transmitted by the bite of a female *Anopheles* mosquito. The nocturnal nature of the *Anopheles* mosquito destines malaria to be transmitted from dusk to dawn.[14] There are five parasite species that cause malaria in humans, *Plasmodium falciparum*, *Plasmodium vivax*, *Plasmodium malariae*, *Plasmodium ovale* and *Plasmodium knowlesi*. Of these five species, *P. falciparum* is the most fatal and prevalent species in sub-Saharan Africa. The other *Plasmodium* species cause significant morbidity but are less life-threatening. *P. vivax* is second to *P. falciparum* in terms of fatality, where it is predominant in the regions of Southeast Asia and Latin America. The fifth species, *P. knowlesi* was rarely reported to cause malaria in humans until more recent years. The species infects primates, which has led to human malaria by which the mode of transmission remains unclear.[15,16]

The malarial infection begins when the malaria-infected female *Anopheles* mosquito inoculates sporozoites into a human host during a blood meal so she can produce eggs. The life cycle of the malaria parasite is illustrated in Figure 2.2.[17] On average, 100 sporozoites are inoculated per mosquito. It takes only minutes for the sporozoites to traverse through the dermis where vigorous, random motility to the blood vessel has been noted. The sporozoites travel to the liver in the bloodstream, where they are able to pass through Kupffer cells. The major surface proteins on *Plasmodium* sporozoites bind to heparan-like oligosaccharides on the liver's main cell type, hepatocytes, thereby mediating invasion. Within the hepatocyte, the sporozoites feed and grow to mature into merozoites over 2 to 16 days, depending on the *Plasmodium* species, and produce thousands of merozoites per hepatocyte. In the blood stage of the cycle, the merozoites rupture into the bloodstream where they invade red blood cells (RBCs; mature erythrocytes and reticulocytes). Here, the parasite feeds and replicates asexually to produce daughter cells that invade new RBCs to continue the blood stage cycle through ring, trophozoite and schizont stages. The other merozoites replicate sexually into male and female gametocytes to be consumed by a mosquito from a blood meal and develop in the mosquito to become fertilised, eventually becoming sporozoites again. The cycle is continued in this way.[18–23]
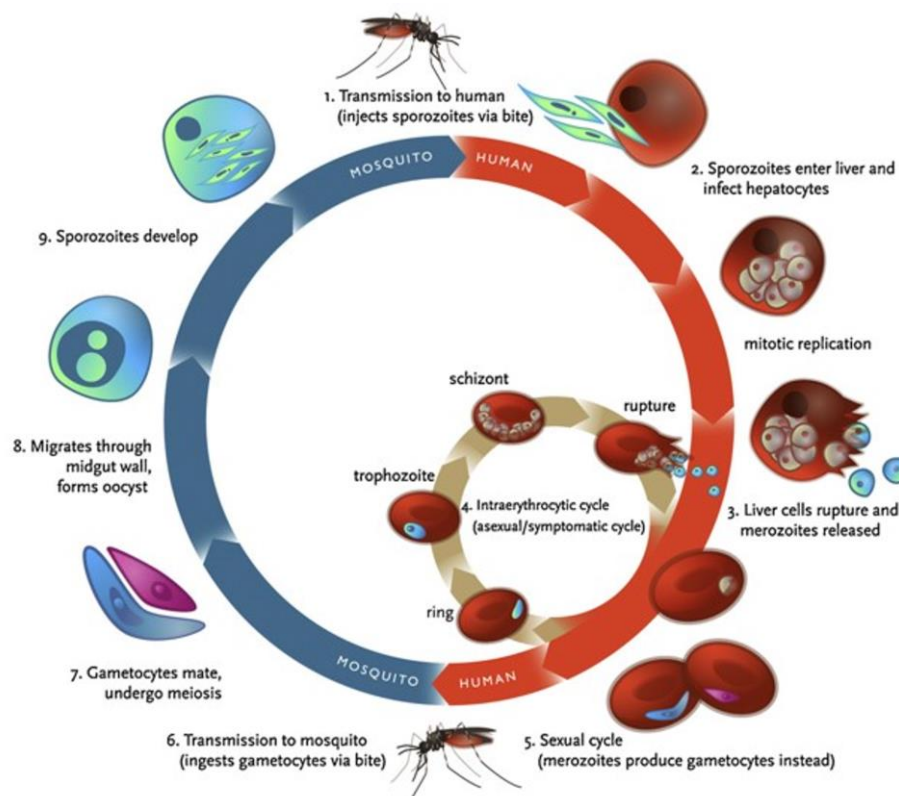
Figure 2.2 Life cycle of the malaria parasite.

2.1.3 The growing resistance to antimalarial drugs

The first antimalarial treatment documented by Europeans was as early as the 1600s in the form of the medicinally active tree bark of *Cinchona calisaya*, found in South America. The tree was so named after the Countess of Chinchón who brought the bark back from Peru after the daughter of a local chief had given her the remedy to cure her of malaria. The bark contains a number of alkaloids which include the antimalarial compound quinine as well as the antiarrhythmic compound quinidine.

Interestingly, as a way to stave off mosquitoes during the colonisation of India by the British, a more palatable way to drink the bitter, daily dose was concocted. Quinine was combined with water, sugar, lime and gin to create the predecessor to the modern-day 'gin and tonic'. Moreover, the tonics used today still contain small amounts of quinine, proven by their fluorescence under ultra-violet light. Quinine's synthesis and efficacy to produce the antimalarial chemotherapy later spurred the development of 4-aminoquinolones, one of which is chloroquine.[24,25] For several decades, chloroquine was regarded as the gold standard for the prevention and treatment of malaria due to its fast-acting ability, minimal toxicity and affordability.[26] The efficacy of this class of drugs has, however, declined to a nadir in recent years as drug-resistant forms of the parasite prevail.

Antimalarial drug resistance can be described as the ability of the parasite to survive and/or multiply despite the recommended drug doses. The mechanism of resistance is believed to be due to the reduced susceptibility of genetic mutations that occur spontaneously, and are then transmitted.[27] In other words, it is when the drug concentrations are adequate to reduce the susceptible parasite population, but inhibit less or do not inhibit the multiplication of the mutant parasites.[28] Drug resistant malaria is largely as a consequence of the species *P. falciparum*, where it is reported that the parasite has developed resistance to nearly all antimalarials currently in use.[11]

The World Health Organisation (WHO) was impelled to change its treatment policy regarding *P. falciparum* towards a recommendation of artemisinin-based combination therapy (ACT).[12] Artemisinin is a derivative of sweet wormwood, or *Artemisia annua*, isolated and synthesised by the Chinese in response to the Vietnam War. Youyou Tu received a Nobel prize in 2015 for her discovery and isolation of this compound.[29] Artemisinin is a sesquiterpene lactone which is known to be a potent drug in the rapid termination of blood stage parasites. The short half-lives of artemisinin and its derivatives led to the conception of combination therapy, where a second drug having a longer half-life is combined to reduce the parasitaemia over a longer time, ingeniously impeding the development of resistance.[25] The combination of two synergistic antimalarial drugs with different modes of action has therefore been used as a strategy to inhibit the development of resistance to either component. Among the artemisinin-based therapies, artemether and lumefantrine in combination is the first-line treatment for uncomplicated *P. falciparum* malaria.[30]

Artemether is rapidly eliminated in the body, with a plasma terminal half-life of approximately 1 h. During that time, however, the active metabolite dihydroartemisinin swiftly reduces the number of parasites to provide pronounced and rapid symptomatic relief. Lumefantrine works to inhibit residual parasites as it has a longer plasma terminal half-life of 3 to 5 days. The absorption of lumefantrine into the

bloodstream is therefore much slower, though more erratic. The peak drug concentration occurs approximately 6 h after oral administration. At any given time, the parasites are never exposed to the singular form of artemether due to its rapid elimination. This is thought to minimise the development of resistance. The parasites may, however, be exposed to the singular form of lumefantrine, but the probability of the parasite developing a resistance to both drugs is thought to be low.[31,32]

Despite the combination's high success rate, there are major complications associated with the oral dosage form such as the requirement to take these drugs along with fat-supplemented food to avoid low and/or erratic absorption, the requirement of drug administration twice per day (usually for a total of three days) as well as the degradation of the drugs in the gastric fluid.[33] Besides these inherent challenges, the WHO is monitoring the efficacy of ACT in most malaria-endemic countries. Alarmingly, there have been some reports of delayed parasite clearance during routine therapeutic efficacy studies of ACT conducted in Africa.[34] Reports of resistance have arisen in parts of Thailand and Cambodia to artesunate-mefloquine, and others to dihydroartemisinin-piperaquine. The species *P.vivax* has even developed a resistance to chloroquine and primaquine in some regions. So, although ACT remains the only viable chemotherapeutic line of defence against malaria, it needs to be supplemented to inhibit the emergence of resistant forms of the parasite in the long-run.

To prevent drug resistance in malaria therapy, new strategies should therefore be put forth. It is not economically or technologically viable to develop new antimalarial drugs faster than the rate at which parasites develop chemotherapeutic resistance. Thankfully, a boom of technology has emerged which is instilling optimism in many fields. Nanotechnology has equipped scientists with the tools to design inventive structures to improve their efficacy and revive those agents able to combat complex diseases such as malaria.

2.2 Nanotechnology

2.2.1 An overview

The newest wave of technology is upon us and it is revolutionising the way we are endeavouring to solve age-old and neoteric problems alike. Nanotechnology can generally be defined as the man-made creation of devices or components produced to have at least one dimension in the range of 1 – 100 nm. Interesting phenomena occur as a consequence of unique quantum and surface events. The true brilliance of nanotechnology is that it has the potential to alter every industry. This is because nanotechnology envelops more than just operating at the nanoscale or even at the atomic scale, it is also the advancements which have allowed us to study the phenomena occurring spontaneously when matter is organised at this level. It is the ability of scientists to use this information to alter various physicochemical and mechanical properties of the devices or components designed to achieve a particular end-goal. Moreover, we are now able to mimic the biological processes which inherently occur on this scale to create new and interesting structures, models and designs.

To provide temporal context, it was in the 1940s when the Austrian economist Joseph Schumpeter noted a number of long waves of industrial activity which had occurred in rhythmic incline and decline

after the Industrial Revolution. With each wave a new economy flourished, bringing about greater investment and exorbitance in the market and then eventually, a massive rationalisation. This has ultimately propelled the world forward in terms of development.[35] An economist at Merrill Lynch, Norman Poire, used Schumpeter's theory in a model which he projected out to the 21st century (Figure 2.3).[36] We are currently at the intersection of the computer and distributed intelligence, examples of which are evidenced by automatic face recognition and the advent of cryptocurrencies. If we follow this model it is also clear that we are at the cusp of the nanotechnology wave. We are only now beginning to experience the effects of this technology, observably set to change the development of our world as we know it.
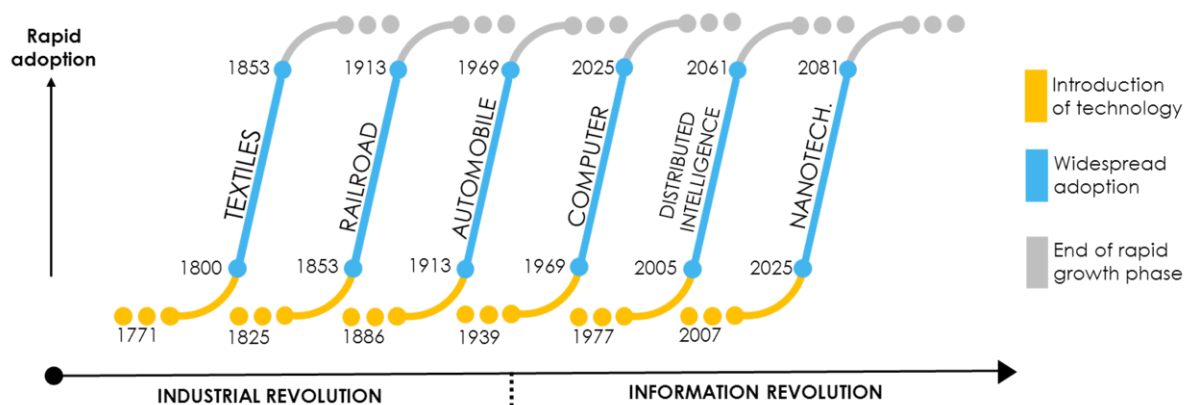
Figure 2.3 Long waves of industrial activity as modelled by the economist Norman Poire.

2.2.2 The beginnings

The conceptual beginnings and systematic discussions of nanotechnology occurred in a talk given by the American physicist and Nobel-prize winner, Richard Feynman. The talk was titled: "There's plenty of room at the bottom" and it was given at the American Physical Society's conference hosted at Caltech in 1959. In his speech, he emphasised the importance of manipulating and controlling things on a small scale and the ways in which they could shed light on the strange phenomena that occurred in complex conditions. He also posed two challenges, the first was to create a nanomotor, and the second, to scale down the letters of the whole Encyclopaedia Britannica to fit onto the head of a pin.

It is interesting to note that it was only much later that the term 'nanotechnology' was independently coined by Taniguchi in 1974 to describe semi-conductor processes, and then by Drexler in 1986 who wrote a book called 'Engines of Creation: The Coming Era of Nanotechnology'. Drexler was truly inspired by Feynman's talk[37] and was unaware of Taniguchi's work at the time.

Feynman foresaw that the progress made in chemistry and biology would rapidly increase if the electron microscope could be made 100 times more sensitive. He said, "We have friends in other fields – in biology, for instance. We physicists often look at them and say, 'You know the reason you fellows are

making so little progress?' (Actually, I don't know any field where they are making more rapid progress than they are in biology today.) 'You should use more mathematics, like we do.' They could answer us – but they're polite, so I'll answer for them: 'What *you* should do in order for *us* to make more rapid progress is to make the electron microscope 100 times better.'"

The progress in these fields, and in nanomotors, was in fact boosted in the 1980s by the invention of the scanning tunnelling microscope and the atomic force microscope, allowing biologists and chemists to observe matter on the atomic scale. This dramatically enhanced the public perception of nanotechnology and furthered the study and manipulation of various nano-phenomena. By the early 2000s, almost all industrialised nations had established nanotechnology initiatives, leading to a worldwide explosion of nanotechnology activity.[38]
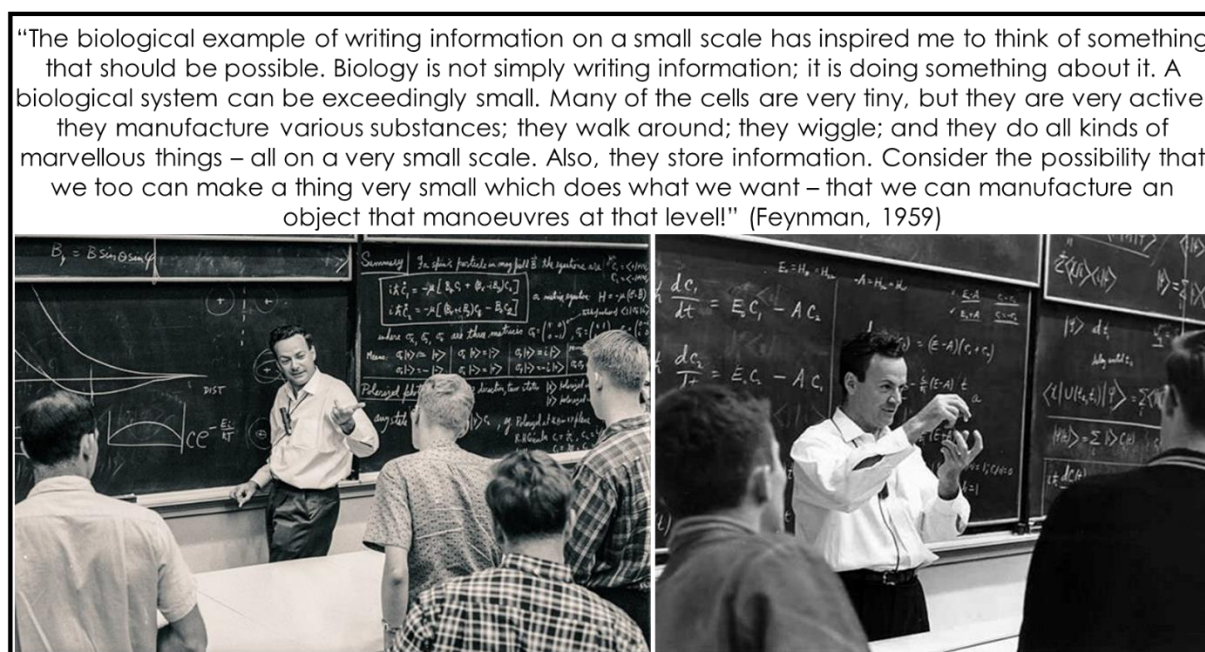
Figure 2.4 An excerpt from Richard Feynman's talk in 1959 at Caltech in California.

Nature has provided us with the ultimate blueprint for nanotechnology. From the locomotion of proteins to the internal pathways of cells, every process occurs at the atomic, molecular or supramolecular level. It is therefore imperative that the structures we design also adhere to the rules of nature to allow for optimal interaction at the atomic scale. The emergence of nanomedicine resulted as a consequence of this design goal. Nanomedicine is the intersection of nanotechnology and medicine. This spin-off of nanotechnology is expected to have an immense impact on health care. As Feynman envisaged, we have reached a point where physics, chemistry and biology have collided in the most orchestrated way possible.

Nanomedicine is also a major division of nanotechnology in monetary terms. The National Science Foundation (NSF) predicted that by 2020, a third of all patents and start-ups in this sector will comprise biomedical applications, and that just less than half of all future pharmaceutical agents will include at

least one nanocomponent.[39] Numerous applications are now deep-rooted in nanomedicine, such as biosensors, tissue engineering, diagnostic devices and particularly, drug delivery systems.

2.2.3 Harnessing nanotechnology to treat malaria

It has been established that the treatment of malaria is directly related to the resistance of the parasite to the drug, and that malaria parasites often form resistance due to low drug concentrations. It is not possible to develop new antimalarial drugs faster than the rate at which resistance to these drugs is occurring. Nanocarriers in this sense can improve the pharmacokinetic profile of drugs by 'packaging' the drug to allow for significantly enhanced circulation times and drug absorption at the targeted site. Antimalarial drug resistance is more likely to occur when patients are required to take a multiple-dose form of the drug compared to a single-dose form, largely attributed to poor patient compliance. Resistance causes treatment failure when drug levels that would normally eliminate the infection can no longer do so.[40–42] The enhancement of the therapeutic profile of the drug and the ability to site-specifically target the drug using nanotechnological systems could reduce the prevalence of resistance by effectively improving the pharmaceutical dosage amount of the drug. We would also be able to apply the same techniques to older drugs, in this way rejuvenating the antimalarial drug reserve that is already available.[43,44]

The malaria parasites are located within the RBCs, so drugs should either have prolonged circulation times and have lower toxicities or they should target the RBCs specifically, making it acceptable to have higher toxicities. Various studies have cited the importance of polymers (macromolecules) in improving the circulation times of the drug after it is assembled with the nanocarrier.[45–47] The polymer therefore plays an integral role in these nanosystems and the ability of matter to be manipulated in such a manner has led to a surge in polymer-based nanotechnology. These tools are complementary, and a particularly appealing application thereof are polymeric prodrugs. This class of nanosized drug delivery system can be manipulated into a wide range of morphologies, more of which will be discussed in Section 2.4.

2.3 Polymeric prodrugs

2.3.1 An overview

A polymeric prodrug stems from the term 'polymer-conjugated drug', where the type of attachment between the polymer and drug is classically covalent. In this type of drug delivery system, the therapeutic agent remains inactive during the time in which absorption takes place and becomes active at the diseased site. The site of action initiates specific events which ultimately lead to the activation of the therapeutic agent at the targeted site. In this sense, the polymer acts as the drug delivery vessel which should safely transport the drug-cargo to the infected site.[48]

The drug in itself is a toxic compound. It was Paracelsus who is credited with the classic toxicology adage, "All things are poison, and nothing is without poison, the dosage alone makes it so a thing is not a poison."[49] In other words, all things, even air and water, can be toxic in high enough quantities. The conventional methods of drug delivery systems (some of which include tablets, ointments and

injectables) result in the drug being distributed throughout the entire body. The drug therefore interacts non-specifically with all of the organs, cells and tissues it encounters through the process of absorption. Much greater than required concentrations of the drug are therefore used to treat the affliction due to this distribution effect. Frequent, high doses are often needed because of the free drug's unfavourable pharmacokinetics (absorption, (bio)distribution, metabolism and elimination; ADME). It is for these reasons that varying degrees of side effects are experienced by patients for any given drug. Antimalarials in particular are known to bring about intensely palpable side effects which include, depending on the drug, fever, nausea, abdominal pain, loss of vision, dizziness and psychiatric episodes.[25]

It is widely known that polymeric prodrugs, compared to the free drug alone, generally demonstrate extended half-lives, enhanced stability, increased aqueous solubility, decreased immunogenicity and antigenicity as well as the ability to specifically target tissues or cells.[40,50] The role of the polymer or polymers is three-fold: to protect the drug, to provide sites for important additional functionalities and to induce an amphiphilic structure to allow for a minimum free energy state to be attained. A minimum free energy state allows for the solvation of the drug due by supramolecular assembly of the polymer-drug conjugate into nanoscopic drug-carriers.

2.3.2 The beginnings

Numerous landmark breakthroughs throughout time are thought to have contributed to the genesis of this field and here only and a few will be highlighted. A good starting point is with Paul Ehrlich, the German Nobel laureate (physiology or medicine, 1908) who coined the terms 'chemotherapy' and 'magic bullet'.[51] In his earlier work he was fascinated by the chemistries of different stains and developed new stains to differentiate between specific organs, tissues and cells. His research on methylene blue was met with promising results when it was discovered to kill malaria parasites. Regarding his concept on the magic bullet, he envisioned a target-specific way of invading microbes, much like a bullet from a gun. He theorised that cells had side chains, or receptors, able to interact specifically with certain toxins. His work was instrumental to that which succeeded his. This is the same Erlich who invented the method for fixing RBCs a year before Lavern discovered the cause of malaria, and had Lavern known about his technique at the time, he might not have been able to see the wriggling motion of the parasite in the wet blood samples that he was analysing.

The first practical instance of a polymer-drug conjugate was used to achieve a depot formulation for the hallucinogenic alkaloid, mescaline. In 1955 Jatzkewitz *et al.* conjugated mescaline to poly(*N*-vinylpyrrolidone) (PVP) through use of a dipeptide spacer, glycine-L-leucine.[52] During the 1960s and 1970s, Ushakov's group synthesised various water-soluble polymeric prodrugs, focussing on penicillin as the drug and typically PVP as the polymer.[53–55] PVP was therefore the first polymer to be conjugated to a drug. Of course, PEG is a very popular polymer used these days despite its shortfalls. PEGylation is the process of conjugating PEG to a therapeutic agent, the start of which was initiated by Davis in the late 1960s. Davis and co-workers conjugated a protein to PEG and proved that it could decrease the recombinant protein's immunogenicity and antigenicity, whilst increasing its bioavailability.[56]

Helmut Ringsdorf pioneered the field by actively conceptualising and detailing a rational model for the synthesis of a polymeric prodrug. By many he is seen as the person who catalysed the era of polymeric prodrugs when he published a paper in 1975 specifying the rationale and giving examples of macromolecular drugs.[57] It is without a doubt that he was inspired by the work preceding him, even though many were sceptical of the field for practical and theoretical reasons. His rational approach to the design of polymeric prodrugs is important, because it emphasised cross-disciplinary collaboration and disproved the initial doubt within the field.

Ringsdorf's model consists of various components bound to a biocompatible polymer backbone. A solubilising group is attached so as to impart a degree of hydrophilicity to the polymer for water solubility and enhanced bioavailability. The drug molecules are covalently conjugated to the backbone through a spacer molecule, which can be designed to include 'breaking points' to ensure the release of the drug from the polymer. In modern terms it is largely referred to as a stimuli-responsive or cleavable linker. Lastly, the polymer conjugate can also include targeting groups which are disease specific, allowing for the transport of the prodrug to certain antigens or receptors on the surface of the diseased site of interest. Ringsdorf's model is exemplified in Figure 2.5.
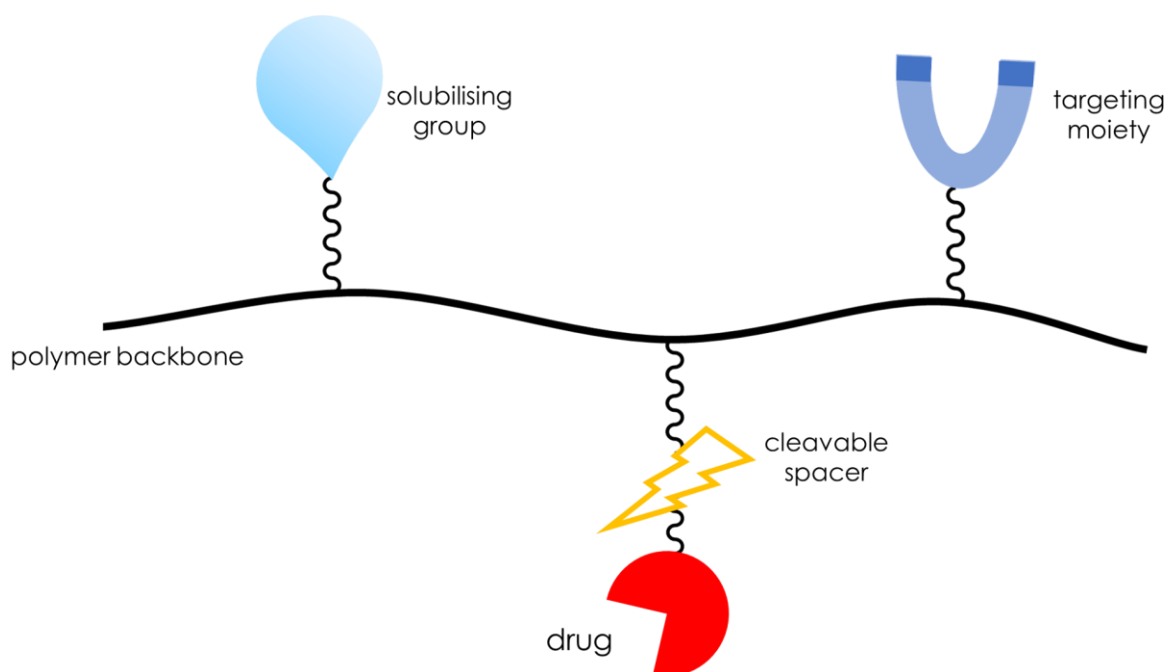
Figure 2.5 Ringsdorf's model for a polymeric prodrug.

2.3.3 Polymer selection

It has been established that a polymeric prodrug is not a singular construct but rather a compilation of various components allied as a whole. Designing a drug delivery system therefore involves forethought. The choice of polymer constituting the polymeric prodrug is of utmost importance. It should allow for its modification with the appropriate functional groups necessary to link the various components together and should also have favourable properties *in vivo*, allowing for non-cytotoxic disintegration once the drug has been delivered.

Modern techniques for the synthesis of polymers have favourably impacted this field making it possible to synthesise controlled, specifically tailored polymers. The polymer architecture, molecular weight, molecular weight distribution and the placement of pendant or terminal functionalities can be controlled to meet the requirements entailed by Ringsdorf's model for a polymeric prodrug. Reversible deactivation radical polymerisation (RDRP) techniques including stable free radical polymerisation (SFRP), transition-metal-catalysed atom transfer radical polymerisation (ATRP) and reversible addition-fragmentation chain transfer (RAFT) mediated polymerisation, as well as ring opening polymerisation (ROP) are largely employed to achieve these constructs with functional moieties.

To reiterate, it is preferable that the polymers used in drug delivery systems are biodegradable, biocompatible, non-immunogenic, have long circulation times and should have the ability to be chemically tailored to release the drug when it is triggered by an external stimulus. A number of polymers, synthetic and natural, have been studied for this purpose. Natural polymers generally present superior *in vivo* properties, yet synthetic polymers are still largely preferred over natural polymers. Natural polymers often suffer from microbial contamination, batch-to-batch variation, uncontrollable rates of hydration and in cases, heavy metal contamination.[58] Although natural polymers represent an essential branch of polymer science with improving characterisation and modifications thereof occurring steadily, for the purpose of controlled drug delivery, synthetic polymers most commonly constitute at least one component in the drug delivery system.

Frequently used synthetic polymers and copolymers include poly(ethylene glycol) (PEG), poly(*N*-vinylpyrrolidone) (PVP), poly(*N*-(2-hydroxypropyl)methacrylamide) (PHPMA), poly(*N,N*-dimethylacrylamide) (PDMA), poly(acrylic acid) (PAA), poly(styrene-*co*-maleic acid/anhydride) (SMA) and aliphatic polyesters such as poly(ε-caprolactone) (PCL), seen in Figure 2.6.
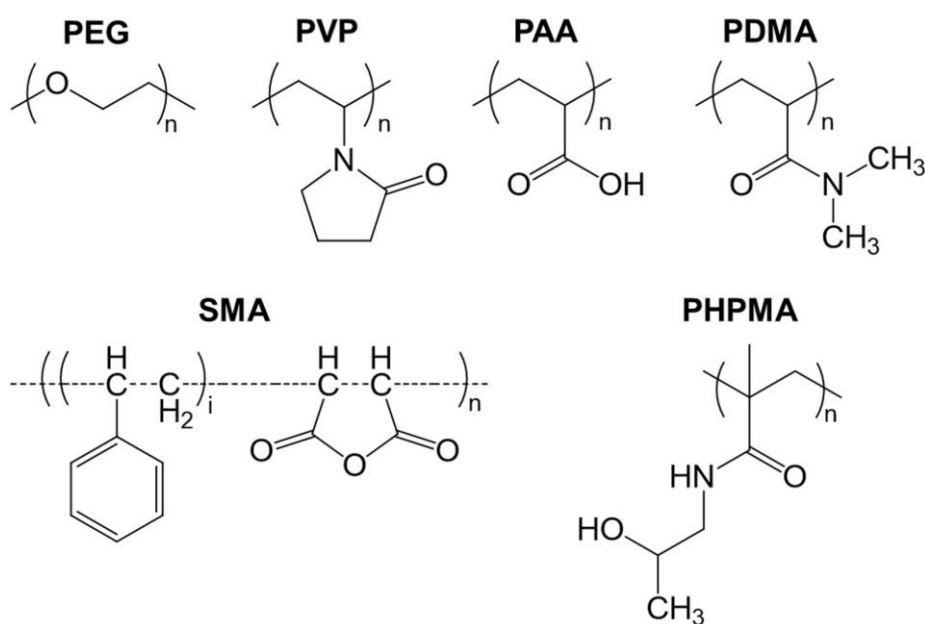
Figure 2.6 Common synthetic polymers used in drug delivery systems. Note that α- and ω-chain ends are omitted for simplicity but can be an array of moieties depending on the method of polymerisation.

From these examples, PEG is the gold standard for drug delivery systems. This is clear by the number of marketed drugs approved by the United States Food and Drug Administration (FDA) that are of PEGylated nature.[59] Its most relevant attributes are intrinsic of hydrophilic polymers in polymer-drug conjugates and include prolonged circulation in the body, increased metabolic stability and decreased immunogenicity compared to the free therapeutic agent alone. Other advantages include its cost effectiveness and the range of commercially available PEG polymers with a wide array of functional groups available for further PEGylation, affording facile synthesis of the prodrug.[60]

Despite PEG's clinical success and numerous proven advantages, unfavourable effects have also been documented. Studies have confirmed the accelerated blood clearance (ABC) phenomenon for PEG conjugates.[61,62] Findings show that the circulation times of PEGylated liposomes decreased after subsequent doses in rats. It has been postulated that this could be as a result of anti-PEG anti-bodies that are produced upon repeated injections of PEG-coated liposomes.[63] The existence of these anti-PEG antibodies is correlated with a loss of therapeutic efficacy and additional adverse effects. PEG is a nonbiodegradable polymer, so its chain length and molecular weight should be controlled as hygroscopic PEG can accumulate in the lysosome and can ultimately result in lysosomal distension and vacuolation.[64] PEG, with its ether backbone structure, is readily degraded through oxidative and mechanical means, which could explain certain irregularities in the pharmacokinetic behaviour of PEG-based carriers, compared to polymers with a carbon backbone, *e.g.* PVP.[59]

a) Poly(*N*-vinylpyrrolidone)

Poly(*N*-vinylpyrrolidone) (PVP) was first synthesised by Reppe and co-workers in 1939 from its monomer *N*-vinylpyrrolidone (NVP).[65] It is a versatile polymer with a unique set of physicochemical characteristics that distinguish it as a fore-runner in biomedical polymers. The monomer is composed of a hydrophilic group (the amide moiety) and hydrophobic alkyl substituents. PVP is highly soluble in water and many organic solvents as a result of its highly polar amide group within the pyrrolidone ring as well as the non-polar methine and methylene groups in the ring and along its backbone. Other important properties include its bulky, non-ionic nature, its non-toxicity, biocompatibility, biodegradability, chemical stability and affinity for complexation with both hydrophilic and hydrophobic compounds.[66,67]

PVP was used as a blood plasma expander to treat trauma victims who were in shock,[68] as a dispersant in cosmetics[69] and in a host of other applications due to its excellent film-forming ability. The complex of PVP and iodine was found to have impressive disinfectant properties as a function of time and is marketed under the name Betadine™, among others. This product is so successful that it was chosen by NASA in 1969 to sterilise the Apollo 11 spacecraft against any bacteria possibly found in space.[70] Iodine is the active agent and PVP ensures the slow release thereof, among other less-understood effects that PVP may invoke, thus reducing the irritation-inducing effects of iodine alone. PVP is also used as an additive in a number of food products as it was confirmed based on toxicokinetics that PVP is negligibly absorbed in the digestive tract and is directly excreted by the body.[71]

It is likely that PEG is better suited for biomedical applications which should confer a degree of antimicrobial activity, such as medical scrubs or medical instruments. The monomer of PVP has a much more electron donating ability compared to that of PEG.[72] This character lends itself to greater cell proliferation and binding ability, which could be more suitable for applications such as polymeric prodrugs or tissue engineering. With regard to its use as a polymeric carrier of therapeutics, Kaneda *et al.* conducted a study to determine which polymeric carrier could most effectively extend the plasma half-life of drugs, where PVP showed the longest mean residence time (MRT) after intravenous injection compared to other non-ionic polymers (PEG, PDMA, polyacrylamide (PAM), poly(vinyl alcohol) (PVA) and dextran) of similar molecular weight.[73] In another study it was concluded that PVP and poly(*N*-acryloyl morpholine) showed promising potential and similar physicochemical properties compared to PEG for ibuprofen-conjugated prodrugs with polymer molecular weights of around 2000 g·mol^{-1}.[74] Furthermore, Baganizi *et al.* bioconjugated interleukin-10, an anti-inflammatory cytokine, to carboxylated PVP-coated Ag nanoparticles which increased their storage stability and improved anti-inflammatory efficacies.[75]

The application of PVP in antimalarial drug delivery systems is not well-described in literature. An example is the formation of solid dispersions and nanosuspensions of dihydroartemisinin in PVP obtained by methods of mechanical co-grinding and solvent evaporation, respectively. PVP improved the solubility of the dihydroartemisinin in the solid dispersion 60-fold and was theorised and concluded to have formed hydrogen bonds with the drug. Nanosuspensions with PVP showed a higher antiplasmodial activity compared to microsuspensions and the free drug alone.[76,77]

b) Aliphatic polyesters

Aliphatic polyesters such as PCL, poly*(*δ-valerolactone) (PVL), poly(L-lactide) (PLA), poly(glycolide) (PGA), poly(ρ-dioxanone) (PDO) and poly(D,L-lactide-*co*-glycolide) (PLGA) are frequently used in biomedical applications such as drug delivery systems due to their properties of high biodegradability, biocompatibility and non-toxicity (Figure 2.7). In many of these applications, particularly for drug delivery purposes, their value lies in their facile and effective degradation into non-toxic substituents, able to be rapidly eliminated by the body through normal metabolic pathways.[78] These polymers contain labile ester bonds or ester derivatives in their backbone structures which can undergo hydrolytic cleavage. The polymer degradation process is, however, relatively gradual so it is not a limiting factor in polymeric prodrug design.

Aliphatic polyesters are synthesised via step-growth polymerisation, the polycondensation of diols and diacids or acid anhydrides, or the ring opening polymerisation (ROP) of cyclic ester monomers (lactones). The latter is preferred because it minimises the risks associated with polycondensation including precise stoichiometry, continuous removal of by-products, high temperatures, long reaction times and difficulty in attaining high molecular weight polymers.[79] ROP is not restricted by these limitations and is therefore the preferred option for specifically tailored polymers. Polymerisation mechanisms will be discussed in the prelude to each relevant section.
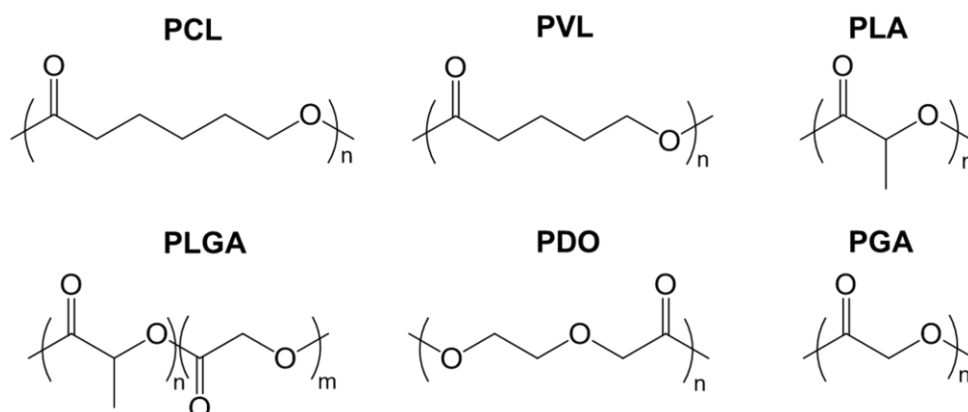
Figure 2.7 Aliphatic polyesters frequently used in drug delivery systems.

Aliphatic polyesters are typically hydrophobic and crystalline, and from a circumscribed perspective this could be seen as a disadvantage, posing certain practical challenges. These polymers also suffer from a lack of chemical functionality which generally restricts their utility as polymeric prodrug candidates. A way to overcome this limitation is to chemically modify the precursor monomer. The monomer can be functionalised to have a reactive handle from which to attach other monomers, targeting ligands, cleavable linkers or drugs.

Of particular interest are PCL and PVL, which are excellent candidates for pre-polymerisation monomer modification. These polymers, differing by only one carbon atom in the cyclic ester monomer, exhibit superior viscoelastic and rheological properties compared to other aliphatic polyesters. Their rates of degradation are also much slower than that of other aliphatic esters. These features, along with the fact that these polymers are also relatively inexpensive and that PCL has been FDA approved, has led to their influx in biomedical applications over recent years.[80] Examples of PCL and PVL in drug delivery systems are abundant in literature. A paper published in 1989 by Fukuzani *et al.* details a drug delivery system of L-lactic acid and δ-valerolactone for estramustine which degraded completely after five weeks *in vivo* (rat animal-model).[81] In a more recent study, triphenylphosphonium-conjugated PCL-based nanostructures were developed for mitochondria-targeting, cationic anticancer nanospheres.[82] Moreover, methoxy-PEG/PCL block copolymer nanospheres were also synthesised with folic acid as the targeting ligand and were loaded with paclitaxel, thereby improving the therapeutic effect of this anticancer drug.[83]

2.3.4 Stimuli-responsive linkers

The controlled release of the drug payload has become a primary concern in modern prodrug design and development. Rather than a passive drug delivery vessel, the nanocarrier of the drug has become an active and integral partner in the manifestation of favourable therapeutic effects. The enhanced efficacy of stimuli-responsive carriers results when the stimulus is unique to the pathology of the diseased site, as off-site drug delivery is concomitantly minimised. A few examples of stimuli that can be used to elicit a response in the polymeric prodrug are temperature, redox potential and pH. This response to an external stimulus is due to the chemical constitution of the specific linker separating the drug from the polymeric system.

For the treatment of malaria, a temperature-responsive linker would be a less founded approach due to the early stages in development of hyperthermia treatment as well as the complexity of the parasitic compartment within the red blood cell (RBC). Current hyperthermia treatment has implemented the use of superparamagnetic iron oxide nanoparticles which can be targeted to the cancerous tumour by an external magnet and once there, an alternating magnetic field can be applied so that the nanoparticles are elevated in temperature, causing ablation.[84] Other approaches make use of the targeted milieu having a temperature which is inherently higher than the normal bodily temperature of 37 °C. In another approach that is especially utilised in cancer therapy, the significant redox potential that exists between cancerous tumours and endosomal tissues is exploited as a stimulus for redox-responsive linkers. These linkers are therefore designed to take advantage of this feat through their constitution of readily reducible disulfide bonds.[85]

The biochemistry of *Plasmodium* is complex and differs to that of cancerous tumours. Many potential drug targets and stimuli for drug release from a polymeric prodrug exist because of the parasite's various metabolic pathways which encompass energy production, lipid metabolism, amino acid metabolism, redox metabolism and the enhanced permeability of the actively growing parasite for small molecular metabolites. There are various cellular barriers that the pharmaceutical agent must traverse through to reach the parasitic terminus. These barriers include the host cell membrane, the parasitic plasma membrane and the digestive vacuole membrane.[86] There exists a pH gradient along these intracellular partitions which can be exploited using pH-responsive, otherwise known as acid-labile or acid-degradable, drug delivery systems. The pH gradient reaches its nadir in the direction of the red arrow, as illustrated in Figure 2.8. Here, TEM images aided with diagrams were used to view the cross-section of infected RBCs over different phases of infection.
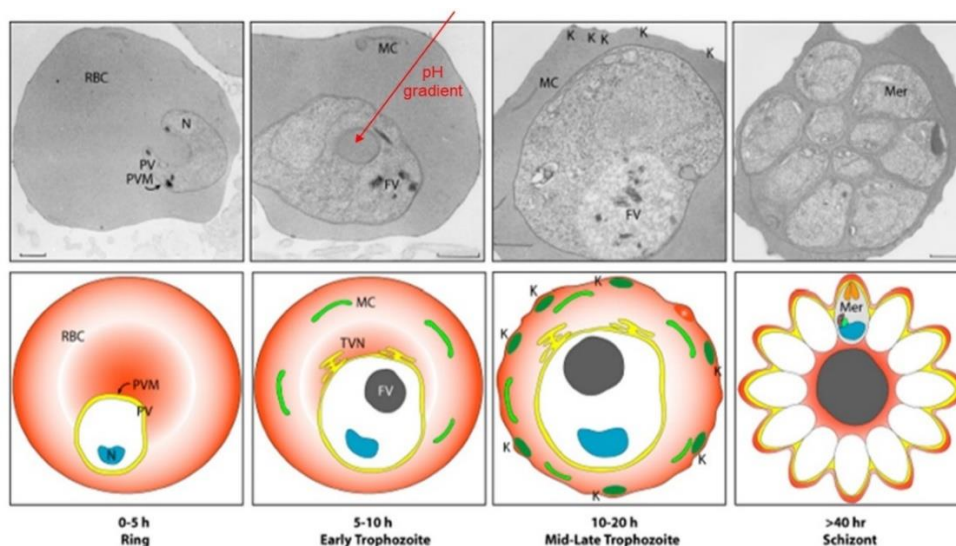
Figure 2.8 Asexual development of malaria parasites in the infected RBC. 0 - 5 h: after invasion, parasites become surrounded by a parasitophorous vacuole (PV) and are visible as ring-like structures in the RBC. 5 - 10 h: the ring stage parasite induced membranous extensions of the parasitophorous vacuole membrane (PVM) into the host cell, which forms a tubulovesicular network (TVN) and RBC membrane-tethered Maurer's clefts. The products of haemoglobin digestion become visible and the decomposition of hemozoin crystals in the food vacuole (FV). 10 - 20 h: as the parasite progresses to the trophozoite stage, it continues to increase its volume considerable and induced knob (K) formation on the iRBC surface. >40 h: after invasion, the parasite starts several rounds of asexual division, resulting in 16 - 32 daughter merozoites, which are still surrounded by the PVM until they rupture free and invade uninfected RBCs. Merozoite (Mer), nucleus (N). Scale bars, 0.5 µm.[87]

Acid-degradable linkages are generally defined as chemical bonds that are stable under physiological pH conditions and are destabilised under lower pH conditions, for instance, in the digestive vacuole of the infected RBC, which has a pH of 5.2 – 5.0.[88] We have within our grasp centuries of development in organic chemistry which has led to a variety of documented cleavable linkers for the application of drug delivery systems. A balance between understanding the existing chemistry available and a curiosity to develop that which is new is required to design an optimally functioning system. Broadly, the triggered release of the payload is achieved through the protonation of acid-degradable functional groups linking the drug to the core-forming polymer. When the pH is reduced below the pK_a of these functional groups, electrostatic repulsion within the polymeric chains causes their destabilisation and hence the release of the therapeutic payload. A more detailed discussion regarding the ability of amphiphilic compounds and polymers to undergo spontaneous self-assembly into nanosized drug-carriers due to solvophobic forces will be provided in Section 2.4. Some frequently used pH-responsive linkers are esters,[89,90] hydrazones,[91,92] *cis*-aconityls,[93,94] orthoesters,[95,96] β-thiopropionates,[97,98] vinyl ethers,[99,100] imines[101,102] and acetals.[103,104] Their structures and hydrolytic degradation products are shown in Table 2.1.

Table 2.1 Common acid-labile linkers and their degradation products

An important factor to consider is the fate of the degradation products post hydrolysis. It is imperative that the degradation products that form as a result of the destabilisation process are (i) biocompatible and (ii) capable of being expelled by the body without causing any harm to healthy tissues, organs or cells.[88] The specific linker chosen should be compatible with the functional groups present in the drug delivery system and the release kinetics should be considered for the final application of the system. If the dissociation of the linkage is too rapid, it could lead to a spike in the concentration of the parent drug leading to off-target toxicity. In the opposite case, too slow a release could hamper the efficacy of the system, even causing drug resistance.

2.3.5 Targeting

The pharmaceutical payload can be delivered to the pathological site by two prominently applied strategies, namely active and passive targeting. Active targeting can be regarded as those systems specifically synthesised with targeting ligands tethered to the nanocarrier so as to enable their affinity with the surface chemistry of the target site. Passive targeting does not utilise this donor-receptor mechanism and instead relies on the inherent ability of nanosized carriers to reach the infected site via biological processes which take place as a result of the disease and the nature of the drug carrier.

In a broader context, for those drug delivery systems designed to deliver chemotherapy to tumours, passive targeting is often relied on. The rationale behind this is a phenomenon called the enhanced permeability and retention (EPR) effect and it is one of the most cited terms in the field of drug delivery. It is an effect coined by Hiroshi Maeda in 1986 and describes the unique vasculature architecture of solid tumours which allows macromolecules from blood vessels to enter into the tissue interstitium. The widespread acceptance of this effect, which describes the natural tendency of nanoparticles to accumulate more in tumour tissues as opposed to healthy tissues, led to an upsurge in nanocarrier therapeutics as cancer therapies.[105]

Although in some cases this effect has been well documented, recently, there has been some controversy surrounding this phenomenon due to a report which reviewed ten years of nanotherapeutics reliant on the EPR effect. It concluded that the median drug accumulation inside cancerous tumours was as low as 0.7%.[106] Progress in developing effective prodrugs using this approach is likely in-part hampered by the heterogeneity of the EPR effect in different tumours and limited human experimental data on the efficacy of this mechanism as related to enhanced nanocarrier accumulation. Different tumour types have different vasculature and pore sizes, for example, fast-growing tumours such as carcinomas have more porous vasculature and slow-growing tumours such as sarcomas possess less porous vasculature.[107,108] These findings and challenges have also been thoroughly researched and discussed by Maeda and co-workers in retrospect since the inception of this phenomenon. It is clear that as with any intersection of technology with biological process, a 'one-size-fits-all' approach will not suffice. Inroads into the tracking of nanoparticles *in vivo* using biomarkers will be beneficial in this field of science, and it may become a requirement to conduct a patient screening study with these biomarkers before the chemotherapy is introduced.

The primary goal of malaria therapy is to deliver a high concentration of the chemoprophylaxis to the intracellular parasitophorous vacuole, where the parasite is hosted. The targeting of antimalarial prodrugs, in particular, is typically active due to the locality of the disease. A part of the human stage of *P. falciparum* takes place inside the RBCs of its host, transforming the RBC by developing a number of unusual metabolic and cell biological functions to sustain its life. The parasite ingests the host cell's haemoglobin by proteases within an acidic food vacuole. The amino acids released are then used for protein synthesis and extracellular media, eventually generating the crystalline by-product called haemozoin (seen under the microscope as dark malaria pigments).[21,86]

It is believed that artemisinin-related antimalarials are activated by these iron-containing digestion products, though the precise mechanism of action is unknown. During the invasion step, the parasite develops within the parasitophorous vacuole, and to make life more hospitable, an estimated 400 proteins are exported by the parasite to the host cell. These proteins include kinases, lipases, adhesins, proteases and chaperone-like proteins. The increased membrane permeability of infected RBCs compared to healthy RBCs is well-documented with regard to a range of low molar mass compounds. This heightened permeability results in membrane channels which appear 12 – 16 h after the invasion takes place. These membrane channels have been termed as 'new permeability pathways' (NPPs) and are unique to infected RBCs. It has been established that macromolecules such as dextran, protein A, heparin and the IgG2a antibody can gain access to the inner parasitophorous vacuole by means of these NPPs.[86,109,110] Through their conjugation, or the conjugation of other discriminating proteins and small molecules to the polymeric nanocarrier, it becomes possible to actively target infected RBCs.

Though active targeting is the preferred strategy in malaria therapy, passive targeting techniques have also been recognised. One such technique, as recorded by Goodyer *et al.*, confirmed that fluorescent carboxylate and amidine-modified latex spheres of diameter 50 – 70 nm were able to traverse across the aforementioned intraerythrocytic barriers to reach the intracellular parasite. The permeation of the spheres is hypothesised as being due to their small size of less than 70 nm, which allowed for their deposition to the parasite likely via NPPs.[111] Studies like these are instrumental to understanding the phenomena which occur at the nanoscale and utilising this power has become synonymous with modern-day drug delivery design. Malaria therapy will be contextualised in the sections to follow, which will delve into the specific design parameters that affect the function and efficacy of polymer-based nanocarriers for therapeutic agents.

2.4 Nano-assembly of polymeric prodrugs

2.4.1 An overview

Immense endeavours into the design and development of nanosized materials have led to the rejuvenation of tools used for the prevention, diagnosis and treatment of an array of diseases. Despite the awakening of this field, the driving force for its existence is not a new concept. Molecular self-assembly is ubiquitous in nature, from the origami formations of DNA and the folding of proteins to the photonic crystals in a scale on a butterfly's wing. These molecular self-assemblies require no human

intervention, and are defined through their spontaneous adoption of structurally defined, ordered assemblies through non-covalent bonds under equilibrium conditions.[112]

The various morphologies of self-assembled small molecule amphiphiles have been studied for decades. Some of these morphologies include spherical micelles, cylindrical micelles (nanorods), bicontinuous structures, vesicles and lamellae. Earlier studies in malaria therapy focussed on liposomal formulations for malaria treatment and demonstrated positive results. Liposomes are nanosized vesicles containing one or more phospholipid bilayers, and have been extensively studied as drug delivery systems since their introduction in the 1960s. Owais *et al.* showed that chloroquine-resistant *P. berghei* (rodent species model of malaria) infected mice could be cured of infections using antibody-bearing liposomes (cholesterol based) to specifically target *P. berghei* RBCs.[113] Studies like these were important in laying the ground work for nanocarriers of antimalarial drugs.

Later, Mosqueira *et al.* encapsulated the antimalarial drug halofantrine within a nanocapsule of PLA homopolymer grafted with PEG chains to form a block copolymer. They found that the nanocapsules improved the efficacy and therapeutic profile of the drug, hence reducing the dosage amount required and therefore the toxicity.[114] The self-assembly of block copolymers to form nanomorphologies has been an active division of polymer chemistry for many years. Other approaches which bypass the requirement of block copolymers for self-assembly exist where sufficient amphiphilicity can be induced by proportions of polymer adjoined to another compound, *e.g.* peptides, antibodies, sugars or drugs.

The self-assembly of amphiphilic block copolymers in water is based on non-polar and hydrophobic interactions between the lipophilic core-forming polymer chains. The process is driven by a gain in entropy of the of the solvent molecules as the hydrophobic components withdraw from the aqueous media to minimise the interfacial free energy of the system. This phenomenon can be extended to any selective solvent system as long as insoluble and soluble components exist. The self-assembly behaviour of block copolymers may also be obtained through mechanical or electrical forces, and self-assembly can also take place in bulk conditions.[115] For the purpose of this study, the self-assembly of block copolymers in a part-aqueous phase will further be referred to. The resulting defined architectures are governed by the volume ratios and concentrations of the soluble and insoluble domains of the block copolymer. The enforced curvature in the assembly arising from the relation of these domains is of primary concern when designing or elucidating the nanoscale structure. This curvature can be expressed mathematically as the dimensionless packing parameter, ρ, which is illustrated in Figure 2.9.

In the expression $\rho = v/a_0 l$, v and l are the volume and length of the solvophobic segment, respectively, and a_0 is the optimal surface area of the solvophobic block at the interface between the solvophobic and solvophilic blocks. In general, spherical micelles are formed when $\rho \leq 1/3$, cylindrical micelles are formed when $1/3 < \rho \leq 1/2$ and vesicles and lamellae are formed when $1/2 < \rho \leq 1$. A prerequisite for this general rule is that the architectures should be in equilibrium. The packing parameter was originally investigated by Israelachvili, Mitchell and Ninham[116] for small molecule surfactants which generally conform to their equilibrium structures. Block copolymers, though similar to surfactants, are much more complex and can adopt kinetically trapped, out-of-equilibrium structures which are not readily

predictable. In order to more efficiently reach the structure at equilibrium, a cosolvent approach has been recommended when creating nano-assemblies. This entails the addition of a cosolvent which is a fair solvent for both blocks, instead of a good solvent for a selective block, to transition the copolymer into a morphology closest to its equilibrium structure. The packing parameter is not commonly calculated for block copolymers because of the complexity and margin of error in determining it experimentally. As a result, the mass fractions which relate to the volume fractions of the hydrophobic and hydrophilic blocks are the generally applied alternative parameters.[117,118]
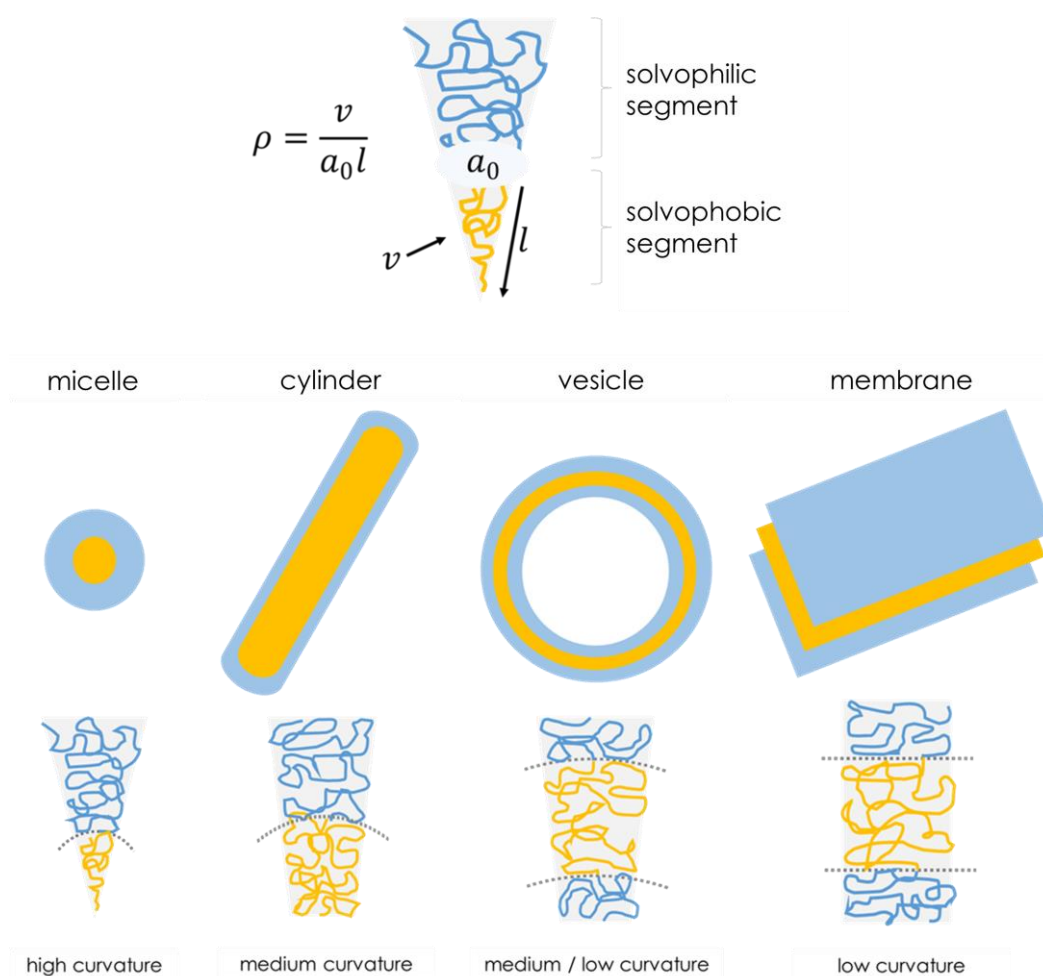
Figure 2.9 The self-assembly characteristics of amphiphilic compounds relating to their curvature as expressed by the packing parameter, ρ.

2.4.2 Nanocarrier stability

Upon intravenous injection, micelles undergo numerous environmental changes including exposure to fluctuations in pH and salt concentration as well as significant dilution effects.[119] Micellar carriers are also prone to dissociation in the blood via plasma proteins, which are able to traverse through nanocarriers into the core, thereby triggering disassembly. Additionally, the adsorption of superficial opsonin proteins has also been thought to elicit micellar disassembly.[120] For polymeric prodrugs, the micelles should remain stable and therefore the drugs should remain in-tact until reaching the targeted cells. Nanocarrier systems can be assessed for their stability in terms of thermodynamic stability (potential of disassembly) and kinetic stability (rate of disassembly).[121]

In a selective solvent, the so-called closed association process can be used to describe the self-assembly of block copolymers into micelles. The critical micelle concentration (CMC) is the minimum concentration at which single polymer chains (unimers) are able to self-assemble into micelles in solution. Below this concentration, polymers exist only as unimers. Above this concentration, micelles are in equilibrium with unimers. The CMC value is an indicator of the thermodynamic stability of the micelle and is related to the thermal energy and the effective activation energy between the polymer and the solution, where lower values indicate higher thermodynamic stabilities. The stability of polymeric micelles compared to surfactant micelles is significantly improved, as evidenced by CMC values generally in the range of 10^{-4} - 10^{-7} M for polymeric micelles and 10^{-2} - 10^{-4} M for surfactant micelles. Micelles with sufficiently low CMC values would be able to withstand the severe dilution which occurs in the blood, an effect that would occur instantaneously upon intravenous administration. The length of the hydrophobic domain correlates directly with the micelle's thermodynamic stability, as increasing the cohesion of the hydrophobic core would lead to a more packed structure with a lower CMC. It has also been shown that the incorporation of hydrophobic drugs can, in this way, increase the stability of the micelles.[115,119,122]

The effect of temperature can be approximated from $\Delta G° = RT\ ln(CMC)$, which begins with defining the standard free energy $\Delta G°$ associated with micelle formation. Here, R is the gas constant, T is the temperature in Kelvin and CMC is the critical micelle concentration. Then since $\Delta G° = \Delta H° - T\Delta S°$, where $\Delta H°$ is the standard enthalpy and $\Delta S°$ is the change in entropy, substituting into the first equation and solving for $ln(CMC)$ results in $ln(CMC) = \Delta H°/RT - \Delta S°/R$. The plot of $ln(CMC)$ as a function of $1/T$ would result in a straight line where the gradient is equal to $\Delta H°/R$ and its intercept is $-\Delta S°/R$, assuming that the standard enthalpy is independent of temperature. In a practical sense, for polymer drug delivery systems with a positive $\Delta H°$, this implies that increasing the temperature would decrease the CMC so that unimers could aggregate into micelles at lower concentrations. A system with a lower CMC value has greater resistance to dissociation in a physiological milieu. Conversely, for systems with a negative $\Delta H°$, the CMC would increase with increasing temperature.[123,124]

Once the micelles are formed, individual chains stay dynamic and are able to switch between micelles and the bulk solution. After a certain amount of time, the micelles disassemble due to dilution effects or changes in the environment. The kinetic stability of a micellar system describes its disassembly

behaviour over time in an aqueous-based solution. It is important to characterise this parameter to ensure the drug is not released prematurely. There are several methods of analysis regarding kinetic stability, and in essence any drug release assay would be an indication of the kinetic stability of the micelle. A classical approach is to monitor the hydrodynamic volume of the micelles in solution using DLS, where typically the solution would be phosphate buffered saline (PBS) or a physiologically-mimicking serum such as fetal bovine serum (FBS)-supplemented PBS. Other strategies include the use of fluorescence microscopy and NMR spectroscopy as characterisation techniques.[119,125]

2.4.3 Micelle shape and size

The nanocarriers' size and shape are considerations which are not ordinarily preconceived and planned but rather analysed as a consequence of the existing system's resulting morphology and size. This is due to the fact that molecular self-assembly is regarded as a 'bottom-up' approach, where the final structure is in fact encoded within the physicochemical properties of the molecules applied to make up the structure. Several studies have, however, been conducted which delve into the specific shapes of effective nanocarriers and the sizes which are best received *in vivo*. Most polymeric micelles in drug delivery systems are reported to be spherical, and a shift to ellipsoid, cylindrical and lamellar micelles may occur as the proportion of core to shell-forming block, concentration of electrolytes, copolymer concentration and composition, organic solvent and the method of micellar preparation are altered.

Micelle diameters of less than 200 nm, sizes generally akin to viruses (5 – 300 nm), prevents their uptake by the reticuloendothelial system (RES) and facilitates the passive targeting of nanovessels.[126] Those micelles larger than 200 nm are mechanically filtered in the spleen, and micelles smaller than 100 nm traverse through blood vessels through fenestrations in the endothelial lining.[127] The ideal diameter of an antimalarial-loaded nanocarrier would therefore be in the range of 100 - 200 nm.

Like size, shape is another important parameter and this is most exquisitely evidenced biologically through viruses, which constitute a nucleic acid molecule within a protein capsid, and replicate within the living cells of various organisms. They therefore provide the ultimate blueprint for biomimicry due to their knack in infiltrating various cells. Viruses are present in a diversity of shapes which drastically govern their function. These efficient biological carriers have undoubtedly been influential in the field of drug delivery, accordingly prompting a focus on shape. One notable feature of some viruses is the presence of filamentous virions extruding from the central structure, which can be short and highly rigid, or long and highly flexible.[128]

In a study by Geng *et al.*, the circulating and cellular uptake of three types of micellar shapes were analysed: spherical, highly deformable worm-shaped particles 'filamicelles' and long filamicelles. They found that there was an estimated 10-fold increase in the circulating time of highly deformable filamicelles to circulate in the bloodstream, compared to spherical micelles. Relating to cellular uptake, the spherical and filamicelles were more efficient under fluid conditions than the long filament micelles which showed the slowest cellular uptake due to their long fibrillar structure.[129] In another study, Loverde, Klein and Discher proved, through all-atom molecular dynamics (MD) simulations, that worm-like nanocarriers could more efficiently deliver the anticancer drug Taxol to a tumour, compared to its

spherical counterpart.[130] Similar studies have also attested to this trend, where it might seem that future steps in drug delivery could aim to impart a slightly elongated or elliptical structure to micelles.[131] These results provide the basis of exploring shapes other than the classical spherical shape of micelles, although the effects of which are not yet fully understood.

2.4.4 Nanocarrier drug loading

Polymer nanocarrier drug loading refers to the concentration of the drug within the core or inner domain of the nanocarrier. The most typical drug loading strategy is via the physical entrapment of the drug (nanoprecipitation) during the self-assembly of previously synthesised polymers in aqueous solution. In this instance, where the hydrophobic drug is non-covalently entrapped within the hydrophobic domain of the carrier, spontaneous molecular assembly is the primary driving force of drug entrapment which occurs so as to minimise the interfacial free energy of the system. Although convenient, there are several drawbacks related to this strategy. These include (i) burst release (the untimely release of a large proportion of drug), (ii) the difficulty in encapsulating low miscibility drugs in the polymer matrix, and (iii) the very low drug loading contents that can be obtained.[132]

Compared with the physical encapsulation method, polymeric prodrugs are excellent candidates for high drug-loaded nanotherapeutics. Here, the drug and polymer are joined via a covalent linkage.[48] Incorporating the drug using this approach is often preferred due to the ability to (i) trigger the drug release via stimuli-responsive linkages, (ii) protect the drug from exposure to the harsh environment in blood thereby limiting premature release, (iii) alter the drug pharmacokinetics which could enhance the therapeutic profile and (iv) the option to load multiple drugs, including those that are hydrophilic, into the system.[133] The amount of drug per mole of polymeric prodrug can be estimated through standard quantitative techniques, where a high drug loading content is consequential so long as the reaction step between the drug and polymer is relatively efficient.

A good indication of the encapsulated drug and hydrophobic core compatibility, is structural similarity and solubility parameters. The Flory-Huggins interaction parameter can be used to predict and measure the compatibility between the drug and the polymer carrier because the drug loading process is effectively a drug solubilising process within the polymeric matrix. The equation $\chi_{dp}=(\delta_d-\delta_p)^2 V_d/RT$ is used to calculate the Flory-Huggins interaction parameter (χ_{dp}) between the polymer and the drug. Here, δ_d and δ_p are the Scatchard-Hildebrand solubility parameters of the drug and core-forming polymer, respectively, V_d is the molecular volume of the drug, R is the ideal gas constant and T is the absolute temperature. Better drug and core-forming polymer compatibility is expected for lower interaction parameter values, which would lead to a greater drug loading content. This is because, for a small positive enthalpic effect (small χ_{dp}) the entropic effect would be greater than the enthalpic effect leading to greater solubilisation.[134] It is expected that the smaller the interaction parameter, the greater the compatibility between the drug and the core-forming polymer. A higher compatibility would in turn lead to a higher drug loading content.

The drug loading content is not, however, solely reliant on this compatibility and it has been shown that this property can be enhanced by utilising hydrogen bonding, steric effects and π-π stacking. Hydrogen bonding can occur between the drug molecule(s) and the polymeric carrier to form strong interactions which contribute to enhanced core-periphery support. The aforementioned steric effects are due to the ideal use of vacant space within the polymer network of the inner core, and lastly, π-π stacking, the attractive interactions between aromatic rings, can also be a contributing factor to drug loading efficiencies.[135] For typical micellar drug delivery systems, drug loading contents of approximately 5 – 20% are reported. A higher loading content means that a greater proportion of the nanocarrier will be active at the pathological site, so that less inactive components need to be administered. This could lead to less treatment failure in the form of patient reliance. In certain cases, this factor is also understood to contribute towards drug resistance.

Yamamoto *et al*. investigated the hydrophobic drug, camptothecin (CPT) by modulating the micellar inner core and found that stable CPT incorporation likely resulted from the concomitant factors of inner-core hydrophobicity, the rigidity of the inner core and the steric configuration.[136] In another study by Liang *et al*., the anticancer drug doxorubicin (DOX) was incorporated into the core of a PEG-green tea catechin conjugate which was self-assembled into micelles.[120] DOX contains within its structure a series of aromatic rings and sites for hydrogen bonding, a structure which is mimicked by the green tea catechin (epigallocatechin-3-*O*-gallate). It was therefore hypothesised that highly-effective binding occurred via hydrogen bonding, hydrophobic interactions and π-π stacking interactions of the catechin to DOX to form ultra-stable, high (88%) drug loaded complexes.

Cai *et al*. were also able to obtain a relatively high drug loading content (55%) of their synthesized nanocomplex of a dimeric drug conjugate of CPT entrapped within a methoxy-PEG and PLA block copolymer micelle.[137] It was hypothesised that their approach of introducing structural defects (dimerising) the drug made it structurally less rigid to decrease its packing efficiency and long-range order. The dimeric prodrug was also thought to have increased hydrogen-bonding compared to the free drug as well as greater drug mobility about the σ bonds for desirable intermolecular drug interactions.

In a recent publication, Lv *et al*. could also ascertain that other interactions besides hydrophobic interactions must come into play when designing a highly efficient drug delivery system. In this case, they hypothesised that the drug loading content of 50% was obtained due to donor-receptor coordination interactions. This form of coordination bonding is commonly exemplified between electron donors and acceptors of π-donor/organometallics or Lewis acids/bases. The donor−acceptor bond energy is usually weaker than covalent bonds and stronger than hydrophobic interactions. To create this system, a PEG-*b*-poly(*N*-2-hydroxyethyl)-aspartamide block copolymer was modified with the Lewis acid phenyl boronic acid on its hydrophobic chains to serve as electron acceptors for coordination with DOX.[138] An increasing awareness of these influential interactions is leading to more efficient drug-loaded nanocomposites as we begin to understand their influences on the self-assembled system.

2.4.5 Drug release

When comparing a free drug to a drug-conjugated carrier system, a clear advantage lies in the fact that the latter approach allows for the modulation of drug release kinetics, while the former does not. Changes to the composition of the carrier by varying the monomer class, functional groups conjugated to the backbone or the crosslinker type and density, can all lead to extended or quickened drug release. To increase the efficacy of the free drug alone, the dosage would need to be increased. This could lead to a plethora of complications including patient non-compliance, drug resistance and exacerbated side-effects due to toxicity.

The stability of the drug-loaded micelle is a prerequisite for sustained drug release. One of the major pressure points for drug delivery systems is the ability to control and quantify the drug release kinetics. For drugs covalently linked to the polymeric carrier, release is governed by the kinetics of the stimuli-responsive linker. For drugs that are physically entrapped within the core of micelles, the release is controlled by the rate of diffusion in the core or the disassembly rate of the micelles. The diffusion rate is dependent on the aforementioned drug-core interactions and can be low for stronger drug and core-forming polymer interactions.[139]

Burst release is the rapid initial release of the drug leading to a deviation from zero-order controlled release, as shown in Figure 2.10. This effect could be problematic in some instances where the carrier would need time to reach the targeted site. If the release of the drug from the polymeric carrier is too rapid, then it will lead to the accumulation of the hydrophobic drug in the body leading to off-target toxicity. Conversely, if the drug is released too slowly, then it will render the drug carrier ineffective to treat the disease and could even cause drug resistance.
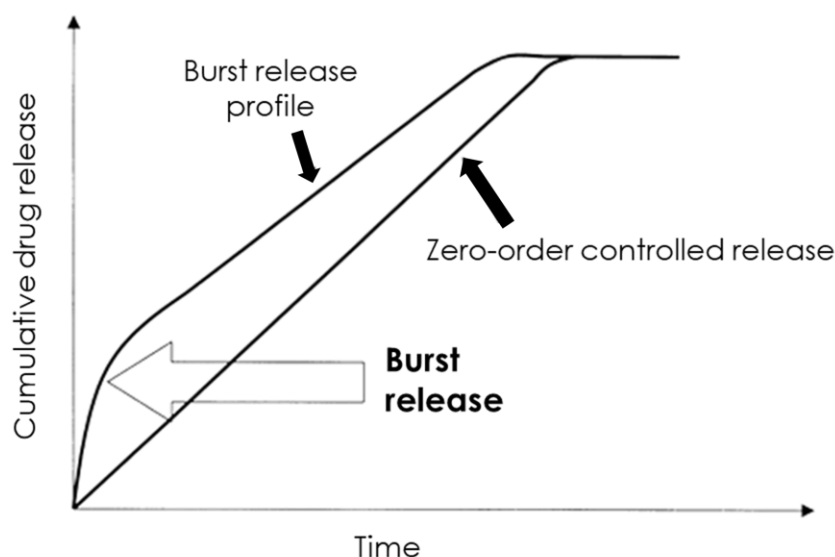
Figure 2.10 Burst release profile.

2.4.6 Cellular uptake

Generally, polymeric prodrugs can be designed to take advantage of the various cellular uptake mechanisms within the body. Some of these mechanisms are not yet fully understood, though our understanding thereof is steadily increasing as more drug delivery systems are being tested *in vivo,* preceding clinical trials. This section will provide a generalised overview of nanocarrier cellular uptake, as malaria-specific RBC targeting strategies have already been discussed.

Free drugs traverse through cell membranes via simple diffusion mechanisms. This diffusion is contingent on the diffusion and partitioning coefficients of the particular drug. A drug that is highly hydrophilic may not be able to traverse the plasma membrane with ease, leading to decreased bioavailability. In this case, the only means of doing so would be to either increase the dosage of the drug or the frequency of the drug dose, which could, once again, lead to the increased likelihood of drug resistance.[43] Nanosized carriers, on the other hand, can be specifically designed for maximum accumulation within cells leading to high therapeutic efficiencies.

Nanosized hydrophilic macromolecules are typically transported into the cell through the process of endocytosis, a pathway responsible for the ingestion of cargo-containing vesicles derived from the plasma membrane in an energy-dependent manner. The uptake mechanisms of cells can differ depending on the type of cell and the cargo being internalised by the cell. The endocytosis pathway has been classified according to the proteins which play a role in the process. Broadly, these mechanisms can be differentiated into two categories, phagocytosis and pinocytosis. Pinocytosis can then be further classified as clathrin-dependent or clathrin-independent mechanisms, of which the latter can be caveolae-mediated, caveolae- and clathrin-independent and macro-pinocytosis.[140] Phagocytosis is primarily accomplished by specialised mammalian cells such as macrophages, monocytes and neutrophils. These cells internalise particles with diameters larger than 750 nm to create internal phagosomes. Smaller particles of diameters up to a few hundred nanometers are engulfed through pinocytosis or micropinocytosis, processes which take place for almost all cell types. Clathrin-dependent endocytosis is a widely-observed mechanism for the uptake of nanoparticles, where cargo-containing endocytic vesicles of less than 100 nm are engulfed by the cell in an energy-dependent manner. In recent years, additional mechanisms have become apparent which are clathrin-independent, and which rely on the cholesterol-dependent clustering of lipid-anchored proteins into diverse microdomains. Caveolae or lipid rafts consisting of plasma membrane invaginations of 50 - 80 nm in diameter, contain cholesterol, sphingolipids, and caveolins.[141,142]

2.5 Conclusions

It is clear that there are numerous points of consideration to deliberate where nano-assembled polymeric prodrugs are concerned and that we are only beginning to understand all of the phenomena that accompany the application of synthetic processes to biological systems, and further yet, to systems at the nanoscale. With complex systems, however, comes the potential to think creatively. It is evidenced by the leaps-and-bounds accomplished in this field over the past few decades. So, though

we are only beginning to scratch at the surface of what drug delivery could someday be, every creative problem-solving technique, every idea and every collaboration will bring us closer to achieving the future of medicine – absolute precision and ultimate distinction.

2.6 References

(1)   Cox, F. E. *Parasit. Vectors* **2010**, *3* (1), 5.

(2)   Hempelmann, E.; Krafts, K. *Malar. J.* **2013**, *12* (1), 232.

(3)   Brabin, B. J. *Malar. J.* **2014**, *13* (1), 497.

(4)   Games, A. https://wellcomecollection.org (accessed Apr. 3, 2018).

(5)   Copp, C. https://wellcomecollection.org (accessed Apr. 3, 2018).

(6)   Smith, D. C.; Sanford, L. B. *Am. J. Trop. Med. Hyg.* **1985**, *34* (1), 2.

(7)   Kotar, S. L.; Gessler, J. E. *Yellow Fever : A Worldwide History*; McFarland: North Carolina, 2017.

(8)   Ross, R. *Lancet* **1898**, *152* (3912), 488.

(9)   Sherman, I. W. *Malaria*; Wiley: Chichester, 2001.

(10)   Bruce-Chwatt, L. J. *J. R. Soc. Med.* **1981**, *74* (7), 531.

(11)   Bloland, P. B. *Drug Resistance in Malaria;* World Health Organisation: Geneva, 2001.

(12)   *World Malaria Report*; World Health Organization: Geneva, 2017.

(13)   Blumberg, L. http://www.nicd.ac.za (accessed Apr. 1, 2018).

(14)   Richie, T. L.; Saul, A. *Nature* **2002**, *415* (6872), 694.

(15)   Singh, B.; Daneshvar, C. *Clin. Microbiol. Rev.* **2013**, *26* (2), 165.

(16)   Warrell, D. A.; Cox, T. M.; Firth, J. D. *Oxford Textbook of Medicine*; Oxford University Press: Oxford, 2010.

(17)   Klein, E. Y. *Int. J. Antimicrob. Agents* **2013**, *41* (4), 311.

(18)   Frevert, U.; Engelmann, S.; Zougbédé, S.; Stange, J.; Ng, B.; Matuschewski, K.; Liebes, L.; Yee, H. *PLOS Biol.* **2005**, *3* (6), 192.

(19)   Bannister, L. H. *Proc. Natl. Acad. Sci. U. S. A.* **2001**, *98* (2), 383.

(20)   Long, C. A.; Hoffman, S. L. *Science* **2002**, *297* (5580), 345.

(21)   Beeson, J. G.; Drew, D. R.; Boyle, M. J.; Feng, G.; Fowkes, F. J. I.; Richards, J. S. *FEMS Microbiol. Rev.* **2016**, *40* (3), 343.

(22)   Cowman, A. F.; Crabb, B. S. *Cell* **2006**, *124* (4), 755.

(23)   Marques, J.; Valle-Delgado, J. J.; Urbán, P.; Baró, E.; Prohens, R.; Mayor, A.; Cisteró, P.; Delves, M.; Sinden, R. E.; Grandfils, C. *Nanomedicine* **2017**, *13* (2), 515.

(24)   Meyer, C. G.; Marks, F.; May, J. *Trop. Med. Int. Heal.* **2004**, *9* (12), 1239.

(25)   Hobbs, C.; Duffy, P. *Mol. Biol. Rep.* **2011**, *3* (5), 24.

(26)   Fidock, D. A.; Rosenthal, P. J.; Croft, S. L.; Brun, R.; Nwaka, S. *Nat. Rev. Drug Discov.* **2004**, *3* (6), 509.

(27)   White, N. *Philos. Trans. Royal Soc. B.* **1999**, *354* (1384), 739.

(28)   Aranda, J. V. *Pediatr. Clin. North Am.* **2017**, *64* (6), 15.

(29)   Su, X.-Z.; Miller, L. H. *Sci. China. Life Sci.* **2015**, *58* (11), 1175.

(30)   Ehrhardt, S.; Meyer, C. G. *Ther. Clin. Risk Manag.* **2009**, *5* (1), 805.

(31)   Bloland, P. B.; Ettling, M.; Meek, S. *Bull. World Health Organ.* **2000**, *78* (1), 1378.

(32)   Omari, A. A.; Gamble, C.; Garner, P. *Trop. Med. Int. Heal.* **2004**, *9* (2), 192.

(33)   Bhandari, S.; Rana, V.; Tiwary, A. K. *Ther. Deliv.* **2017**, *8* (4), 201.

(34)   *Artemisinin and Artemisinin-Based Combination Therapy Resistance*; World Health Organisation: Geneva, 2016.

(35)   Grinin, L.; Korotayev, A.; Tausch, A. *Economic Cycles, Crises, and the Global Periphery*; Springer: Cham, 2016.

(36)   Rowland-Campbell, A. https://intersticia.com (accessed Apr. 24, 2018).

(37)   Drexler, K. E. *Engines of Creation*; Anchor: New York, 1986.

(38)   Feynman, R. P. *Microelectromech. Syst.* **1992**, *1* (1), 60.

(39)   Ventola, C. L. *Pharm. Ther.* **2012**, *37* (9), 512.

(40)   Neeraj Agrawal, R.; Alok Mukerji, A. J.; Joseph, A.; Mukerji, A. *J. Antivir. Antiretrovir.* **2013**, *11* (15)*,* 72.

(41)   Taylor, W. R. J.; White, N. J. *Drug Saf.* **2004**, *27* (1), 25.

(42)   Peters, W. *Pharmacol. Ther.* **1990**, *47* (3), 499.

(43)   Santos-Magalhães, N. S.; Mosqueira, V. C. F. *Adv. Drug Deliv. Rev.* **2010**, *62* (4), 560.

(44)   Couvreur, P.; Vauthier, C. *Pharm. Res.* **2006**, *23* (7), 1417.

(45)   Klibanov, A. L.; Maruyama, K.; Torchilin, V. P.; Huang, L. *FEBS Lett.* **1990**, *268* (1), 235.

(46)   Maruyama, K.; Takahashi, N.; Tagawa, T.; Nagaike, K.; Iwatsuru, M. *FEBS Lett.* **1997**, *413* (1), 177.

(47)   Green, N. K.; Herbert, C. W.; Hale, S. J.; Hale, A. B.; Mautner, V.; Harkins, R.; Hermiston, T.; Ulbrich, K.; Fisher, K. D.; Seymour, L. W. *Gene Ther.* **2004**, *11* (16), 1256.

(48)   Hoste, K.; De Winne, K.; Schacht, E. *Int. J. Pharm.* **2004**, *277* (1), 119.

(49)   Fagin, D. *Nature* **2012**, *490* (7421), 462.

(50)   Bowman, W. C.; Rand, M. J.; West, G. B. *Textbook of Pharmacology*; Blackwell Scientific: Oxford, 1968.

(51)   Strebhardt, K.; Ullrich, A. *Nat. Rev. Cancer* **2008**, *8* (6), 473.

(52)   Jatzkewitz, H. *Nature* **1955**, *10* (1), 27.

(53)   Givental, N. I.; Ushakov, S. N.; Panarin, E. F.; Popova, G. O. *Antibiot. Med. Biotek.* **1965**, *10* (8), 701.

(54)   Shumikhina, K. I.; Panarin, E. F.; Ushakov, S. N. *Antibiot. Med. Biotek.* **1966**, *11* (9), 767.

(55)   Panarin, E. F.; Ushakov, S. N. *Pharm. Chem. J.* **1968**, *2* (5), 260.

(56)   Hoffman, A. S. *Acta Biomater.* **2016**, *40* (1), 1.

(57)   Ringsdorf, H. *J. Polym. Sci. Polym. Symp.* **2007**, *51* (1), 135.

(58)   Gavasane, A. J.; Pawar, H. A. *Clin. Pharmacol. Biopharm.* **2014**, *3* (2), 1.

(59)   Knop, K.; Hoogenboom, R.; Fischer, D.; Schubert, U. S. *Angew. Chem.* **2010**, *49* (36), 6288.

(60)   Kolate, A.; Baradia, D.; Patil, S.; Vhora, I.; Kore, G.; Misra, A. *J. Control. Release* **2014,** *192* (1), 67.

(61)   Bendas, G.; Rothe, U.; Scherphof, G. L.; Kamps, J. A. A. M. *Biochim. Biophys. Acta* **2003**, *1609* (1), 63.

(62)   Ishida, T.; Maeda, R.; Ichihara, M.; Irimura, K.; Kiwada, H. *J. Control. Release* **2003**, *88* (1), 35.

(63)   Sroda, K.; Rydlewski, J.; Langner, M.; Kozubek, A.; Grzybek, M.; Sikorski, A. F. *Cell. Mol. Biol. Lett.* **2005**, *10* (1), 37.

(64)   Prentice, D. E.; Majeed, S. K. *Toxicol. Lett.* **1978**, *2* (2), 119.

(65)   Aroua, S.; Tiu, E. G. V.; Ayer, M., Ishikawa; T.; Yamakoshi, Y. *Polym. Chem.* **2015**, *6* (14), 2616.

(66)   Koczkur, K. M.; Mourdikoudis, S.; Polavarapu, L.; Skrabalak, S. E. *Dalton Trans.* **2015**, *44* (41), 17883.

(67)   Teodorescu, M.; Bercea, M. *Polym. Plast. Technol. Eng.* **2015**, *54* (9), 923.

(68)   Ravin, H. A.; Seligman, A. M.; Fine, J. *N. Engl. J. Med.* **1952**, *247* (24), 921.

(69)   Yamakoshi, Y. N.; Yagami, T.; Fukuhara, K.; Sueyoshi, S.; Miyata, N. *J. Chem. Soc. Chem.*

Commun. **1994**, *0* (4), 517.

(70)   Lawrence, J. C. *J. Wound Care* **1998**, *7* (8), 421.

(71)   Nair, B. *Int. J. Toxicol.* **1998**, *17* (4), 95.

(72)   Fortuin, L. *Modified Chitosan Nano-Substrates for Mycobacterial Capture [MSc Thesis]*; Stellenbosch University, 2015.

(73)   Kaneda, Y.; Tsutsumi, Y.; Yoshioka, Y.; Kamada, H.; Yamamoto, Y.; Kodaira, H.; Tsunoda, S.; Okamoto, T.; Mukai, Y.; Shibata, H. *Biomaterials* **2004**, *25* (16), 3259.

(74)   Sartore, L.; Peroni, I.; Ferruti, P.; Latini, R.; Bernasconi, R. *J. Biomater. Sci. Polym. Ed.* **1997**, *8* (10), 741.

(75)   Baganizi, D. R.; Nyairo, E.; Duncan, S. A.; Singh, S. R.; Dennis, V. A. *Nanomater.* **2017**, *7* (7), 165.

(76)   Ansari, M. T.; Sunderland, V. B. *Arch. Pharm. Res.* **2008**, *31* (3), 390.

(77)   Chingunpitak, J.; Puttipipatkhachorn, S.; Chavalitshewinkoon-Petmitr, P.; Tozuka, Y.; Moribe, K.; Yamamoto, K. *Drug Dev. Ind. Pharm.* **2008**, *34* (3), 314.

(78)   Ikada, Y.; Tsuji, H. *Macromol. Rapid Commun.* **2005**, *21* (3), 117.

(79)   Löfgren, A.; Albertsson, A.-C.; Dubois, P.; Jérôme, R. *J. Macromol. Sci. Part C Polym. Rev.* **1995**, *35* (3), 379.

(80)   Woodruff, M. A.; Hutmacher, D. W. *Prog. Polym. Sci.* **2010**, *35* (10), 1217.

(81)   Hironobu, F.; Masaru, Y.; Masaharu, A.; Minoru, K.; Tooru, M.; Hisako, Y.; Kyoichi, I.; Hidetoshi, Y.; Umeko, K.; Keiji, S. *J. Control. Release* **1989**, *10* (3), 293.

(82)   Cho, D. Y.; Cho, H.; Kwon, K.; Yu, M.; Lee, E.; Huh, K. M.; Lee, D. H.; Kang, H. C. *Adv. Funct. Mater.* **2015**, *25* (34), 5479.

(83)   Park, E. K.; Lee, S. B.; Lee, Y. M. *Biomaterials* **2005**, *26* (9), 1053.

(84)   Ahmed, M.; Lukyanov, A. N.; Torchilin, V.; Tournier, H.; Schneider, A. N.; Goldberg, S. N. *J. Vasc. Interv. Radiol.* **2005**, *16* (10), 1365.

(85)   Huo, M.; Yuan, J.; Tao, L.; Wei, Y. *Polym. Chem.* **2014**, *5* (5), 1519.

(86)   Tilley, L.; Dixon, M. W. A.; Kirk, K. *Int. J. Biochem. Cell Biol.* **2011**, *43* (6), 839.

(87)   Marti, M.; Baum, J.; Rug, M.; Tilley, L.; Cowman, A. F. *J. Cell Biol.* **2005**, *171* (4), 587.

(88)   Binauld, S.; Stenzel, M. H. *Chem. Commun.* **2013**, *49* (21), 2082.

(89)   Tong, R.; Cheng, J. *J. Am. Chem. Soc.* **2009**, *131* (13), 4744.

(90)   Sengupta, S.; Eavarone, D.; Capila, I.; Zhao, G.; Watson, N.; Kiziltepe, T.; Sasisekharan, R.

Nature **2005**, *436* (7050), 568.

(91)   Patil, R.; Portilla-Arias, J.; Ding, H.; Konda, B.; Rekechenetskiy, A.; Inoue, S.; Black, K. L.; Holler, E.; Ljubimova, J. Y. *Int. J. Mol. Sci.* **2012**, *13* (12), 11681.

(92)   Kale, A. A.; Torchilin, V. P. *Bioconjugate Chem.* **2007**, *18* (2), 363.

(93)   Li, N.; Lu, W.; Yu, J.; Xiao, Y.; Liu, S.; Gan, L.; Huang, J. *Mater. Sci. Eng. C* **2018**, *91* (1), 179.

(94)   Huang, X.; Liao, W.; Xie, Z.; Chen, D.; Zhang, C. Y. *Mater. Sci. Eng. C* **2018**, *90* (1), 27.

(95)   Wang, J.; Wang, X.; Yan, G.; Fu, S.; Tang, R. *J. Colloid Interface Sci.* **2017**, *508* (1), 282.

(96)   Cheng, X.; Qin, J.; Wang, X.; Zha, Q.; Yao, W.; Fu, S.; Tang, R. *Eur. J. Pharm. Biopharm.* **2018**, *128* (1), 247.

(97)   Shi, X.; Hou, M.; Bai, S.; Ma, X.; Gao, Y. E.; Xiao, B.; Xue, P.; Kang, Y.; Xu, Z.; Li, C. M. *Mol. Pharm.* **2017**, *14* (11), 4032.

(98)   Qiu, L.; Liu, Q.; Hong, C. Y.; Pan, C. Y. *J. Mater. Chem. B* **2016**, *4* (1), 141.

(99)   Xu, Z.; Gu, W.; Chen, L.; Gao, Y.; Zhang, Z.; Li, Y. *Biomacromolecules* **2008**, *9* (11), 3119.

(100)   Boomer, J. A.; Qualls, M. M.; Inerowicz, H. D.; Haynes, R. H.; Patri, V. S.; Kim, J.M.; Thompson, D. H. *Bioconjug. Chem.* **2009**, *20* (1), 47.

(101)   Indira Chandran, V.; Matesic, L.; Locke, J. M.; Skropeta, D.; Ranson, M.; Vine, K. L. *Cancer Lett.* **2012**, *316* (2), 151.

(102)   Cai, X.; Dong, C.; Dong, H.; Wang, G.; Pauletti, G. M.; Pan, X.; Wen, H.; Mehl, I.; Li, Y.; Shi, D. *Biomacromolecules* **2012**, *13* (4), 1024.

(103)   Liu, R.; Zhang, Y.; Zhao, X.; Agarwal, A.; Mueller, L. J.; Feng, P. *J. Am. Chem. Soc.* **2010**, *132* (5), 1500.

(104)   Bachelder, E. M.; Beaudette, T. T.; Broaders, K. E.; Dashe, J.; Fréchet, J. M. J. *J. Am. Chem. Soc.* **2008**, *130* (32), 10494.

(105)   Maeda, H.; Tsukigawa, K.; Fang, J. *Microcirculation* **2016**, *23* (3), 173.

(106)   Wilhelm, S.; Tavares, A. J.; Dai, Q.; Ohta, S.; Audet, J.; Dvorak, H. F.; Chan, W. C. W. *Nat. Rev. Mater.* **2016**, *1* (5), 16014.

(107)   Youn, Y. S.; Bae, Y. H. *Adv. Drug Deliv. Rev.* **2018**, *130* (1), 3.

(108)   Prabhakar, U.; Maeda, H.; Jain, R. K.; Sevick-Muraca, E. M.; Zamboni, W.; Farokhzad, O. C.; Barry, S. T.; Gabizon, A.; Grodzinski, P.; Blakey, D. C. *Cancer Res.* **2013**, *73* (8), 2412.

(109)   Kirk, K. *Acta Trop.* **2004**, *89* (3), 285.

(110)   Kirk, K. *Physiol. Rev.* **2001**, *81* (2), 495.

(111)   Goodyer, I. D.; Pouvelle, B.; Schneider, T. G.; Trelka, D. P.; Taraschi, T. F. *Mol. Biochem. Parasitol.* **1997**, *87* (1), 13.

(112)   Whitesides, G. M.; Mathias, J. P.; Seto, C. T. *Science* **1991**, *254* (5036), 1312.

(113)   Owais, M.; Varshney, G. C.; Choudhury, A.; Chandra, S.; Gupta, C. M. *Antimicrob. Agents Chemother.* **1995**, *39* (1), 180.

(114)   Mosqueira, V. C. F.; Loiseau, P. M.; Bories, C.; Legrand, P.; Devissaguet, J.-P.; Barratt, G. *Antimicrob. Agents Chemother.* **2004**, *48* (4), 1222.

(115)   Riess, G. *Prog. Polym. Sci.* **2003**, *28* (7), 1107.

(116)   Israelachvili, J. N.; Mitchell, D. J.; Ninham, B. W. *J. Chem. Soc. Faraday Trans.* **1976**, *72* (1), 1525.

(117)   Smart, T.; Lomas, H.; Massignani, M.; Flores-Merino, M. V.; Perez, L. R.; Battaglia, G. Block *Nano Today* **2008**, *3* (3), 38.

(118)   Doncom, K. E. B.; Blackman, L. D.; Wright, D. B.; Gibson, M. I.; O'Reilly, R. K. *Chem. Soc. Rev.* **2017**, *46* (14), 4119.

(119)   Owen, S. C.; Chan, D. P. Y.; Shoichet, M. S. *Nano Today* **2012**, *7* (1), 53.

(120)   Liang, K.; Chung, J. E.; Gao, S. J.; Yongvongsoontorn, N.; Kurisawa, M. *Adv. Mater.* **2018**, *30* (14), 1706963.

(121)   Lu, J.; Owen, S. C.; Shoichet, M. S. *Macromolecules* **2011**, *44* (15), 6002.

(122)   Adams, M. L.; Lavasanifar, A.; Kwon, G. S. *J. Pharm. Sci.* **2003**, *92* (7), 1343.

(123)   Kabanov, A. V; Batrakova, E. V; Alakhov, V. Y. *J. Control. Release* **2002**, *82* (2), 189.

(124)   Monk, P. M. S. *Physical Chemistry : Understanding Our Chemical World*; Wiley: Manchester, 2004.

(125)   Jones, M. C.; Leroux, J. C. *Eur. J. Pharm. Biopharm.* **1999**, *48* (2), 101.

(126)   Kim, Y.; Pourgholami, M. H.; Morris, D. L.; Stenzel, M. H. *J. Mater. Chem.* **2011**, *21* (34), 12777.

(127)   Mitragotri, S.; Lahann, J. *Nat. Mater.* **2009**, *8* (1), 15.

(128)   Ma, Y.; Nolte, R. J. M.; Cornelissen, J. J. L. M. *Adv. Drug Deliv. Rev.* **2012**, *64* (9), 811.

(129)   Geng, Y.; Dalhaimer, P.; Cai, S.; Tsai, R.; Tewari, M.; Minko, T.; Discher, D. E. *Nat. Nanotechnol.* **2007**, *2* (4), 249.

(130)   Loverde, S. M.; Klein, M. L.; Discher, D. E. *Adv. Mater.* **2012**, *24* (28), 3823.

(131)   Venkataraman, S.; Hedrick, J. L.; Ong, Z. Y.; Yang, C.; Ee, P. L. R.; Hammond, P. T.; Yang, Y. Y. *Adv. Drug Deliv. Rev.* **2011**, *63* (14), 1228.

(132)   Nicolas, J. *Chem. Mater.* **2016**, *28* (6), 1591.

(133)   Shen, S.; Wu, Y.; Liu, Y.; Wu, D. *Int. J. Nanomed.* **2017**, *12* (1), 4085.

(134)   Nagarajan, R.; Barry, M.; Ruckenstein, E. *Langmuir* **1986**, *2* (2), 210.

(135)   Yokoyama, M. *J. Drug Target.* **2014**, *22* (7), 576.

(136)   Yamamoto, T.; Yokoyama, M.; Opanasopit, P.; Hayama, A.; Kawano, K.; Maitani, Y. *J. Control. Release* **2007**, *123* (1), 11.

(137)   Cai, K.; He, X.; Song, Z.; Yin, Q.; Zhang, Y.; Uckun, F. M.; Jiang, C.; Cheng, J. *J. Am. Chem. Soc.* **2015**, *137* (10), 3458.

(138)   Lv, S.; Wu, Y.; Cai, K.; He, H.; Li, Y.; Lan, M.; Chen, X.; Cheng, J.; Yin, L. *J. Am. Chem. Soc.* **2018**, *140* (4), 1235.

(139)   Aliabadi, H. M.; Lavasanifar, A. *Expert Opin. Drug Deliv.* **2006**, *3* (1), 139.

(140)   Sahay, G.; Alakhova, D. Y.; Kabanov, A. V. *J. Control. Release* **2010**, *145* (3), 182.

(141)   Zhao, F.; Zhao, Y.; Liu, Y.; Chang, X.; Chen, C.; Zhao, Y. *Small* **2011**, *7* (10), 1322.

(142)   Kou, L.; Sun, J.; Zhai, Y.; He, Z. *Asian J. Pharm. Sci.* **2013**, *8* (1), 1.

Chapter Three

Acid-degradable linkages

3.1 Introduction

Numerous nanocarriers have already been tested, approved and implemented as chemotherapeutic drug delivery systems.[1] Despite this success, there is still much progress to be made in terms of optimising the drug release characteristics of these systems to attain control over the therapeutic effects thereof. An important shift in nanocarrier design occurred when the strategies of incorporating targeting moieties to enhance nanocarrier accumulation at the desired location (spatial) and the ability to control the payload release (temporal) were implemented.[2]

The payload release by the polymer is a modulable consequence of designing stimuli-responsive polymers, also branded as 'smart' polymers. These polymers can be defined as those which are able to undergo an immense or sudden change in a physical or chemical characteristic in response to an external stimulus. Some systems are even designed to respond to more than one form of stimulus. The response of the polymer to this change in its environment can occur in more ways than one. For instance, the polymer can undergo reversible changes in its chain conformation or degree of intermolecular association, or irreversible bond cleavage.[3] Polymers with ionisable groups in their backbone or acid-degradable linkers are duly pH-sensitive and are thus able to elicit the intended temporal response. For a delivery system to function optimally, the pH-sensitive linker should remain stable in physiological conditions (pH 7.4) until it is activated by more acidic conditions (pH 5.0 – 5.5) found in tumorous tissues or malaria-infected red blood cells. Several types of pH-sensitive linkers are able to elicit this type of degradable behaviour. The majority of polymer-drug conjugates in clinical trials make use of the hydrolytically-labile ester linkage and variations thereof.[4] Other major categories include acetals/ketals, imines, hydrazones and cis-acetonityls,[3] as summarised previously.

Elucidating the stability of the polymer-drug bond is crucial for various applications of polymer-drug conjugates and polymer-protein conjugates. For example, for polymer-protein conjugates associated with prolonged circulation, the half-life of the bond degradation should be greater than the half-life of the conjugate itself. For polymer-drug conjugates intended for circulatory depots, the bond degradation half-life should be shorter than the plasma half-life.[5] Different applications would require slightly different release kinetics. It is therefore important to take into consideration the polymer system and the hydrolysis kinetics of the linker when designing a drug delivery system.

Poly(*N*-vinylpyrrolidone) (PVP) is a desirable biomedical polymer for these systems due to its stability, non-toxicity, neutrality and aqueous/organic solvent solubility. Additionally, it has been approved by the FDA as a food additive, it has been used in contact lenses, as a blood plasma substitute, it resists non-specific adsorption of proteins and it is easily lyophilised.[5,6–8] The functionalisation of PVP has therefore been an important target over the last few decades. The emergence of radical polymerisation by reversible deactivation techniques has made it possible to synthesise PVP with predictable molecular

weights and low dispersities. Where polymerisation techniques such as transition-metal-catalysed atom transfer radical polymerisation (ATRP), nitroxide-mediated polymerisation (NMP), iodine transfer polymerisation (ITP) and organocobalt-mediated radical polymerisation (OCRP) have not succeeded in controlling the polymerisation of NVP, other techniques such as organoheteroatom-mediated polymerisation (OHRP) and reversible addition-fragmentation transfer (RAFT) polymerisation, have.[9] With the advent of the latter by Moad, Rizzardo and Thang in 1998,[10] it is no longer an arduous task to apply radical polymerisation to the formation of complex architectures and advantageous end-groups for further functionalisation.

The RAFT process is accomplished by performing a radical polymerisation in the presence of a thiocarbonylthio compound which acts as a reversible chain transfer agent (CTA) i.e. RAFT agent. These compounds are generally dithioesters, dithiocarbamates, trithiocarbonates or xanthates.[11] When xanthates are used to mediate the polymerisation, it is frequently referred to as a RAFT/MADIX (macromolecular design via the interchange of xanthates) process. In order to control this radical polymerisation, a fine balance between the forward and reverse rates of addition (k_{add} and k_{-add}) and fragmentation (k_{β} and $k_{-\beta}$), along with the rates of reinitiation (k_i) and propagation (k_p) ought to be achieved (Scheme 3.1 a)). The RAFT mechanism begins when an initiator-derived radical and propagates with the monomer (M) to form a polymeric radical ($P_n^{\bullet}$). Ideally, $P_n^{\bullet}$ would react efficiently with the RAFT agent and an intermediate would form which would then fragment quantitatively to create the macro-RAFT agent. This agent then ejects a radical $R^{\bullet}$ thereby re-initiating the polymerisation.
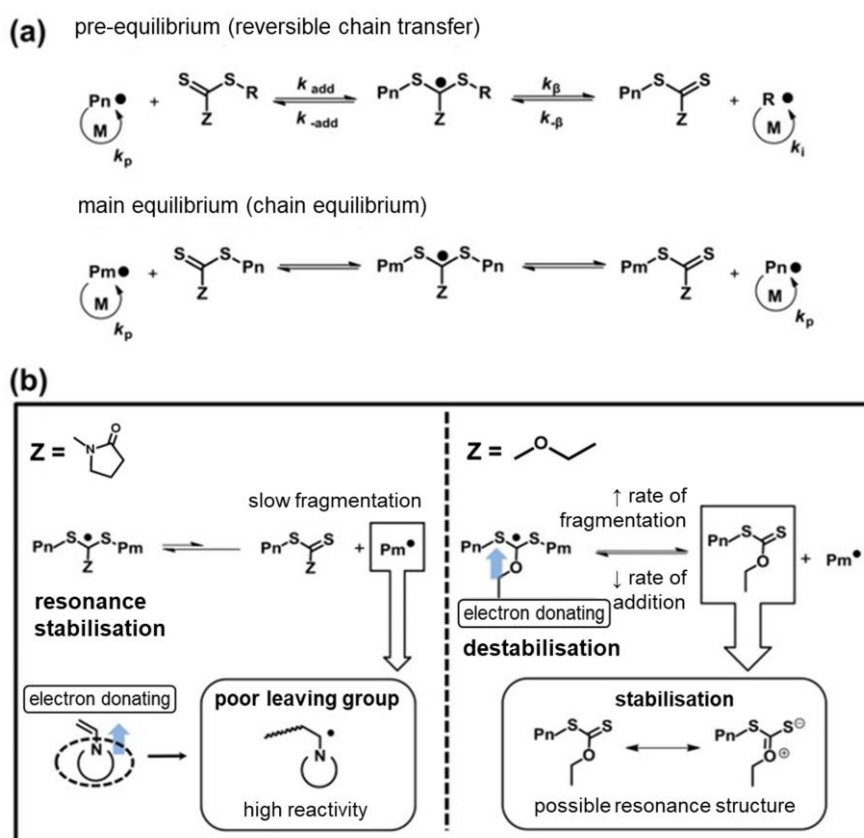
Scheme 3.1 a) The addition-fragmentation chain transfer (RAFT) process's pre-equilibrium and during main equilibrium and b) the proposed mechanism for RAFT-mediated N-vinyl monomer polymerisation.[12]

Radically polymerisable monomers can be divided into 'more activated monomers' (MAMs) and 'less activated monomers' (LAMs) based on the ability of the monomer to react in a free-radical process (MAMs > LAMs). MAMs can be classed as those monomers where the vinylic group is conjugated to an electron-poor neighbouring functionality such as a carbonyl group or an aromatic ring and LAMs can be classed of those monomers where the vinylic group is adjacent to an electron-rich atom such as a nitrogen or oxygen atom, as is the case with *N*-vinylpyrrolidone (NVP) (Scheme 3.1). The MAMs react more readily with radicals due to enhanced electronic stabilisation and additional steric effects, where the opposite is true for LAMs. The RAFT agent should therefore be carefully chosen with the appropriate Z and R groups, where the Z group modulates the reactivity of the thiocarbonyl double bond and the R group is the free radical leaving group.[12–14]

An important attribute of RAFT polymerisation is that it facilitates well-defined end-groups which can readily be used for further functionalisation through direct use of the R group, as it can be chosen to be dually efficient (in terms of reinitiating the RAFT polymerisation) and useful (in terms of future reactions). An example of such, which will later be explored, is the use of a hydroxy-functional RAFT agent where the α-end group is a hydroxyl group and can be used as a macro-initiator post polymerisation to initiate the ring-opening polymerisation (ROP) of a second monomer to form a block copolymer.

The ω-end group can be modified through a process of degradation by a number of reactions to obtain chain-end dormancy or increased activity to build more complex or useful polymer building blocks. It is known that the thiocarbonylthio group can impart instability[15] or interfere with subsequent steps in the synthetic route. These reactions include xanthate thermolysis, hydrolysis and aminolysis.[16] During aminolysis, the ω-end group is reduced to a thiol, providing an orthogonal pathway to a myriad of reactions. The thiol-ene reaction has been classed as a type of 'click' reaction[17] due to its simplicity, high yields and modularity.

PVP was traditionally synthesised in bulk or in organic media at a temperature of approximately 60 °C, yielding polymers with predictable molar masses, low dispersities and high enough conversions near the accepted standard of 60%. This approach required the distillation of NVP as well as the solvent of choice (1,4-dioxane, methanol, toluene or fluorinated alcohols), if used. The freeze-pump-thaw process would then be used during standard Schlenk techniques to obtain an oxygen-free environment for effective RAFT conditions. Pound *et al.* thoroughly investigated the polymerisation of NVP under these conditions and showed that unexpected side-reactions could occur under certain conditions.[18] Other work also conducted in Klumperman's research group continued to delve into the intricacies of RAFT/MADIX for PVP formation,[13,19–22] so that more effective and facile polymerisation processes could be developed for this polymer. A much milder approach for PVP formation was developed most successfully by Guinaudeau *et al.*[9] who used the redox system of *tert*-butyl hydroperoxide/ascorbic acid in water at 25 °C. Much higher conversions of up to 100% can be obtained, as verified by ^{1}H NMR analysis, with limited side-reactions occurring. These advances in the polymerisation of NVP have aided the simplicity of designing drug delivery systems centred around this polymer. This feat, coupled with its impressive biomedical characteristics, provide a strong impetus for its use as a dominant component in modern-day drug delivery systems.

3.1.1 Approach

With RAFT-polymerised PVP consolidated as a central building block of this drug delivery vessel, questions remained regarding the method of drug and linker conjugation as well as the type of acid-sensitive linker to be used. The β-thiopropionate ester linkage was chosen as a starting reference based on previous success in our group.[23] This linkage was reported by Oishi *et al.*[24] to be easily hydrolysed in the mildly acidic pH conditions that would be found in the endosomal organelles (pH 5.0) compared to its relative stability in serum (pH 7.4). A slight modulation of the substitution group or pattern can result in a vastly different hydrolytic profile. It was therefore sought to analyse the effect of substituting the ester group in the β-thiopropionate ester linkage with an amide group and a maleimide group, as well as to analyse the effect of a supplementary methylene unit in each described linkage. To realise this, a model drug compound was conjugated to PVP via each linkage in a one-pot approach, proceeding the synthesis of PVP via RAFT/MADIX polymerisation. ^{1}H NMR kinetic studies were used to monitor the room temperature hydrolytic cleavage of the model drug from PVP. In an additional study, an acetal linker was tested in the same manner so as to form a grounded approach for subsequent studies with this polymer. To this end, seven polymers with different acid-labile groups were synthesised: P1 (PVP conjugated to phenyl acrylate), P2 (PVP conjugated to *N*-phenylacrylamide), P3 (PVP conjugated to *N*-phenylmaleimide), P4 (PVP conjugated to benzyl acrylate), P5 (PVP conjugated to *N*-benzylacrylamide), P6 (PVP conjugated to *N*-benzylmaleimide) and P7 (PVP conjugated to phenyl vinyl ether).
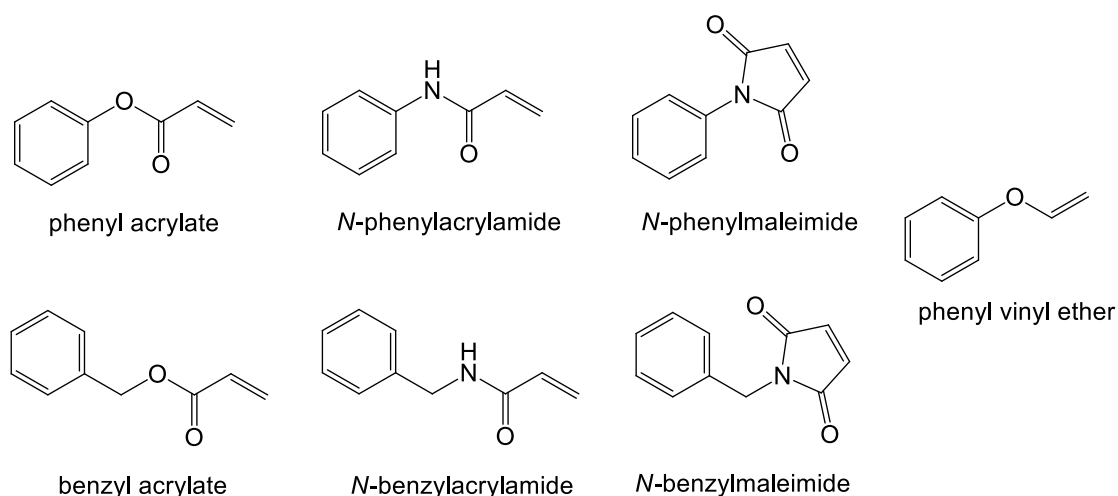
Figure 3.1 Chemical structures of chosen model drug compounds.

3.2 Results and discussion

3.2.1 Polymer-model drug conjugate synthesis

a) Synthesis of poly(*N*-vinylpyrrolidone)

To create the model drug polymers P1 – P6, PVP was synthesised via RAFT polymerisation using the RAFT agent *S*-(2-ethyl propionate) *O*-ethyl xanthate (RAFT-X1), which was chosen due to its ability to control the polymerisation of *N*-vinylpyrrolidone (NVP) in organic media or in the bulk, which was

previously explored in our group.[25] RAFT-X1 was synthesised in high yields and purity as detailed in the experimental section. In Scheme 3.2, the RAFT-X1 mediated polymerisation of NVP in bulk is shown using 4,4'-azobisisobutyronitrile (AIBN) as the radical initiator. The proceeding polymer modification section will elaborate on the removal of the thiocarbonylthio moieties via aminolysis to render free thiols to be conjugated to the model drug compounds through the thiol-Michael addition reaction.
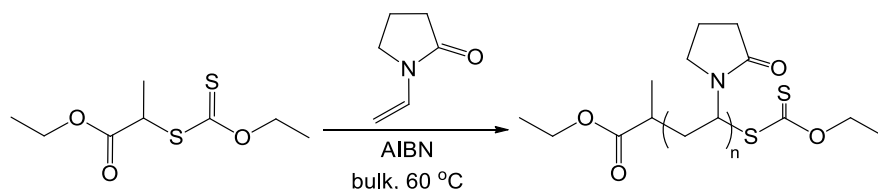
Scheme 3.2 RAFT polymerisation of NVP mediated by RAFT-X1 to yield PVP-X1.

For the seventh model drug polymer (P7), hydroxy-functional PVP (PVP-X2) was synthesised from the hydroxy-functional RAFT agent 2-hydroxyethyl 2-(ethoxycarbonothioylthio)propanoate (RAFT-X2). This was done in order to conjugate phenyl vinyl ether to PVP-X2 via the alcohol functionality on the α-end of the polymer. An acetal linker is conveniently formed between the polymer and the model drug. The acetal functional group is known to be acid labile from literature[26–28] and was included in the set of studied polymers to provide an alternative means of attaching the drug to the polymer, and in so doing, to create a larger potential pool of viable hydrolysis rates and RAFT-related methods to consider when designing known application-driven drug delivery systems. RAFT-X2 was synthesised in high yields and purity as detailed in the experimental section of this chapter.

The approach of synthesising PVP was improved towards the end of this work, which is why the polymerisation conditions differ for PVP-X1 (bulk, 60 °C, AIBN initiator) compared to PVP-X2 (PBS buffer pH 7.4, 25 °C, redox pair initiator). Using distilled, deionised water instead of the PBS buffer also resulted in the efficient polymerisation of NVP but instead, the use of PBS buffer was habituated. This is a conservative approach because it generally decreases the possibility of pH fluctuations and is cost-effective, simple and stable for long periods of time. In a practical sense, an efficient polymerisation here refers to one where a high monomer to polymer conversion and end-group fidelity are obtained reproducibly. This aqueous redox polymerisation of NVP does not have a marked effect on the chemical composition of the polymers as similar RAFT end-group fidelities were obtained as compared to PVP-X1. The polymerisation scheme is shown in Scheme 3.3.
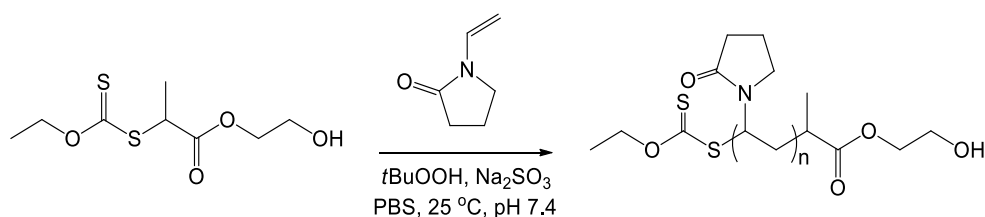
Scheme 3.3 RAFT polymerisation of NVP in aqueous media.

Table 3.1 summarises the polymerisation conditions of NVP to synthesise PVP-X1 and PVP-X2. The NVP monomer was distilled before use for PVP-X1 formation and was used as is (undistilled) for PVP-X2 formation. In the case of PVP-X1, the technique conducted is dependent on several (up to seven) freeze-pump-thaw cycles to thoroughly deoxygenate NVP before allowing the polymerisation to take place. Visually, one should notice the cessation of bubble-formation upon thawing the solution. The polymerisation of NVP in bulk or organic media therefore proved to be more labour-intensive compared to that in aqueous media.

Table 3.1 Polymerisation conditions, conversion and molecular weight of PVP-X1 and PVP-X2

Polymer	$\propto$ [a] %	Time h	Solvent	Temperature °C	$M_{n,target}$ [b] g mol^{-1}	$M_{n,SEC}$ [c] g mol^{-1}	$M_{n,NMR}$ [d] g mol^{-1}	$Đ$ [e]
PVP-X1	61	6	none	60	7000	4600	5400	1.1
PVP-X2	90	6	PBS aqueous buffer	25	4000	4000	3900	1.1

[a] conversion of NVP to PVP, determined gravimetrically
[b] $M_{n,theo} = M_{n,target} \times$ conversion
[c] $M_{n,SEC}$ is based on PMMA standards, eluent DMF
[d] $M_{n,NMR}$ is determined by the ratio of integral signals of the xanthate end-group to polymer backbone
[e] $Đ$ represents the dispersity, from SEC (M_w / M_n)
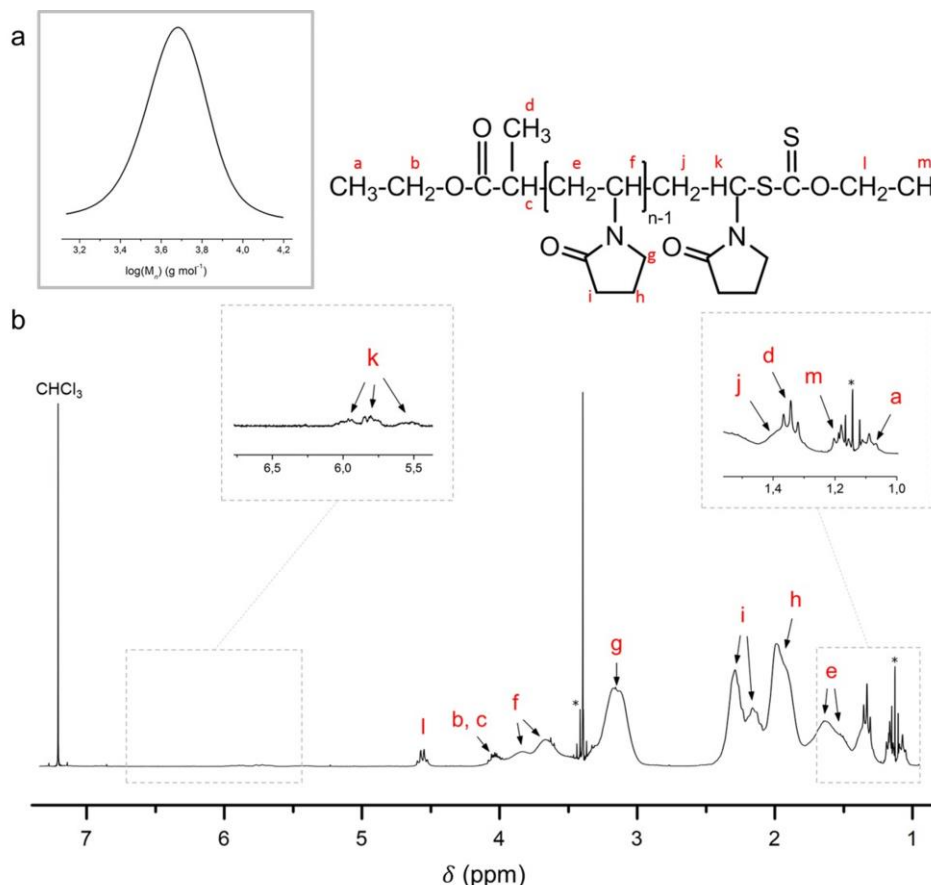
Figure 3.2 a) Molar mass distribution of unmodified PVP (PVP-X1) and b) ^{1}H NMR characterisation of PVP-X1.

^{1}H NMR spectroscopy and SEC were used to characterise pristine PVP before any further modification took place. A monomodal and symmetrical SEC molar mass distribution with a low Đ (≤ 1.2) is indicative of a controlled free-radical polymerisation, which is represented for PVP-X1 in Figure 3.2 a), which has a dispersity of 1.1. Additionally, the good agreement between the theoretical M_n and those calculated by ^{1}H NMR spectroscopy confirms the chain-end fidelity of the xanthate group and the living character of the polymerisation. The ^{1}H NMR peak assignments for PVP-X1 are also shown below in Figure 3.2 b) where a high RAFT end-group fidelity (95%) was obtained. The RAFT end-group fidelity calculation is based on the ratio of the peak intensities of '**I**' (4.55 ppm, 2H) belonging to the methylene protons of the RAFT group to '**i**' (2.5 – 2.1 ppm, 2H) belonging to the pyrrolidone ring of the polymer backbone.

PVP is able to bind with water and other organic solvent molecules such as diethyl ether (*) highly effectively. DOSY further confirms this phenomenon using PVP-X2, which was dried under vacuum and dissolved in chloroform-*d* (Figure 3.3). PVP contains a highly hydrophilic moiety, the pyrrolidone lactam, and a hydrophobic component, the alkyl group. The rapid dissolution in polar and nonpolar solvents can be ascribed to the highly polar amide moiety in the pyrrolidone ring and the nonpolar methine and methylene groups along the polymer backbone and within the ring.[29] The residual diethyl ether molecules interact with PVP to a large extent, which could possibly be credited to the hydrophobic interaction between the hydrocarbon portions of diethyl ether and the alkyl groups of PVP.
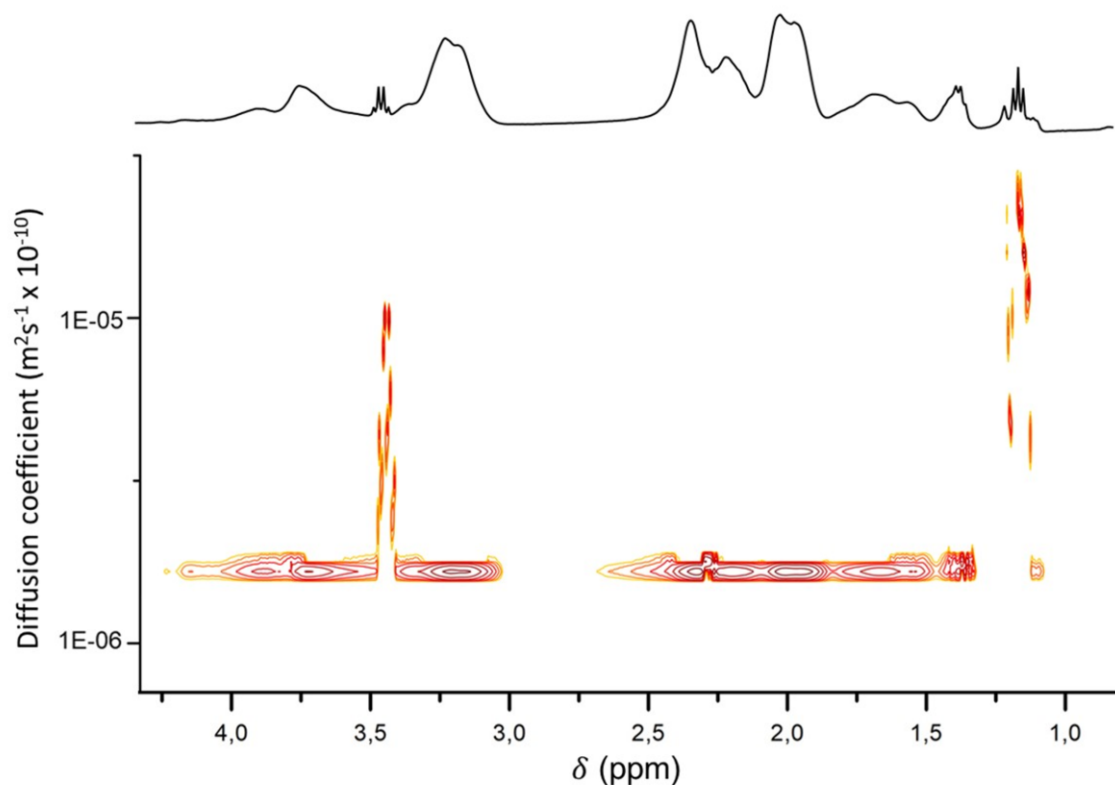
Figure 3.3 DOSY NMR spectrum of hydroxy-functional PVP.
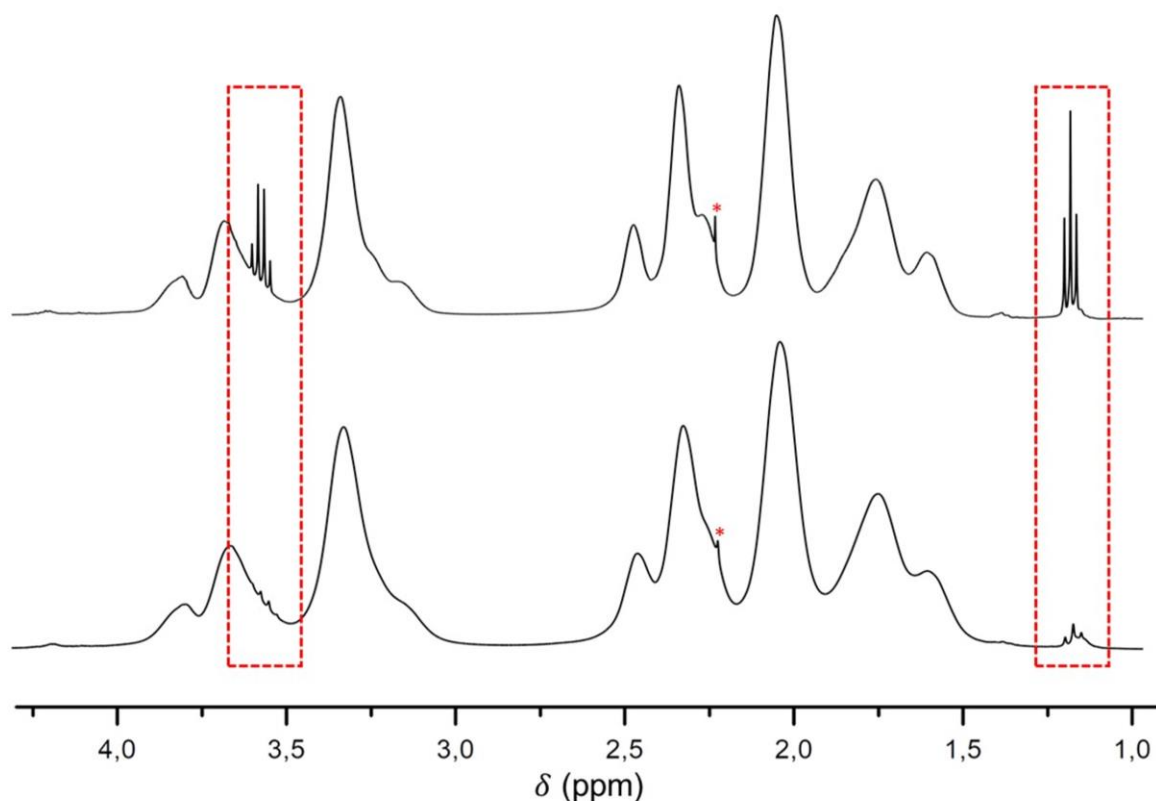
Figure 3.4 Pristine PVP (high MW) with a common organic solvent retention (diethyl ether, red blocks and acetone, asterisk) after vacuum drying (above) and after lyophilisation (below).

In order to remove residual organic solvent from the polymer, one could freeze dry (lyophilise) the polymer solution from a small quantity of water as evidenced in Figure 3.4, though residual solvent could still remain and the process may be repeated only when stringent proceeding steps require it. Care should be taken not to hydrolyse the xanthate chain ends of PVP which was generally observed to occur by comparing the xanthate integral (I) before and after dialysing pristine PVP in water. This form of purification was therefore avoided. The optimum purification technique was therefore to precipitate PVP in ether several times (at least three), followed by lyophilisation. The ideal storage conditions are in an airtight container filled with a blanket of argon and stored in a freezer (temperature -4 °C).

Due to the novelty of the aqueous polymerisation of NVP with regard to RAFT-X2 used to mediate it, and the particular redox pair (*tert*-butylhydroperoxide and sodium sulfite), the polymerisation kinetics were analysed for an $M_{n,target}$ of 10 000 g·mol^{-1}. The conversion of monomer to polymer was quantified via ^{1}H NMR spectroscopy by comparing the peak integrals of the polymer backbone to the vinylic protons of the monomer at 7.08 ppm. After 6 h, 96% conversion was obtained, with a Đ of 1.1. It was confirmed that the polymerisation is a living chain growth process due to the linear increase in M_n with respect to conversion, as evidenced in Figure 3.5 a). The molecular weight and dispersity were determined via SEC, and were related to the conversion determined by ^{1}H NMR spectroscopy. The molar mass distributions in Figure 3.5 b) demonstrate the increasing molecular weight as a function of the elution time. The time-conversion plot consisting of ^{1}H NMR spectra stacked in chronological order

can be found in Addendum A, where the proton signals of NVP are observed to decrease with time concurrent to the broad polymer peaks increasing with time.

For the actual polymer-model drug conjugate, comparable molecular weights of P1 – P7 were required, therefore a $M_{n,target}$ of 4000 g·mol^{-1} was set. PVP-X2 exhibited high RAFT end-group fidelity of 97%. The polymerisation conditions and other significant information are summarised in Table 3.1. The aqueous RAFT polymerisation of NVP has improved the appeal of PVP due to the circumvention of monomer distillation prior to use as well as the need for intensive degassing techniques such as freeze-pump-thaw. It is also more common for near-quantitative conversions and high RAFT end-group fidelity to be obtained, as verified by ^{1}H NMR spectroscopy.
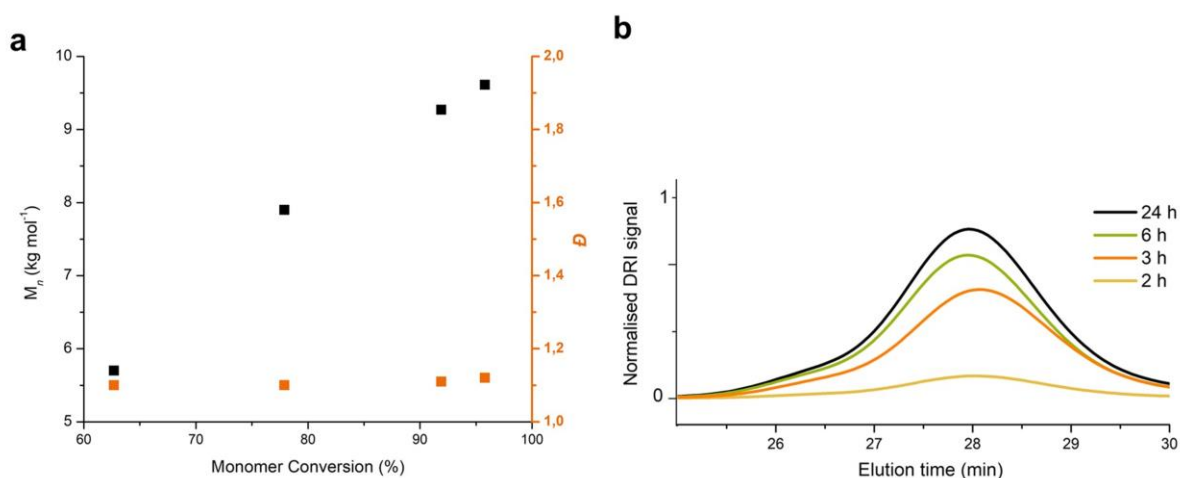
Figure 3.5 a) Evolution of the experimental M_n and dispersity as functions of monomer conversion and b) normalised SEC molar mass distributions of PVP-X2 at various polymerisation times.

b) Modification of PVP with model drug compounds

After PVP was successfully synthesised, the model drug compounds were conjugated to the polymer. The model drug compounds referred to are phenyl acrylate, *N*-phenylacrylamide, *N*-phenylmaleimide, benzyl acrylate, *N*-benzylacrylamide, *N*-benzylmaleimide and phenyl vinyl ether (Figure 3.1). The synthesis and characterisation of the applicable compounds are fully detailed in the experimental section. The conjugation of the first six compounds to the thiol end group of PVP allows for the formation of the β-thiopropionate ester, amide or maleimide linkages. Besides the classical β-thiopropionate ester linkage where the drug is adjacent to the ester group, to the best of our knowledge this group of linkages containing the amide and maleimide moieties have not been explored as acid-degradable linkages for drug delivery design.

The ω-end groups of PVP-X1 were converted to thiols via aminolysis, which could then be conjugated to the vinyl-bearing model drug compounds, chosen for their inclusion of an activated double bond and a phenyl functional group for tracking of the hydrolysis products. A simple iteration is shown in Scheme 3.4 where PVP-X1 which is able to undergo aminolysis with hexylamine to render a thiol-terminated polymer.
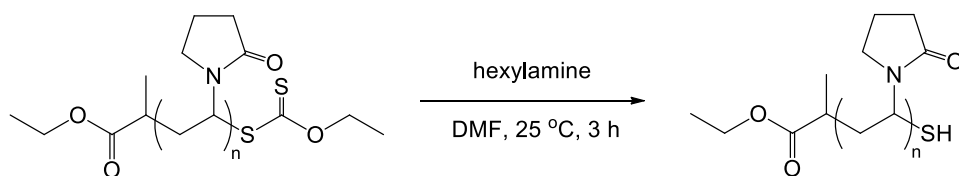
Scheme 3.4 Aminolysis of PVP-X1.

In many cases, the aminolysis and subsequent thiol-ene addition reactions are conducted in two steps, with purification steps in between.[30–32] The inclusion of oxygen in the system readily oxidises thiols to disulfides which would result in an approximate doubling of the molecular weight due to the coupled species, causing a bimodal molecular weight distribution using SEC. A way in which to avoid this is through the use of a reducing agent and stringent oxygen-free conditions.

Figure 3.6 shows an example of PVP-X1 where a reducing agent was not used during the aminolysis reaction. The SEC molar mass distributions with different detectors (differential refractive index (DRI) and ultraviolet (UV)) of PVP-X1 is shown in blue and aminolysed PVP without the presence of a reducing agent is shown in red. In Figure 3.6 b), the thiocarbonylthio moiety absorbs in the UV spectrum at 280 nm, which allows for the detection of unmodified PVP. This is not the case for disulfide-coupled PVP, which shows no UV absorption at that wavelength.
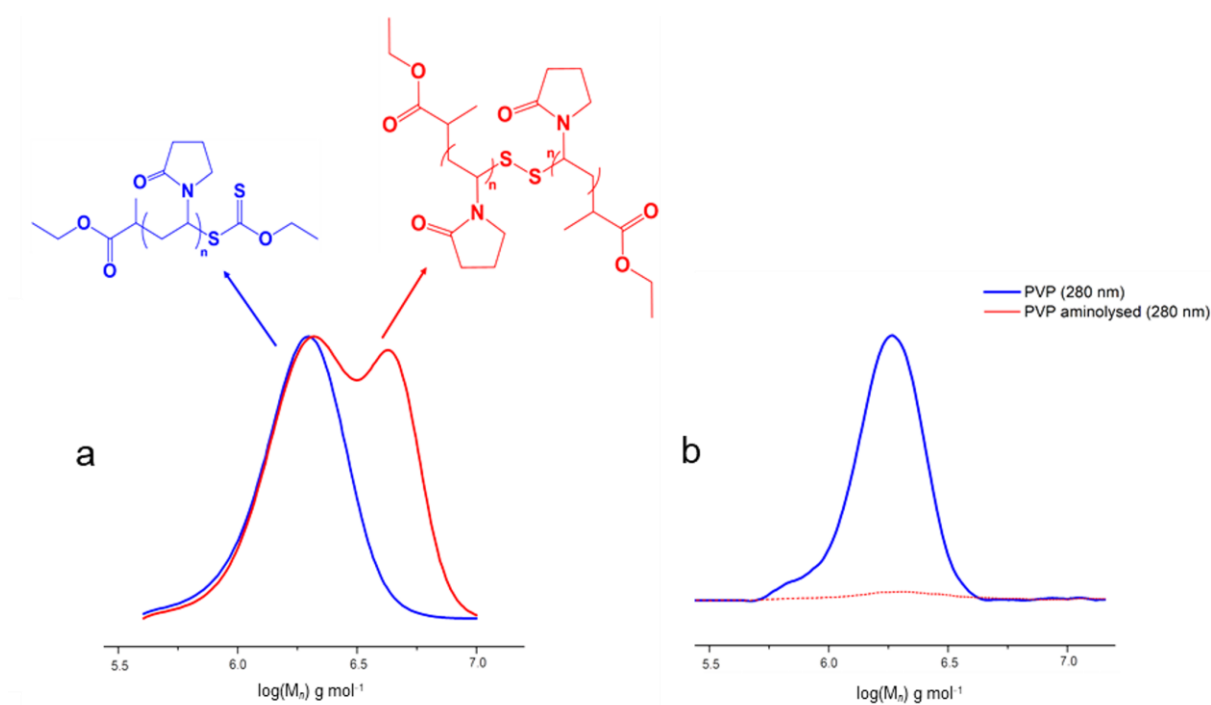
Figure 3.6 SEC molar mass distributions. a) DRI signal response and the b) UV response of PVP-X1 and aminolysed PVP-X1 without the use of a reducing agent.

To avoid multiple reaction steps and possible loss of product due to purification procedures or side-reactions, a one-pot approach was used. This involves the concurrent protection of the thiol and functionalisation of the polymer after aminolysis occurs. The solvent, reducing agent and coreagents should be carefully considered because of the reactive and easily polymerisable nature of the model drug vinyl moieties. Ho *et al.*[33] reported high maleimide %functionality values for the one-pot aminolysis/thiol-maleimide reaction of trithiocarbonate poly(*N*-isopropylacrylamide) using triethylphosphite as the reducing agent. One of the benefits of this synthetic route is the avoidance of phosphines which are toxic and costly.

These model drug polymer conjugates are shown in Scheme 3.5, where P1 is PVP conjugated to phenyl acrylate, P2 is PVP conjugated to *N*-phenylacrylamide, P3 is PVP conjugated to *N*-phenylmaleimide, P4 is PVP conjugated to benzyl acrylate, P5 is PVP conjugated to *N*-benzylacrylamide and P6 is PVP conjugated to *N*-benzylmaleimide. The last polymer, P7, is that of PVP conjugated to phenyl vinyl ether, and due to a different conjugation strategy being used, this will be discussed in the proceeding section.
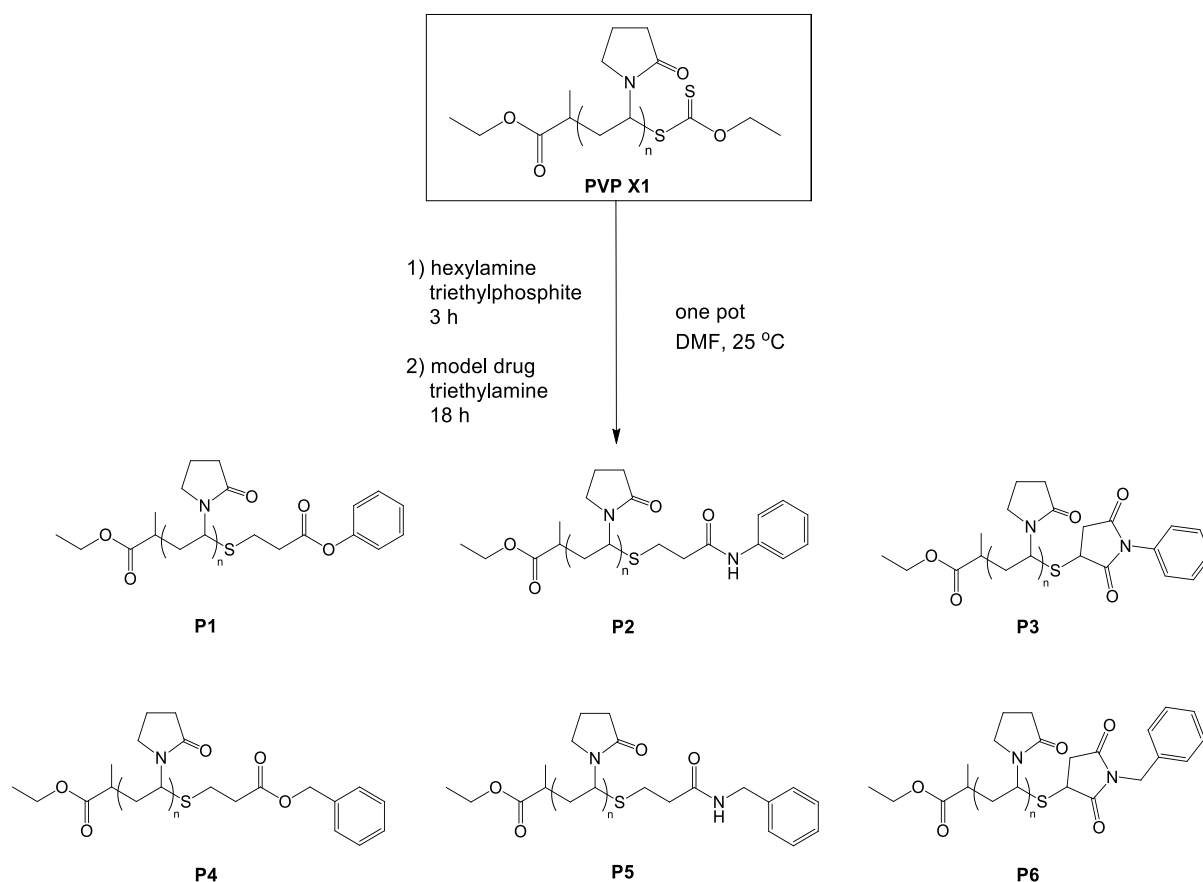
Scheme 3.5 Poly(N-vinylpyrrolidone)-model drug conjugates.

To synthesise the final polymer, P7, PVP-X2 first underwent thermolysis by heating at 120 °C for 16 h to cleave the labile thiocarbonylthio moiety, which was replaced with an unsaturated group (Addendum B). The thiocarbonylthio moiety cleaves easily with heat and hydrolysis, and reacts readily with nucleophiles. This procedure reduces the risk of side-reactions in the next modification step. Following thermolysis, phenyl vinyl ether was reacted with hydroxy-functional PVP under acid catalysis in a reaction which simultaneously produces the acid-degradable acetal group, Scheme 3.6. No side-reactions occurred following the reaction.

Alcohols and vinyl ethers react efficiently via an acetal bond through a 'click'-type reaction, leading to quantitative conversions as previously reported by Mangold *et al.*[34] Activated molecular sieves were added to the reaction mixture so as to remove water as the reaction proceeds. The product would run the risk of hydrolysing back to its hemiacetal form if the necessary precautions are not taken.
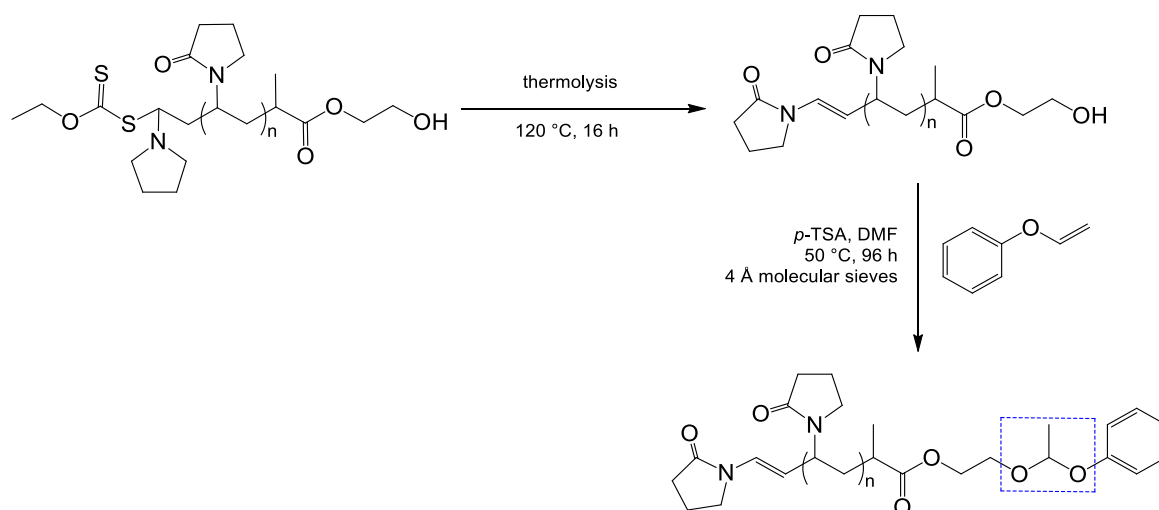
Scheme 3.6 The thermolysis of PVP-X2 and its modification to yield the acetal-linked PVP-model drug conjugate.
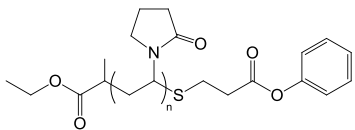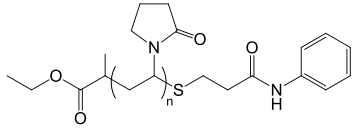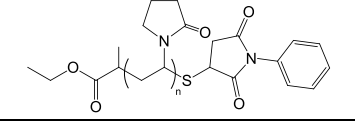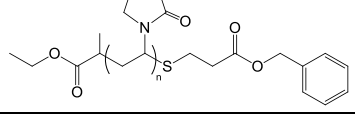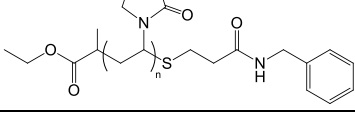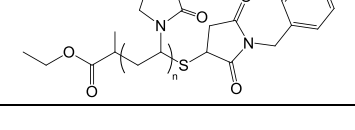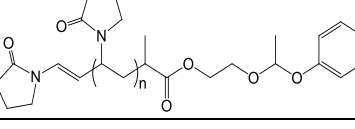
The acetal bond is highlighted in the blue dashed block shown in Scheme 3.6. In acidic media, one of the oxygen atoms becomes protonated which activates the neighbouring carbon, thereby facilitating the nucleophilic attack of water.[3] This results in the cleavage of the acetal to form, in this case, acetaldehyde, phenol and OH-functional PVP. Under low pH conditions, ketals have been shown to hydrolyse at faster rates than acetals thus providing another rate-determining avenue for future research.[35]

3.2.2 Polymer-model drug conjugate characterisation

The polymer-model drug conjugates were fully characterised using ^{1}H NMR spectroscopy, thermogravimetric analysis (TGA) and SEC, the results of which are summarised in Table 3.2.

Table 3.2 Characterisation data of polymers P1 – P7

Polymer	Structure	Model drug %functionality	M_n (g·mol^{-1})	Đ
P1		¹H NMR: 95% TGA: 92%	¹H NMR: 4500 SEC: 4500	1.1
P2		¹H NMR: 90% TGA: 88%	¹H NMR: 4400 SEC: 4600	1.1
P3		¹H NMR: 85% TGA: 84%	¹H NMR: 4600 SEC: 4600	1.2
P4		¹H NMR: 94% TGA: 94%	¹H NMR: 4200 SEC: 4500	1.1
P5		¹H NMR: 90% TGA: 93%	¹H NMR: 4600 SEC: 4700	1.2
P6		¹H NMR: 87% TGA: 85%	¹H NMR: 4600 SEC: 4700	1.2
P7		¹H NMR: 93% TGA: 89%	¹H NMR: 4100 SEC: 4200	1.2

A clear indication of model drug attachment was confirmed in the ¹H NMR spectra of P1 – P7 by analysing the aromatic region. These aromatic groups also provided a simple means of calculating the percentage functionality of model drug compound attached to PVP (%f,$_{NMR}$), by comparing the integrals of the aromatic proton signals to the polymer backbone. A representative spectrum, P1, is shown in Figure 3.7 which was purified by precipitation and lyophilisation to remove residual solvent. For the kinetic studies, only precipitation and no lyophilisation were done so as to avoid untimely hydrolysis from occurring.
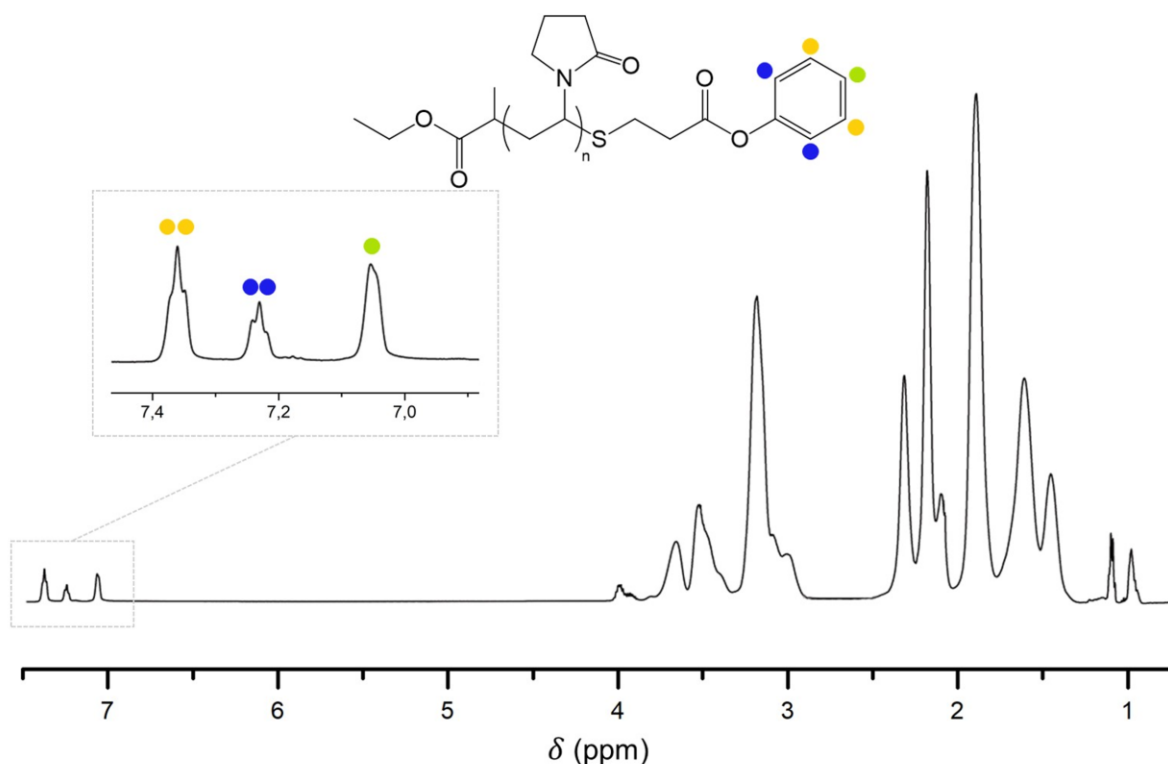
Figure 3.7 ^{1}H NMR spectrum of P1.

The thermal lability of the PVP conjugates were analysed using TGA, which provided another means of corroborating the %f,$_{TGA}$ determination. A representative TGA weight loss curve is shown in Figure 3.8, where the solid lines indicate the weight loss as a function of temperature and the dotted lines indicate the first derivative of weight loss.
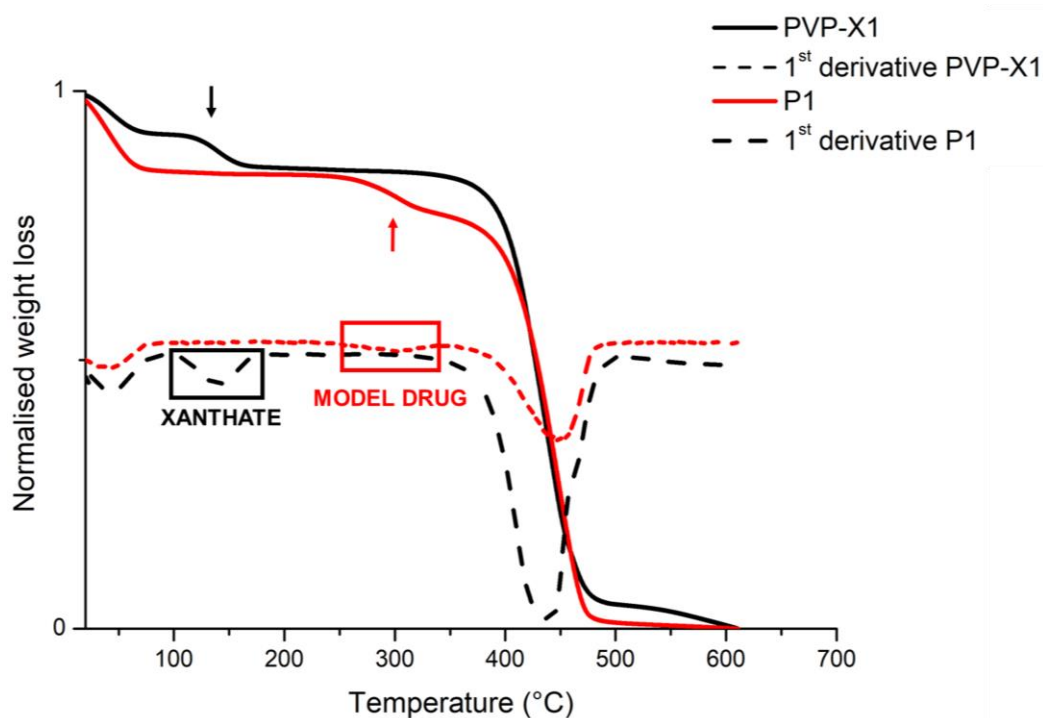
Figure 3.8 Representative normalised TGA weight loss and first derivative weight loss curves for unmodified PVP (PVP-X1, black) and the acrylate-model drug modified PVP (P1, red).

All polymers exhibit a three-stage decomposition profile, with the first loss appearing below 120 °C, attributed to the moisture content. For unmodified PVP, a weight loss at approximately 130 °C is observed, which is attributed to the xanthate end-groups. The stability of RAFT groups varies among the classes, with most being stable above 150 °C. The thiocarbonylthio moiety in conjugation to NVP exhibits a lower than expected temperature of degradation, likely due to electronic effects within the system.

Considering the RAFT agent groups of dithiobenzoates, trithiocarbonates and xanthates, xanthates have been found to be the most thermally labile.[36] As expected, the modified polymers (P1 – P7) exhibit enhanced thermal stability, as evidenced by the higher temperatures (approximately 260 °C) at which the introduced model drug functionalities become thermally labile. The principal weight loss peak is due to the thermal degradation of the polymer backbone. By comparing the wt.% values of the model drug end-group functionalities with reference to PVP-X1 for P1 – P6, and PVP-X2 for P7, the %f_{TGA} was be determined.

3.2.3 Hydrolytic release kinetics

The model drug release was analysed by means of ^{1}H NMR spectroscopy for polymers P1 – P7 at room temperature. The method of Kim *et al.*[37] was followed with minor adaptions for this system, as described in the experimental section. The variable time ^{1}H NMR spectra of P1 at pH 5.0 are represented in Figure 3.9.
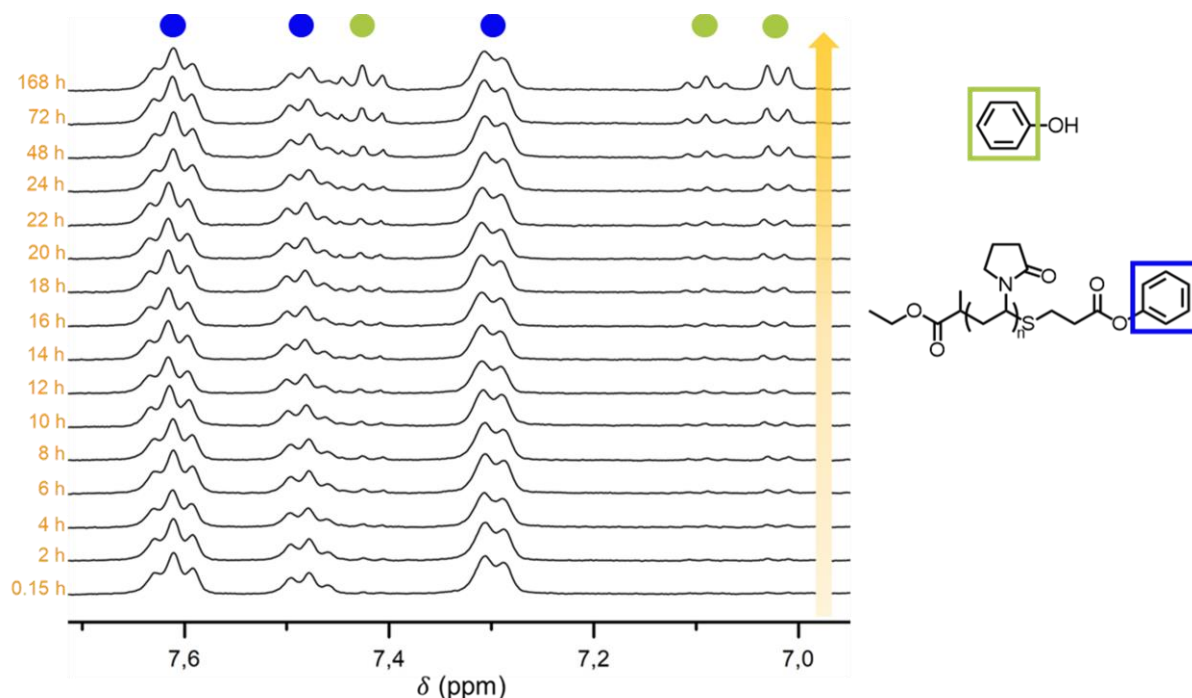
Figure 3.9 Stacked ^{1}H NMR spectra of P1 recorded over time.

The polymer-bound protons of the aromatic groups have chemical shifts at approximately 7.6, 7.5 and 7.3 ppm, which decrease in intensity as the acid-degradable bonds are cleaved between the polymer

and the model drug compounds. This cleavage is also evidenced by the new free-aromatic group signals which appear at 7.4, 7.1 and 7 ppm. The polymer-bound aromatic groups are more deshielded than the free aromatic groups because the ester linkage in the polymer system deshields the aryl protons. When the linkage between PVP and the model drug is cleaved over time, the phenol derivative is liberated which is much less deshielded. These protons therefore appear slightly upfield making it convenient for ^{1}H NMR spectroscopic analysis. These aromatic signals could be quantified relative to an internal standard (DMF, multiplicity = 1, 8.03 ppm). The acrylate-functional polymers, P1 and P4 and the acetal-functional polymer, P7, were the only polymer systems observed to show acid-degradable behaviour, as no net change in the ^{1}H NMR spectra of the acrylamide- and maleimide-functional polymers could be quantified during the time of analysis (one week). It is possible for the acrylamide-functional polymers to degrade via amide hydrolysis which occurs at a rate in orders of magnitude lower than the acrylate-functional polymers (ester hydrolysis), because similar hydrolysis mechanisms come into play. For the purpose of drug delivery systems this hydrolysis rate would not be beneficial as it would be too slow relative to the clearance processes of the body.

For effective acid-degradable linkages, highly selective neutral *vs.* acidic media drug release is sought after to minimise contact with healthy tissues and cells. The desired rate of drug release is dependent on the type of drug delivery system (active or passive targeting) as well as the final application. Ideally, for active targeting (distribution control) drug delivery systems, the majority of drug released should occur at the targeted site. This requires that the polymer-based delivery vehicle be stable for the period of time that is required to reach this site. Drug release should therefore be slow enough so as to curtail the destabilisation of the micelle as the drug diffuses from the core of the system (self-assembled micelle).[38] Perfect sink conditions are maintained when the drug concentration in the release medium does not exceed 10% of the solubility of the drug in the medium under the conditions over the period of analysis. This is often upheld in drug release experiments, as this is assumed by some kinetic models in order to avoid artificial drug saturation limitations *in vitro*.[39] In practice, this would require the replenishment of the buffer medium every time a sample is removed for analysis. In so doing, the initial volume of the release medium is always maintained and an 'infinite dilution' scenario is mimicked *in vitro*. This is not possible during a ^{1}H NMR experiment containing an internal standard, although a highly sufficient model drug dilution ratio is maintained in the first 24 h. This period was used to determine the optimal drug release model by fitting the data to the kinetic models of zero order (Equation 3.1) as cumulative % drug released *vs.* time and first order (Equation 3.2) as log cumulative % drug remaining *vs.* time.

$$C = K_0 t \hspace{6cm} \text{Equation 3.1}$$

In Equation 3.1, K_0 is the zero-order rate constant in units of concentration/time and t is the time in hours. A zero-order release rate describes a system where the drug release rate is independent of its concentration.

$$\log C = \log C_0 - kt/2.303 \hspace{4cm} \text{Equation 3.2}$$

In Equation 3.2, C_0 is the initial concentration of the drug, k is the first order constant and t is the time in hours. A first-order release rate describes a system where the drug release rate is dependent of its concentration.[40] The mode of release kinetics is dependent on the degradation mode and rate, the swelling rate, absorption threshold, polymer molecular weight and polymer composition. This is why it is important to differentiate between simple systems used to theorise drug release kinetics (small compounds) and polymer-bound drug delivery systems.

The data for P1, P4 and P7 were plotted appropriately and the R^2 values were determined for each straight line of best fit. These values as well as a representative zero-order and first-order model drug release kinetic model for P1 at pH 5.0 are shown in Addendum C. As expected for ester and acetal hydrolysis, all three polymers exhibited the highest R^2 values for the best fit lines following first-order drug release kinetics. The data will deviate from perfect first-order kinetics because external factors come into play which affect the hydrolysis. There are numerous mathematical models to describe drug release from controlled systems but each with its own set of particular assumptions to be met.[41]

The rate constants were calculated by multiplying the gradient by -2.303 as per Equation 3.2. Referring to Figure 3.9 again, over extended periods of time (168 h) the compete disappearance of polymer-bound aromatic protons is not observed and this is likely due to the model drug saturation limit being reached, as discussed previously. The half-life of hydrolysis is the is the time it takes in hours for the conjugated drug to decrease by half of its initial value. From Equation 3.2, the half-life of hydrolysis ($t_{1/2}$) can be determined for each polymer at pH 5.0 and pH 7.4 as shown in Equation 3.3.

$$t_{1/2} = 2.303 \cdot log\frac{100}{50}/k$$

∴ $t_{1/2} = 0.693/k$ Equation 3.3

a) The β-thiopropionate ester linkage

Simple carboxylic acids and their esters are weak bases and are only completely protonated in strong acidic media.[42] Scheme 3.7 shows the general mechanism of the hydrolysis of a carboxylic acid ester in acidic media and Scheme 3.8 shows that in basic media, which is the generally accepted mechanism for neutral ester hydrolysis.[43] It is well known that the half-lives of carboxylic acid esters can vary from hours to years,[44] and that their rate constants are highly influenced by structural changes. The β-thiopropionate ester linkage (i.e. 3-sulfanylpropionyl linkage) is a modified ester which is advantageous in drug delivery vehicles due to its favourable hydrolysis rate under low pH conditions and is also reported to be relatively stable under neutral pH conditions.[45–47]

Chapter Three | Acid-degradable linkages
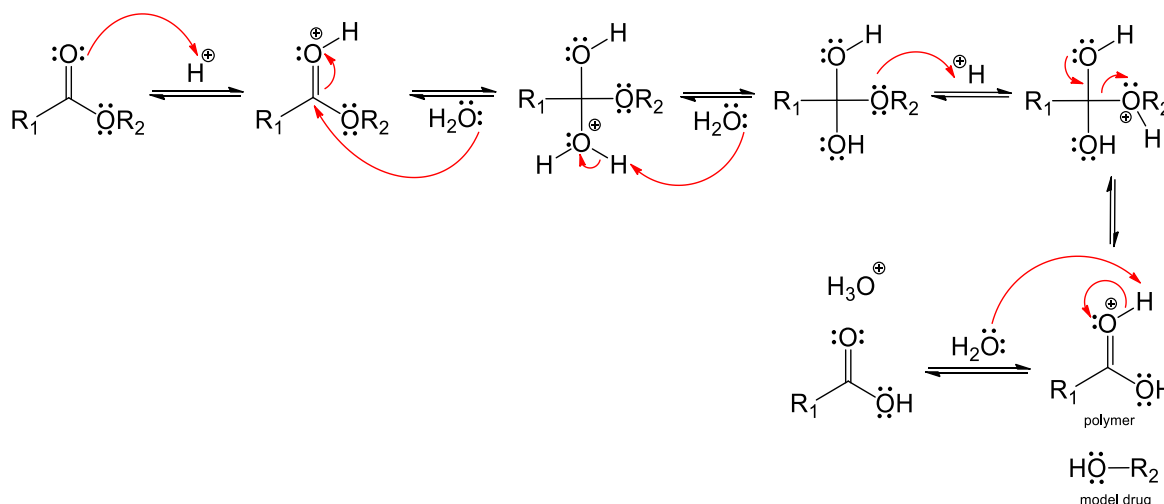
Scheme 3.7 Hydrolysis of an ester in acidic media.
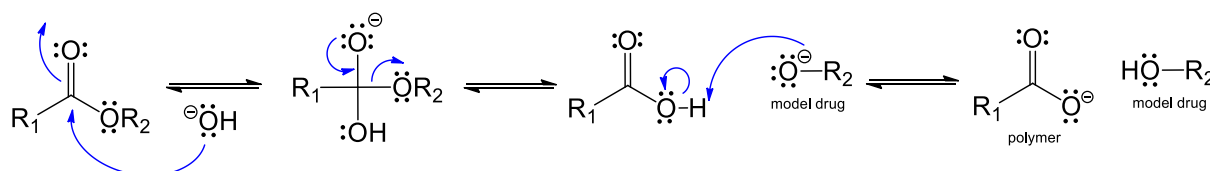
Scheme 3.8 Hydrolysis of an ester in basic media.

It is believed that the difference in hydrolysis of this linkage compared to a simple ester is driven by induction, through the formation of a partial positive charge on the carbonyl of the ester group caused by sulfur, situated three carbon atoms away from the acyl carbon atom.[48] This was further explored with amides (P2 and P5) and maleimides (P3 and P6), where it was observed that similar effects did not result in the acid-degradable behaviour of these polymers at pH 5. It was found that the inductive effects of sulfur in this case had little effect on the lability of those linkages. It is likely that the carbonyl group could not become adequately protonated due to the electron donating resonance characteristics of the amide nitrogen.[49]

P1 and P4 did, however, show acid-degradable behaviour. These model drug-conjugates have subtle structural/electronic differences (Figure 3.10). The log cumulative % drug remaining as a function of time is shown for P1 and P4 in Figure 3.11. P4 was observed to have a slower hydrolysis rate than P1 at both pH values. For ester hydrolysis, only the rate constants of neutral- and base-catalysed reactions are highly sensitive to structural changes.[50] This is likely why the hydrolyses at pH 5 for P1 and P4 are more comparable than for that at pH 7.4. The stability of carboxylic acid esters is generally determined by the ability of the carbonyl carbon to be nucleophilically attacked, and by the leaving group ability of the alcohol group. The methine group is electron donating and can cause the carbonyl group to be less electrophilic and reactive in this way.
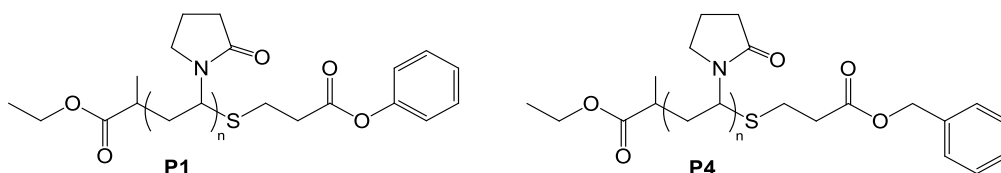
Figure 3.10 Chemical structures of P1 and P4.
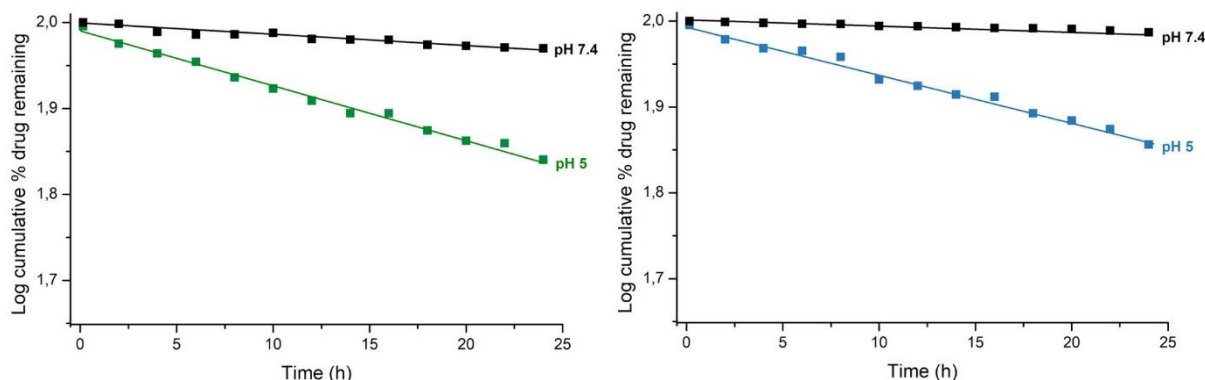
Figure 3.11 Log cumulative % model drug remaining as a function of time at pH 5.0 and pH 7.4. P1 is left and P4 is right for both pH values.

Table 3.3 Half-lives of hydrolysis for P1, P4 and P7 at pH 5.0 (acetate buffer) and pH 7.4 (PBS buffer)

Sample	Half-life of hydrolysis, pH 5.0	Half-life of hydrolysis, pH 7.4
P1	49 h	752 h
P4	53 h	1034 h
P7	107 h	-

The calculated half-lives of hydrolysis are shown in Table 3.3. At pH 5, P4 has a half-life of 53 h and P1 of 49 h. In the neutral buffer, P4 exhibits a slower hydrolysis rate at pH 7.4 ($t_{1/2}$ = 1034 h) compared to P1 ($t_{1/2}$ = 752 h). Benzyl alcohol has a higher pK_a than phenol, which would make it a poorer leaving group thus corroborating the practical findings. P4 is more selective than P1 and could therefore be used in drug delivery vehicles that require more stringent neutral pH control, as compared to the classic β-thiopropionate ester linkage.

b) The acetal linkage

Acetals show great potential as acid-degradable linkers. A variety of hydroxyl groups (primary, secondary, tertiary, syn-1,2- and -1,3-diols) can be used to render the respective acetal, each with its own hydrolysis rate which can be modified based on the substituents of the acetal.[26] The mechanism for acetal and ketal acid-catalysed hydrolysis is shown in Scheme 3.9. The acetal group is generally stable in neutral and basic conditions because of the lack of good leaving groups, the nucleophilicity of the acetal oxygens and stereoelectronic effects.
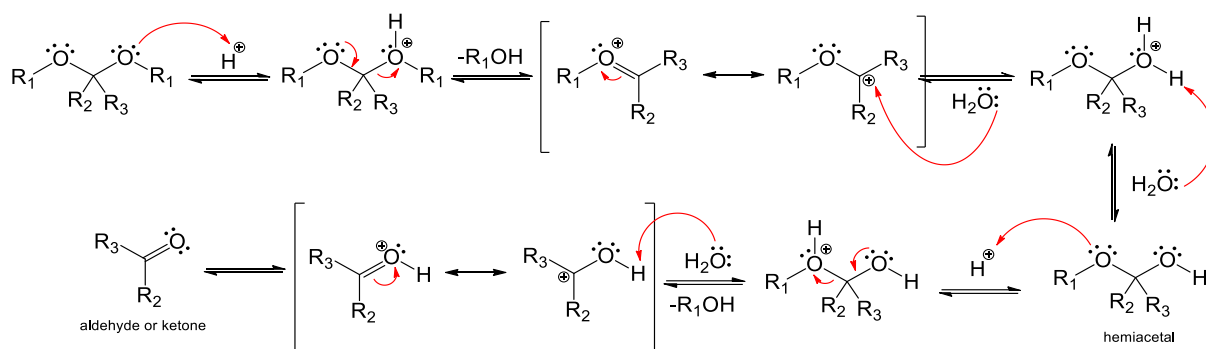
Scheme 3.9 Hydrolysis of acetals and ketals.

It is generally accepted that acetals, hydrazones and imines have much higher hydrolysis rates compared to the β-thiopropionate ester.[51,52] Since slower release rates are often preferred (especially for passive targeting), acetals from time-to-time are overlooked in drug delivery design. As seen thus far, structural changes can make a notable influence on the hydrolysis profile of a prodrug. A specific acetal was therefore chosen in this study for its reported ability to hydrolyse slowly. It was previously shown that an acetal which hydrolyses into substituents of acetaldehyde and primary alcohols had a half-life of approximately 100 h at pH 5.[53] For the acid-catalysed hydrolysis of acetals, the formation of the resonance-stabilised carboxonium ion intermediate has been proposed and generally accepted as the rate-determining step of the process. The stability of the carboxonium ion would therefore prescribe the hydrolysis rate of the acetal. In the case of ketals which hydrolyse into formaldehyde as opposed to acetals which hydrolyse into acetaldehyde, higher hydrolysis rates would result from the more electron-donating character of the methyl substituent group, which stabilises the intermediate.[35] The simple acetal of P7 should therefore hydrolyse more slowly, its chemical structure reiterated in Figure 3.12.
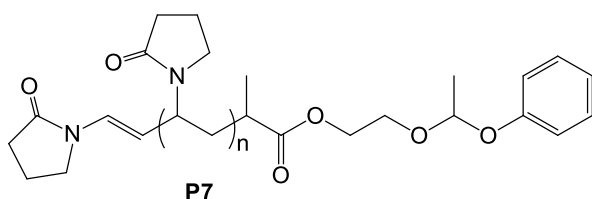
Figure 3.12 Chemical structure of P7.

The release kinetics for P7 are shown in Figure 3.13 at pH 5 and pH 7.4. At pH 5 the $t_{1/2}$ is 107 h (Table 3.3), which is aligned with initial expectations. P7 remained stable at pH 7.4, as no hydrolysis of the model drug was observed. Prolonged acetal stability (years) in neutral and basic media is a well-documented characteristic of the functional group with few exceptions.[54] In this case, through use of an acetal derived from acetaldehyde, a slower release rate is obtained as compared to the β-thiopropionate ester linkage at pH 5, and additionally, complete stability over the time-scale of this study at pH 7.4 is observed.
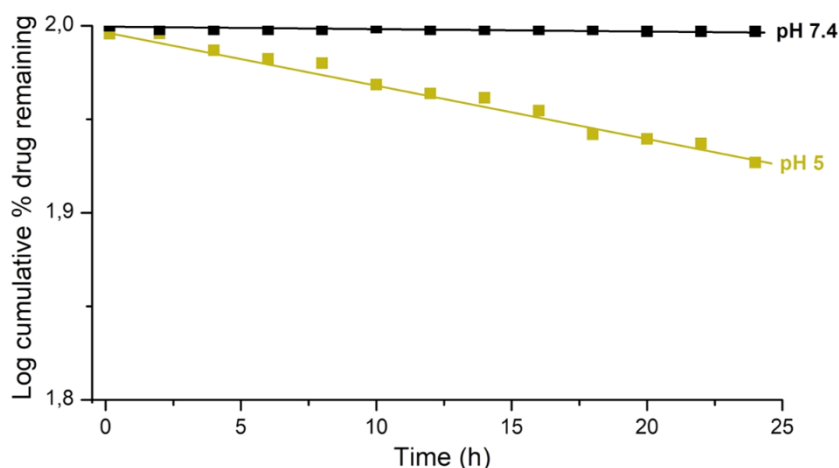
Figure 3.13 Log cumulative % model drug remaining from P7 as a function of time at pH 5.0 and pH 7.4.

3.3 Conclusions

Two different methods of incorporating acid-degradable linkers to RAFT-derived polymers have been shown. Substituent effects were investigated for a series of linkers based on the β-thiopropionate linkage for esters, amides and maleimides. The ester-based polymers, P1 and P4, were unique in exhibiting acid-lability at pH 5. The differences in the structural/electronic effects of these polymers resulted in different rates of model drug release for these systems. In acidic pH conditions P4 and P1 exhibited similar hydrolysis rates, with P4 hydrolysing slightly more slowly than P1. Under neutral pH conditions a marked decrease in the hydrolysis rate occurred thus increasing selectivity of P4 compared to P1. The ability of polymeric prodrugs to remain stable at physiological conditions is a highly sought-after characteristic. The acetaldehyde-liberating acetal linkage was compared in this study and it was shown to have a slower hydrolysis rate compared to the β-thiopropionate ester linkage. The acetal-bound model drug polymer (P7) is highly stable at the physiologically-mimicking neutral pH, indicating a higher selectivity compared to P1 and P4.

It is clear from this study that substituent effects in the near-vicinity of the acid-degradable linkage should be thoroughly assessed when considering the acid-degradable linker for a given application. Based on this study and other studies similar to it, it can be assumed that a degree of tunability of the hydrolysis rate exists regardless of the linkage functional group if substituent effects are considered. Moving forward, the acetal linkage exhibited by P7 holds promise for the development of slow-release polymeric prodrugs where acetalisation can take place. These drug delivery systems would potentially fulfil the requirements of high specificity and the rendering of non-toxic hydrolysis products *in vivo*. Meeting these requirements is imperative for the acceleration of viable nanocarriers being approved and implemented for the treatment of malaria and other diseases.

3.4 Experimental

3.4.1 General details

Phenol (≥99.5%, Sigma-Aldrich), TEA (≥99.5%, Sigma-Aldrich), acryloyl chloride (≥96.0%, Sigma-Aldrich), aniline (≥99.5%, Sigma-Aldrich), *N*-phenylmaleimide (97%, Sigma-Aldrich), *N*-benzylamine (99%, Sigma-Aldrich), *N*-benzylacrylate (97%, Alfa Aesar), benzyl amine (99%, Sigma-Aldrich), phosphorous pentoxide (99%, Sigma-Aldrich), ethyl-2-bromopropionate (99%, Sigma-Aldrich), potassium *O*-ethyl xanthate (96%, Sigma-Aldrich), anhydrous ethylene glycol (99.8%, Sigma-Aldrich), DMAP (≥99%, Sigma-Aldrich), 2-bromopropionyl bromide (97%, Sigma-Aldrich), *tert*-butyl hydroperoxide solution (70% in water, Sigma-Aldrich), sodium sulfite (≥98%, Sigma-Aldrich), triethyl phosphite (98%, Sigma-Aldrich), hexylamine (99%, Sigma-Aldrich), phenyl vinyl ether (97%, Sigma-Aldrich), hydroquinone (≥99%, Sigma-Aldrich), *p*-toluenesulfonic acid monohydrate (99%, Sigma-Aldrich), glacial acetic acid (100%, Merck), sulfuric acid (98%, Merck), sodium bicarbonate (≥99.7%, Merck), potassium carbonate (≥99%, Holpro) and magnesium sulfate (≥99.5%, Merck) were used without further purification. *N*-vinylpyrrolidone (≥99.5%, Sigma-Aldrich) stabilised with ~0.001% *N*,*N'*-di-*sec*-butyl-*p*-phenylenediamine was distilled by vacuum distillation when applicable. Maleic anhydride (99%, Sigma-Aldrich) was sublimed under reduced pressure and stored in an airtight container until use. AIBN (Riedel-de Haën) was recrystallised twice from anhydrous methanol and dried under vacuum. PBS tablets (pH 7.4) and anhydrous DMF were purchased from Sigma Aldrich. Acetone was left over sodium carbonate for 24 h and was distilled from sodium carbonate prior to use. DCM was stored over activated molecular sieves. Distilled, deionised water was obtained from a Millipore Milli-Q purification system. Other solvents were purchased from Kimix and were used without further purification. The NMR solvents used were CDCl$_3$ (99.9%, Aldrich), DMSO-d$_6$ (99.9%, MagniSolv) and D$_2$O (99.9%, MagniSolv). TLC plates (0.2 mm silica gel 60 with fluorescent indicator UV254) and silica gel 60 (0.063 – 0.2 mm / 70 – 230 mesh) were purchased from Machery-Nagel.

^{1}H and ^{13}C NMR spectra were obtained with a Varian VXR-Unity spectrometer (400 MHz unless stated otherwise) with samples dissolved in deuterated solvents with tetramethylsilane (TMS) as the internal reference. All DOSY experiments were performed using the bipolar pulse longitudinal eddy current delay pulse sequence (BPPLED). The spoil gradients were also applied at the diffusion period and eddy current delay. Typically, a value of 0.5 -1 ms was used for the gradient pulse length (δ), 100 - 120 ms for the diffusion time (Δ) and the gradient strength (g) was incremented in 20 – 30 steps along a linear ramp from 5 to 95% of its full strength of 60.2 G·cm^{-1} using a square gradient pulse. Each parameter was chosen to obtain over 85% signal attenuation for the slowest diffusion species at the last step experiment. The pulse repetition delay (including acquisition time) between each scan was larger than 10 s. Monoexponential fitting for selected resonances was applied to create the DOSY spectra using MestreNova 12.0.4 software using the automatic Baysian DOSY transform following manual phase and baseline correction. Liquid chromatography-mass spectroscopy (LC-MS) was conducted using a Waters Synapt G2 with electron spray ionisation (ESI) in the positive mode using a Waters UPLC C18 column of dimensions 2.1 × 100 mm. SEC data were obtained from a Shimadzu LC-10AT isocratic

pump, a Waters 717+ autosampler, a column system fitted with a PSS guard column (50 × 8 mm) in series with three PSS GRAM columns (300 × 8 mm, 10 μm, 2 × 3000 Å and 1 × 100 Å) kept at 40 °C, a Waters 2487 dual wavelength UV detector and a Waters 2414 differential refractive index (DRI) detector. DMF was used as eluent, stabilized with 0.05% 2,6-di-*tert*-butyl-4-methylphenol (BHT) and 0.03% LiCl (w/v) at a flow rate of 1 mL·min^{-1}. The calculated molar masses were relative to poly(methyl methacrylate) (PMMA) calibration standards (Polymer Laboratories) ranging from 690 to 1.2×10^6 g·mol^{-1}. Data acquisition was performed using Millennium software version 4. Attenuated total reflectance Fourier transform infrared spectroscopy (ATR-FTIR) was performed using a Nexus infrared spectrometer equipped with a Smart Golden gate attenuated total reflectance diamond from Thermo Nicolet with ZnSe lenses and data acquisition on Omnic Software version 7.2. TGA was performed using a Q500 TA instrument in the temperature range of 0 - 590 °C, using Pt crucibles with typically 5 mg dried samples, under dynamic N_2 atmosphere (50 mL·min^{-1}) and a heating rate of 10 °C·min^{-1}. Samples were weighed in a sample component that was dried and flushed with nitrogen gas.

3.4.2 Synthetic procedures

3.4.2.1 Synthesis of small molecules

a) Phenyl acrylate

The synthetic procedure is found in literature.[55] Briefly, phenol (3.76 g, 0.04 mol) and TEA (4.55 g, 0.045 mol) were dissolved in THF (40 mL) in a 100 mL three-neck round-bottom flask (RBF) under argon gas flow. Acryloyl chloride (4.07 g, 0.045 mol) was added dropwise to this solution over a period of 10 min via syringe. After 3 h of stirring, the triethylammonium chloride salt could be removed by filtration and the solvent was rotor evaporated from the filtrate. The residue was dissolved in diethyl ether and extracted in acetic acid (5%, v/v), water and a saturated solution of sodium bicarbonate, respectively. The organic phases were combined and dried over sodium sulfate to obtain a pale, yellow oil following solvent removal (3.62 g, 61%). ^{1}H NMR (400 MHz, CDCl$_3$) δ (ppm) 7.34 – 7.25 (m, 2H, -C**H**- ×2 (aromatic)), 7.14 (t, *J* = 7.4 Hz, 1H, -C**H**- (aromatic)), 7.04 (d, *J* = 8.6 Hz, 2H, -C**H**- ×2 (aromatic)), 6.51 (dd, *J* = 17.3, 1.3 Hz, 1H, -C**H₂**), 6.23 (dd, *J* = 17.3, 10.4 Hz, 1H, -C**H**-), 5.90 (dd, *J* = 10.4, 1.3 Hz, 1H, -C**H₂**). ^{13}C NMR (400 MHz, CDCl$_3$) δ (ppm) 164.51, 150.67, 132.55, 129.44, 127.94, 125.88, 121.53. Major IR absorptions (cm^{-1}): 3468, 3047, 1738, 1583, 1632, 1402, 1292, 1249, 1195, 1146, 1021, 973, 916, 800, 876, 748, 685. MS (ESI): m/z = 171.10 (calculated: 171.15 for [M + Na]$^+$).
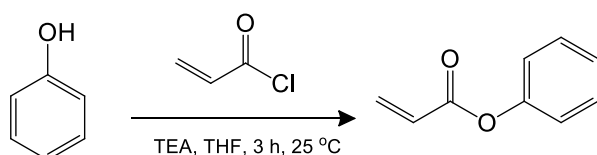
Scheme 3.10 Synthesis of phenyl acrylate.

b) *N*-Phenylacrylamide

The synthetic procedure is found in literature.[56] Briefly, aniline (1.86 g, 0.02 mol) and potassium carbonate (4.15 g, 0.03 mol) were added to a stirring solution of water/acetone (2:1, 60 mL) in a 100 mL three-neck RBF which was cooled in an ice-bath. Acryloyl chloride (2.26 g, 0.025 mol) was added dropwise and this mixture over 10 min and was left to react for 2 h, after which it was transferred into cold water (100 mL). The resulting precipitate was collected and recrystallised from hexane/diethyl ether (1:1, v/v) to yield the product as off-white crystals (2.70 g, 92%). ^{1}H NMR (400 MHz, CDCl$_3$) δ (ppm) 7.95 (s, 1H, -N**H**-), 7.48 (dd, J = 25.3, 7.90 Hz, 2H, -**CH**- ×2 (aromatic)), 7.39 – 7.11 (m, 2H, -**CH**- ×2 (aromatic)), 7.03 (t, J = 7.4 Hz, 1H, -**CH**- (aromatic)), 6.33 (dd, J = 16.9, 1.5 Hz, 1H, -**CH**-), 6.22 (dd, J = 16.9, 10.0 Hz, 1H, -**CH**$_2$), 5.64 (dd, J = 10.0, 1.6 Hz, 1H, -**CH**$_2$). ^{13}C NMR (400 MHz, CDCl$_3$) δ (ppm) 162.97, 136.78, 130.25, 127.94, 123.51, 119.19. Major IR absorptions (cm^{-1}): 3262, 3202, 3145, 3047, 1660, 1596, 1551, 1490, 1435, 1402, 1323, 1250, 943, 746, 676. MS (ESI): m/z = 148.01 (calculated: 148.08 for [M + H]$^+$), 170.01 (calculated: 170.16 for [M + Na]$^+$).
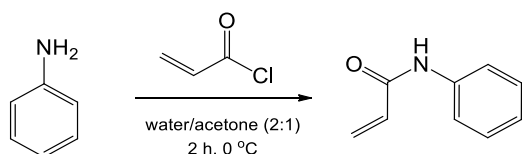
Scheme 3.11 Synthesis of N-phenylacrylamide.

c) *N*-Benzylacrylamide

Benzylamine (2.14 g, 0.02 mol) and potassium carbonate (4.15 g, 0.03 mol) were added to a stirring solution of water/acetone (2:1, 60 mL) in a 100 mL three-neck RBF, which was cooled in an ice-bath. Acryloyl chloride (2.26 g, 0.025 mol) was added dropwise, and the mixture was left to react for 2 h, after which it was poured into cold water (100 mL). The resulting precipitate was collected and recrystallised from hexane/diethyl ether (1:1, v/v) to give the product as off-white crystals (2.84 g, 88%). ^{1}H NMR (600 MHz, CDCl$_3$) δ (ppm) 7.39 – 7.14 (m, 5H, aromatic), 6.35 – 6.22 (m, 1H, -**CH**-), 6.09 (dd, J = 17.0, 10.3 Hz, 1H, -**CH**$_2$), 6.00 – 5.83 (s, 1H, -N**H**-), 5.63 (dd, J = 10.3, 1.3 Hz, 1H, -**CH**$_2$), 4.47 (d, J = 13.4 Hz, 2H, -**CH$_2$**-). ^{13}C NMR (600 MHz, CDCl$_3$) δ (ppm) 165.36, 137.99, 130.62, 128.69, 127.85, 127.54, 126.70. Major IR absorptions (cm^{-1}): 3278, 3062, 3030, 1648, 1623, 1532, 1489, 1453, 1401, 1356, 1300, 1232, 1071, 991, 952, 800, 743, 691, 585. MS (ESI): m/z = 162.07 (calculated: 162.21 for [M + H]$^+$), 184.05 (calculated: 184.20 for [M + Na]$^+$).
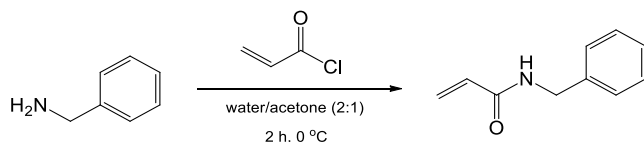
Scheme 3.12 Synthesis of N-benzylacrylamide.

d) *N*-Benzylmaleimide

N-benzylmaleimide was synthesised in two steps in a one-pot reaction. In the first, maleic anhydride (15 g, 0.153 mol) was dissolved in anhydrous DMF (75 mL) under argon gas flow. Then, benzylamine (14.57 g, 0.136 mol) in DMF (50 mL) was added over the period of 1 h, and the solution was allowed to stir for 6 h at room temperature. In the second step, a solution of phosphorus pentoxide (7.75 g, 0.055 mol) and sulfuric acid (3.25 g, 0.033 mol) in DMF (50 mL) was added slowly. The solution was brought to 95 °C and stirred for a further 12 h. After cooling to room temperature, the reaction mixture was poured in ice water and effectively extracted into diethyl ether, dried over magnesium sulfate and concentrated to yield the crude product as a yellow solid. The crude product was recrystallized from isopropanol to yield bright yellow crystals and then recrystallized from acetone to yield colourless spindle-like crystals (23.2 g, 91%). ^{1}H NMR (600 MHz, CDCl$_3$) δ (ppm) 7.34 – 7.12 (m, 5H, aromatic), 6.63 (s, 2H, -C**H** ×2), 4.60 (s, 2H, C**H$_2$**). ^{13}C NMR (600 MHz, CDCl$_3$) δ (ppm) 170.33, 136.12, 134.15, 128.68, 128.64, 128.30, 127.81, 127.72. Major IR absorptions (cm^{-1}): 3448, 3100, 1765, 1673, 1611, 1605, 1586, 1580, 1458, 1387, 1357, 1342, 1311, 1290, 1159, 1145, 1137, 1081, 1036, 1004, 881, 843, 782, 724, 644, 625, 578. MS (ESI): m/z = 188.04 (calculated: 188.20 for [M + H]$^+$).
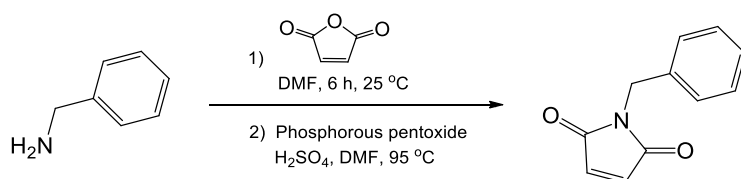
Scheme 3.13 Synthesis of N-benzylmaleimide.

e) RAFT agent *S*-(2-ethyl propionate) *O*-ethyl xanthate (RAFT-X1)

The synthesis of RAFT-X1 was adapted from literature.[57] The compound ethyl-2-bromopropionate (4.88 g, 0.027 mol) was dissolved in ethanol (30 mL). After cooling to 0 °C, potassium *O*-ethyl xanthate (4.75 g, 0.03 mol) was added in portions and the reaction mixture was stirred for 16 h at 25 °C. A large portion of the potassium bromide salt was removed by filtration and the filtrate was extracted in pentane/diethyl ether (2:1, v/v). The organic phases were washed, dried over magnesium sulfate and concentrated under reduced pressure. The crude product was further purified by column chromatography using hexane/ethyl acetate (95:5, v/v) as the eluent (4.83 g, 81%). ^{1}H NMR (400 MHz, CDCl$_3$) δ (ppm) 4.57 (q, *J* = 7.1 Hz, 2H, -C**H$_2$**-), 4.37 – 4.25 (m, 1H, C**H**), 4.13 (q, *J* = 7.1 Hz, 2H, -C**H$_2$**-), 1.50 (dd, *J* = 7.4, 2.4 Hz, 3H, -C**H$_3$**), 1.35 (t, *J* = 7.1 Hz, 3H, -C**H$_3$**), 1.25 – 1.17 (m, 3H, -C**H$_3$**). ^{13}C NMR (400 MHz, CDCl$_3$) δ (ppm) 212.33, 171.54, 70.40, 61.90, 47.40, 17.11, 14.31, 13.87. Major IR absorptions (cm^{-1}): 2960, 1733, 1444, 1372, 1299, 1259, 1208, 1149, 1043, 858, 788, 691. MS (ESI): m/z = 223.18 (calculated: 223.33 for [M + H]$^+$), 245.15 (calculated 245.31 for [M + Na]$^+$).
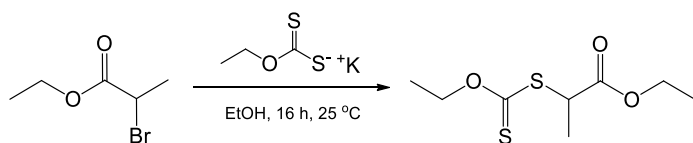
Scheme 3.14 Synthesis of RAFT- X1.

f) RAFT agent 2-hydroxyethyl 2-(ethoxycarbonothioylthio)propanoate (RAFT-X2)

The synthetic procedure from literature[15] was adapted to avoid the use of pyridine, and the work-up was adjusted. The precursor to RAFT-X2, 2-hydroxyethyl 2-bromopropionate is first synthesised. Briefly, ethylene glycol (28 mL, 0.5 mol), TEA (8 mL, 0.057 mol) and DMAP (0.7 g, 5.7×10^{-3} mol) were dissolved in THF (150 mL) was placed in a 250 mL RBF. After cooling to 0 °C, 2-bromopropionyl bromide (10.8 g, 0.05 mol) was added dropwise over 15 min under argon gas flow. The precipitate triethylamine hydrobromide is observed to form instantaneously. The reaction mixture was then left to react for 24 h at 25 °C, after which it was poured into acidic water (pH 2, 800 mL) and filtered. The mixture was extracted into DCM (6×100 mL), washed with water and dried over magnesium sulfate. The solvent was removed under reduced pressure to yield a colourless liquid (6.30 g, 64%). ^{1}H NMR (600 MHz, chloroform-*d*) δ 4.37 (q, $J = 7$ Hz, 1H, -C**H**Br-CH$_3$), 4.24 (t, $J = 4.7$ Hz, 2H, HO-CH$_2$-C**H$_2$**-O-), 3.88 (t, $J = 4.7$ Hz, 2H, HO-C**H$_2$**-CH$_2$-), 2.35 (s (broad), 1H, **H**O-CH$_2$-CH$_2$-), 1.78 (d, $J = 7.0$ Hz, 3H, -C**H$_3$**-CHBr).

In the second step, potassium *O*-ethyl xanthate (3.65 g, 0.023 mol) was dissolved in acetone (15 mL) in a 50 mL three-neck RBF. 2-Hydroxyethyl 2-bromopropionate (4 g, 0.02 mol) dissolved in acetone (15 mL) was then added to this solution via dropping funnel over 0.5 h, and the mixture was stirred for 12 h at 25 °C. Following this, the white potassium bromide salt was removed through filtration to afford a clear, yellow solution which was concentrated under reduced pressure. The crude product was purified by column chromatography with hexane/ethyl acetate (3:1 v/v, $R_f = 0.44$) as eluent. The fractions were collected and dried over magnesium sulfate and concentrated to afford an oily, yellow liquid (3.81 g, 84%). ^{1}H NMR (600 MHz, CDCl$_3$) δ (ppm) 4.60 (q, $J = 7.0$ Hz, 1H, -C**H**Br-CH$_3$), 4.38 (t, 2H, HO-CH$_2$-C**H$_2$**-O-), 3.80 (d, 2H, -C**H$_2$**-CH$_2$-), 2.01 (br, 1H, -O**H**), 1.56 (d, 3H, -C**H$_3$**-CH-), 1.25 – 1.17 (t, 3H, -C**H$_3$**-CH$_2$-). ^{13}C NMR (600 MHz, CDCl$_3$) δ (ppm) 212.38, 171.73, 70.46, 67.30, 61.02, 47.07, 16.86, 13.93. Major IR absorptions (cm^{-1}): 3410, 2950, 1652, 1493, 1461, 1423, 1287, 647. MS (ESI): m/z = 239.19 (calculated: 239.33 for [M + H]$^+$), 261.02 (calculated 261.31 for [M + Na]$^+$).
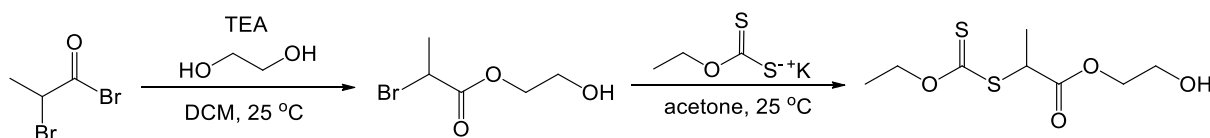
Scheme 3.15 Synthesis of 2-hydroxyethyl 2-bromopropionate leading to the formation of RAFT-X2.

3.4.2.2 Synthesis of polymers and their functionalisation

a) RAFT-mediated polymerisation of *N*-vinylpyrrolidone in bulk

The following procedure was typical for $M_{n,\text{target}}$ of 4000 g·mol^{-1}: a 50 mL oven-dry Schlenk flask was charged with AIBN (87 mg, 5.3×10^{-4} mol), RAFT-X1 (0.59 g, 2.65×10^{-3} mol) and distilled *N*-vinylpyrrolidone (10 g, 0.09 mol). The Schlenk flask was thoroughly degassed by multiple freeze-pump-thaw cycles until the absence of gas bubbles was observed during the thaw cycle. The flask was backfilled with argon, sealed and immersed in an oil bath preheated and thermostated at 60 °C. The polymerisation was left to run overnight for 6.5 h, whereupon the stir bar ceased to move due to the apparent polymer formation. The crude polymer was dissolved in dichloromethane and precipitated thrice from diethyl ether. The resulting off-white, powdery polymer (PVP-X1) was then dried in a vacuum oven for 24 h. The theoretical molecular weight ($M_{n,\text{theo}}$) was calculated using Equation 3.4. The conversions (α) were determined gravimetrically and in this way the theoretical molecular weights could be determined and confirmed for agreement with ^{1}H NMR spectroscopy and SEC.

$$M_{n,\text{theo}} = \frac{[\text{NVP}]_0}{[\text{RAFT agent}]_0} \cdot M_{r,\text{NVP}} \cdot \alpha + M_{r,\text{RAFT agent}} \qquad \text{Equation 3.4}$$

b) RAFT-mediated polymerisation of *N*-vinylpyrrolidone in aqueous media

The following procedure was typical for $M_{n,\text{target}}$ of 4000 g·mol^{-1}: a 25 mL pear-shaped flask was charged with *tert*-butyl hydroperoxide (70% aqueous solution, 34 mg, 3.77×10^{-4} mol), RAFT-X2 (0.32 g, 1.32×10^{-3} mol), undistilled *N*-vinylpyrrolidone (5 g, 0.045 mol) and PBS pH 7.4 (3 mL). The Schlenk flask was thoroughly degassed by argon bubbling for 0.5 h. Concurrently, sodium sulfite (33.3 mg, 2.64×10^{-4} mol) and PBS pH 7.4 (0.2 mL) was transferred to a small vial which was equipped with a rubber septum and purged with argon over the same period. This solution was then transferred to the Schlenk flask via a degassed, air-tight syringe and bubbling was resumed for 10 min. The polymerisation was left to run for 6 h in a preheated water bath at 25 °C. The crude polymer was lyophilised for 24 h, precipitated thrice from diethyl ether and the off-white, powdery polymer (PVP-X2) was dried in a vacuum oven at 25 °C for 16 h. $M_{n,\text{theo}}$ was calculated as per Equation 3.4.

c) PVP with β-thiopropionate linkages

The general procedure for conjugating PVP-X1 with the capping agents of phenyl acrylate, benzyl acrylate, *N*-phenylacrylamide, *N*-benzylacrylamide, *N*-phenylmaleimide and *N*-benzylmaleimide is described here as adapted from literature.[33] Briefly, PVP-X1 (0.89 g, 1.16×10^{-4} mol), triethyl phosphite (0.28 g, 1.68×10^{-3}) and hexylamine (0.2 mL, 3.0×10^{-4} mol) were dissolved in DMF (5 mL) in a 25 mL three-neck round-bottom flask. The solution was degassed thoroughly with argon and left to stir for 3 h at 25 °C. After this time, a degassed solution of the model drug compound (3.75×10^{-4} mol) and TEA (0.25 mL, 3.59×10^{-4} mol) in DMF (2 mL) was added slowly via syringe. The reaction mixture was left to stir for 18 h at 25 °C, after which the respective polymer was precipitated from diethyl ether three times and dried overnight in a vacuum oven at 25 °C.

d) PVP with acetal linkage

PVP-OH (1.65 g, 5.5 × 10^{-4} mol) and *p*-toluenesulfonic acid (2.8 mg, 2 × 10^{-5} mol) were dissolved in DMF (30 mL) in a 100 mL pear-shaped flask containing five molecular sieves (4 Å). The solution was degassed by argon bubbling for 0.5 h. Separately, a solution of phenyl vinyl ether in DMF (0.24 g, 2.0 × 10^{-3} mol, 2 mL) was thoroughly degassed. The phenyl vinyl ether solution was then transferred to the pear-shaped flask, sealed securely and left to react for 72 h at 50 °C. After this time, the mixture was decanted and precipitated from diethyl ether four times. The resulting polymer was dried overnight in a vacuum oven at 25 °C.

3.4.3 General procedures

a) Polymerisation kinetics of PVP-X2

During the polymerisation procedure outlined for PVP-X2, a kinetic study based on the conversion of monomer to polymer at different time intervals (1, 0.5, 1, 2, 3, 6 and 24 h). PVP with a $M_{n,target}$ of 12 000 g·mol^{-1} was analysed and DMF was used as the internal standard. The measurements were based on the integration values of vinyl protons (4.33 ppm, 2H for NVP) of unreacted monomer and the downfield proton signal of DMF (7.95 ppm, 1H). The procedure is as follows: to a pear-shaped flask was added undistilled NVP (1 g, 9.0 × 10^{-3} mol), RAFT-X2 (18.9 mg, 8.0 × 10^{-5} mol), *tert*-butyl hydroperoxide (70% aqueous solution, 2.6 mg, 2.0 × 10^{-5} mol), DMF (32 mg, 5 mol% of NVP) and PBS pH 7.4 (0.4 mL). The flask was sealed with a rubber septum, degassed with argon and submerged in a pre-heated water bath at 25 °C. An aliquot (0.1 mL) was removed before the initiator was added. Separately, an initiator solution of sodium sulfite (2.7 mg, 2 × 10^{-5} mol) in PBS pH 7.4 (0.2 mL) was thoroughly degassed. The initiator solution was then transferred to the monomer-containing pear-shaped flask via a degassed, air-tight syringe. Aliquots of 0.1 mL were removed at the stipulated time intervals, where a portion was kept for SEC analysis and ^{1}H NMR (D$_2$O). Hydroquinone (1.33 mg·mL^{-1} in D$_2$O, 0.05 mL) was used to quench each sample in order to terminate the reaction. For SEC analysis, the samples containing PBS were dried under reduced pressure. The samples were then diluted in DCM and precipitated from diethyl ether twice.

b) ^{1}H NMR kinetics of model drug release

Deuterated buffers (PBS pH 7 and acetate buffer pH 5.0) were prepared on a small-scale (2 mL) by using deuterated water for each buffer, afterwards confirming the pH with a pH meter. The hydrolysis measurements were performed by dissolving a known amount of the model drug compound in each deuterated buffer, along with the internal standard DMF (15 μL). ^{1}H NMR spectra were recorded at periodic intervals at 25 °C. Samples were kept at 25 °C in between measurements.

3.5 References

(1)   Mura, S.; Nicolas, J.; Couvreur, P. *Nat. Mater.* **2013**, *12* (11), 991.

(2)   Fleige, E.; Quadir, M. A.; Haag, R. *Adv. Drug Deliv. Rev.* **2012**, *64* (9), 866.

(3)   Binauld, S.; Stenzel, M. H. *Chem. Commun.* **2013**, *49* (21), 2082.

(4)   Duncan, R. *Nat. Rev. Drug Discov.* **2003**, *2* (5), 347.

(5)   D'Souza, A. J. M.; Schowen, R. L.; Topp, E. M. *J. Control. Release* **2004**, *94* (1), 91.

(6)   Moffitt, E. A. *Can. Anaesth. Soc. J.* **1975**, *22* (1), 12.

(7)   Salpekar, A. *U.S. Patent No. 5,364,601*; U.S. Patent and Trademark Office: Washington DC, 1994.

(8)   Nair, B. *Int. J. Toxicol.* **1998**, *17* (4), 95.

(9)   Guinaudeau, A.; Mazières, S.; Wilson, D. J.; Destarac, M. *Polym. Chem.* **2012**, *3* (1), 81.

(10)   Chiefari, J.; Chong, Y. K.; Ercole, F.; Krstina, J.; Jeffery, J.; Le, T. P. T.; Mayadunne, R. T. A.; Meijs, G. F.; Moad, C. L.; Moad G.; Rizzardo, E. A. *Macromolecules* **1998**, *31* (16), 5559.

(11)   Thang, S. H.; Chong, Y. K.; Mayadunne, R. T. A.; Moad, G.; Rizzardo, E. A. *Tetrahedron Lett.* **1999**, *40* (12), 2435.

(12)   Nakabayashi, K.; Mori, H. *Eur. Polym. J.* **2013**, *49* (10), 2808.

(13)   McLeary, J. B.; Klumperman, B. *Soft Matter* **2006**, *2* (1), 45.

(14)   Moad, G.; Rizzardo, E.; Thang, S. H. *Aust. J. Chem.* **2006**, *59* (10), 669.

(15)   Nicolaÿ, R.; Kwak, Y.; Matyjaszewski, K. *Chem. Commun.* **2008**, *0* (42), 5336.

(16)   Barner-Kowollik, C*. Handbook of RAFT polymerization; Wiley: Weinheim, 2008.*

(17)   Dondoni, A. *Angew. Chemie Int. Ed.* **2008**, *47* (47), 8995.

(18)   Pound, G.; Eksteen, Z.; Pfukwa, R.; McKenzie, J. M.; Lange, R. F. M.; Klumperman, B. *J. Polym. Sci. A.* **2008**, *46* (19), 6575.

(19)   Pound, G.; McLeary, J. B.; McKenzie, J. M.; Lange, R. F. M; Klumperman, B. *Macromolecules* **2006**, *39* (23), 7796.

(20)   Pound, G.; McKenzie, J. M.; Lange, R. F. M.; Klumperman, B. *Chem. Commun.* **2008**, *0* (27), 3193.

(21)   Pound, G.; McLeary, J. B.; McKenzie, J. M.; Lange, R. F.; Klumperman, B. *Macromolecules* **2006,** *39* (23), 7796.

(22)   Ilchev, A.; Pfukwa, R.; Hlalele, L.; Smit, M.; Klumperman, B*. Polym. Chem.* **2015**, *6* (46), 7945.

(23)   Reader, P. W.; Pfukwa, R.; Jokonya, S.; Arnott, G. E.; Klumperman, B. *Polym. Chem.* **2016**, *7* (42), 6450.

(24)   Oishi, M.; Nagatsugi, F.; Sasaki, S.; Nagasaki, Y.; Kataoka, K. *ChemBioChem.* **2005**, *6* (4), 718.

(25)   Pound, G. *Reversible Addition Fragmentation Chain Transfer (RAFT) Mediated Polymerization of N-Vinylpyrrolidone [PhD Thesis]*; Stellenbosch University, 2008.

(26)   Gillies, E. R.; Goodwin, A, P.; Fréchet, J. M. *Bioconjug Chem. 2004*, *15* (6), 1254.

(27)   Murthy, N.; Thng, Y. X.; Schuck, S.; Xu, M. C.; Fréchet, J. M. *J. Am. Chem. Soc.* **2002**. *124* (42), 12398.

(28)   Cui, W.; Qi, M.; Li, X.; Huang, S.; Zhou, S.; Weng, J. *Int. J. Pharm.* **2008**, *361* (1), 47.

(29)   Koczkur, K. M.; Mourdikoudis, S.; Polavarapu, L.; Skrabalak, S. E. *Dalton Trans.* **2015**. *44* (41), 17883.

(30)   Boyer, C.; Bulmus, V.; Davis, T. P. *Macromol. Rapid Commun.* **2009**, *30* (7), 493.

(31)   Scales, C. W.; Convertine, A. J.; McCormick, C. L. *Biomacromolecules* **2006**, *7* (5), 1389.

(32)   Nakayama, M.; Okano, T. *Biomacromolecules* **2005**, *6* (4), 2320.

(33)   Ho, H. T.; Levere, M. E.; Pascual, S.; Montembault, V.; Soutif, J. C.; Fontaine, L. *J. Polym. Sci. Part A Polym. Chem.* **2012**, *50* (8), 1657.

(34)   Mangold, C.; Dingels, C.; Obermeier, B.; Frey, H.; Wurm, F. *Macromolecules* **2011**, *44* (16), 6326.

(35)   Liu, B.; Thayumanavan, S. *J. Am. Chem. Soc.* **2017**, *139* (6), 2306.

(36)   Legge, T. M.; Slark, A. T.; Perrier, S. *J. Polym. Sci. A.* **2006**, *44* (24), 6980.

(37)   Kim, S.; Linker, O.; Garth, K.; Carter, K. R. *Polym. Degrad. Stab.* **2015**, *121*, 303.

(38)   Nimesh, S. *Gene Therapy: Potential Applications of Nanotechnology*; Woodhead Publishing: Cambridge, 2013.

(39)   Siepmann, J. *Adv. Drug Deliv. Rev.* **2012**, *64* (1), 163.

(40)   Merchant, H. A.; Shoaib, H. M.; Tazeen, J.; Yousuf, R. I. *AAPS PharmSciTech* **2006**, *7* (3), 178.

(41)   Siepmann, J.; Siepmann, F. *Int. J. Pharm.* **2008**, *364* (2), 328.

(42)   Kirby, A. J. *Compr. Chem. Kinet.* **1972**, *10* (1), 57.

(43)   da Silva, P. L.; Guimarães, L.; Pliego, J. R. *J. Phys. Chem. B* **2013**, *117* (21), 6487.

(44)   Rayne, S.; Forest, K. *Flavour Fragr. J.* **2016**, *31* (5), 385.

(45)   Wang, X.; Liu, L.; Luo, Y.; Shi, H.; Li, J.; Zhao, H. *Macromol. Biosci.* **2012**, *12* (11), 1575.

(46)   Oishi, M.; Nagasaki, Y.; Itaka, K.; Nishiyama, N.; Kataoka, K. *J. Am. Chem. Soc.* **2005,** *127* (6), 1624.

(47)   Tamura, A.; Yui, N. *J. Mater. Chem. B* **2013**, *1* (29), 3535.

(48)   Dan, K.; Pan, R.; Ghosh, S. *Langmuir* **2011**, *27* (2), 612.

(49)   Jackson, G. L. *Hydrolysis of amides: a kinetic study of substituent effects on the acidic and basic hydrolysis of aliphatic amides [PhD thesis]*; University of Wollongong, 1969.

(50)   Hilal, S. H.; Karickhoff, S. W.; Carreira, L. A.; Shrestha, B. P. *QSAR Comb. Sci.* **2003**, *22* (910), 917.

(51)   Qiu, L.; Li, J. W.; Hong, C. Y.; Pan, C. Y. *ACS Appl. Mater. Interfaces* **2017**, *9* (46), 40887.

(52)   Jacques, S. A.; Leriche, G.; Mosser, M.; Nothisen, M.; Muller, C. D.; Remy, J. S.; Wagner, A. *Org. Biomol. Chem.* **2016**, *14* (21), 4794.

(53)   Kreevoy, M. M.; Taft, R. W. *J. Am. Chem. Soc.* **1955**, *77* (21), 5590.

(54)   Schelhaas, M.; Waldmann, H. *Angew. Chemie Int. Ed. English* **1996**, *35* (18), 2056.

(55)   Bisjak, C. P.; Lubbad, S. H.; Trojer, L.; Bonn, G. K. *J. Chromatogr. A* **2007**, *1147* (1), 46.

(56)   Chen, I. L.; Wang, T. C.; Chen, Y. L.; Tzeng, C. *J. Chinese Chem. Soc.* **2000**, *47* (1), 155.

(57)   Destarac, M.; Brochon, C.; Catala, J. M.; Wilczewska, A.; Zard, S. Z. *Macromol. Chem. Phys.* **2002**, *203* (16), 2281.

Chapter Four

Block copolymer synthesis and self-assembly

4.1 Introduction

Block copolymers are largely defined as macromolecules consisting of two or more distinct segments, i.e. blocks, of different monomer compositions combined together in some architecture by a covalent bond.[1] The self-assembly of block copolymers to form nanomorphologies is currently a topic of active research in drug delivery design. The traditional approach used to create nanosized vessels is through the self-assembly of a block copolymer in a solvent that is selective for one of the blocks. There are certain parameters of the block copolymer which affect the equilibrium morphologies in the solution state, namely, solubility, the relative volume fraction and the length of the blocks.[2,3] The transition between morphologies can therefore be induced by altering the solvent characteristics or the block ratios of the amphiphilic macromolecule. Most often, spherical micelles are obtained from the self-assembly of diblock copolymers in a selective solvent because a high curvature (Figure 4.1) is more likely to occur.[4] Block copolymers composed of amorphous or semi-crystalline blocks are able to undergo the necessary microphase separation that underlies the self-assembly.
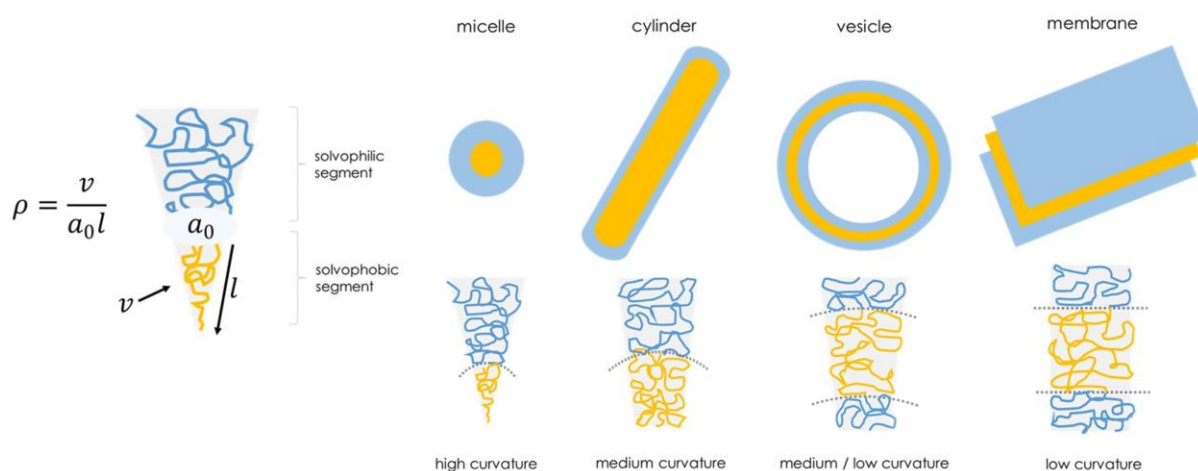
Figure 4.1 The different morphologies obtained with different packing parameters, ρ.

The movement of spheres is more predictable due to symmetry, but non-spherical particles may tumble and rebound in the presence of circulatory flow.[5] Some impetus has therefore been placed on the formation of cylindrical or rod-like micelles due to research demonstrating their improved performance *in vivo* compared to spherical micelles for properties such as circulation time[6] and shape-influenced interactions with cells.[7] Platelet-shaped micelles have also received attention in recent years.[8,9] These lamellae-type, 2D high aspect ratio materials are important as additives in composites and thermosets and in drug delivery as scaffolds and as templates for nanoparticles.[10] Zhu *et al.* reported that truncated lozenge 'bamboo leaf' shaped micelles were formed from a poly(ethylene oxide)-*block*-poly(ε-caprolactone) (PEO-*b*-PCL) block copolymer via crystallisation-driven self-assembly (CDSA)

and interestingly, these micelles displayed selective internalisation upon their exposure to various cell types.[11] The formation of cylindrical micelles and platelets is not a simple task using conventional solvent-driven self-assembly methods because there exists only a small window of opportunity to create low curvature nanostructures. CDSA provides an alternative means of creating nanomorphologies with low curvatures that would otherwise have been more challenging to obtain. A prerequisite to accomplish this is that one block of the block copolymer block is semi-crystalline, as CDSA is driven by the crystallisation of the core as long as the temperature is kept below the T_m of the crystalline block.[12]

PCL is a polymer derived from the seven-membered cyclic ester, ε-caprolactone (CL). It is an excellent choice of semi-crystalline polymer for biological systems because it is FDA-approved, biodegradable, biocompatible and releases non-toxic degradation products. It also exhibits superior viscoelastic and rheological properties compared to many other aliphatic polyesters.[13] The six-membered cyclic ester, δ-valerolactone (VL), when polymerised to poly(δ-valerolactone) (PVL), however, remains relatively unexplored despite similarly favourable physicochemical properties.[14–16] A few biomedical applications of these polymers are shown in Figure 4.2.
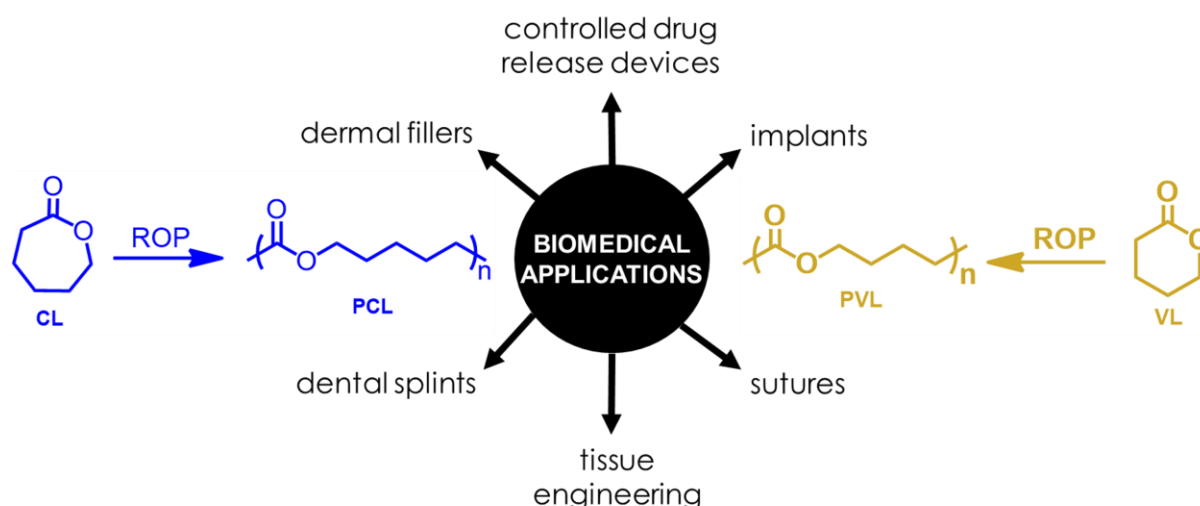
Figure 4.2 Possible biomedical applications of poly(ε-caprolactone) and poly(δ-valerolactone).

PVL has a reported T_g of -67 °C and a T_m of between 52 – 59 °C, compared to PCL where it is reported as -60 °C and between 59 – 64 °C for the T_g and T_m, respectively.[17] Both polymers are rubbery and flexible at physiological and at room temperatures.[18,19] PVL is more hydrophilic than PCL, likely due to the shorter nonpolar aliphatic chains in the backbone, where longer chains would impart a higher degree of hydrophobicity.[20,18] The long degradation times (years) recorded for PCL limit the extent of its applications as a biodegradable polymer.[21] On the other hand, poly(D,L-lactide-co-glycolide) (PLGA), another commonly used aliphatic polyester, exhibits very short degradation times (<6 months). In terms of degradation, PVL represents a valuable polyester intermediate where its degradation time is shorter than that of PCL but longer than that of PLGA. To the best of our knowledge, there are no reports on the CDSA behaviour of a block copolymer composed of PVL as the core-forming block. We wish to bridge this gap by providing insights into the PVL-based block copolymer, PVP-*b*-PVL.

Ring-opening polymerisation (ROP) is a convenient method of synthesising PVL and has led to the synthesis of polymers with predictable molecular weights, low dispersities and high end-group fidelities.[22] It is especially beneficial when applied in tandem to other forms of controlled radical polymerisations such as RAFT or ATRP. A block copolymer can be synthesised using an alcohol macroinitiator in the form of a hydroxy end-functional polymer which can used to initiate the ROP of a cyclic ester. ROP can proceed via anionic, cationic, coordination and radical mechanisms depending on the monomer type and catalyst system.[23] The most frequently used catalyst for anionic ROP is tin(II) ethylhexanoate ($Sn(oct)_2$) at high temperatures. While highly effective for some uses, certain disadvantages such as the high-energy demand, the formation of brown-tinged products due to oxidation and the presence of residual metal catalyst, could cause restriction in certain applications.[24] This is especially true for polymers intended in microelectronics and drug delivery systems, where metal contaminants could pose a risk by reducing the efficiency of the devices or could cause cytotoxicity, respectively.[25]

The first instance of organocatalysed (metal-free) ROP was reported by Nederberg *et al*. in 2001 for the ROP of lactide catalysed by DMAP in the presence of a primary alcohol as the initiator.[26] Since then, many organocatalysts have been explored. The guanidine organocatalyst 1,5,7-triazabicyclodecene (TBD) and the amidine organocatalyst 1,8-diazabicycloundec-7-ene (DBU) have become popular for the ROP of lactones.[22] Their chemical structures are shown in Figure 4.3. These highly basic *N*-heterocyclic carbenes are powerful organocatalysts which are able to mediate the formation of well-defined polyesters.[27] TBD is more active than DBU and catalyses the ROP of VL and CL under conditions where DBU cannot.[28] It was shown by Lohmeijer *et al*. that TBD is distinctive in its ability to bifunctionally activate both the alcohol and the monomer, whereas DBU can only activate the alcohol.[27] DBU therefore requires a cocatalyst, usually in the form of thiourea for the ROP of VL and CL. Aside from DBU's ability to form hydrogen bonds with alcohol initiators (thereby activating the alcohol for nucleophilic attack), new research has revealed that DBU is also a competent nucleophile, capable of acting as a nucleophilic catalyst.[29] As with metal catalysts, organocatalysts also require anhydrous conditions. Water can act as an initiator and could therefore lead to polymers with different end-groups and lower-than-targeted molecular weights.[30]

TBD   **DBU**
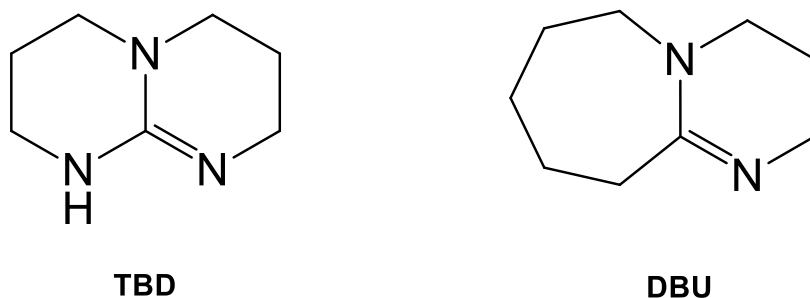
Figure 4.3 Chemical structures of 1,5,7-triazabicyclodecene (left) and 1,8-diazabicycloundec-7-ene (right).

RAFT polymerisation and ROP have proven to be essential tools in the synthesis of complex and well-defined polymers. A drug delivery system that is inspired by Ringsdorf's rationale is composed of a polymer backbone, solubilising functional groups, a labile bond, the drug and a targeting moiety.[31] The polymeric prodrug should therefore be robust to allow for the chemistry needed to include these components into the system. One disadvantage of aliphatic polyesters is their lack of functionality. A way in which to realise this is through the use of functional cyclic esters which provide a means of conjugating the drug to the aliphatic polyester block of the block copolymer.

4.1.1 Approach

The amphiphilic block copolymer, or carrier, is a central focus in creating drug delivery systems. This work encompasses the synthesis steps and procedures necessary to obtain the block copolymer used as the vessel for the delivery of the synergistic drug combination artemether-lumefantrine. A hydroxy-functional RAFT agent was used to synthesise PVP as described in Chapter 3 as PVP-X2, which will further be referred to as PVP-OH for simplicity. This polymer was protected with pyridyl disulfide (PDS) to render PDS-PVP-OH. The PDS group is important for future conjugation to the targeting ligand which will be described in Chapter 5. Furthermore, α-allylvalerolactone (AVL) was synthesised as the functional cyclic ester to undergo ROP initiated by PDS-PVP-OH. This allylated lactone provides a pathway for the conjugation of lumefantrine post-polymerisation. The simplified parent block copolymer, PVP-*b*-PVL served as a means to determine the optimum polymerisation conditions for this system and in this way, the organocatalysts DBU + thiourea (TU) as well as TBD were explored. Various conditions were optimised to allow for the efficient synthesis of PVP-*b*-PVL using standard Schlenk techniques. The self-assembly of PVP-*b*-PVL was also explored and a range of nanomorphologies were observed using TEM, with characterisation techniques including DLS, DSC, FTIR and P-XRD being conducted on selected samples to gain further insights.

4.2 Results and discussion

4.2.1 Synthesis and polymerisations

a) Synthesis of α-allylvalerolactone monomer

The functional lactone, α-allylvalerolactone (AVL), was synthesised according to the procedure by Molander and Harris (Scheme 4.1).[32] In this method, allylated lactones were synthesised to serve as intermediates in the study of Barbier cyclisations. Parrish *et al.*[33] drew on this and further proved that this monomer was able to undergo ROP to form its homopolymer as well as copolymers with CL and VL by simply mixing the functionalised and pristine monomers in the reaction vessel prior to implementing the required ROP conditions. To date, accounts of poly(α-allylvalerolactone) (PAVL) in literature have been based on its copolymerisation with CL and VL.[14,34]
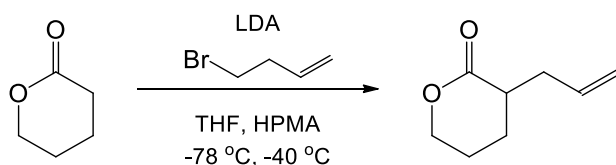
Scheme 4.1. Synthesis of the monomer α-allylvalerolactone.

Modifications to the synthesis of AVL using *n*-butyllithium were inspired by the work of Li, Buzon and Castaldi,[35] because initially, lower than expected yields were obtained (approximately 20%), possibly as a result of dialkylation. The dry ice/acetone cooling bath was carefully monitored and maintained well below -70 °C upon addition of allyl bromide. This is an important consideration as it is an extremely exothermic reaction. An added precaution was to precool the allyl bromide/HPMA solution before its addition. By making these small changes, the yield was increased to 65%. Some product loss is very likely as a result of the double-step purification technique (column chromatography and vacuum distillation) because monomers free of impurities are required for ring-opening polymerisations. The ^{1}H NMR spectrum of AVL can be found in Addendum D. The second temperature phase required that the cooling bath be maintained at -40 °C. A convenient way of ensuring this was by mixing ethylene glycol and ethanol in dry ice in a ratio of 60/40 (v/v). In this way, any temperature over the range of -12 to -78 °C can be sustained over long periods of time depending on the mixing ratio, which is especially useful when there is no single solvent to achieve this.[36] Additionally, *n*-butyllithium should be titrated before use so as to determine its concentration if it is unknown as it is known to degrade upon ageing. This procedure is described in the Experimental section.

b) Protection of PVP-OH with 2,2'-pyridyldisulfide

To prepare the macroinitiator for the ROP of AVL, hydroxy-functional PVP (PVP-OH) was synthesised as described in Chapter 3 as 'PVP-X2' using RAFT-X2. In this instance, instead of removing the thiocarbonylthio group on the ω-end of the polymer through thermolysis, it was converted to a pyridyl disulfide (PDS) protected thiol. After this procedure, PVP-OH is further referred to as PDS-PVP-OH (Figure 4.4 a)). This thiol-protecting strategy is well-described in literature[37] and is frequently applied in biological systems as a convenient strategy for thiol-disulfide exchange. Examples of the synthesis conditions for PVP-OH and PDS-PVP-OH are shown in Table 4.1.

Table 4.1 Synthesis conditions and analytical details of PVP-OH and PDS-PVP-OH

Polymer	∝ [a] / yield %	Time h	Solvent	Temperature °C	$M_{n,target}$ [b] g·mol^{-1}	$M_{n,SEC}$ [c] g·mol^{-1}	$M_{n,NMR}$ [d] g·mol^{-1}	Đ
PVP-OH	90	6	PBS aqueous buffer	25	4000	4000	3900	1.1
PDS-PVP-OH	99	24	acetonitrile	25	-	4000	3900	1.1

[a] conversion of NVP to PVP-OH, determined gravimetrically
[b] $M_{n,target}$ = ([NVP]/[RAFT agent]) · $M_{r,NVP}$ · α + $M_{r,RAFT\ agent}$ where ∝ = 1
[c] $M_{n,SEC}$ is based on PMMA standards, eluent DMF
[d] $M_{n,NMR}$ is determined by the ratio of integral signals of the xanthate end-group to polymer backbone
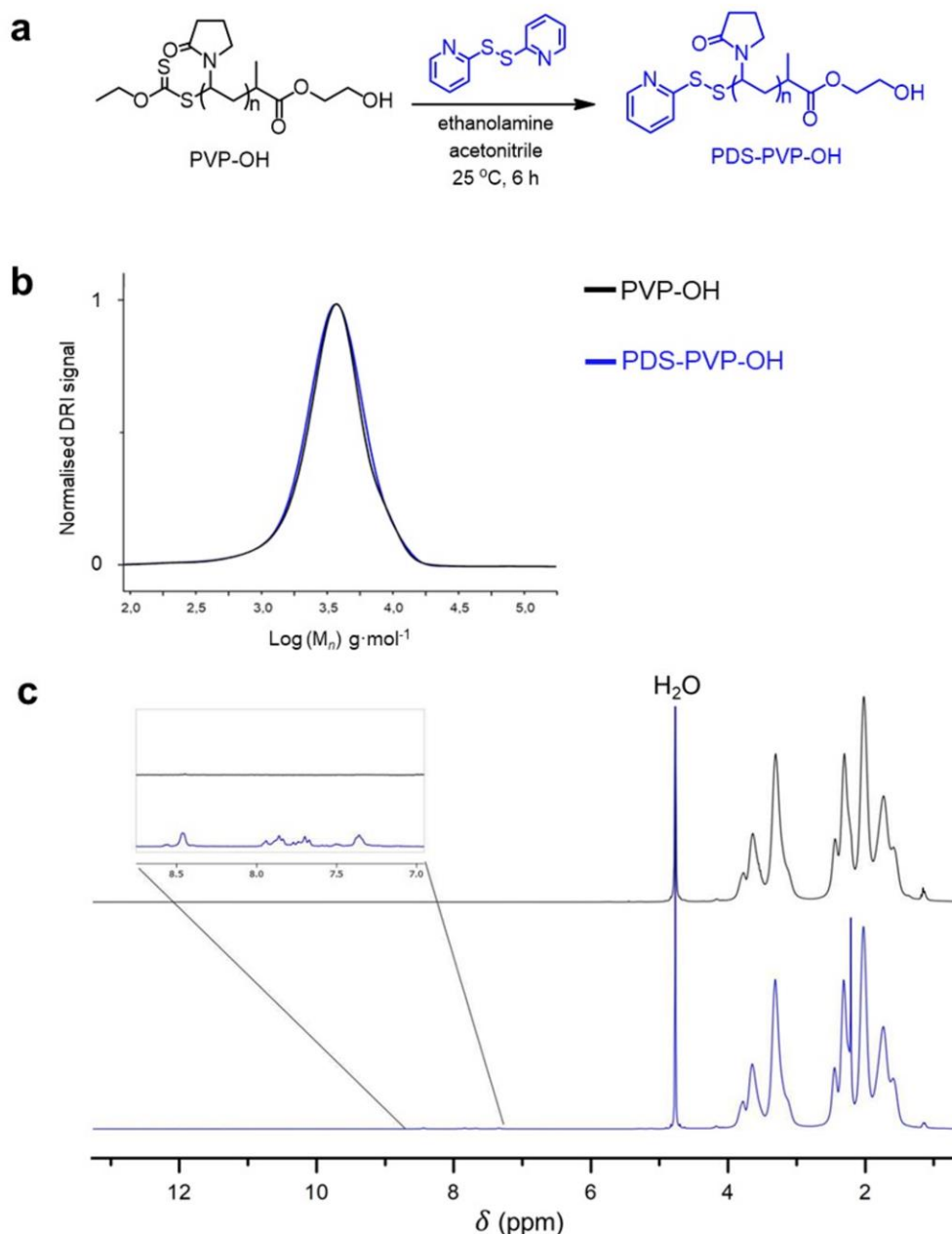
Figure 4.4 a) Synthesis of PDS-PVP-OH. b) Molar mass distributions and c) ^{1}H NMR stacked spectra of PVP-OH (black) and PDS-PVP-OH (blue).

It is well established in literature that trithiocarbonate and dithioester RAFT end groups can be facilely converted to thiols via aminolysis.[38] PDS-terminated PVP-OH was prepared in near-quantitative conversions by the aminolysis of PVP-OH in the presence of ethanolamine, reacted *in situ* with excess 2,2'-pyridyldisulfide. PDS sufficiently protects the thiol end-groups of PVP-OH during the subsequent ring-opening polymerisations and post-polymerisation modification reactions, which will be described first. The driving force of the reaction is the release of pyridine-2-thione, which is a chemically inert compound with a distinct UV absorbance which can be used to quantify the efficacy of PDS conjugation or subsequent bioconjugation reactions.[39] The ability of PDS to undergo disulfide exchange efficiently and site-selectively with the biological targeting ligand will be discussed in Chapter 5.

The SEC molar mass distributions and ^{1}H NMR spectra of PVP-OH and PDS-PVP-OH are shown in Figure 4.4 b) and c), respectively. The successful conjugation of PDS was confirmed with the appearance of the characteristic signals of the pyridyl ring at δ 8.4, 8 – 7.6 and 7.3 ppm in the ^{1}H NMR spectrum. SEC analysis of the polymers revealed similar molar masses and monomodal distributions indicating that there was no disulfide coupling between the polymer chains. The polymers were dissolved in deuterium oxide as the solvent for ^{1}H NMR spectroscopy analysis because PDS is insoluble in water.

Any signals observed in the spectrum are therefore attributed to the PVP-bound protons of PDS and not of free PDS, although thorough purification steps were followed. During an initial attempt only a 15% PDS end-group functionality (%f,$_{NMR}$) was obtained. The PDS %f,$_{NMR}$ is calculated from the ratio of the integral signal of the pyridyl protons of PDS (2H, 8.4 ppm) to that of the methyl group on PVP's α-end (3H, 1.1 ppm). After certain reaction conditions were optimised, including increasing the reaction time and the molar excess of 2,2'-dipyridyl disulfide to the polymer, as well as improving the degassing technique from argon gas bubbling to freeze-pump-thaw (Addendum E), the near-quantitative coupling of PDS to the polymer was obtained.

c) ROP of δ-valerolactone using 1-pyrenemethanol

Before utilising the synthesised PDS-PVP-OH as a macroinitiator to initiate the ROP of the synthesised AVL monomer, various model studies were conducted. This was done so as to minimise the risk of loss of compounds associated with unsuccessful polymerisations. Additionally, the block copolymer system of PVP-*b*-PVL has not yet been reported so its optimisation is important.

The TBD promoted ROP of VL, initiated from 1-pyrenemethanol (1-PM), was conducted in DCM at room temperature in the ratio of 50/1/1 for [VL] / [1-PM] / [TBD] (Table 4.2, run 1). The DBU + TU promoted ROP of VL, initiated from 1-PM was also conducted in DCM at room temperature in the ratio of 50/1/1/1 for [VL] / [1-PM] / [DBU] / [TU] (Table 4.2, run 2). TBD and DBU + TU both afforded PVLs at room temperature over short to appreciable periods of time, with experimental molar masses independently determined by SEC (with THF as the eluent, M$_{n,SEC}$) and ^{1}H NMR (M$_{n,NMR}$) in good to excellent agreement with the theoretical molar masses. With DBU + TU, the experimental data were systematically lower than the calculated ones (Table 4.2).

ROPs catalysed by TBD should not be run for extended periods of time because TBD is known to catalyse the transesterification reactions of the resulting polyesters due to the high activity of this catalyst.[27] The polymerisation was therefore quenched within minutes when visually, the presence of solidified polymer was observed after that time. DBU + TU-catalysed polymerisations were more sluggish and required longer periods of time to obtain similar conversions to TBD-catalysed PVLs.

Table 4.2 Polymerisation conditions and analytical details for TBD-catalysed VL (run 1) and DBU + TU-catalysed VL (run 2)

Run	Catalyst loading	$\propto$ [a] %	Time h	Temperature °C	$M_{n,\text{target}}$ [b] g·mol⁻¹	$M_{n,\text{SEC}}$ [c] g·mol⁻¹	$M_{n,\text{NMR}}$ [d] g·mol⁻¹	$Đ$ [e]
1	2 mol%	95	0.1	25	5200	4900	5300	1.1
2	5 mol%	82	3	25	5200	4100	4100	1.2

[a] conversion of VL to PVL, determined gravimetrically

[b] $M_{n,\text{target}} = ([\text{monomer}]/[\text{initiator}]) \cdot \propto \cdot M_{r,\text{monomer}} + M_{r,\text{initiator}}$ where $\propto = 1$ for 100% conversion

[c] $M_{n,\text{SEC}}$ is determined by SEC based on polystyrene standards, eluent THF

[d] $M_{n,\text{NMR}}$ is determined by ^{1}H NMR spectroscopy in CDCl₃ as the ratio of the signals of pyrene (9H, 8.3 – 8.0 ppm) to the polymer backbone (2H, 4.1 ppm)

[e] $Đ$ represents the dispersity, from SEC (M_w / M_n)

Figure 4.5 shows the molar mass distributions from SEC of the obtained PVL polymers catalysed by TBD and DBU + TU using a differential refractive index (RI) and UV detector at 340 nm. Through use of the UV-active initiator 1-PM, a clear indication of its incorporation into the polymer is obtained, where the dashed curves represent the UV signal of 1-PM in the PVLs. The solid curves represent the molar mass distributions calibrated from RI detector data which are monomodal and narrow. As is evident from the overlaid RI and UV signals, the initiator is clearly attached to the polymers. The wavelength of 340 nm was chosen specifically because no other UV-active functional groups of the polymer would absorb here, for instance, the thiocarbonylthio moiety absorbs at 280 nm so this wavelength region was avoided.
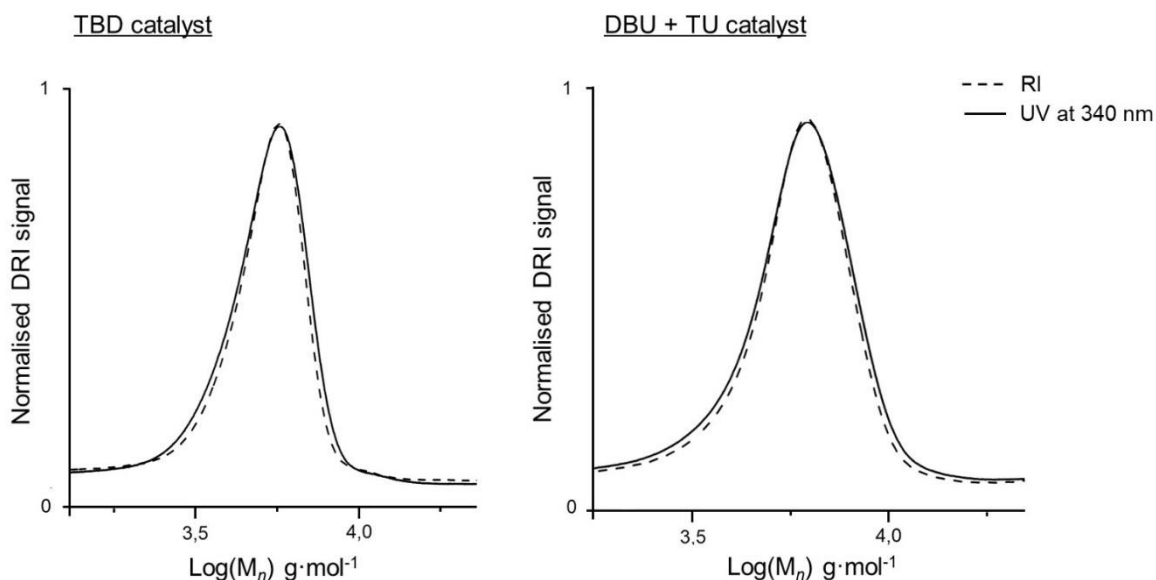
Figure 4.5 Molar mass distributions of TBD- (left) and DBU + TU- (right) catalysed ROP of PVL homopolymers detected by RI and UV (340 nm) detectors.
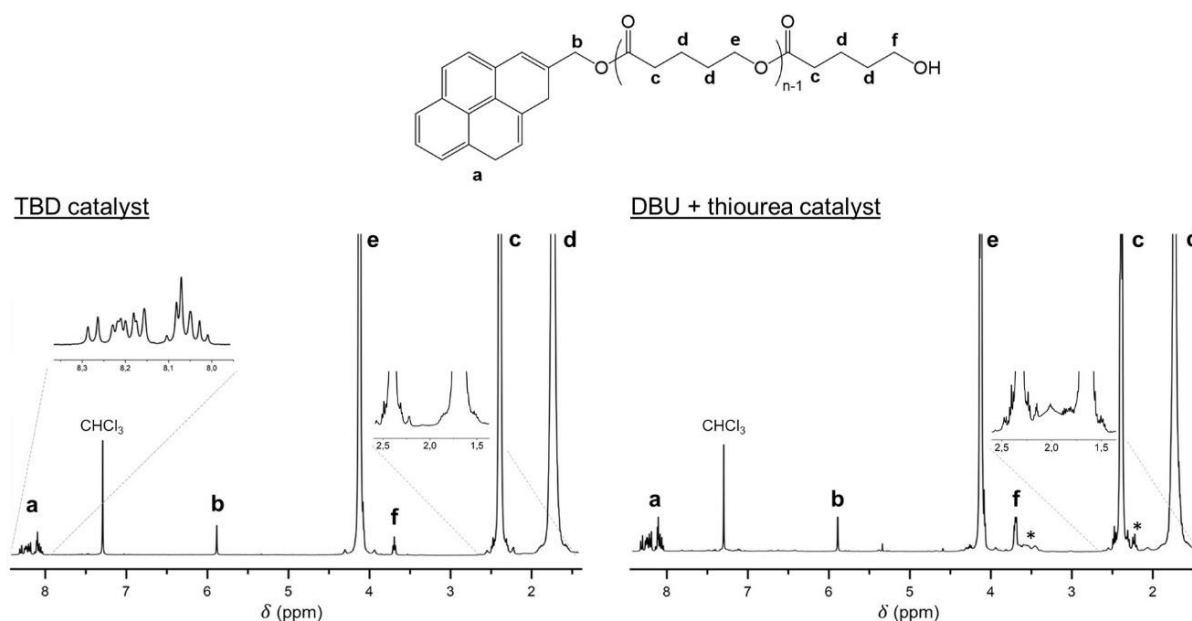
Figure 4.6 ^{1}H NMR spectra of TBD (left) and DBU + thiourea (right) catalysed ring-opening polymerisations of VL.

The fraction of initiator-derived polymer chains was further explored by ^{1}H NMR spectroscopy. Figure 4.6 shows the assigned chemical structure of PVL and the ^{1}H NMR spectra of the TBD-catalysed and DBU + TU-catalysed ROPs of VL. The characteristic peaks due to the initiator, 1-PM, are observed as the pyrene protons in the upfield region (**a**, 9H, 8.3 – 8 ppm) and the methylene protons (**b**, 2H, 5.8 ppm) which are more downfield in both spectra. The ratios of signal **b** on the α-chain end of both polymers can be related to those of signal **f** (2H, 3.6 ppm) on the ω-chain end adjacent to the hydroxyl group. When TBD was used, the α- and ω-chain end groups (**b** : **f**) integrated to a ratio of 1:1. When DBU + TU was used, the α- and ω-chain end groups (**b** : **f**) integrated to a ratio of 1:2. The relative intensity of peak **b** (α-end group) to peak **f** (ω-end group) should indicate that there is a 1:1 ratio of the end groups originating from the initiator and from the hydrolysis of the propagating species, respectively.

This is the ideal case when TBD was used, as signal **b** relative to signal **f** integrated to 1:1, but when DBU was used this ratio was 1:2. The signals marked with an asterisk could be due to DBU-initiated chains. Cyclic amidines such as DBU have been shown to be strong nucleophiles,[38] exhibiting a more nucleophilic nature compared with TBD. DBU therefore has the potential to interact directly with highly polarised bonds such as those of esters found in lactone monomers used in ROPs, *i.e.* VL. A nucleophilic-attack pathway has been established, which describes the potential of DBU to function as a nucleophile by attacking the carbonyl bond of the monomer, thereby initiating polymerisation.[40] TBD was therefore chosen as the succeeding organocatalyst over DBU + TU because of the greater certainty over the end-group fidelity, as well as faster polymerisation kinetics, *i.e.* quantitative monomer conversions in less than one minute. This powerful catalyst is, however, highly water and air-sensitive, so the polymerisation conditions were continually improved in order to reach the maximum conversion in the shortest amount of time.

Steps that were taken to ensure this:

1. Drying TBD in a vacuum oven for 24 h before the polymerisation

2. Distilling DCM and storing it over activated molecular sieves for 24 h before the polymerisation

2. Storing VL over activated molecular sieves in an air-tight container under argon

3. Stirring VL over activated molecular sieves in DCM for 24 h under argon before the polymerisation

4. In a separate vessel, stirring the initiator over activated molecular sieves in DCM for 24 - 48 h under argon before the polymerisation

5. Maintaining a positive flow of argon gas during the transfer of the initiator solution to the monomer solution

6. Using degassed, air-tight syringes

d) ROP of δ-valerolactone using a macroinitiator

After the appropriate polymerisation conditions and catalyst were chosen for the homopolymerisation of VL, hydroxy-functional PVP was used as the macroinitiator (starting hydrophilic block) instead of 1-PM to create the PVP-*b*-PVL block copolymer (BCP). The macroinitiated ROP of VL generally proceeded to substantial conversions within 5 min when appropriate airtight and water-free conditions were upheld. The polymerisation was quenched when visually, the stir bar ceased to move due to the high viscosity of the polymerisation mixture at high conversions. If there was any presence PVP or PVL, then it was removed via successive precipitations in methanol (to remove any residual VL and PVP) and then in ethyl acetate (to remove any PVL). The SEC molar mass distributions of the crude and purified block copolymer are shown in Addendum F, where the presence of homopolymer in a crude sample was generally observed for the DBU + TU-catalysed system. Many block copolymers are liquids at room temperature or are sticky and therefore challenging to handle due to the disparate properties of each block, making it difficult to find solvent combinations for effective purification. Often much time is invested in tedious purification techniques. For PVP-*b*-PVL, however, only precipitation needs to be applied to effectively purify the block copolymer. Fine, white powders are obtained which are easy to handle practically and store. Since PVP is an outstanding lyoprotectant, it would impart a degree of physical stability during the sublimation of water during the process of lyophilisation of the PVP-*b*-PVL and PVP-*b*-PVL micelles.[41] Excellent long-term storage has been reported for PVP-based micelles following lyophilisation.[42] This would aid in the protection of the structure and payload of the self-assembled micelles. The block copolymers were able to dissolve in water without forming precipitates, indicating the absence of free PVL. The polymers also dissolved in solvents such as ethanol and methanol in which PVL is insoluble. This emphasises the altered physical properties of the block copolymers.

In ^{1}H NMR spectroscopy, evidence of chain extension to form the block copolymer is shown in the purified product by the presence of VL peaks along with those peaks that are characteristic of the PVP macroinitiator. A typical ^{1}H NMR spectrum of PVP-*b*-PVL is shown in Figure 4.7 a) where it is compared with the spectra of PVP and PVL. The characteristic peaks of PVP and PVL are clearly observed in the spectrum of the purified block copolymer, as indicated by arrows. The monomodal molar mass

distribution curve of PVL-*b*-PVP is shown in Figure 4.7 b) (Table 4.3, BCP 1), obtained from SEC. The analytical details of six PVP-PVL block copolymers are shown in Table 4.3. These block copolymers have different block ratios of the hydrophilic (PVP) and hydrophobic (PVL) segments because it was important to understand this effect in terms of self-assembly, which will be discussed towards the end of this chapter. By simply using macroinitiators of different molecular weights or by targeting different block copolymer molecular weights, a range of PVP-*b*-PVLs were synthesised.
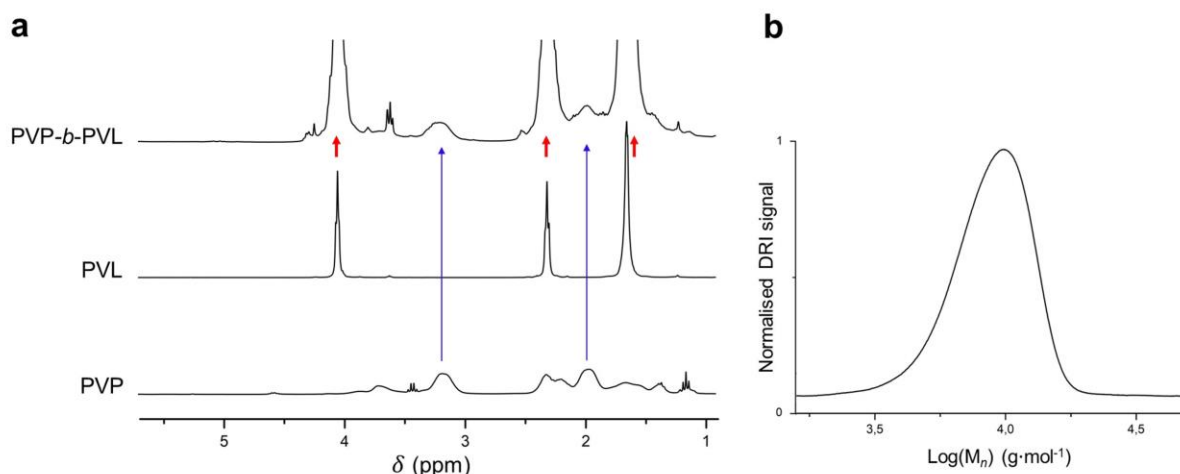
Figure 4.7 a) ^{1}H NMR spectra of PVP$_{36}$-b-PVL$_{53}$ (top), PVL (middle) and PVP (bottom) and b) the SEC molar mass distribution of PVP$_{36}$-b-PVL$_{53}$ (M$_{n,SEC}$ = 9300 g·mol^{-1}, Đ = 1.1).

It should be mentioned that SEC data is likely not to reflect the true molar masses due to calibration with PMMA standards. In addition, SEC analysis of block copolymers can be inaccurate when the blocks have different polarities as well as different interactions with the column and the solvent. Due to overlapping peaks in the ^{1}H NMR spectra, however, it was challenging to accurately integrate the ratios of blocks using this method. The SEC data, where DMF was used as the eluent for both the macroinitiator and the block copolymers, were found to be more aligned with the expected theoretical molecular weights. A relative comparison of the block copolymer compositions was therefore made based on SEC data.

Table 4.3 PVP-b-PVL block copolymers of varying block ratios

BCP	BCP composition	M$_{n,theoretical}$ [a] g·mol^{-1}	M$_{n,SEC}$ [b] g·mol^{-1}	Đ [c]
1	PVP$_{87}$-*b*-PVL$_{19}$	10 200	11 700	1.1
2	PVP$_{87}$-*b*-PVL$_{41}$	12 380	13 900	1.1
3	PVP$_{138}$-*b*-PVL$_{100}$	22 540	25 400	1.2
4	PVP$_{138}$-*b*-PVL$_{127}$	24 180	28 100	1.2
5	PVP$_{27}$-*b*-PVL$_{53}$	5880	8 300	1.1
6	PVP$_{138}$-*b*-PVL$_{346}$	35 010	41 400	1.2

[a] M$_{n,theoretical}$ = ([monomer]/[macroinitiator]) · ∝ · M$_{r,monomer}$ + M$_{r,macroinitiator}$ where ∝ is the gravimetric conversion
[b] M$_{n,SEC}$ is determined by SEC based on PMMA standards, eluent DMF
[c] Đ represents the dispersity, from SEC (M$_w$/ M$_n$)

PVP is exceptionally hygroscopic and should be thoroughly dried before use. When PDS-PVP-OH was attempted to be azeotropically distilled, however, ^{1}H NMR spectroscopy indicated that the protecting group had been removed likely due to the high temperatures needed for this procedure. A mild drying protocol for PVP was therefore developed, as was described for the PVL homopolymer, where the polymer was left to stir in DCM over activated molecular sieves for at least 24 h before the polymerisation took place, under a blanket of inert gas. After this time, the solution was transferred into a flame-dried polymerisation vial containing activated molecular sieves. In this way the use of a glovebox was avoided and reproducible block copolymers were synthesised with high purity and conversions. The work by Williams and Lawton[43] on the enhanced ability of activated molecular sieves to remove water compared to the conventional methods of distilling certain solvents such as THF, promoted this approach. This approach to synthesising the PVP-PVL block copolymer is considered successful as there are good agreements between the theoretical and SEC molar masses as well as low $Đ$ values.

e) ROP of α-allylvalerolactone

The ROP of α-allylvalerolactone (AVL) was catalysed by TBD (2 mol% relative to the monomer) as shown in Scheme 4.2 using the same conditions that were described for the synthesis of PVP-*b*-PVL. PVP-*b*-PAVL had proceeded to 76% conversion when the reaction was quenched after 5 min. PAVL formation is known to occur at similar rates to the formation of PVL.[33]
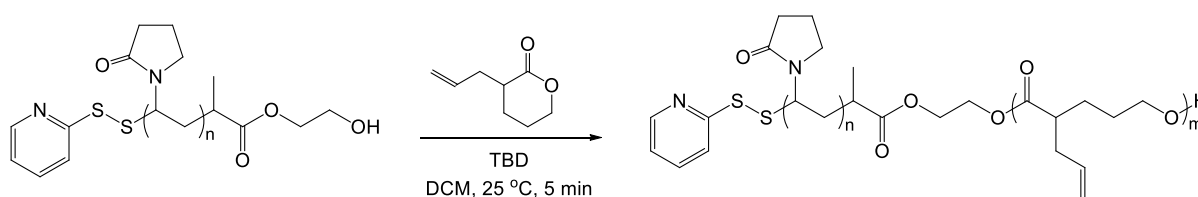
Scheme 4.2 ROP of AVL catalysed by TBD and initiated by the macroinitiator, PDS-PVP-OH.

Reasonably high monomer conversions (~70 %) and low $Đ$ values were obtained by using rigorously dried PVP macroinitiator and purified AVL monomer. Additionally, the attempts at achieving full conversion with the block copolymers by running the polymerisations over longer periods of time (hours) resulted in the broadening of the molar mass distribution curves resulting in higher $Đ$ values. This is presumably due to transesterification events occurring at high monomer conversions achieved at long reaction times.[44] The block copolymers were easily recovered and purified by several precipitations from methanol and ethyl acetate. The ^{1}H NMR spectrum of PVP-*b*-PAVL is shown in Figure 4.8, where the PDS groups are observed to remain intact (expansion in the region of 8.1 – 7.2 ppm). In Addendum G the monomodal molar mass distribution of PVP-*b*-PAVL is shown ($M_{n,\text{theoretical}}$ = 7800 g·mol^{-1}, $M_{n,\text{SEC}}$ = 9300 g·mol^{-1}, $Đ$ = 1.2).
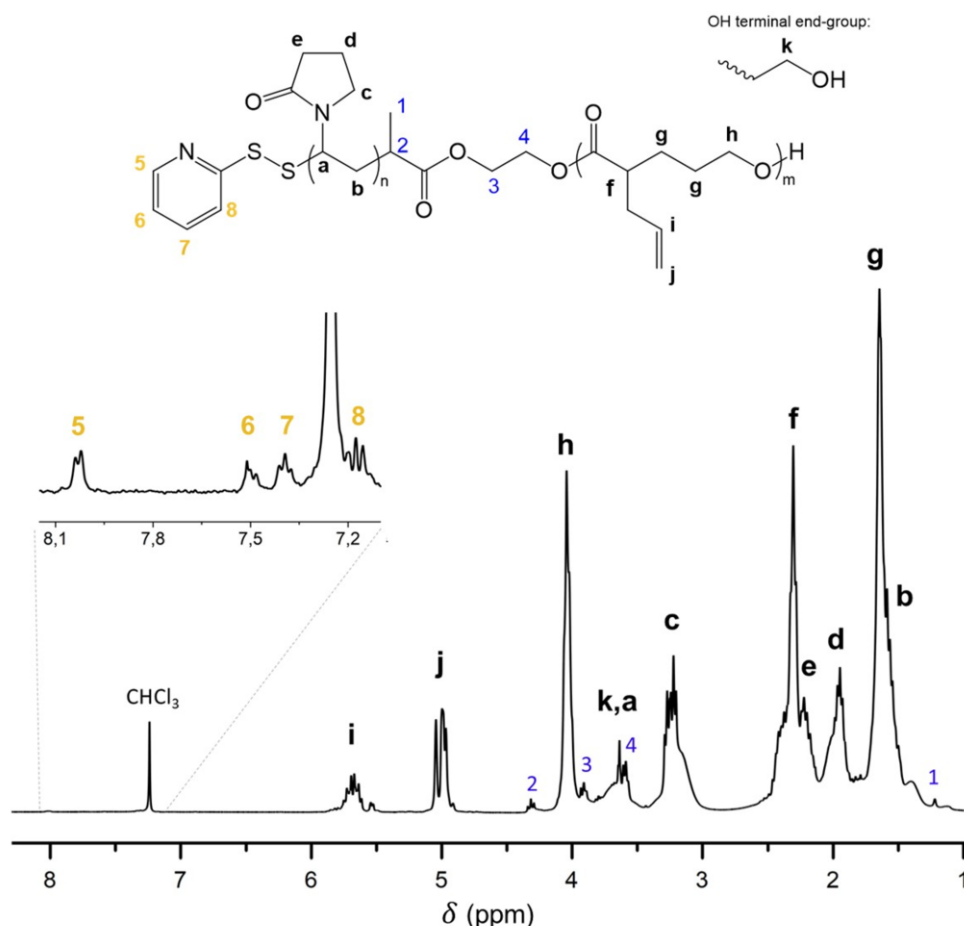
Figure 4.8 ^{1}H NMR spectrum of PVP-b-PAVL using PDS-PVP-OH as the macroinitiator and TBD as the organocatalyst.

4.2.2 Self-assembly

a) Self-assembly in water

The aqueous self-assembly behaviour of PVP-*b*-PVL was examined using block copolymers composed of varying block ratios (Table 4.3). Selective solvation leads to the arrangement of micelles with a core comprised of the insoluble block surrounded by a corona of the soluble block. Intrinsic parameters such as solubility, relative volume fractions and the lengths of the blocks of the block copolymer are important in determining the resulting structures.[3] The complexity of the system is enhanced when one block is semi-crystalline and additional parameters related to crystallinity need to be considered. PVP-*b*-PAVL was investigated in order to gain a full understanding of this block copolymer, however, it should be noted that in the PVP-PAVL block copolymer, PAVL is amorphous because the allyl groups make it stereoirregular.[33] Crystallinity therefore does not influence this block copolymer's self-assembly behaviour. The protocol for the self-assembly of the parent block copolymer is described in the Experimental section, but briefly, THF was used as a common solvent and upon complete dissolution, water was added at a slow, controlled rate. THF was then allowed to evaporate overnight through a needle made in the centre of the lid of a scintillation vial. TEM and DLS analyses were conducted at micelle concentrations of 0.5 mg·mL^{-1} in water.

Visually, the transparent organic solutions became opaque as a critical amount of the selective nonsolvent (water for PVL) was added to each vial. This is an early indication of micelle formation as the diameters of the micelles in water are large enough to diffract light, causing the cloudy appearance. DLS was then used as a rapid and convenient method to confirm that nanosized morphologies had been created. The hydrodynamic radii obtained from DLS, however, are derived using the Stokes–Einstein equation where particles are assumed to be spherical. In the instance where non-spherical morphologies are recorded, such an equation is invalid. For the purpose and scope of this study, however, it was useful in determining the size of spherical micelles in solution and for detecting the presence of multiple populations and large aggregates in solution before subsequent TEM analysis. The hydrodynamic diameters obtained from DLS (D_h, Table 4.4) indicate the presence of large and much smaller aggregates present in solution. It is important to note that DLS measures the intensity-weighted particle size distributions and therefore severely overestimates the true mole fraction of larger aggregates, possibly leading to larger than true dimensions.[45]

TEM analysis of the aqueous micelles self-assembled at room temperature revealed a range of nanomorphologies. Addendum H contains the TEM images obtained from the aqueous micelles self-assembled from BCP 1 – 6 in acetone and then in THF. Acetone was first used as the organic solvent for the PVP-PVL block copolymers and this led to the observation of spherically-shaped micelles of different diameters. The organic solvent was then changed to THF and this led to observations of a variety of micelle morphologies. It is not uncommon for the spherical morphology to occur across a range of block ratios.[45,46] This observation could be related to the solubility parameters of the block copolymer in each solvent. The series consisting of the block copolymers PVP_{138}-PVL_{100}, PVP_{138}-PVL_{127} and PVP_{138}-PVL_{346} makes it apparent that a dependence on the block ratio exists, as all other parameters during the self-assembly process were kept constant. Figure 4.9, 4.10 and 4.11 show the self-assembled structures of PVP_{138}-b-PVL_{100} (higher curvature), PVP_{138}-b-PVL_{127} (medium curvature) and PVP_{138}-b-PVL_{346} (lower curvature), respectively, after one day of ageing, one week of ageing and after one week of ageing with 10 min of sonication, using TEM analysis. The ageing process takes place after the slow evaporation of THF from the aqueous micelle media at room temperature.

After one day of ageing each sample, the higher curvature sample having a PVL wt. fraction (W_{PVL}) of 0.42 is observed to form a mixed morphology. Spherical micelles, lamellae (sheet) micelles and irregularly shaped cylindrical micelles are observed after this time (PVP_{138}-b-PVL_{100}, Figure 4.9 and magnified in Figure 4.12). The medium curvature sample with a W_{PVL} of 0.48 is observed to form ribbon-like micelles with a regular width of 12 ± 1.2 nm, seemingly composed of smaller spherical micelles (PVP_{138}-b-PVL_{127}, Figure 4.10 and magnified in Figure 4.12). Previous studies have corroborated the observation of having morphologies of lower curvature being composed of subunits of morphologies with higher curvatures,[45,47] in this example, spherical micelles. The curvature of the morphology generally follows spheres > cylinders > vesicles > lamellae and platelets. After one day of ageing, the sample with the greatest degree of hydrophobicity with a W_{PVL} of 0.71, was observed to form platelet-like ('lozenge' or 'bamboo-leaf' shaped) morphologies, with micelles of length 180 ± 15 nm and width

65 ± 5 nm observed along with spherical micelles. These results are fairly consistent with the trend of lower interfacial curvature morphologies being expected from the block copolymers with a larger proportion of hydrophobic block lengths.
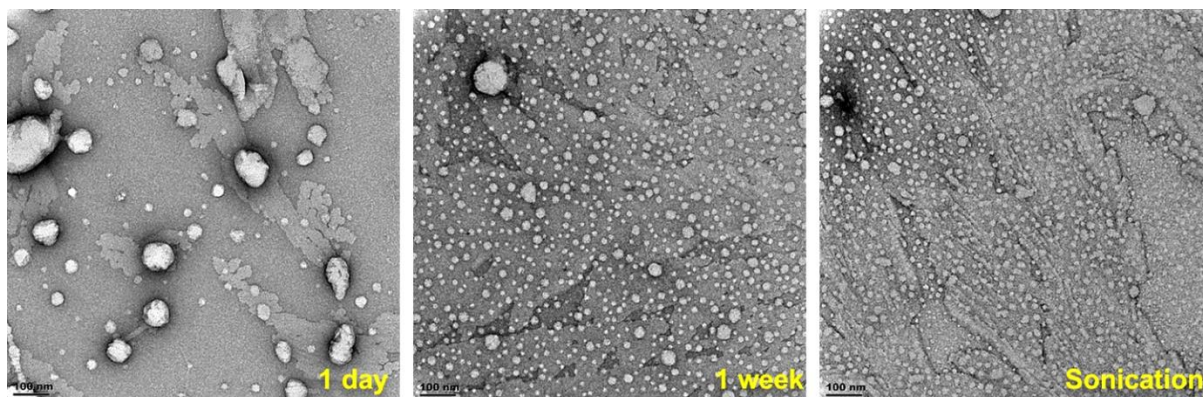
Figure 4.9 TEM images of micelles self-assembled from PVP$_{138}$-b-PVL$_{100}$ and aged for one day, one week and one week with sonication (10 min).
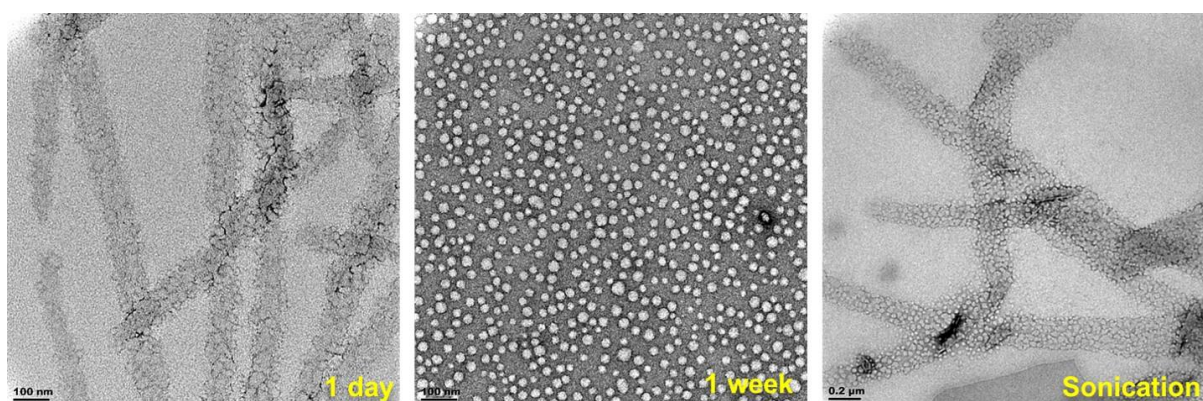
Figure 4.10 TEM images of micelles self-assembled from PVP$_{138}$-b-PVL$_{127}$ and aged for one day, one week and one week with sonication (10 min).
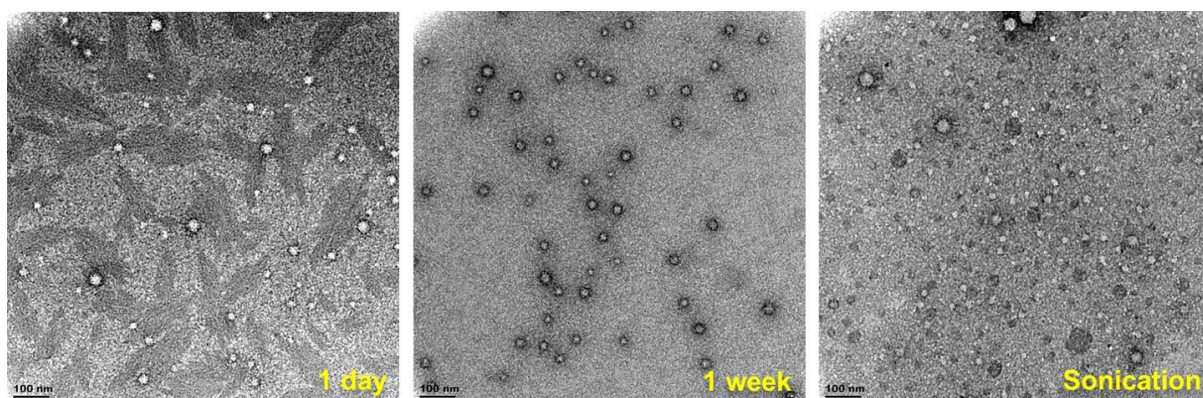
Figure 4.11 TEM images of micelles self-assembled from PVP$_{138}$-b-PVL$_{346}$ and aged for one day, one week and one week with sonication (10 min).
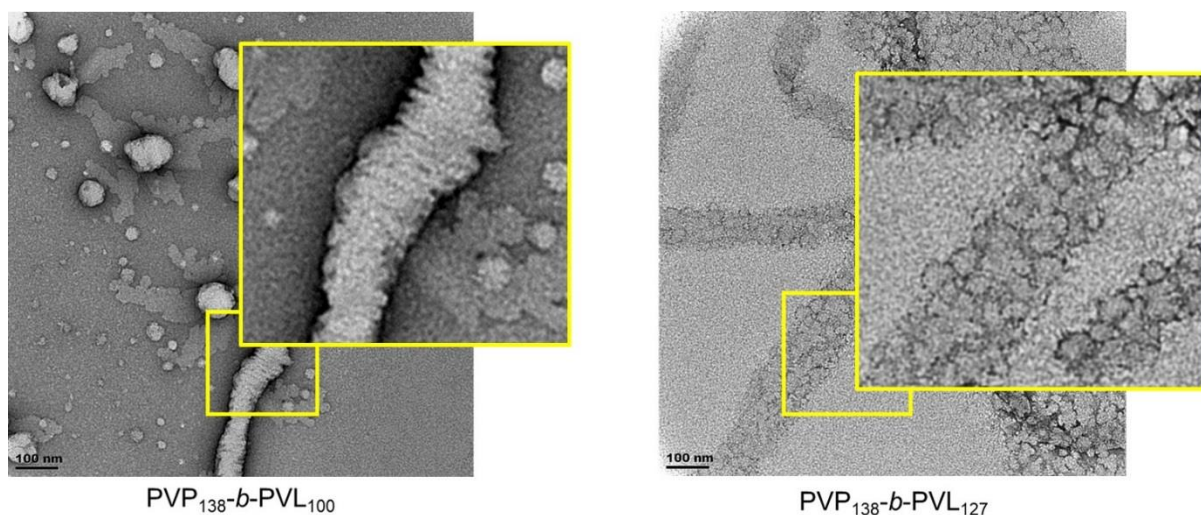
Figure 4.12 TEM images of micelles self-assembled from PVP$_{138}$-b-PVL$_{100}$ (left) and PVP$_{138}$-b-PVL$_{127}$ (right).

After one week of ageing, spherical micelles are observed to form for all samples in the series. This could occur above the original lamellae structures either from self-assembled unimers in the aqueous medium or as a result of the reorganisation of unimers in the self-assembled morphologies. After energy is added into the system by means of sonication, some surface roughage is observed in the form of cylindrical indentations for PVP$_{138}$-*b*-PVL$_{100}$ micelles after one week of ageing (Figure 4.9). Cylindrical micelles have been documented to pack lengthwise over time eventually creating lamellae structures for some systems.[3] These findings are corroborated in this work as the implementation of sonication would cause the reverse direction of micelle growth (micelle fragmentation) from smooth lamellae to lamellae with cylindrical micelle-like surface roughage. After one week of ageing and sonication, the medium curvature sample is affected back into ribbon-like micelles (PVP$_{138}$-*b*-PVL$_{127}$, Figure 4.10). The lower curvature sample maintains its spherical morphology (PVP$_{138}$-*b*-PVL$_{346}$, Figure 4.11) although crater-like depressions are observed which could be as a result of displaced spherical micelles from the originally-formed lamellae. A negative staining technique was used during quantitative TEM analysis which would render the periphery of the micelles to be dark, contrasting with the core which is much lighter.

Any crystallisation which could occur over time as the micelle solutions are left to age, would cause a stiffening of the core-forming segment which would shift morphologies based on PVL's ability to crystallise. PVP$_{27}$-*b*-PVL$_{53}$ self-assembled micelles having a W$_{PVL}$ of 0.66 exhibit a lamellae micelle morphology along with spherical micelles (Figure 4.13). After one week of ageing a similar morphology is observed with fused cylindrical micelles being more apparent at the periphery of the lamellae, likely indicating that the lamellae are composed of cylindrical micelles. Sonication of the samples after one week of ageing does not significantly alter the morphology although similar morphologies are seen after sonication compared to after one day of ageing. The prevalence of spherically shaped micelles is also diminished. These lamellae micelles were observed across a range of samples so further investigation into the physical parameters of the block copolymers and block copolymer micelles was conducted in order to gain more insight.
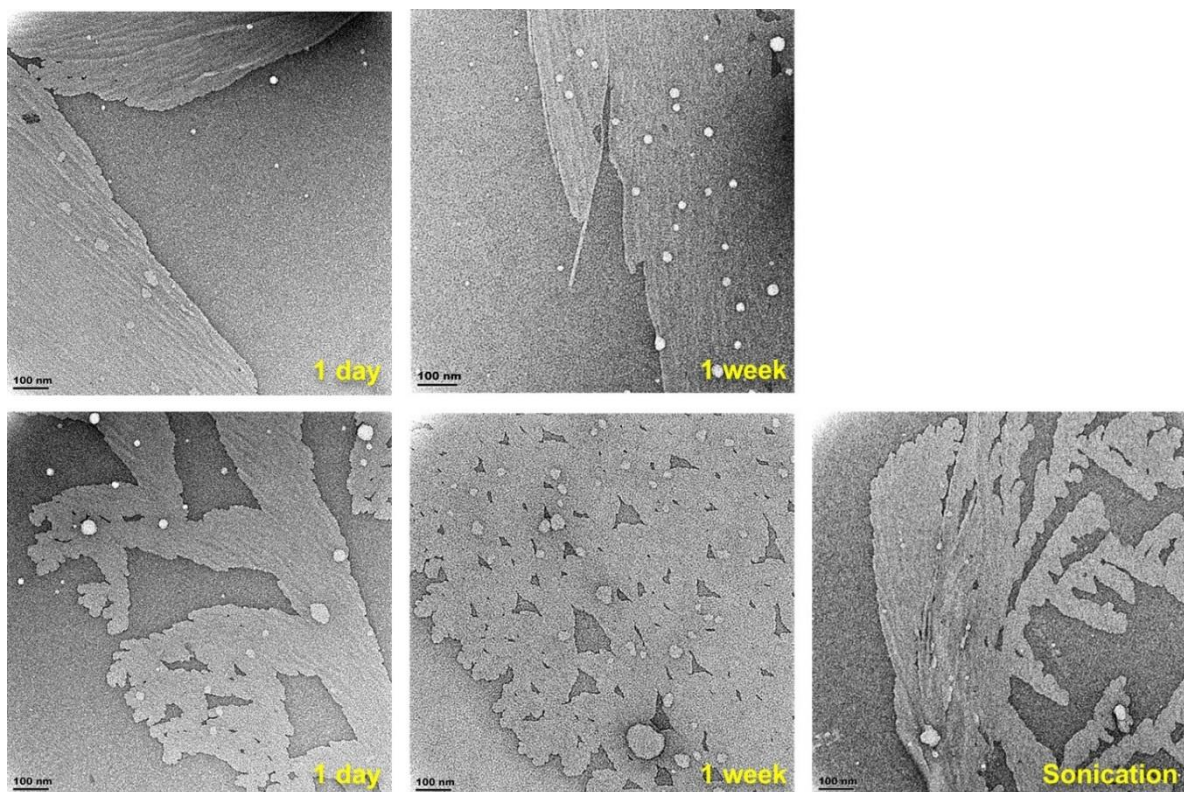
Figure 4.13 TEM images of micelles self-assembled from PVP$_{27}$-b-PVL$_{53}$ aged for one day, one week and one week with sonication (10 min).

To confirm that this room temperature self-assembly process is crystallisation driven, the thermal properties of the block copolymers and block copolymer micelles were analysed via DSC. The aqueous micelle suspensions were lyophilised for DSC analysis on the same day that TEM and DLS were conducted. The degree of crystallinity in each sample was estimated by comparing the enthalpies of fusion to the theoretical value of the enthalpy of fusion of 100% crystalline PVL as outlined in the Experimental section. The measurement of the degree of crystallinity is therefore an indirect method of estimating these values but provides a precise means of analysing each sample in relation to one another and the process that was conducted. Before the self-assembly process, the crystallinity of the PVL block in the block copolymers varied between 28 – 36 % and after, increased to 45 – 58% upon ageing of the micelles in water (%crystallinity, Table 4.4). A considerable increase in the %crystallinity therefore occurred after self-assembly had taken place.

P-XRD was used to collect the X-ray diffraction data of the PVL homopolymer, the block copolymer PVP$_{138}$-*b*-PVL$_{127}$ and the self-assembled PVP$_{138}$-*b*-PVL$_{127}$ micelles recovered after lyophilisation. The diffractograms are shown in Figure 4.14. The semi-crystalline structure of pristine PVL is closely related to its chain architecture. Two well resolved characteristic diffraction peaks for PVL are observed for all samples with the intense peak at $2\theta = 21.7^o$ and the weak one at $2\theta = 24.3^o$ which are assigned to the diffraction of the (110) and (200) lattice planes, respectively.[48] The crystallographic analysis of PVL reported by Furuhashi *et al.*[49] indicated that PVL crystallised with an orthorhombic unit cell structure. The crystal structure is in fact very similar to PCL which also has an orthorhombic unit cell structure.

The similarity is further exemplified by the values obtained from the specific volume of PVL crystals (0.840 cm$^3 \cdot$g^{-1}) compared to PCL crystals (0.833 cm$^3 \cdot$g^{-1}). It is likely that PVL has similar intrinsic flexibility and similar configurational entropy compared to PCL.[17] From literature, the melting curve of PVL is relatively sharp compared to other polylactones, signifying its high tendency towards crystallisation.[14,50]

When analysing the block copolymer of PVP and PVL in the bulk state and after self-assembly, the presence of less intense crystalline peaks of PVL at $2\theta = 10° - 15°$ disappear and this signifies that a more amorphous component has been included, *i.e.* PVP. PVP exhibits two broad peaks at approximately $2\theta = 13°$ and $21°$ related to its completely amorphous nature.[51] This would cause those less intense crystalline peaks to become less apparent along with the clear incidence of the amorphous halo. When comparing the XRD patterns of the homopolymer PVL, the block copolymer and micelles, it is found that the peak ratio of the (110) reflection to the (200) reflection ($A_{(110)}/A_{(200)}$) is 2.7 for the homopolymer, 1.8 for the block copolymer and 2.2 for the micelles after self-assembly. This demonstrates the significant decrease in the relative intensity of the (200) reflection from the PVL homopolymer upon PVP incorporation in the block copolymer. After self-assembly of this block copolymer and ageing, there is an increase in the relative intensity of the (200) reflection. This is an indication that crystallisation occurred along the (200) crystal plane. These results corroborate the degree of crystallinity estimations derived from DSC thermograms.
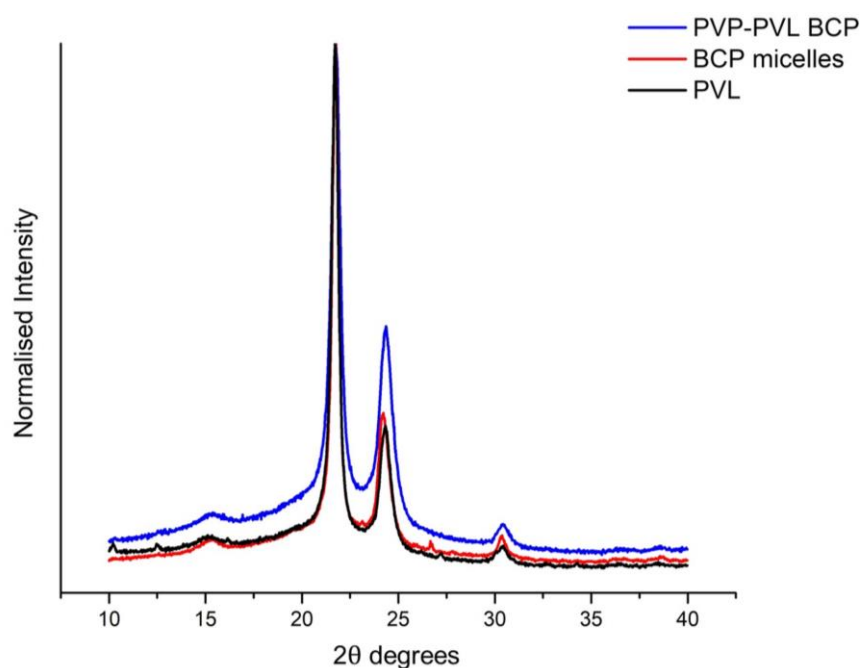
Figure 4.14 P-XRD patterns of bulk PVP$_{138}$-b-PVL$_{127}$ (blue), lyophilised micelles (red) and PVL homopolymer (black). The wavelength of X-ray (λ) is 1.54 Å.

Bragg's Law was used to calculate *d*-spacing values according to Equation 4.1, where *n* is an integer, *λ* is the wavelength of the incident X-ray, *θ* is the angle of incidence and *d* is the *d*-spacing value which is the interplanar spacing of the crystal.[52] The *d*-spacing of the (200) crystal plane was found to be less than that of the (110) crystal plane which shows that the PVL chains are closer here and the covalently linked PVP blocks are more crowded along this direction.

$$n\lambda = 2d\sin\theta \hspace{4cm} \text{Equation 4.1}$$

An analysis of some of the parameters pertaining to these block copolymers and block copolymer micelles are summarised in Table 4.4. After one week of ageing, all block copolymer micelles exhibited spherical morphologies which had likely formed above lamellae. For these spherical micelles, quantitative TEM analysis was applied to determine the diameters of the PVL core (d_{core}). The diameter of the PVL core was determined using negative staining (uranyl acetate, PVP: dark, PVL: bright). The number of PVL chains (aggregation number, N_{agg}) filling the sphere with a diameter of d_{core} can be estimated according to Equation 4.2.

$$N_{agg} = \frac{1}{6} \cdot \pi \cdot d_{core}^3 / (m_0 \cdot n / \rho_0 \cdot N_L) \hspace{3cm} \text{Equation 4.2}$$

In this equation, m_0 is the molecular weight of the monomer (100.12 g·mol^{-1}), *n* is the average number of lactone units, ρ_0 is the crystal density of PVL taken as 1.17 g·cm^{-3} from literature[53,54] and N_L is Avogadro's number. From the aggregation number, the distance *b* between neighbouring chains at the core-corona interface can be estimated from Equation 4.3. [55,56]

$$b = (\pi \cdot d_{core}^2 / N_{agg})^{0.5} \hspace{4cm} \text{Equation 4.3}$$

A graphical representation of these parameters is shown in Figure 4.15. The micelles self-assembled from block copolymers with varying PVL contents in the PVP$_{138}$ series are largely observed to form spherical morphologies after one week of ageing in water at room temperature. The aggregation numbers increased slightly with increasing PVL chain lengths from the higher curvature sample to the lower curvature sample. High aggregation numbers are related to more densely populated micelles with small distances between neighbouring chains. The aggregation number for those micelles self-assembled from PVP$_{138}$-*b*-PVL$_{127}$ are higher than expected. This sample exhibited the least stable morphological state because sonication caused the spherical micelles (resulting after one week of ageing) to revert back to ribbon-like micelles (resulting after one day of ageing) after 10 minutes of sonication. For the other samples, sonication had a much less pronounced effect. The ribbon-like micelles were observed to be composed of spherical micelles so it could be that the external morphological construct of the ribbons caused densely populated spherical micelles to form.
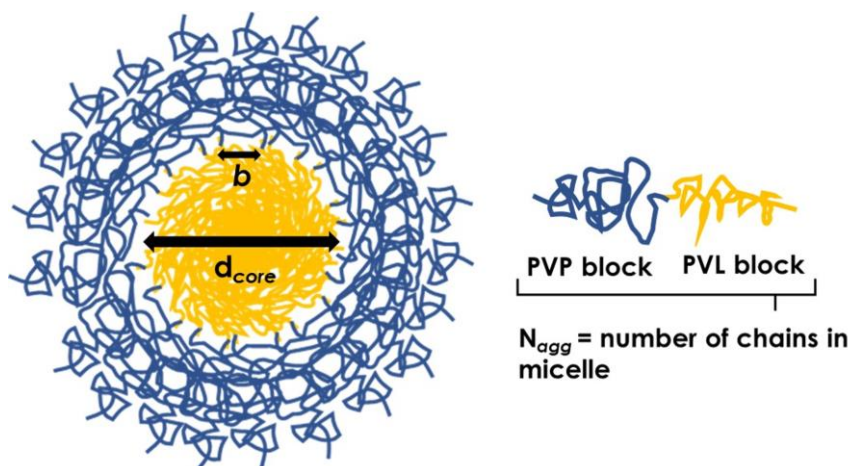
Figure 4.15 Graphical depiction of a block copolymer micelle with parameters including the aggregation number (N_{agg}), the interchain distance (b) and the diameter of the PVL core (d_{core}).

Table 4.4 Characteristics of PVP-PVL block copolymers and block copolymer micelles

BCP composition	W_{PVL}	Crystallinity [a] %	D_h [b] nm	d_{core} [c] nm	N_{agg} [d]	b [e] nm
PVP_{138}-b-PVL_{100}	0.42	$28 \rightarrow 45$	82	15.6 ± 5.8, 65.2 ± 4.1	570	1.2
PVP_{138}-b-PVL_{127}	0.48	$30 \rightarrow 47$	109	21.3 ± 3.4	610	1.5
PVP_{138}-b-PVL_{346}	0.71	$44 \rightarrow 63$	130	56.2 ± 3.2	600	4.1
PVP_{27}-b-PVL_{53}	0.66	$36 \rightarrow 58$	827	-	-	-

[a] The crystallinity of PVL in the BCPs and $\rightarrow$ BCP micelles was determined using DSC

[b] The hydrodynamic diameter ($D_h = 2 R_h$) was determined by DLS after 1 week ageing

[c] The diameter of the PVL core of micelles was determined by TEM analysis of 100 particles

[d] N_{agg} is the aggregation number of the chains forming the spherical crystalline micelles

[e] b is the distance between neighbouring chains at the core-corona interface of the micelles

A number of key processes could describe the formation of these crystalline-coil micelles. It could be that microphase separation occurs due to the effect of solvent quality over shorter timescales. Morphological transitions likely occur due to the competition between the stretching of the soluble block (PVP) and the crystallisation energy of the core-forming block (PVL) which would determine the initial micellar shape boundaries. Adjunct to improving the solvation conditions of the core-forming block, it is also believed that an initially low crystallinity of the newly-formed micelles is responsible for the rearrangement and recrystallisation events to take place. This is likely the case as the initial block copolymer degrees of crystallinity were estimated to be low in relation to the self-assembled structures. Crystallisation takes place over longer timescales compared to microphase separation. In this instance it is likely due to hierarchical assembly, where equilibrium structures may be created from the reorganisation and recrystallisation of kinetically trapped metastable crystalline micellar morphologies. These metastable structures which were formed at an earlier stage in core crystallisation can undergo aggregation either by fusion or coalescence, which is accompanied by a secondary crystallisation which ultimately has preference for the arrangement of more stable structures. It is clear that lamellae micelles

occur over short periods of time, relating to the high crystallisation ability of PVL, and that different forms of energy might needed to fragment these micelles as they are highly stable.[3,57,58]

b) Inducing morphological transitions

A short study was conducted on the ability of certain external stimuli to induce micellar morphological transitions. The investigation of these transformations is important as they would provide opportunities to tailor existing self-assembled structures to suit particular applications. The formation of cylindrical micelles is of particular interest in the biomedical field, as this morphology has been shown to exhibit improved circulation times *in vivo* as well as different cellular internalisation pathways compared to spherical micelles.[6,7] The CDSA of BCPs was thought to be unidirectional and irreversible due to the vitrification effect of crystallisation. This was later refuted as it was found that bidirectional transformations could occur, which conveniently leads to flexible applications of BCP micelles created through CDSA. To reverse the direction of micelle growth (induce micelle morphology fragmentation), work has been focused on intensive forms of external stimuli, such as sonication, heating and hydrogen bonding.[3] Here, a novel and less-intensive external stimulus was found to induce micelle fragmentation in the form of freeze-thawing.

A low temperature study was conducted on the micelles self-assembled from PVP_{27}-*b*-PVL_{53} using TEM analysis. The sample was aged for one week at room temperature to allow for the formation of lamellae micelles and after this had occurred, the sample was aged at -10 °C in a freezer for one month. After this time, cylindrical micelles monodisperse in length (65.3 ± 8 nm) and width (11.1 ± 2 nm) were observed, as shown in Figure 4.16. A small number of spherical micelles (approximately 0.5% relative to cylindrical micelles) were observed in the samples (diameter 11.7 nm ± 3 nm).
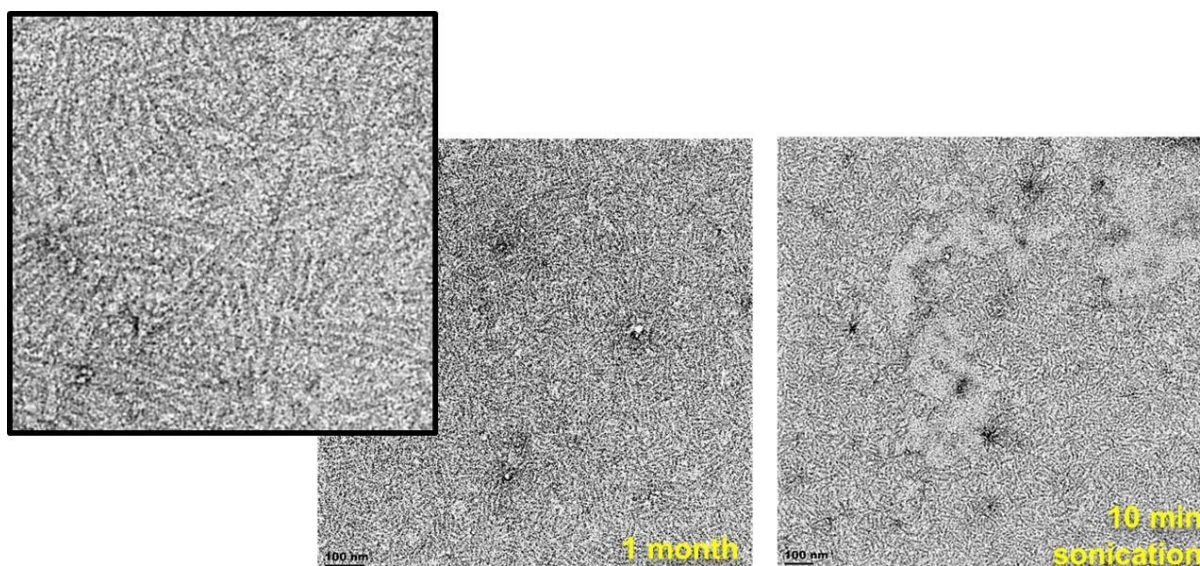
Figure 4.16 TEM images of micelles self-assembled from PVP_{27}-b-PVL_{53} after room temperature ageing for one week and -10 °C ageing for one month (left) and this sample after 10 min sonication (right).

The same sample aged for one month at room temperature was not found to form these cylindrical structures, as only consolidated lamellae were observed (Addendum I). After 10 min of sonication, certain areas between the cylindrical micelles separate whilst other areas remain relatively unchanged. It is likely that the freeze-thaw process caused enough stress to the lamellae micelles to spur the reorganisation events which led to the formation of cylindrical micelles. The freeze-thaw process is potentially a new method for effecting morphological transitions from lamellae micelles to cylindrical micelles. This method is highly beneficial because it does not require the use of additives or sophisticated laboratory processes such as sonication. The simplicity of this method lies in the fact that the sample is merely frozen and thawed in order to achieve the transformation. The results are reproducible and the cylindrical micelles obtained are uniform in width and length. Current work is focussed on the investigation into the mechanism of this transformation, and the ability to control the lengths of the cylindrical micelles by exploring different freeze-thaw conditions and methods.
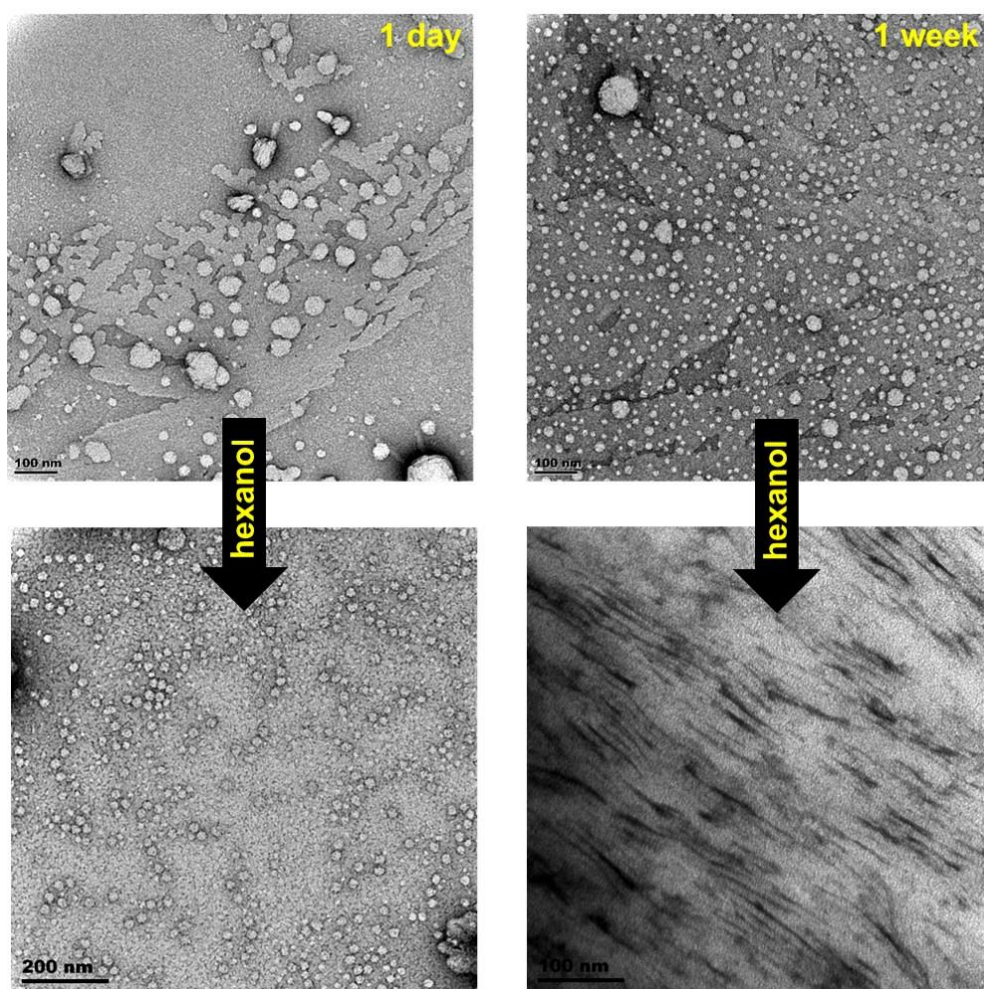
Figure 4.17 TEM images of mixed lamellae of PVP-b-PVL a) aged for one day with the addition of hexanol became more monodisperse and spherical and b) aged for one week and with the addition of hexanol became more monodisperse and cylindrical (additive 10% v/v of solvent).

Following the freeze-thaw method, hydrogen bonding was investigated as the external stimulus to induce micellar morphological transitions. It has been reported that hydrogen bonding is able to modify the self-assembled morphologies of amorphous block copolymers.[59] More recently, small organic molecules such as phenol, salicylic acid and other H-bond donors have been discovered to prompt morphological transformations in crystalline core-containing block copolymer micelles in aqueous solutions, where PEO- and PCL-based systems have been studied with regard to these effects.[60–63] This method was applied to PVP-PVL block copolymer micelles as a way in which to regulate the highly stable lamellae micelles which were often observed to form in aqueous media at room temperature. TEM was used to visualise the effect that the additive 1-hexanol (hexanol) had on PVP_{138}-b-PVL_{100} self-assembled micelles that were aged for either one day or one week (Figure 4.17).

Upon addition of hexanol, either monodisperse spherical or cylindrical micelles were observed indicating that fragmentation of the lamellae had occurred. A degree of order is observed in the system through the addition of hexanol. In this study, the ageing time of the micelles preceding additive addition was found to dictate whether the formation of spherical or cylindrical micelles occurred. To target cylindrical micelles, a longer ageing time is required (one week) compared with the formation of spherical micelles, where a shorter ageing time is required (one day), preceding hexanol addition. It was therefore shown in this study that the ageing time of the sample can be a complementary tool in the use of additives in micelle fragmentation.

Hexanol is commonly used as a solvent for the growth of single crystals from PCL[55] which has similar solvation characteristics to PVL and signifies that hexanol is able to partially solubilise the core. Improving the solvation conditions of the core-forming block is believed to be one of the driving forces to spur rearrangement and recrystallisation events. Besides these hierarchical events, H-bonding is thought to be responsible for the initial disruption of crystallinity, causing lamellar or cylindrical structures to revert back to elongated or spherical structures preceding reorganisation into monodisperse morphologies. Hexanol has one H-bond site, *i.e.* its hydroxyl functionality, which is able to bind to the polymer chains in the micelle and cause stress to the core. In this way, the fragmentation of micelles (in the reverse direction) takes place.

This effect has not yet been investigated for PVL and was explored by analysing FTIR spectra and XRD diffractograms before and after mixing with hexanol and ageing for 24 h (Figure 4.18). Figure 4.18 a) shows the FTIR spectra of PVL (above) and a mixture of PVL and hexanol (below) fit with Lorentz functions. For pristine PVL, the main peak and shoulder peak are indicative of the carbonyl groups in the crystalline and amorphous regions, respectively.[64] An additional shoulder peak is observed in the FTIR spectrum of PVL + hexanol at 1656 cm^{-1} after mixing and ageing, which is attributed to the H-bonded carbonyl groups of PVL.
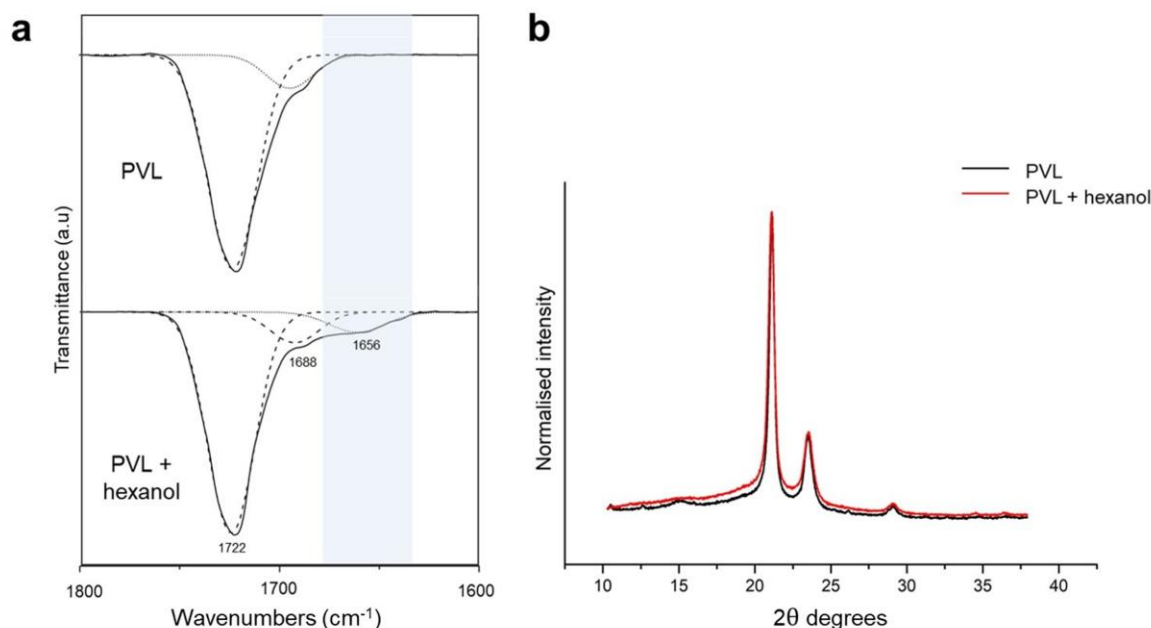
Figure 4.18 a) FTIR spectra and b) P-XRD patterns of PVL and the PVL + hexanol mixture.

The apparent decrease in crystallinity was then confirmed using P-XRD as seen in Figure 4.18 b), where the addition of hexanol is clearly observed to increase the broad amorphous halo. Deconvolution of these peaks indicated that the crystallinity of the sample decreased by approximately 3% after the addition of hexanol. Only a small reduction in crystallinity is calculated after 24 h which attests to the slow disassembly process of the micelles in hexanol. This is corroborated by observing the FTIR peak corresponding to crystalline PVL which remains largely unchanged before and after mixing. Hexanol is therefore able to disrupt the crystallisation process without completely eradicating the crystalline structure of the homopolymer and therefore the block copolymer micelles. Moreover, we are able to selectively target specific morphologies based on the amount of time that the block copolymer micelles are allowed to age in water at room temperature. Over short periods of time (one day), the addition of hexanol affected the morphological shift to the appearance of monodisperse spherical micelles. Over longer periods of time (one week) the addition of hexanol affected the morphological shift to the appearance of monodisperse cylindrical micelles.

c) Self-assembly in ethanol

PVP-*b*-PVL was dissolved in ethanol by annealing the block copolymer at 60 °C. The self-assembly kinetics were monitored using TEM. Arno *et al.* showed that 1D cylindrical and 2D platelet micelles were obtained from the epitaxial growth of PCL-*b*-PDMA block copolymers.[65] When the polymer system of PVP-*b*-PVL was investigated, however, a dynamic process was recorded where butterfly-like morphologies were observed after only 1 h of ageing (PVP$_{138}$-*b*-PVL$_{100}$, Figure 4.19). With time, all surfaces of these structures developed cylindrical indentations. The butterfly morphologies seem to coalesce after 24 h of ageing in ethanol and seem to separate after 3 days of ageing. After one month the individual morphologies become large conjoining lamellae, and with even more time are observed to form 'stacks' (Figure 4.19, 2 months). The partitioning and coalescence of the structures were

observed to occur over similar periods of time for different samples. In order to obtain individual butterfly micelles, it is recommended to age the sample in ethanol for four days. After this time the micelles can be dialysed against water to remove ethanol and can be recovered using lyophilisation. The micelles maintained their morphology in water after one month of ageing in water indicating that the removal of ethanol in an excess of water followed by lyophilisation (Addendum J). Moving from water to ethanol would have the effect of kinetically trapping the butterfly morphology, since water has a higher enthalpy penalty for interactions with the core-forming block.
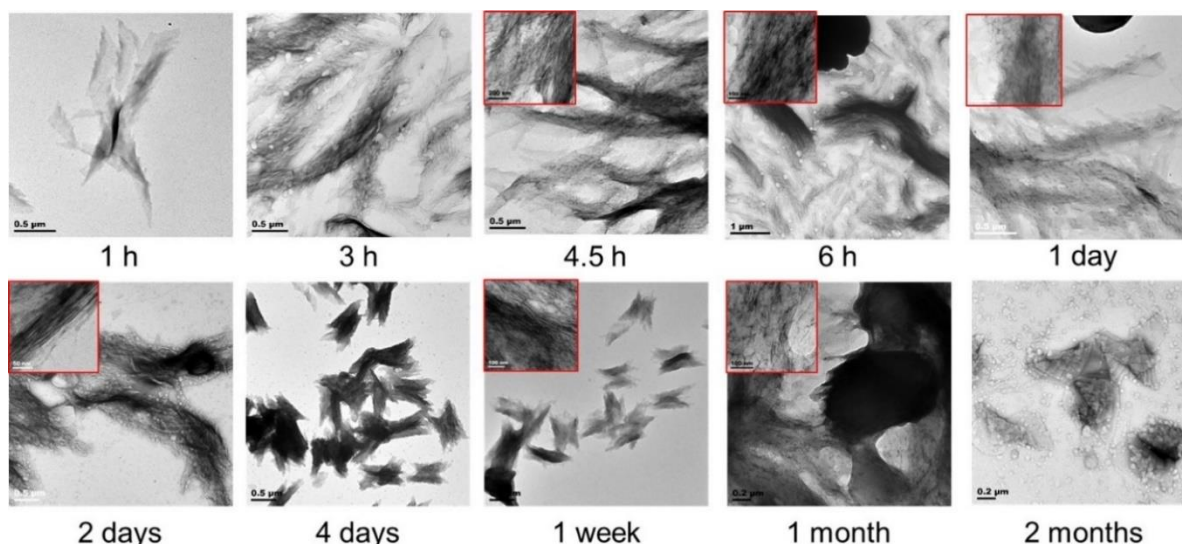
Figure 4.19 TEM images showing the kinetic progression of PVP$_{138}$-b-PVL$_{100}$ structures in ethanol.

4.3 Conclusions

In this chapter the foundations were laid for the formation of the block copolymer necessary to act as the carrier for the antimalarial drug combination artemether-lumefantrine. An important goal was to synthesise a carrier system which had the necessary potential for future incorporation of drug delivery components. After PVP-OH was synthesised, the thiol was protected using PDS to ensure that it would not interfere with subsequent ROP and post-polymerisation modification reactions. Moreover, the protected thiol should provide an avenue for the bioconjugation of the targeting ligand. The allylated lactone, AVL, was synthesised so as to provide a pathway for the conjugation of lumefantrine post-polymerisation. The ROP of AVL was catalysed by TBD and initiated by PDS-PVP-OH to synthesise the block copolymer PVP-*b*-PAVL, where the PDS groups remained intact. To synthesise PVP-*b*-PAVL, the organocatalysts DBU + TU and TBD were first applied to the ROP of VL, which served as a model study. TBD was chosen as the organocatalyst instead of DBU + TU because of the greater certainty over the end-group fidelity, as well as faster polymerisation kinetics, *i.e.* quantitative monomer conversions in less than a minute.

Furthermore, the self-assembly of the parent block copolymer of PVP-*b*-PVL was studied because it has not been explored in literature with regard to CDSA. It is known that the complexity of self-assembled systems is enhanced when one block is semi-crystalline. Using THF as the good solvent

and water as the selective solvent at room temperature, a range of nanomorphologies were observed. The amount of time that the micelle solutions were allowed to age largely dictated their resulting morphologies which by large and eventually, preferred to adopt mixed morphologies consisting of lamellae and spherical micelles. This feature was used as an advantage when the additive hexanol was applied for its H-bonding ability with the core-forming block, PVL. The addition of hexanol imparted a degree of order into the micellar systems to render monodisperse spherical or cylindrical micelles. Moreover, a novel method was developed to induce micellar morphological transitions from lamellar to cylindrical micelles in the form of the freeze-thaw process. This method is highly beneficial because of its simplicity, as it does not require the use of additives or sonication. The results are reproducible and the cylindrical micelles obtained are fairly uniform in width and length.

Another advantage to this system is the prevalence of the PDS groups attached to the PVP blocks in micelles self-assembled from PVP-*b*-PVL, which is easily prepared. These PDS groups can be bioconjugated to a slew of ligands thus positioning this system for its potential use in a range of applications. This block copolymer holds exciting prospects for further research in the study of high aspect micellar morphologies and the influence that they may have on the classical drug delivery facets such as drug loading, micelle stability, cellular uptake and therapeutic activity.

4.4 Experimental

4.4.1 General details

Triethylamine (≥99.5%, Sigma-Aldrich), diisopropylamine (≥99%, Sigma-Aldrich), *n*-butyllithium (2.5 M in hexanes, Sigma-Aldrich), δ-valerolactone (technical grade, Sigma-Aldrich), allyl bromide with ≤1000 ppm propylene oxide as stabiliser (97%, Sigma-Aldrich), hexamethylphosphoramide (99%, Sigma-Aldrich), 2,2'-dipyridyldisulfide (98%, Sigma-Aldrich), ethanolamine (≥98%, Merck), 1-pyrenemethanol (98%, Sigma-Aldrich), phenol (≥99.5%, Sigma-Aldrich), 1-hexanol (98%, Sigma-Aldrich), sodium chloride (≥99.0%, Sigma-Aldrich) and ammonium chloride (≥99.5%, Merck) were used without further purification. 1,5,7-triazabicyclo[4.4.0]dec-5-ene (98%, Sigma-Aldrich) was dried in a vacuum oven at 25 °C for 24 h before use and 1,8-diazabicyclo[5.4.0]undec-7-ene (98%, Sigma-Aldrich) was distilled before use and stored over activated 3 Å molecular sieves until needed. Other solvents such as ethanol, acetone, diethyl ether and ethyl acetate were purchased from Kimix and the ice-bath component ethylene glycol from ReAgent was used without further purification. Reaction grade THF and acetonitrile were purchased from Sigma-Aldrich and the former was passed through a basic alumina column and kept over 3 Å molecular sieves for 24 h prior to the synthesis reaction. Dichloromethane was purchased from Kimix, distilled prior to ROPs and stored over activated 3 Å molecular sieves until needed. Distilled, deionised water was obtained from a Millipore Milli-Q purification system. Thiourea ($C_{33}O_3F_{18}N_7H_{27}$) was kindly prepared according to literature[66] by Shane van Wyk in our research group. Hydroxy-functional poly(*N*-vinylpyrrolidone) (PVP-OH, $M_{n,NMR}$ = 3900 g·mol⁻¹, $M_{n,SEC}$ = 4000 g·mol⁻¹, Đ = 1.1) was synthesised as per PVP-X2 using RAFT-X2 as

detailed in Chapter 3. The NMR solvents used were $CDCl_3$ (99.9%, Aldrich), DMSO-d_6 (99.9%, MagniSolv) and D_2O (99.9%, MagniSolv).

^1H spectra were obtained with a Varian VXR-Unity spectrometer (400 MHz unless stated otherwise) with samples dissolved in deuterated solvents with tetramethylsilane (TMS) as internal reference. MestreNova 11.0.4 software was used to process the spectra. LC-MS was conducted using a Waters Synapt G2 with electron spray ionisation (ESI) in the positive mode using a Waters UPLC C18 column of dimensions 2.1 × 100 mm. SEC data were obtained from a Shimadzu LC-10AT isocratic pump, a Waters 717+ autosampler, a column system fitted with a PSS guard column (50 × 8 mm) in series with three PSS GRAM columns (300 × 8 mm, 10 μm, 2 × 3000 Å and 1 × 100 Å) kept at 40 °C, a Waters 2487 dual wavelength UV detector and a Waters 2414 differential refractive index (DRI) detector. DMF was used as eluent, stabilised with 0.05% 2,6-di-*tert*-butyl-4-methylphenol (BHT) and 0.03% LiCl (w/v) at a flow rate of 1 mL·min^{-1}. The calculated molar masses were relative to poly(methyl methacrylate) (PMMA) calibration standards (Polymer Laboratories) ranging from 690 to 1.2×10^6 g·mol^{-1}. Data acquisition was performed using Millennium software version 4. DLS was conducted to determine the particle size and particle size distribution of the block copolymers using a Malvern Instrument ZetaSizer Nano ZS90 equipped with a 4 mW He-Ne laser, operating at a wavelength of 633 nm. The scattered light was detected at a scattering angle of 90° at 25 °C or 37 °C. The final particle size and size distribution were obtained from three measurements, each comprising 10 – 15 sub-runs, and calculated via the Malvern Zetasizer software. TEM analysis was conducted to observe the morphology of the self-assembled block copolymers. The samples were imaged using the Tecnai 20 transmission electron microscope (Thermo Fisher) fitted with a LaB$_6$ emitter and operating at 200 kV and a Gatan Tridiem 863 UHS (Gatan). The images were collected using the embedded Gatan CCD camera (2048 × 2048 pixels). A drop of the sample solution was deposited onto a copper grid and dried at room temperature. The samples were negatively stained with uranyl acetate. ImageJ software was used for nanomorphology measurements where 100 micelles were measured to record the average and standard deviation. P-XRD was conducted using a Siemens D8 Advance diffractometer using Cu Kα radiation (λ = 1.54 Å) operated at 40 kV and 30 mA. Diffractograms were recorded in the range 10 - 40° (2θ) with a scan step of 0.015°. Care was taken to ensure uniform packing in the sample holder. The analysis software X'pert HighScore Plus and Orgin Pro were used to analyse the data. ATR-FTIR was performed using a Nexus infrared spectrometer equipped with a Smart Golden gate attenuated total reflectance diamond from Thermo Nicolet with ZnSe lenses and data acquisition was conducted using Omnic Software version 7.2. The absorbance peaks were deconvolved using Origin Software with multiple Lorentz functions. DSC measurements were recorded on a TA Instruments Q100 DSC. The instrument was calibrated using indium standards with a standard cooling and heating rate of 10 °C min^{-1} over a temperature range of -25 – 220 °C. Three cycles of data were acquired and the second cycle was used to determine the degree of crystallinity. Samples of 3 mg were prepared for analysis in aluminium pans. The data were analysed using the TA Universal Analysis program and the degree of crystallinity was determined using Equation 4.4,[67] where χ_C is the degree of crystallinity, ΔH_m is the

enthalpy of fusion of PVL and $\Delta H_{100\%}$ is the enthalpy of fusion of 100% crystalline PVL taken as 144 J·g^{-1} from literature.[14]

$$\chi_C = \Delta H_m / \Delta H_{100\%} \hspace{4cm} \text{Equation 4.4}$$

4.4.2 Synthetic procedures

4.4.2.1 Synthesis of α-allylvalerolactone monomer

The synthesis of α-allylvalerolactone (AVL) was conducted as previously reported by Parrish *et al.*[33] with adjustments. Briefly, diisopropylamine (4.6 mL, 0.033 mol) was added to THF (250 mL) in a flame-dried 3-neck RBF under argon, in an acetone/dry ice cooling bath held constant at -78 °C. Following this, standard air-tight techniques were used to transfer *n*-butyllithium (20.6 mL, 0.033 mol) to the solution via a degassed air-tight syringe and this was stirred for 15 min to form lithium diisopropylamide *in situ*. The cyclic ester, δ-valerolactone (VL) (2.8 mL, 0.033 mol) was slightly thawed and added dropwise over 30 min, and the mixture was allowed to stir for 1 h. A solution of allyl bromide (3.1 mL, 0.036 mol) in hexamethylphosphoramide (6.3 mL, 0.036 mol) was pre-cooled over an ice bath containing NaCl and was added dropwise to the reaction vessel via a syringe. A different cooling bath containing a ratio of ethylene glycol and ethanol in dry ice at a temperature of -40 °C then replaced the previous cooling bath and the mixture was left to stir for 4 h. After this time, a saturated solution of NH$_4$Cl (1 mL) was used to quench the reaction and the reaction vessel was warmed to room temperature by removing it from the cooling bath. The volatiles were then removed via rotor evaporation and the crude was dissolved in diethyl ether, washed with brine and concentrated under reduced pressure. The process was repeated with hexane as the organic phase. The product was purified by column chromatography (hexane / ethyl acetate, 6:1) and vacuum distilled (95 °C) to produce a colourless, viscous liquid with the distinct aroma of peppermint and pinecones. Yield = 65% ^{1}H NMR (600 MHz, Chloroform-d) δ (ppm) 5.77 (m, 1H), 5.09 (m, 2H), 4.28 (m, 2H), 2.55 (m, 2H), 2.28 (m, 1H), 2.08 (m, 1H), 1.89 (m, 2H), 1.56 (m, 1H). ^{13}C NMR (400 MHz, CDCl$_3$) δ (ppm) 173, 135, 118, 69, 39, 36, 25, 22. MS (ESI): m/z = 141.09 (calculated: 141.19 for [M + H]$^+$).
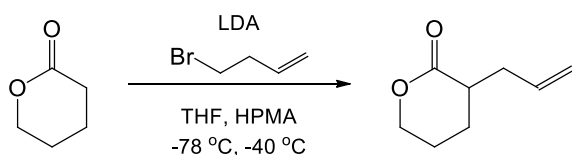
Scheme 4.1 Synthesis of monomer α-allylvalerolactone.

4.4.2.2 Pyridyl disulfide-protection of PVP

The synthesis of pyridyl disulfide (PDS)-protected PVP (PDS-PVP-OH) was conducted as per the method described by Shi *et al.*[68] Briefly, PVP-OH (0.1 g, 2.56 × 10^{-5} mol) and 2,2'-dipyridyl disulfide (84.6 mg, 2.56 × 10^{-4} mol) were added to a Schlenk flask and acetonitrile (2.5 mL) was added. The solution was degassed thoroughly with multiple freeze-pump-thaw cycles until the presence of oxygen

bubbles upon thawing was no longer observed. Separately, ethanolamine (15.6 mg, 2.56×10^{-4} mol) and acetonitrile (0.5 mL) were degassed by bubbling with argon for 30 min, after which the solution was transferred to the Schlenk flask via a degassed, air-tight syringe. The Schlenk flask was left to stir at 25 °C for 6 h, upon which a colour change was observed from lightly tinged yellow to an orange hue. The solution was purified by precipitation in diethyl ether four times, dissolving in water and filtering. PDS-protected PVP was recovered by lyophilisation. $M_{n,NMR}$ = 3900 g·mol^{-1}, $M_{n,SEC}$ = 4000 g·mol^{-1}, $Đ$ = 1.1
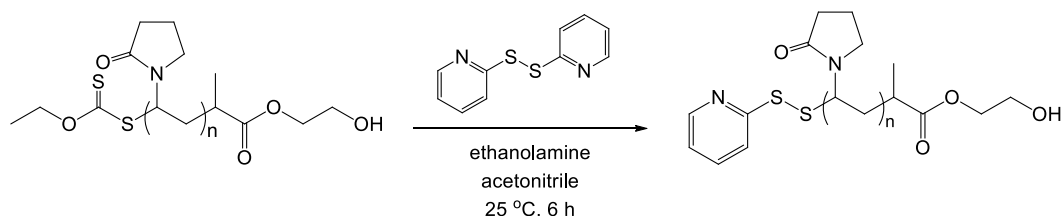
Scheme 4.3 Synthesis of PDS-terminated PVP-OH.

4.4.2.3 Synthesis of poly(δ-valerolactone) homopolymers

Typical procedures are described below for the homopolymerisation of VL.

a) ROP of δ-valerolactone with TBD

Under argon, VL (100 mg, 1.0×10^{-3} mol) and 1-pyrenemethanol (4.6 mg, 2.0×10^{-5} mol) were dissolved in DCM (0.5 mL) in a flame-dried pear-shaped reaction vial equipped with a magnetic stir bar and 3 beads of activated 3 Å molecular sieves. This mixture was stirred and thoroughly degassed for 0.5 h. Simultaneously, TBD (2 mol% of monomer) was degassed in DCM (0.2 mL). Following this, the TBD solution was transferred to the reaction vial via a degassed air-tight syringe under a positive argon gas flow at all times. Degassing was continued as the polymerisation was left to commence at 25 °C for 10 min. The resultant solidified polymer was diluted with DCM, quenched with benzoic acid (5 mg, 4.1×10^{-5} mol), withdrawn via pipette and precipitated in methanol. The white, solid powder was recovered via centrifugation (4000 rpm, 10 min) and dried in a vacuum oven overnight.

b) ROP of δ-valerolactone with DBU + thiourea

Under argon, in a flame-dried pear-shaped reaction vial were added successively, DCM (0.5 mL), VL (100 mg, 1.0×10^{-3} mol), thiourea (45.6 mg, 5.0×10^{-5} mol), DBU (7.6 mg, 5.0×10^{-5} mol), 1-pyrenemethanol (4.6 mg, 2.0×10^{-5} mol), a magnetic stir bar and 3 beads of activated 3 Å molecular sieves. The reaction mixture was left to stir at 25 °C for 3 h. The resultant solidified polymer was diluted with DCM, quenched with benzoic acid (5 mg, 4.1×10^{-5} mol), withdrawn via pipette and precipitated in methanol. The white, solid powder was recovered via centrifugation (4000 rpm, 10 min) and dried in a vacuum oven overnight.

4.4.2.4 Synthesis of PVP-*b*-PVL and PVP-*b*-PAVL block copolymers

Typical procedures are described below for the homopolymerisation of VL and AVL.

a) ROP of δ-valerolactone and α-allylvalerolactone with TBD

Under argon, VL (100 mg, 1.0×10^{-3} mol) or AVL (140.2 mg, 1.0×10^{-3} mol) and the PDS-PVP-OH macroinitiator (56 mg, 1.4×10^{-5} mol) were dissolved in DCM (1 mL) in a flame-dried pear-shaped reaction vial equipped with a magnetic stir bar and 3 beads of activated 3 Å molecular sieves. This mixture was stirred and thoroughly degassed for 0.5 h. Simultaneously, TBD (2 mol% of monomer) was degassed in DCM (0.2 mL). Following this, the TBD solution was transferred to the reaction vial via a degassed air-tight syringe under a positive argon gas flow at all times. Degassing continued as the polymerisation was left to commence at 25 °C for 10 min. The resultant solidified polymer was diluted with DCM and quenched with benzoic acid (10 mg, 8.2×10^{-5} mol). The block copolymer was purified by precipitation in methanol followed by ethyl acetate. The white, solid powder was recovered via centrifugation (4000 rpm, 10 min) and dried in a vacuum oven overnight.

b) ROP of δ-valerolactone with DBU + thiourea

Under argon, in a flame-dried, pear-shaped reaction vial were added successively, DCM (0.5 mL), VL (100 mg, 1.0×10^{-3} mol), thiourea (45.6 mg, 5.0×10^{-5} mol), DBU (7.6 mg, 5.0×10^{-5} mol), PDS-PVP-OH macroinitiator (56 mg, 1.4×10^{-5} mol), a magnetic stir bar and 3 beads of activated 3 Å molecular sieves. The reaction mixture was left to stir at 25 °C for 1 h. The resultant solidified polymer was diluted with DCM and quenched with benzoic acid (10 mg, 8.2×10^{-5} mol). The block copolymer was purified by precipitation in methanol followed by ethyl acetate. The white, solid powder was recovered via centrifugation (4000 rpm, 10 min) and dried in a vacuum oven overnight.

4.4.3 General Procedures

a) Titration of *n*-butyllithium

Generally, *n*-butyllithium was purchased in single-use bottles where the concentration was precisely known. When this was not possible, the following procedure was followed. Briefly, in a flame-dried Schlenk flask under argon was added the indicator *N*-benzylbenzamide (100 mg, 4.73×10^{-4} mol) in THF (5 mL). The flask was cooled to -45 °C in a dry ice/acetonitrile bath. To this colourless solution was added the *n*-butyllithium solution dropwise via a 0.5 mL syringe until the end-point was reached (persistent royal blue hue). The molarity of the solution is calculated as the number of moles of indicator used multiplied by the volume of *n*-butyllithium added.

b) Aqueous self-assembly

In a typical procedure, the PVP-PVL or PVP-PAVL block copolymer (10 mg) was completely dissolved in an appropriate organic solvent (acetone or THF, 2 mL) by stirring in a scintillation vial equipped with a screw-top lid at 25 °C for 2 h. Following this, water (0.4 mL) was added via syringe using a metered flow pump at a slow rate (0.015 mL·min^{-1}). After this time, the solution was observed to be opaque and

an excess of water was added (9.6 mL). The organic solvent was removed by closing the vial and pricking a needle tip through the centre of the lid to let the solvent evaporate slowly, overnight. The micellar liquid could then be recovered by lyophilisation to obtain an aerated white powder which could be stored in the freezer until further use. A portion of the micellar liquid was always stored in liquid state *sans* lyophilisation for further characterisation.

c) Self-assembly in alcohol with heat

In a typical procedure, the PVP-*b*-PVL block copolymer (10 mg), ethanol (10 mL) and a stir bar were added to a scintillation vial equipped with a screw-top lid and stirred at 25 °C for 1 h. After this time, the stir bar was removed and the solution was heated to 60 °C in an oil-bath without stirring for 24 h. After this time, the heating plate was switched off without removing the sample from the oil-bath and the sample was left to age for a predetermined amount of time. The sample was diluted (1:1, v/v) with ethanol for further characterisation.

4.5 References

(1) Mai, Y.; Eisenberg, A. *Chem. Soc. Rev.* **2012**, *41* (18), 5969.

(2) Zhang, L.; Eisenberg, A. *Polym. Adv. Technol.* **1998**, *9* (10), 677.

(3) Crassous, J. J.; Schurtenberger, P.; Ballauff, M.; Mihut, A. M. *Polymer* **2015**, *62* (1), 1.

(4) Cao, L.; Manners, I.; Winnik, M. A. *Macromolecules* **2002**, *35* (22), 8258.

(5) Toy, R.; Hayden, E.; Shoup, C.; Baskaran, H.; Karathanasis, E. *Nanotechnology* **2011**, *22* (11), 115101.

(6) Truong, N. P.; Whittaker, M. R.; Mak, C. W.; Davis, T. P. *Expert Opin. Drug Deliv.* **2015**, *12* (1), 129.

(7) Champion, J. A.; Katare, Y. K.; Mitragotri, S. *J. Control. Release* **2007**, *121* (1), 3.

(8) Hudson, Z. M.; Boott, C. E.; Robinson, M. E.; Rupar, P. A.; Winnik, M. A.; Manners, I. *Nat. Chem.* **2014**, *6* (10), 893.

(9) He, X.; Hsiao, M. S.; Boott, C. E.; Harniman, R. L.; Nazemi, A.; Li, X.; Winnik, M. A.; Manners, I. *Nat. Mater.* **2017**, *16* (4), 481.

(10) Inam, M.; Cambridge, G.; Pitto-Barry, A.; Laker, Z. P. L.; Wilson, N. R.; Mathers, R. T.; Dove, A. P.; O'Reilly, R. K. *Chem. Sci.* **2017**, *8* (6), 4223.

(11) Zhu, W.; Peng, B.; Wang, J.; Zhang, K.; Liu, L.; Chen, Y. *Macromol. Biosci.* **2014**, *14* (12), 1764.

(12) Pitto-Barry, A.; Kirby, N.; Dove, A. P.; O'Reilly, R. K. *Polym. Chem.* **2014**, *5* (4), 1427.

(13) Woodruff, M. A.; Hutmacher, D. W. *Prog. Polym. Sci.* **2010**, *35* (10), 1217.

(14) Le Devedec, F.; Boucher, H.; Dubins, D.; Allen, C. *Mol. Pharm.* **2018**, *15* (4), 1565.

(15)   Lou, X.; Detrembleur, C.; Jérôme, R. *Macromolecules* **2002**, *35* (4), 1190.

(16)   Zeng, F; Lee, H; Chidiac, M; Allen, C. *Biomacromolecules* **2005**, *6* (4), 2140.

(17)   Aubin, M.; Prud'homme, R. E. *Polymer* **1981**, *22* (9), 1223.

(18)   Gagliardi, M.; Di Michele, F.; Mazzolai, B.; Bifone, A. *J. Polym. Res.* **2015**, *22* (2), 17.

(19)   Hombreiro Pérez, M.; Zinutti, C.; Lamprecht, A.; Ubrich, N.; Astier, A.; Hoffman, M.; Bodmeier, R.; Maincent, P. *J. Control. Release* **2000**, *65* (3), 429.

(20)   Toncheva, V. *J. Environ. Polym. Degrad.* **1996**, *4* (2), 71.

(21)   Báez, J. E.; Martínez-Richa, A.; Marcos-Fernandez, A. *Macromolecules* **2005**, *38* (5), 1599.

(22)   Kamber, N. E.; Jeong, W.; Waymouth, R. M.; Pratt, R. C.; Lohmeijer, B. G.; Hedrick, J. L. *Chem. Rev.* **2007**, *107* (12), 5813.

(23)   Nuyken, O.; Pask, S. D. *Polymers **2013**, 5* (2), 361*.*

(24)   Hege, C. S.; Schiller, S. M. *Green Chem.* **2014**, *16* (3), 1410.

(25)   Kakuchi, R.; Tsuji, Y.; Chiba, K.; Fuchise, K.; Sakai, R.; Satoh, T.; Kakuchi, T. *Macromolecules* **2010**, *43* (17), 7090.

(26)   Nederberg, F.; Connor, E. F.; Möller, M.; Glauser, T.; Hedrick, J. L. *Angew. Chem.* **2001**, *40* (14), 2712.

(27)   Lohmeijer, B. G.; Pratt, R. C.; Leibfarth, F.; Logan, J. W.; Long, D. A.; Dove, A. P.; Hedrick, J. L. *Macromolecules* **2006**, *39* (25), 8574.

(28)   Simón, L.; Goodman, J. M. *J. Org. Chem.* **2007**, *72* (25), 9656.

(29)   Brown, H. A.; De Crisci, A. G.; Hedrick, J. L.; Waymouth, R. M. *ACS Macro Lett.* **2012**, *1* (9), 1113.

(30)   Dove, A. P. *ACS Macro Lett.* **2012**, *1* (12), 1409.

(31)   Ringsdorf, H. *J. Polym. Sci. Polym. Symp.* **2007**, *51* (1), 135.

(32)   Molander, G. A.; Harris, C. R. *J. Am. Chem. Soc.* **1995**, *117* (13), 3705.

(33)   Parrish, B.; Quansah, J. K.; Emrick, T. *J. Polym. Sci. A* **2002**, *40* (12), 1983.

(34)   Wu, L.; Zhang, Y.; Li, Z.; Yang, G.; Kochovski, Z.; Chen, G.; Jiang, M. *J. Am. Chem. Soc.* **2017**, *139* (41), 14684.

(35)   Li, B.; Buzon, R. A.; Castaldi, M. J. *Org. Process Res. Dev.* **2001**, *5* (6), 609.

(36)   Jensen, C. M.; Lee, D. W. *J. Chem. Educ.* **2000**, *77* (5), 629.

(37)   Goethals, F.; Frank, D.; Du Prez, F. *Prog. Polym. Sci.* **2017**, *64* (1), 76.

(38)   Willcock, H.; O'Reilly, R. K. *Polymer Chemistry* **2010**, *1* (2), 149.

(39)   Wang, L.; Kristensen, J.; Ruffner, D. E. *Bioconjugate Chem.* **1998**, *9* (6), 749.

(40)   Reed, R.; Réau, R.; Dahan, F.; Bertrand, G. *Angew. Chem.* **1993**, *32* (3), 399.

(41)   Benahmed, A.; Ranger, M.; Leroux, J. C. *Pharm. Res.* **2001**, *18* (3), 323.

(42)   Ravenelle, F.; Vachon, P.; Rigby-Jones, A. E.; Sneyd, J. R.; Le Garrec, D.; Gori, S.; Lessard, D.; Smith, D. C. *Br. J. Anaesth.* **2008**, *101* (2), 186.

(43)   Williams, D. B. G.; Lawton, M. *J. Org. Chem.* **2010**, *75* (24), 8351.

(44)   Ren, Y.; Gao, Q.; Zhou, C.; Wei, Z.; Zhang, Y.; Li, Y. *RSC Adv.* **2015**, *5* (35), 27421.

(45)   Noack, S.; Schanzenbach, D.; Koetz, J.; Schlaad, H. *Macromol. Rapid Commun.* **2019**, *40* (1), 1800639.

(46)   Petzetakis, N.; Walker, D.; Dove, A. P.; O'Reilly, R. K. *Soft Matter* **2012**, *8* (28), 7408.

(47)   Mihut, A. M.; Crassous, J. J.; Schmalz, H.; Drechsler, M.; Ballauff, M. *Soft Matter* **2012**, *8* (11), 3163.

(48)   Ren, Y.; Wei, Z.; Wu, T.; Bian, Y.; Leng, X.; Zhou, C.; Li, Y. *RSC Adv.* **2016**, *6* (51), 45791.

(49)   Furuhashi, Y.; Sikorski, P.; Atkins, E.; Iwata, T.; Doi, Y. *J. Polym. Sci. B.* **2001**, *39* (21), 2622.

(50)   Harrison, K. L.; Jenkins, M. J. *Polym. Int.* **2004**, *53* (9), 1298.

(51)   Abdelrazek, E. M.; Abdelghany, A. M.; Badr, S. I.; Morsi, M. A. *J. Mater. Res. Technol.* **2018**, *7* (4), 419.

(52)   Bragg, W. H. *Nature* **1913**, *88* (605), 428.

(53)   Schneiderman, D. K.; Hill, E. M.; Martello, M. T.; Hillmyer, M. A. *Polym. Chem.* **2015**, *6* (19), 3641.

(54)   Ponting, M.; Lin, Y.; Keum, J. K.; Hiltner, A.; Baer, E. *Macromolecules* **2010**, *43* (20), 8619.

(55)   Iwata, T.; Furuhashi, Y.; Su, F.; Doi, Y. *Riken Rev.* **2001**, *1* (1), 15.

(56)   Förster, S.; Zisenis, M.; Wenz, E.; Antonietti, M. *J. Chem. Phys.* **1996**. *104* (24), 9956.

(57)   Raez, J.; Manners, I.; Winnik, M. A. *J. Am. Chem. Soc.* **2002**, *124* (35), 10381.

(58)   Raez, J.; Manners, I.; Winnik, M. A. *Langmuir* **2002**, *18* (19), 7229.

(59)   Lee, C. F. *Phys. Rev. E.* **2009**, *80* (3), 31922.

(60)   Parekh, P.; Ganguly, R.; Aswal, V. K.; Bahadur, P. *Soft Matter* **2012**, *8* (21), 5864.

(61)   Mata, J. P.; Majhi, P. R.; Kubota, O.; Khanal, A.; Nakashima, K.; Bahadur, P. *J. Colloid Interface Sci.* **2008**, *320* (1), 275.

(62)   Yang, J. X.; Fan, B.; Li, J. H.; Xu, J. T.; Du, B. Y.; Fan, Z. Q. *Macromolecules* **2016**, *49* (1), 367.

(63)   Wang, X. Y.; Wang, R. Y.; Fan, B.; Xu, J. T.; Du, B. Y.; Fan, Z. Q. *Macromolecules* **2018**, *51* (5), 2138.

(64)   Wang, J.; Cheung, M. K.; Mi, Y. *Polymer* **2002**, *43* (4), 1357.

(65)   Arno, M. C.; Inam, M.; Coe, Z.; Cambridge, G.; Macdougall, L. J.; Keogh, R.; Dove, A. P.; O'Reilly, R. K. *J. Am. Chem. Soc.* **2017**, *139* (46), 16980.

(66)   Fastnacht, K. V.; Spink, S. S.; Dharmaratne, N. U.; Pothupitiya, J. U.; Datta, P. P.; Kiesewetter, E. T.; Kiesewetter, M. K. *ACS Macro Lett.* **2016**, *5* (8), 982.

(67)   Li, L.; Zheng, S. *J. Polym. Sci. B.* **2008**, *46* (21), 2296.

(68)   Shi, H.; Liu, L.; Wang, X.; Li, J. *Polym. Chem.* **2010**, *3* (5), 1182.

Chapter Five

Polymeric prodrug assembly and application

5.1 Introduction

The *Plasmodium falciparum* parasite has developed a degree of resistance to all known antimalarial drug classes,[1] and warrants a sophisticated approach to drug therapy. Recently, the combination of two synergistic antimalarial drugs with different modes of action has been used as a strategy to inhibit the development of resistance to either component.[2] Among the artemisinin-based therapies, artemether and lumefantrine used in combination is highly potent, and is currently used as the first-line treatment for uncomplicated malaria.[3]

Artemether (Figure 5.1) and other artemisinin derivatives exhibit a broad spectrum of activity which extends from the young ring stage of the parasite through to the early schizont stage. The peroxide group in artemether, and other endoperoxides, reacts with ferrous ion in haem during the break down of haemoglobin in the malaria parasite's digestive food vacuole. This leads to the production of a carbon-centred free radical which inactivates proteins in the vicinity by alkylation.[4] Artemisinin derivatives are the most potent of all antimalarials and have even been known to cause a substantial reduction in gametocyte (mature sexual stage parasite) carriage which limits malaria transmission.[5] Despite the high activity of artemether, its action is short lived due to its short plasma half-life (2 – 3 h) and it has been reported that an estimated 100 – 100 000 residual parasites remain after the drug is used singularly over a three-day course of treatment.[6,7] Lumefantrine (Figure 5.1) is a fluorene derivative with a mode of action that is attributable to the arylamino alcohol group. This group is also found in antimalarials such as quinine, mefloquine and halofantrine.[8] Like other arylamino carbinol blood schizontocides, it binds powerfully with haemin, produced during the break down of haemoglobin in the parasite's food vacuole, preventing the polymerisation of the toxic iron porphyrin to non-toxic crystalline haemozoin (malaria pigment).[4,9] Lumefantrine has a longer plasma half-life (3 – 6 days) with a different mode of action and lifecycle target compared with artemether. Lumefantrine is therefore able to eliminate the residual parasites which remain after artemether is cleared, minimising the risk of recrudescence.[10]
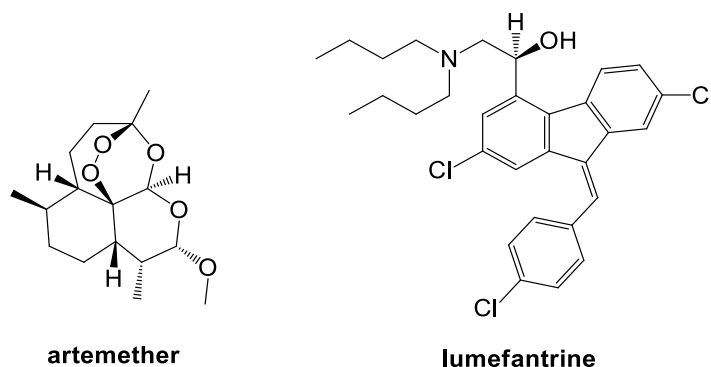
Figure 5.1 Chemical structures of artemether and lumefantrine.

Despite the combination's high success rate, there are major complications associated with the oral dosage form such as the requirement to accompany these drugs with fat-supplemented food to avoid low and/or erratic absorption, the requirement of drug administration twice per day and the degradation of the drugs in the gastric fluid.[10,11] These challenges can be overcome through their incorporation into biodegradable, targeted polymeric prodrugs, in this way improving the therapeutic profile of the loaded drugs. Amphiphilic block copolymers are able to self-assemble into well-defined micellar structures at the nanoscale under the appropriate conditions. These micelles are promising for the development of precision nanomedicine because of their ability to solvate poorly water-soluble compounds such as artemether. This feature is based on the compatible microenvironment within the core of the micelles and the largely hydrophobic drugs.[12] Poor drug solubility is a major bottleneck in the screening and development of drugs to treat life-threatening diseases such as cancer and malaria. Many otherwise viable drugs are rejected because of a lack of aqueous solubility, which is a prerequisite for effective biodistribution and uptake in the body.[13] Besides solubilisation, polymeric micelles also impart other desirable pharmaceutical characteristics such as the ability to control the release and protect the payload from releasing prematurely, thereby increasing the blood circulation time of the micelles. This would lead to longer interaction times with the diseased site, minimising the toxicity to healthy cells.

There is no general consensus on the ideal block ratio (hydrophilic:hydrophobic segments) for block copolymer micelles in drug delivery applications. From literature, however, it can be concluded that increasing the hydrophobicity of the core-forming block increases the thermodynamic stability of the micelles and decreases the release rate of the hydrophobic drug.[14,15] The characteristics of thermodynamic stability as well as the prolonged blood circulation of the polymeric micelle are highly sought after. These characteristics are, however, influenced by opposing parameters. Regarding prolonged blood circulation, from literature it has been found that a higher proportion of the hydrophilic block compared to the core-forming block will cause longer circulation times in the bloodstream.[16,17] Richter *et al.* conducted a study where the drug solubilisation of sagopilone, a poorly water-soluble anticancer drug, was investigated. They found that the ideal hydrophilic to hydrophobic ratio was approximately 1:1 for PEG-*b*-PCL micelles in terms of balancing the parameters of corona hydration, micelle thermodynamic stability and drug solubilisation.[18]

The subject of micelle size is more agreed upon over the spectrum of known diseases. In general, the hydrodynamic diameter should be less than approximately 150 nm in order to avoid rapid clearance by the reticuloendothelial system (RES).[19] For cancer therapy, nanoparticles of approximately 50 nm in diameter were found to display the maximum cellular uptake as higher and lower diameters lead to decreased endocytosis.[20,21] In general, micelles smaller than 100 nm have been shown to traverse through blood vessels through fenestrations in the endothelial lining.[22] For malaria therapy, it is known that *Plasmodium*-infected RBCs (iRBCs) have increased permeability to a range of compounds through channels called 'new permeation pathways' (NPPs), which develop approximately 12 – 16 h after the *Plasmodium* invasion of the RBC.[23] These NPPs have been shown to facilitate the passive targeting of nanoparticles approximately 80 – 50 nm in diameter,[24] leading to the assertion that differentiation between iRBCs and healthy RBCs could in-part be mediated by these size effects.

5.1.1 Approach

In Chapter 3, different acid-labile linkages were explored and it was confirmed that the acetal linkage held potential in drug delivery systems. In Chapter 4, the block copolymer poly(*N*-vinylpyrrolidone-*block*-poly(δ-valerolactone) (PVP-*b*-PVL) was investigated as well as its derivative, poly(*N*-vinylpyrrolidone-*block*-poly(α-allylvalerolactone) (PVP-*b*-PAVL). In this chapter, the simple steps necessary to conjugate lumefantrine through its hydroxy-functionality to PVP-*b*-PAVL via an acetal linkage will be described and its successful conjugation confirmed using SEC, ¹H NMR and DOSY spectroscopy. Artemether can be incorporated into the system by physical entrapment using the cosolvent technique, which will lead to the simultaneous formation of artemether entrapped, lumefantrine-conjugated micelles. Additionally, the peptide 'GSRSKGT' has been explored for its ability to actively target iRBCs.[25] For this purpose, it was modified to bear a thiol groups in order to achieve its bioconjugation to the prodrug micelles.

5.2 Results and Discussion

5.2.1 Synthesis of acetal-linked lumefantrine prodrugs based on PVP-*b*-PAVL

The antimalarial drug, lumefantrine (LUM), was conjugated to the block copolymer PVP-*b*-PAVL ($M_{n,theoretical}$ = 7800 g·mol⁻¹, $M_{n,SEC}$ = 9300 g·mol⁻¹, Đ = 1.2) in three successive steps (Scheme 5.1) to synthesise the acetal-conjugated LUM block copolymer (LUM prodrug). In the first step, the pendant allyl groups were quantitatively converted to carboxylic acid groups. In the second step, those carboxylic acid groups underwent Steglich esterification to obtain the vinyl-ether functionalised block copolymer. Finally, LUM was conjugated via its hydroxy-functionality to the vinyl ether groups to simultaneously render the acid degradable acetal linkage.
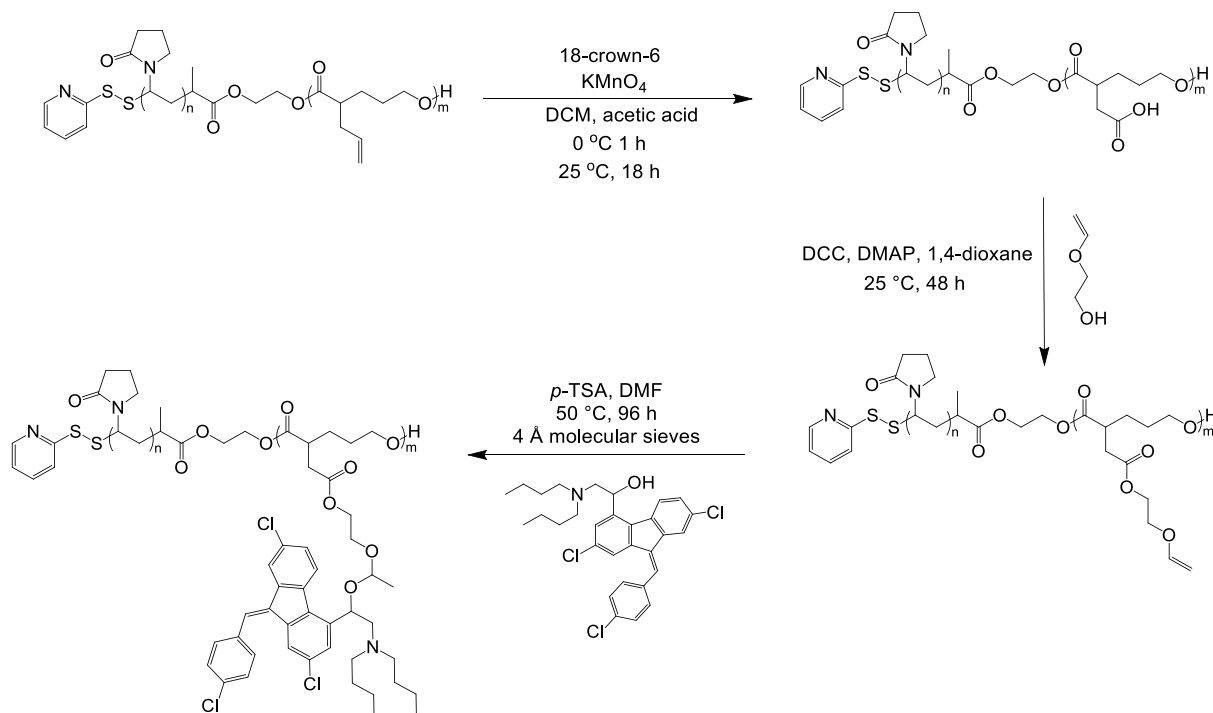
Scheme 5.1 Synthesis route to the LUM prodrug.

The oxidation of the pendant alkene groups of PAVL in the block copolymer, PVP-*b*-PAVL, occurred in a biphasic medium of DCM and acetic acid with $KMnO_4$ in the presence of 18-crown-6 to yield carboxylic acid groups. The method of Kurth *et al.* was used to achieve this,[26] which resulted in the quantitative conversion of the allyl groups to carboxylic acid groups, as evidenced by ^{1}H NMR and ^{13}C NMR spectroscopy. $KMnO_4$ was used as the oxidation agent and 18-crown-6 as the phase transfer and dissociating agent of $KMnO_4$. For the permanganate ion (MnO_4^-) to be used as an effective oxidation agent, close contact is needed between the ions and the species to be oxidised (vinyl groups). This would not be possible if a crown ether were not used as a dissociating agent because alkali metal salts such as $KMnO_4$ are virtually insoluble in non-polar organic solvents such as DCM. The cavity of the crown ether molecule is lined with oxygen atoms and is large enough to accommodate the potassium ion in its centre (complexation with ether oxygen atoms), while its periphery is non-polar. Upon oxidation, the aldehyde groups which form and terminate the block copolymer are rapidly oxidised to carboxylic acid groups and the liberated methanoic acid groups are oxidised to CO_2 and water.[27–29]

Ethylene glycol vinyl ether was conjugated to the carboxylated block copolymer using Steglich esterification using DCC and DMAP as the coupling reagent and acylation catalyst, respectively.[30] The reaction was left to proceed for 48 h in anhydrous 1,4-dioxane and after purification, the incorporation of EGVE was confirmed using ^{1}H NMR spectroscopy, where the signals attributed to the vinyl and methylene protons of EGVE between δ 6.5 – 3.5 ppm were noted. The ^{1}H NMR spectra of carboxylated and EGVE-terminated PVP-*b*-PVL are shown in Addendum K. The drug, lumefantrine, could then be conjugated to EGVE-functionalised PVP-*b*-PVL via an acetal linkage through a 'click'-type reaction between the hydroxyl groups of lumefantrine and the pendant vinyl ether groups, similar to the approach reported by Mangold *et al.*[31] Figure 5.2 shows the colour coded, stacked ^{1}H NMR spectra of PVP-*b*-PAVL (top) and the LUM prodrug (bottom).
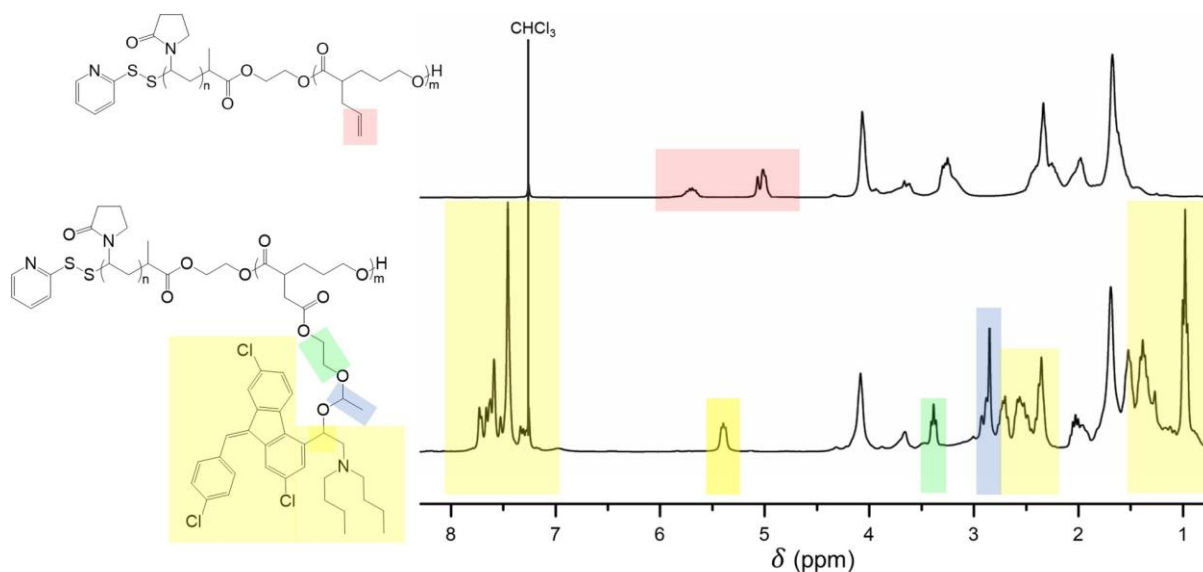
Figure 5.2 Colour coded, stacked ^{1}H NMR spectra and chemical structures of PVP-b-PAVL, top, and the LUM prodrug, bottom.

The signals attributed to lumefantrine are highlighted in yellow, where a clear indication of drug functionalisation can be seen in the aromatic region of the ^{1}H NMR spectrum. Other noteworthy indicators are the peaks assigned to the acetal methine protons (blue, 2.8 ppm) and the ethylene glycol bridge protons (green, 3.4 ppm). The lumefantrine %functionalisation was estimated to be 22 mol% using ^{1}H NMR analysis, by comparing the integral ratios of lumefantrine (5.4 ppm, methine proton, 1H) to the polymer carrier (4.05 ppm, methylene protons, 2H).

The molar mass distribution of the LUM prodrug ($M_{n,SEC}$ = 15 600 g·mol^{-1}, $Đ$ = 1.4) is shown in Figure 5.3 a) which is symmetrical in shape and has a monomodal distribution. $Đ$ increased upon introduction of lumefantrine, an observation also found in literature for similar systems.[32,33] This indicates that the molar mass is more distributed, and that there are more polymer chains of different lengths present after the drug is conjugated to the block copolymer. It is possible that some ester bonds were cleaved during the reaction time needed to conjugate lumefantrine to the block copolymer or during the purification steps. DOSY was therefore used to further investigate the conjugation of lumefantrine to the block copolymer and the extent of hydrolysis as it can be used to correlate the ^{1}H NMR signals with the diffusion coefficients in solution. Figure 5.3 b) shows the DOSY spectrum of the LUM prodrug. From the spectrum only one main diffusional behaviour is observed for the LUM prodrug which indicates the absence of unbound lumefantrine or polymer chains of vastly different diffusional behaviour. Compounds or macromolecules with lower molar masses would diffuse faster, as seen with the solvent, chloroform. The successful conjugation of lumefantrine to PVP-*b*-PAVL was therefore confirmed using this technique and the extent of hydrolysis was concluded to be limited.
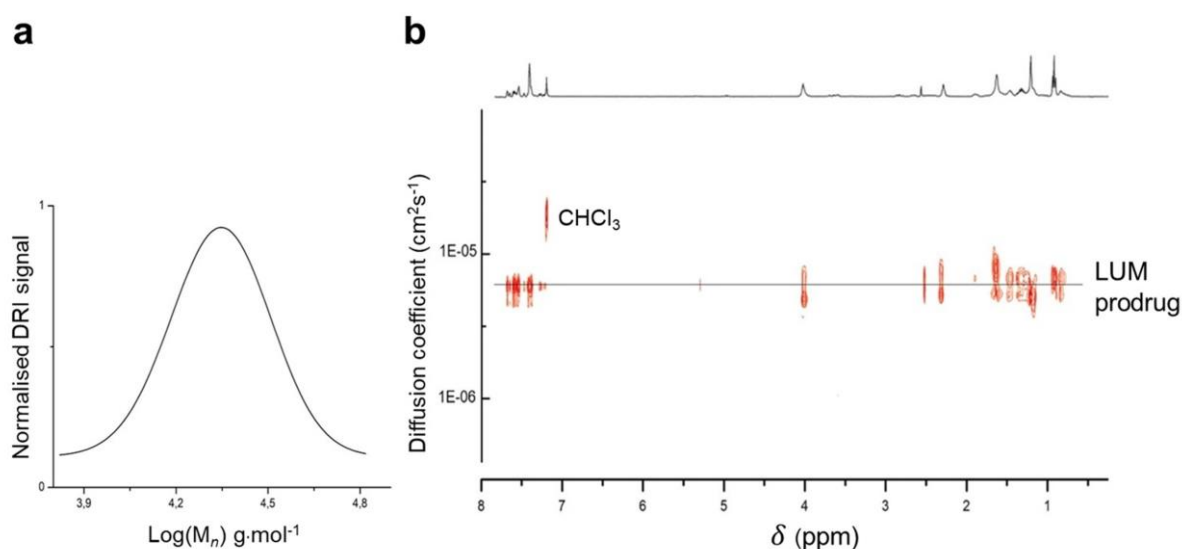
Figure 5.3 a) Molar mass distribution from SEC and b) DOSY spectrum of the LUM prodrug.

5.2.2 Physical entrapment of artemether

Artemether (AM) is a poorly water-soluble drug with a water solubility of 114 mg·L^{-1} at pH 7.[34] It is therefore possible to entrap this drug within the hydrophobic core of LUM prodrug micelles via aqueous self-assembly. This would occur in order to minimise the overall enthalpy of the system by minimising artemether's contact with the surrounding polar water molecules. The entrapment of artemether within the hydrophobic core of LUM prodrug micelles would render artemether-lumefantrine (AL) prodrug micelles.

To achieve this, artemether and the LUM prodrug were fully dissolved in an appropriate organic solvent followed by the controlled, slow addition of water to cause the spontaneous self-assembly of the LUM prodrug with artemether molecules harboured within the hydrophobic core of the micelles. TEM was used to observe the precursory and ultimate morphology of the AL prodrug micelles under various conditions (Figure 5.4).
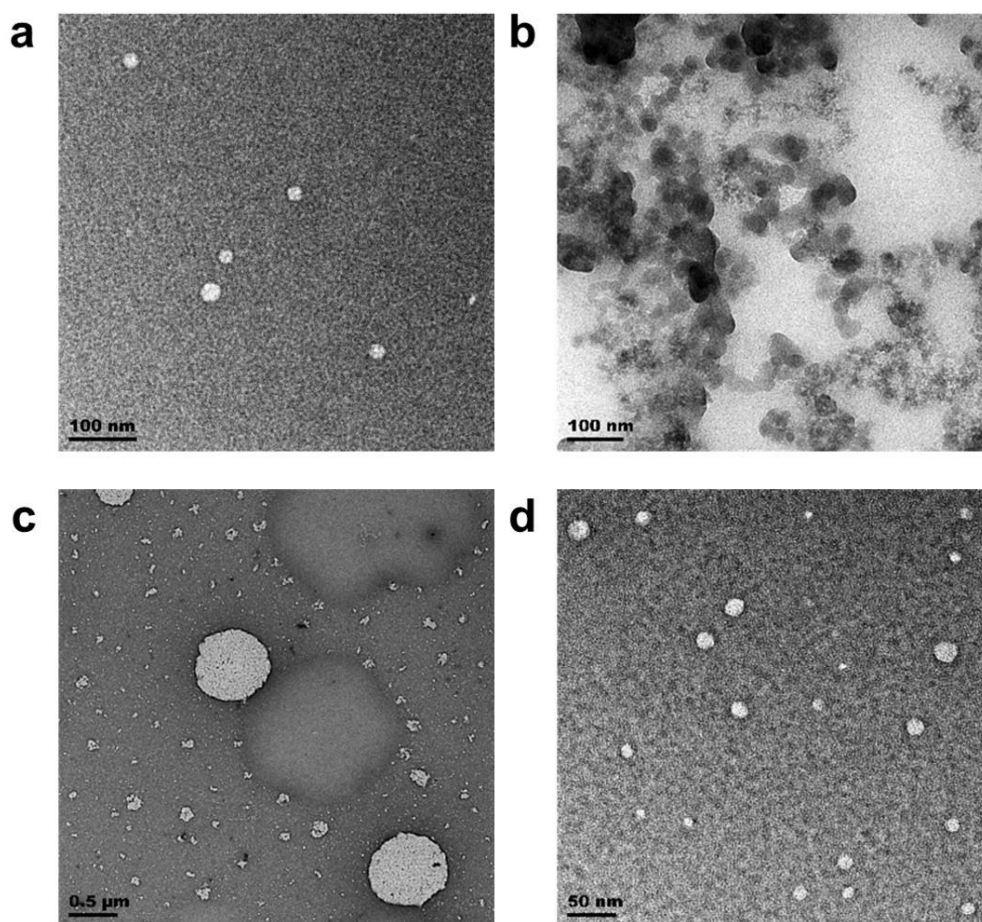
Figure 5.4 TEM images of a) PVP-b-PAVL micelles (THF), b) LUM prodrug micelles (THF), c) AL prodrug micelles (acetone) and d) AL prodrug micelles (THF). The organic solvent in parenthesis indicates the good solvent used to dissolve the BCPs, and water was used as the selective solvent. One drop of each unfiltered aqueous micelle dispersion was dropped onto a carbon coated TEM grid and dried under ambient conditions after being stained with uranyl acetate (20 wt.% in water).

Figure 5.4 a) shows the TEM image of PVP-*b*-PAVL micelles obtained after using THF as the good solvent for both blocks and water as the selective solvent for PAVL. Similar conditions were used for the LUM prodrug micelles, as shown in the TEM image seen in Figure 5.4 b). The incorporation of LUM was observed to change the morphology from spherical micelles to quasi-spherical aggregates of different size populations, as the hydrophobicity of the core-forming segment was altered. Figure 5.4 c) and d) show the AL prodrug micelles (after artemether entrapment) using acetone and THF as the good solvent, respectively, and water as the selective solvent.

The entrapment of artemether led to the observation of irregular-shaped aggregates and vesicles when self-assembly was conducted in acetone. Under the same conditions, using THF led to the observation of spherical micelles. Artemether is freely soluble in acetone and lumefantrine is only moderately soluble; whereas both drugs are freely soluble in THF.[35] During the addition of the selective solvent (water) the common solvent (acetone or THF) is present in the hydrophobic domains of the micelles. It is likely that in THF, the polymeric prodrug was more uncoiled and freer to move, allowing for the morphological transitions into stable structures to take place over a shorter period of time compared with the process in acetone.

Table 5.1 Block copolymer and polymeric prodrug micelle diameters estimated from TEM and DLS

Sample	Description	Morphology observation	d_{core} [a] nm	D_h [b] nm
PVP-*b*-PAVL	'empty' micelles (THF)	spherical micelles	29.5 ± 3.2	125.3
LUM prodrug	LUM-conjugated micelles (THF)	quasi-spherical micelles	38.0 ± 14.9	183.4
AL prodrug	AM entrapped LUM-conjugated micelles (acetone)	large aggregates irregular micelles	754.5 ± 39.8 92.6 ± 24.7	1049.3, 297.9
AL prodrug	AM entrapped LUM-conjugated micelles (THF)	spherical micelles	25.4 ± 3.3	114.1

[a] The diameter of the core of micelles was determined by TEM analysis of 100 micelles
[b] The average hydrodynamic diameter ($D_h = 2\,R_h$) was determined via DLS after three measurements.

The observations and analyses obtained from TEM and DLS (micelle concentration of 0.5 mg·mL^{-1} in water) are shown in Table 5.1. From DLS, the hydrodynamic sizes of the micelles in aqueous-based media can be obtained. In combination with TEM, DLS is highly useful in estimating what the approximate hydrodynamic size of the micelles would be once administered, as normal human whole blood consists of 45 vol% blood cells and 55 vol% blood plasma, which is 90% water.[36] In an aqueous environment, the PVP corona would be in the hydrated state (more unbound) as the polymer chains

are allowed to take up space. TEM analysis is conducted on micelles which are more compact due to drying effects. Furthermore, TEM analysis would provide the number-based particle size distribution whereas from DLS it would be intensity-based. A combination of both techniques is necessary as aggregates and irregular micelle shapes can be identified through TEM. Based on TEM and DLS results, artemether-encapsulated, LUM-conjugated PVP-*b*-PVL block copolymers self-assembled into spherical micelles of approximately 114 nm in hydrodynamic size from DLS and 25 nm in diameter from TEM analysis.

The diameters of the micelles decreased slightly once artemether was loaded into the hydrophobic core of the block copolymer micelles. A similar occurrence was observed for poly(ε-caprolactone)-*block*-poly(ethylene glycol) (PCL-*b*-PEG) loaded with doxorubicin.[37] This could be due to non-covalent intermolecular interactions between artemether and the core-forming segment, PVL, leading to a slightly more compact structure. In order to gain a better understanding of the interactions which could be taking place between the loaded drug and the polymer carrier, it is beneficial to know whether the drug exists within the micelle in the crystalline or amorphous state. The superimposed, DSC thermograms of pristine artemether and artemether-loaded micelles are shown in Figure 5.5 over artemether's characteristic melting endotherm temperature region. Artemether has a melting endotherm reported to occur between 86 – 90 °C.[38] Fully amorphous materials do not exhibit melting endotherms as this transition is first-order, and occurs in order to destroy the existing order.[39] Pristine artemether was found to have a melting endotherm at 88.1 °C (ΔH: 61.2 J·g^{-1}) demonstrating its crystallinity. After artemether was loaded into the block copolymer micelles and lyophilised, no distinct melting endotherm for artemether can be observed which indicates that artemether is present in its amorphous state.
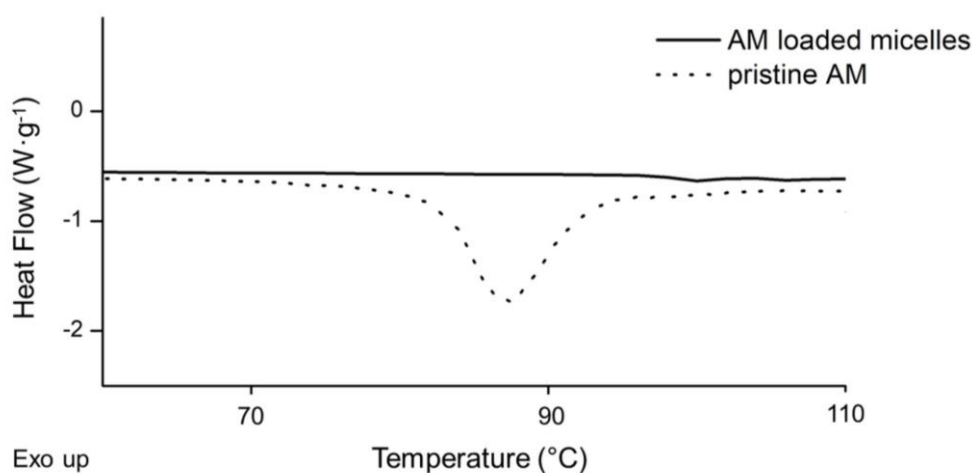
Figure 5.5 DSC thermograms of pristine artemether (dotted curve) and artemether-loaded micelles (line curve) over the characteristic melting endotherm area of crystalline artemether. Second heating cycle shown.

It is well known that the physical entrapment of hydrophobic drugs such as artemether is driven by the hydrophobic-hydrophobic interactions between the drug and the hydrophobic segments of the core-forming block. In this instance, the hydrophobicity of PVL is largely due to the methylene units in the polymer backbone. Besides hydrophobic interactions, other factors such as the crystallinity of the polymer and drug, hydrogen-bonding interactions and van der Waals forces are thought to play a role

in the drug loading outcomes.[40] Drugs in the amorphous state have a disordered structure and possess a high free energy which improves the bioavailability of the drug. In this regard, molecular non-covalent interactions such as H-bonding between PVP and hydrophobic drugs in the amorphous state have been reported.[41] Furthermore, deprotonated artemether contains hydroxyl groups which can form hydrogen bonds with the carbonyl groups of the amorphous PVL.

After the preparation of AM entrapped LUM-conjugated micelles, the entrapment efficiency (EE) of the drug and the drug loading content (DLC) of the micelles were determined. The EE is defined as the fraction of initial drug that is entrapped within the micelles relative to the initial mass of the drug used in the formulation of the micelles. The DLC is defined as the mass fraction of the drug relative to the mass fraction of the micelles recovered after the entrapment. Equation 5.1 and 5.2 were used to determine the EE and DLC, expressed as percentages.[17,42]

$$\text{EE \%} = \frac{\text{amount of drug entrapped}}{\text{drug initially used in formulation}} \times 100 \qquad\qquad \text{Equation 5.1}$$

$$\text{DLC \%} = \frac{\text{amount of drug in micelles}}{\text{amount of micelles recovered}} \times 100 \qquad\qquad \text{Equation 5.2}$$

Artemether does not contain any chromophores so its detection using UV-Vis spectroscopy or fluorescence spectroscopy is restricted. Derivatization can be induced by the addition of concentrated hydrochloric acid to allow for its detection at $\lambda = 254$ nm, from the acid decomposition product of a α,β-unsaturated decalone.[35,43] Due to possible interference by the polymer's absorption in the UV-Vis spectrum and the pH-dependency of the system, LC-MS was used as an alternative method to determine its concentration using external calibration with standard protocols (Addendum L). The DLC and EE of artemether in AL prodrug micelles was found to be 14 wt.% and 60%, respectively. The DLC of lumefantrine in the AL prodrug micelles derived using LC-MS was found to be 27 wt.%. The tendency of the DLC to be greater for systems with greater inclusions of hydrophilic segments has been noted in literature.[44,45] The amount of the hydrophilic segment (PVP content) should not be so high that it compromises the thermodynamic stability (or self-assembly) of the micelles as higher thermodynamic stability has been reported for drug delivery systems with greater inclusions of hydrophobic contents,[46] as will be elaborated on in the section to follow. A block copolymer composition of PVP$_{36}$-b-PAVL$_{38}$ was chosen so as to balance these opposing attributes and it was also based on studies which have indicated that an approximate 1:1 ratio of the hydrophobic to the hydrophilic segment yielded a good balance of stability and appreciable DLCs.[18,47]

Based on literature, the DLC of the hydrophobic drug is often in between 5 and 30 wt. %.[48] In fact, very low DLCs (between 2 – 5 wt.%) have been reported for PCL-based block copolymer drug delivery vessels which was attributed to the high crystallinity of the core-forming block. This means that there are less amorphous regions available to accommodate the drug entrapped within the core. For this drug delivery system, however, the AL prodrug is synthesised from PVP-b-PAVL. Unlike PVL, PAVL is amorphous due to the functionalisation with allyl groups which introduced stereoirregularities in the

mainchain backbone, also confirmed using DSC analysis. This could account for the higher DLC found for the AL prodrug micelles.

5.2.3 Stability studies

a) Thermodynamic stability

The thermodynamic stability of block copolymer micelles upon dilution is an important consideration for various *in vivo* applications. The primary driving force leading to the self-assembly of amphiphilic polymers is the lowering of free energy in an aqueous environment by minimising the interactions with hydrophobic block segments. The critical micelle concentration (CMC) is the threshold at which unimers assemble into micelles, therefore, the lower the CMC value, the more stable the micelles are to dilution effects.[49] These dilution effects would occur once the micelles are intravenously injected into the bloodstream of a patient. The CMC can be determined by measuring the abrupt changes in certain physical parameters such as the optical clarity of a micelle solution, its viscosity, surface tension or micelle size changes at this point.[50]

Here, the CMC of selected PVP-PVL block copolymers and the AL prodrug micelles were measured using the fluorescence technique with pyrene as the hydrophobic fluorogen. Pyrene is a widely used fluorescent agent because of its propensity to associate within the micelle core, its easy detection and its low detection limit. When pyrene partitions into the hydrophobic core of micelles, its spectroscopic properties change.[51] As a hydrophobic molecule, pyrene exhibits weak fluorescence in polar media; this changes drastically once pyrene partitions into nonpolar domains, duly demonstrating strong fluorescence. To determine the concentration of block copolymer micelles that elicit the partitioning of pyrene into the core, concentrations of micelles from 1×10^{-4} to 1 mg·mL^{-1} were dispersed in water and treated with a fixed concentration of pyrene in acetone, as described in the Experimental section. As shown in Figure 5.6, a red shift in the excitation spectra was observed at the peak maxima of pyrene shifting from 333 nm to 337 nm as indicated by the dashed lines. With it, the relative peak intensity increased concomitantly.
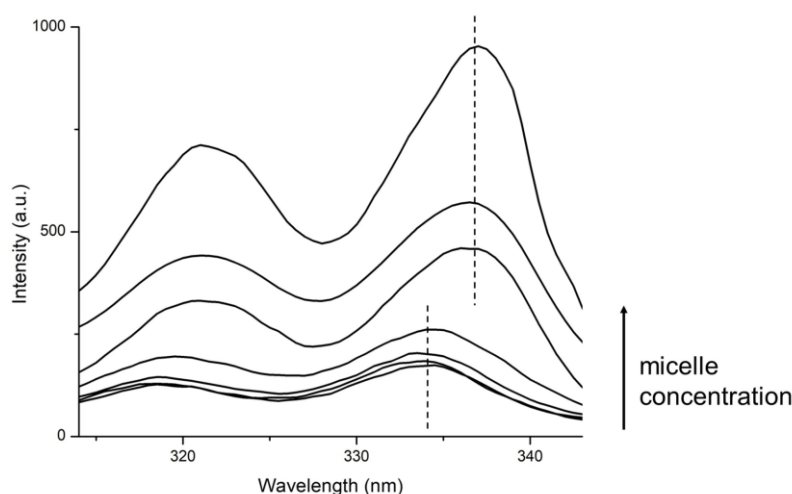
Figure 5.6 Fluorescence excitation spectra of pyrene (6×10^{-7} M) containing PVP-b-PVL micelles at different concentrations between 1×10^{-4} and 1 mg·mL^{-1}.

The CMC is calculated by measuring the intersection point of the ratio of intensities of $I_{337\,nm}/I_{333\,nm}$ from the pyrene excitation spectra *versus* the logarithm of the concentration of the micelles (Figure 5.7 and 5.8). The ratio of the intensity of fluorescence from pyrene has a linear gradient which is smaller at low block copolymer micelle concentrations and from a particular concentration, increases considerably with higher concentrations. The points of inflection are indicated by arrows in Figure 5.7. Here, two block copolymers with highly disparate block ratios, PVP_{138}-*b*-PVL_{100} and PVP_{138}-*b*-PVL_{346}, in the series PVP_{138} were compared for their thermodynamic stability. The CMC values for micelles self-assembled from PVP_{138}-*b*-PVL_{100} and PVP_{138}-*b*-PVL_{346} were 5.4×10^{-3} and 2.3×10^{-3} mg·mL^{-1}, respectively. The block copolymer with the higher weight fraction of PVL has a lower CMC value and is therefore more thermodynamically stable. An increase in the hydrophobic block length effectively lowers the CMC, indicating that the hydrophobic block length is critical in determining the thermodynamic stability of block copolymer micelles, a phenomenon described in literature.[48,52] It should be noted that hydrophobic effects are not solely responsible for micelle stability and that intermolecular interactions also play a role. For example, Me *et al*. found that crystallisation, especially stereocomplexation, of polyester core-forming blocks enhanced the thermodynamic stability of the self-assembled micelles.[53]
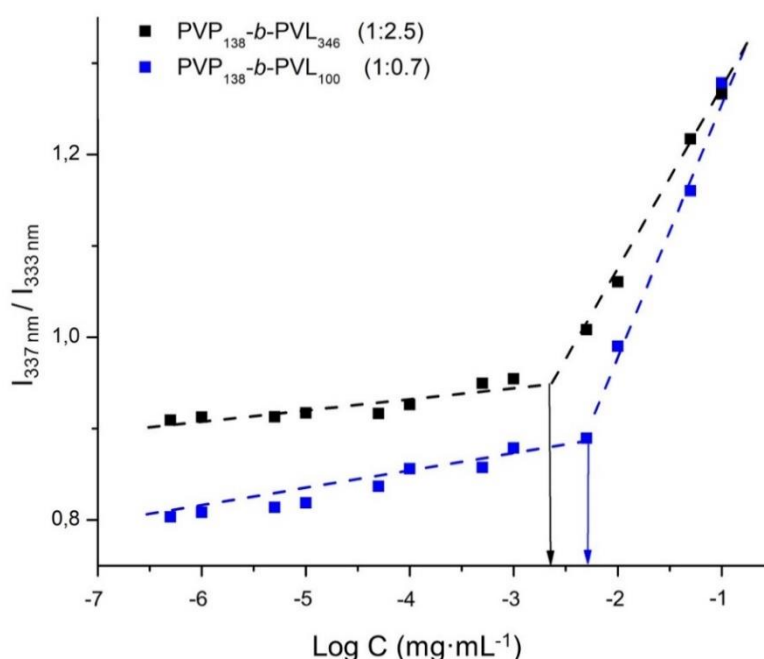
Figure 5.7 Fluorescence intensity of $I_{337\,nm}/I_{333\,nm}$ for pyrene as a function of the logarithm of concentration of micelles self-assembled from the PVP_{138} series block copolymers.

Drug-core interactions are able to affect the thermodynamic stability of block copolymer micelles.[46] This is seen in Figure 5.8, where the AL prodrug micelles, with artemether loaded into the core, are more thermodynamically stable than the precursor 'empty' block copolymer micelles self-assembled from PVP_{36}-*b*-$PAVL_{38}$. Here, the CMC decreased from 5.2×10^{-3} to 2.0×10^{-3} mg·mL^{-1} for the artemether-entrapped micelles. It is documented in literature that the encapsulated, hydrophobic drug is able to stabilise the micelle through the additional hydrophobic interactions between the nonpolar groups of the core-forming block and the drug, which result after the drug has been entrapped within the hydrophobic core.[54–56] It is the tendency of these non-polar groups to associate and cluster in order to be shielded

from an aqueous environment that is the driving force for these interactions. The CMC value of AL prodrug micelles is sufficiently low, as it is in the millimolar region. This indicates that these micelles should be able to withstand the plasma dilution effect once administered into the body.[44]
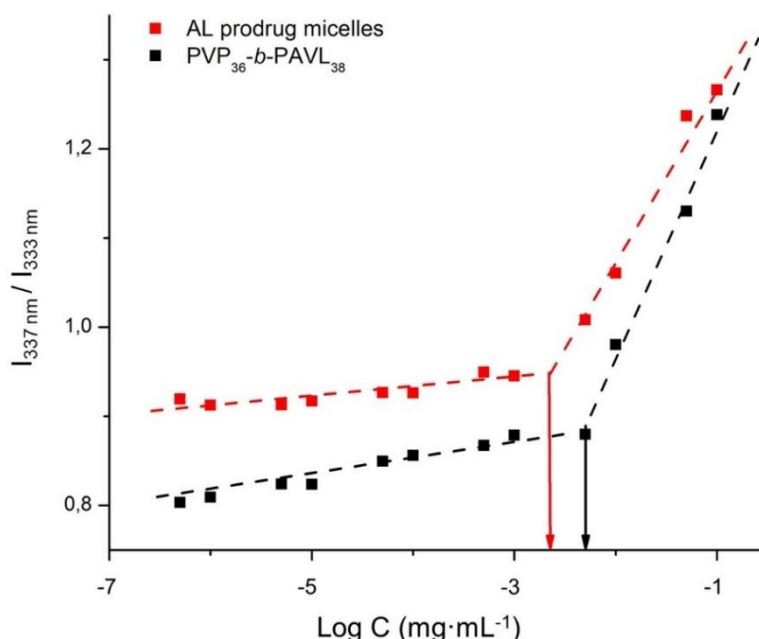
Figure 5.8 Fluorescence intensity of $I_{337\,nm}/I_{333\,nm}$ for pyrene as a function of the logarithm of concentration of micelles self-assembled from PVP$_{36}$-b-PAVL$_{38}$ and the AL prodrug.

b) Kinetic stability

The kinetic stability of the AL prodrug was investigated by measuring the average hydrodynamic diameter of the micelles as a function of time in phosphate buffered saline (PBS) and in a simulated physiological environment. In order to more accurately mimic *in vivo* conditions, it is important to investigate the kinetic stability of the micelles in biologically relevant media. A simulated physiological environment was therefore achieved by dispersing AL prodrug micelles in PBS containing 10% fetal bovine serum (PBS/FBS) at 37 °C. DLS was used to measure the change in micelle size over time.

It is important to determine the stability of the micelles in serum because a major concern for drug carriers is their destabilisation by opsonin proteins. Plasma proteins are able to partition into the core of drug-loaded micelles which would trigger disassembly. The adsorption of opsonin proteins on the surface of micelles can also trigger destabilisation.[57] Opsonisation is the process whereby a foreign body is covered with nonspecific opsonin proteins, making it more visible to phagocytic cells. After opsonisation, phagocytosis can occur which is the engulfing and removal of the foreign body from the bloodstream.[58] Neutrally charged micelles have been found to have lower opsonisation rates compared to charged micelles.[59] Furthermore, block copolymer micelles composed of greater hydrophilic:hydrophobic block segments were found to decrease opsonisation rates, as polymers that are highly flexible and hydrophilic can help to 'shield' hydrophobic or charged particles from blood proteins.[60]

Figure 5.9 shows the particle size stability of the AL prodrug micelles (0.5 mg·mL^{-1}) incubated in PBS (pH 7.4) and PBS/FBS (PBS pH 7.4 containing 10% FBS) at 37 °C. The micelles were self-assembled from the resulting AL prodrug using THF as the good solvent and water as the selective solvent. The AL prodrug micelles were found to be stable for four days in the various media, as after this time a drastic decrease in the hydrodynamic sizes were recorded. The relative stability of PVP-*b*-PVL micelles in serum is likely as a result of the of the hydrophilic PVP corona of the micelles. The composition of approximately 1:1 wt. fraction of hydrophilic to hydrophobic segments likely adequately shielded the hydrophobic cores of micelles from the aqueous medium. If, however, the hydrophobic constituents are at some point subjected to the surrounding aqueous environment, the micelle will lose integrity and disassemble.[61]
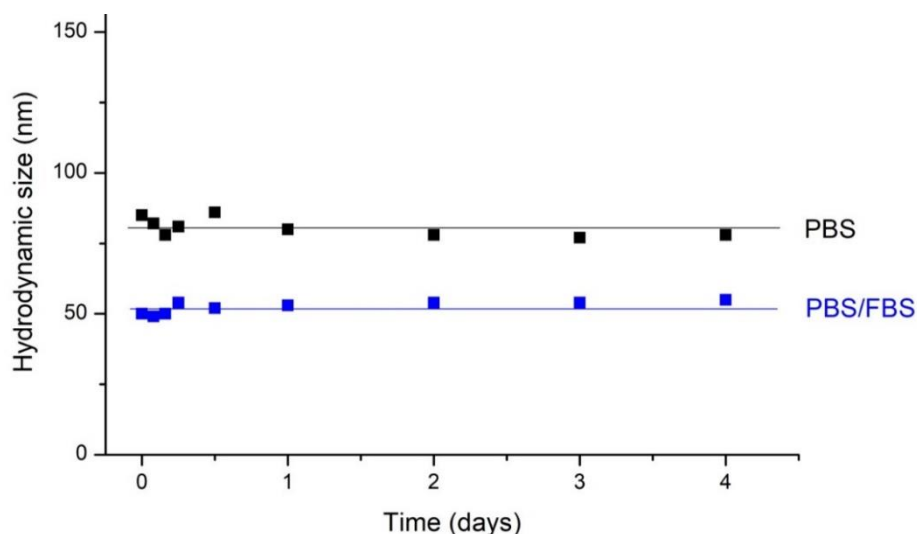
Figure 5.9 Kinetic stability of AL prodrug micelles at 37 °C in PBS (pH 7.4) and PBS/FBS over four days.

5.2.4 Drug release

Lumefantrine was conjugated to the block copolymer by means of an acid degradable acetal linkage. This linkage was found to be stable at physiological pH and labile at a low pH of 5, as confirmed in the model study using ^{1}H NMR spectroscopy in Chapter 3. The ability of the drug delivery system to degrade in acidic media and remain relatively stable in neutral media is important because the optimal functioning of the system is based on the physiological triggers that are utilised *in vivo* for malaria-burdened patients. More specifically, there exists a pH gradient from the blood plasma through the various intracellular compartments in the *Plasmodium*-infected red blood cell (iRBC). The pH is the lowest in the parasitophorous food vacuole.

The human malarial parasite *P. falciparum* has to ingest substantial amounts of haemoglobin during its development in the RBC so as to meet its nutrient requirements and maintain the necessary osmotic stability within the host cell.[62,63] The haemoglobin, which is internalised through endocytosis, is eventually hydrolysed in the parasite's digestive food vacuole. Cysteine, various enzymes and aspartic proteases are involved in the degradation of haemoglobin. These compounds are able to do so at an optimal pH range of 4.5 – 5.0, which implies that the food vacuole would maintain this acidic

environment. Another signal is that a low food vacuolar pH would promote the biomineralization of haem to haemozoin, which appears to be the primary pathway used by the parasite to detoxify large quantities of haem liberated during haeomoglobin degradation.[64–66] In reality, it is challenging to accurately determine the pH of the food vacuole due to the techniques required to do so as many previous studies have relied on lysed or isolated parasites. The general consensus is that the pH is estimated to be pH 5.0 – 5.8.[67–69] A study using a non-invasive *in vivo* pH measurement technique by Kuhn, Rohrbach and Lanzer indicated that the true value is likely towards the lower region of this pH zone.[66] The drug release of lumefantrine and artemether was therefore analysed at a pH of 5 and at a pH of 7.4 *in vitro* to simulate the environment that the micelles would be exposed to upon parenteral administration to the patient.

The drug release from the AL prodrug micelles was studied in a PBS buffer (pH 7.4) and in an acetate buffer (pH 5.0) at 37 °C using the dialysis technique. An equal amount of fresh buffer was used to replace each withdrawn sample after a predetermined time to maintain sink conditions and the sample was analysed for its drug concentration using LC-MS following the same protocols that were conducted for the determination of the DLCs. Complete release (100%) was taken as the total amount of each drug released after the addition of HCl (0.1 M, pH 2) and further incubation. The cumulative % drug release curve of lumefantrine is shown in Figure 5.10. Of primary concern was that at a low pH, the cleavage of the acetal bond conjugating lumefantrine to the block copolymer occurs. The results indicate that lumefantrine release is enhanced under the acidic environment condition and that no burst release is observed. After three days, approximately 74% of lumefantrine was released at a pH of 5 and approximately 22% was released at a pH of 7.4.
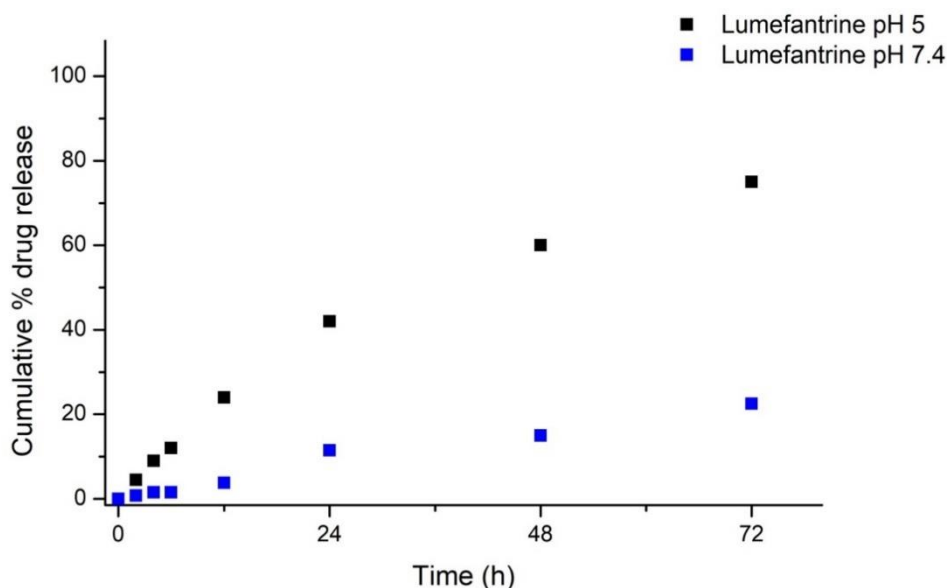
Figure 5.10 Cumulative % drug release of lumefantrine at pH 5.0 (acetate buffer) and at pH 7.4 (PBS buffer).

Similar to lumefantrine, artemether's drug release was enhanced under the acidic environment and no sign of burst release was observed. It is, however, likely that during the dialysis purification technique used to remove free artemether from the AL prodrug micelles, some entrapped artemether could also have been removed which would not result in an accurate representation of the drug release curve for artemether. This is not a limiting factor for covalently-bound lumefantrine.

5.2.5 Bioconjugation of the targeting ligand

Acute changes in the plasma membrane of iRBCs render the surface of those RBCs to become dissimilar to those of uninfected ones. It has been confirmed through extensive biochemical and molecular biological analyses that iRBCs are discernible from healthy RBCs through the following features, (i) the appearance of nanosized protrusions or 'knobs' on the surface of the membrane which leads to the stiffening of the cell, (ii) the possession of modified host proteins, (iii) the insertion of parasite-derived proteins, (iv) changes in the lipid composition and (v) having exposure of phosphatidylserine.[70,71]

These distinct features have led to the development of several screening methods used to identify a variety of compounds that are able to selectively bind to the surface of iRBCs. Of these compounds, low molecular weight peptides are particularly interesting as targeting ligands for antimalarial polymeric prodrug micelles because they are the less likely to interfere with self-assembly and the formation of micelles with defined core-shell structures. Furthermore, an ideal targeting ligand density has not been reported due to the idiosyncrasies of each drug delivery system and targeting mechanism. It has, however, been reported by Elias *et al.* that a lower targeting ligand density on the surface of the micelles or nanoparticles can prevent overcrowding, therefore leading to more effective target binding through achieving the correct orientation with the designated receptor.[72] A small molecule targeting ligand was previously used due to its hydrophilicity, molecular weight and *N*-terminus handle able to undergo the applicable bioconjugation chemistry.[73] It is the most hydrophilic peptide of the targeting ligands screened by Eda, Eda and Sherman, with sequence 'GSRSKGT' (Gly-Ser-Arg-Ser-Lys-Gly-Thr) as shown in Figure 5.11.[25]
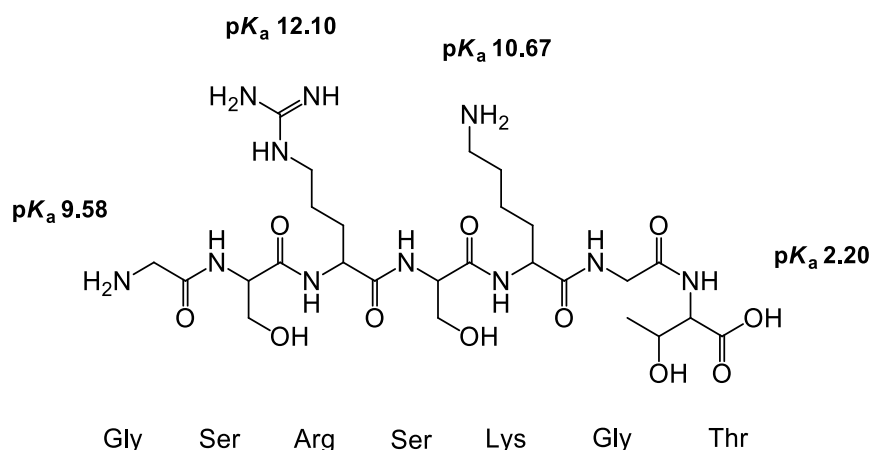
Figure 5.11 Small molecule targeting ligand, peptide 'GSRSKGT'.

This peptide 'GSRSKGT' was easily modified using succinimidyl 3-(2-pyridyldithio)propionate (SPDP) to introduce disulfide bonds at the *N*-terminus of the peptide on the α-amino glycine residue. The amine-reactive portion of SPDP is the *N*-hydroxysuccinimide (NHS) ester, and the reaction proceeds optimally in physiological to slightly alkaline conditions from pH 7.2 to 9, as shown in Scheme 5.2. At pH values above 8, the reaction proceeds rapidly because the rate of degradation and hydrolysis increase with increasing pH (the half-life of NHS ester is 10 min at pH 9 compared to 4 – 5 h pH 7).[74]

The internal lysine and arginine residues also contain amino groups which could possibly react with NHS-ester reagents. The glycine *N*-terminus should therefore be preferentially modified, which is achieved by maintaining a pH that will lead to the other available amino groups being very rarely in the protonated state, a technique frequently used in peptide chemistry.[74,75] The pH should be at least two units lower than the pK_a of the ε-amino groups to render limited activity.[76] Here, the lysine and arginine ε-amino groups have pK_a values which are higher than that of the *N*-terminus and a pH of 8.5 was used as it allowed for sufficient reactivity with the *N*-terminus. The pH values of 7, 7.5 and 8 had previously resulted in lower SPDP modification ratios.
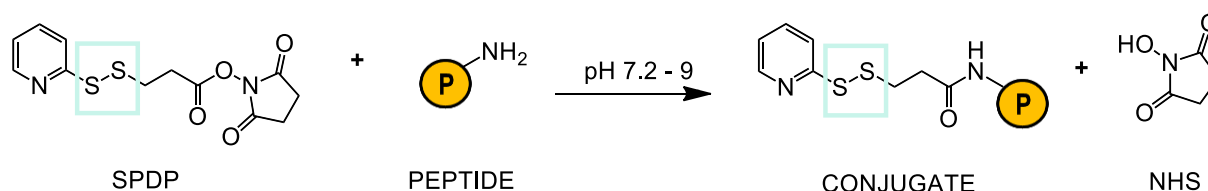
Scheme 5.2 NHS-ester reaction scheme for chemical conjugation to a primary amine.

The peptide 'GSRSKGT' was purchased and modified to be pyridyl disulfide (PDS)-terminated, as confirmed with the dithiothreitol (DTT) assay, as detailed in the Experimental section. This assay involves quantitatively measuring the release of pyridine-2-thione using UV-Vis spectroscopy (ϵ = 8080 M^{-1}·cm^{-1} at 340 nm in PBS-EDTA). DTT is a powerful reducing agent which can be used to efficiently convert PDS end groups to thiols. The number of moles of pyridine-2-thione released upon treating the PDS-terminated peptide with DTT is equal to the number of moles of PDS groups that were conjugated to the peptide prior to the reduction. In this way, the modification ratio of PDS/peptide was found to be approximately 1:1 indicating that the modification with SPDP had been successful. The formation of the modified peptide was further confirmed using ESI-MS in the positive mode. The ESI-MS spectra of the unmodified and modified 'GSRSKGT' peptide are shown in Figure 5.12. The molar mass ion peak at *m/z* 692 corresponds with the theoretical molar mass of the unmodified peptide which is 691.73 g·mol^{-1}. After the SPDP modification reaction and reduction using DTT, the thiol-terminated peptide (SH-peptide) was isolated. The molar mass ion peak at m/z 781 corresponds with the theoretical molar mass of the modified peptide which is 779.86 g·mol^{-1}.
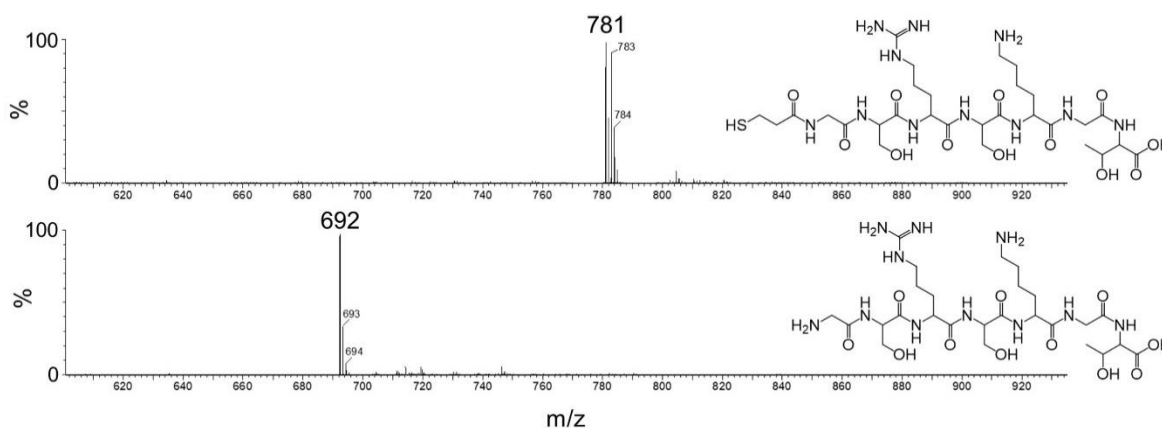
Figure 5.12 ESI-MS spectrum of the native peptide (m/z 692), bottom, and the thiol-functional peptide (m/z 781), top.

In the next step, the thiol-terminated peptide (SH-peptide) was conjugated to the AL prodrug. As detailed in Chapter 4, PDS-terminated PVP-OH (PDS-PVP-OH) was prepared in near-quantitative conversions and was used as the macroinitiator in the ROP of AVL which led to the synthesis of the LUM prodrug. The PDS moiety was confirmed to still be attached to the block copolymer after the post-polymerisation reactions had taken place. The SPDP-modified peptide was maintained in its protected thiol state until just prior to the bioconjugation reaction. At this time, DTT was used to deprotect the thiol and excess DTT was removed using dialysis. The bioconjugation reaction then proceeded through disulfide exchange between the SH-peptide and the AL prodrug micelles, which readily occurred at a neutral pH of 7 in PBS over 1 h. After this time, the peptide-functionalised AL prodrug micelles (pep-AL prodrug micelles) were purified using dialysis against PBS at pH 7.

The reaction was monitored by means of UV-Vis spectroscopy by measuring the displacement of pyridine-2-thione, which indirectly measures the number of moles of PDS groups that were attached to the compound following the DTT assay protocol. An assay was conducted on the SH-peptide to confirm that all of the PDS groups had been reduced prior to the reaction. Following this, an assay was conducted on the AL prodrug micelles before and after the bioconjugation reaction had taken place. The decrease in the number of moles of pyridine-2-thione could therefore be quantified after the SH peptide had displaced an amount of the PDS groups terminated to the AL prodrug. Approximately 12 ± 3 mol% of the polymer chains were found to be tethered to the peptide when this method was repeated three times. Figure 5.13 shows the UV-Vis spectra of the SH-peptide and the pep-AL prodrug (LUM 286 nm in PBS-EDTA) after the bioconjugation reaction had taken place. The UV-Vis spectra were recorded after DTT reduction so that the characteristic signal of pyridine-2-thione is clearly observed at 340 nm (ϵ = 8080 $M^{-1} \cdot cm^{-1}$, PBS-EDTA).
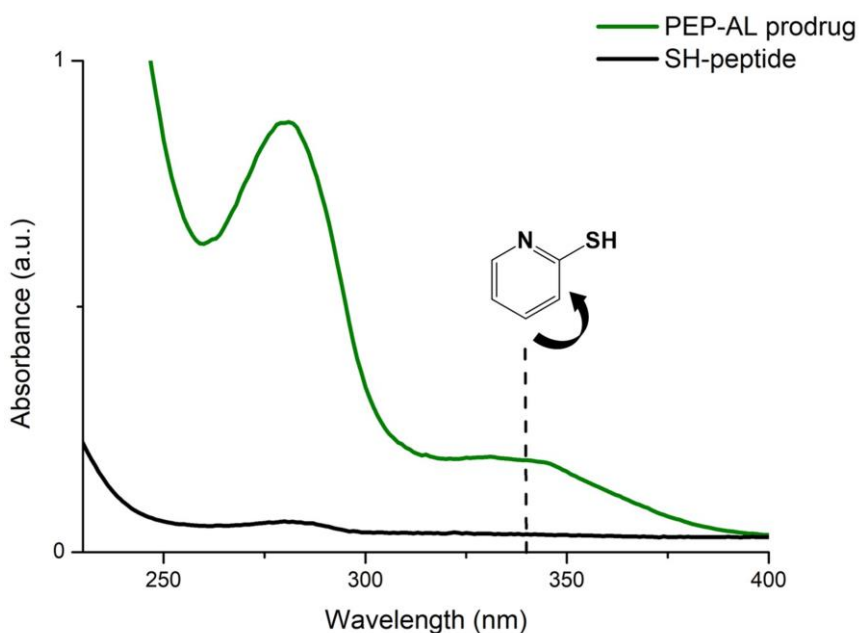
Figure 5.13 UV-Vis spectra of the thiol-terminated peptide (black) and the peptide-conjugated AL prodrug (green) after DTT reduction.

5.2.6 Biological analysis

Artemether-lumefantrine (AL) used in combination is a highly potent, synergistic drug combination therapy that is currently advocated by the WHO for the treatment of malaria because *P. falciparum* has not yet developed a resistance to it.[1] Drug resistance is a major concern for antimalarials as the parasite is ever-evolving. The longer plasma half-life of lumefantrine compared with artemether aids in the eradication of residual parasites once artemether has cleared from the bloodstream. Polymeric drug delivery systems can be highly beneficial in extending the blood circulation times of drugs and reducing their exposure to healthy cells. Artemether has a higher activity (lower IC_{50}) compared with lumefantrine which has a lower activity (higher IC_{50} value).[3,7,12] Without lumefantrine to extend the antimalarial action of the combination therapy, drug resistance to artemether would eventually develop, rendering treatment with artemether alone to be less effective. Here, the activity of lumefantrine is not its primary attribute, but rather its ability to extend the activity of the combined system that is highly beneficial. In these biological assays, the toxicity of the free drug (artemether and lumefantrine mixed in a ratio of 1:6) was compared with the prodrug micelles and the activity of the micelles was investigated against *P. falciparum* parasites.

a) *In vitro* toxicity

The haemolytic toxicity of the free drug, the PVP-*b*-PAVL micelles devoid of therapeutics ('empty' micelles), the LUM-conjugated prodrug micelles and the AL prodrug micelles bearing the peptidic targeting ligand (pep-AL prodrug micelles) were determined using RBCs from three different donors at varying concentrations. Haemolysis is the lysis of red blood cells and the expulsion of their components into the blood plasma. Regarding polymeric prodrugs used for parenteral purposes, it is one of the most important toxicological concerns.[77] The haemolytic toxicity was therefore determined for the polymeric prodrug over a period of 96 h, following a method by Rautenbach *et al.*[78] where decreasing concentrations of the compounds were tested for their ability to break down healthy RBCs.
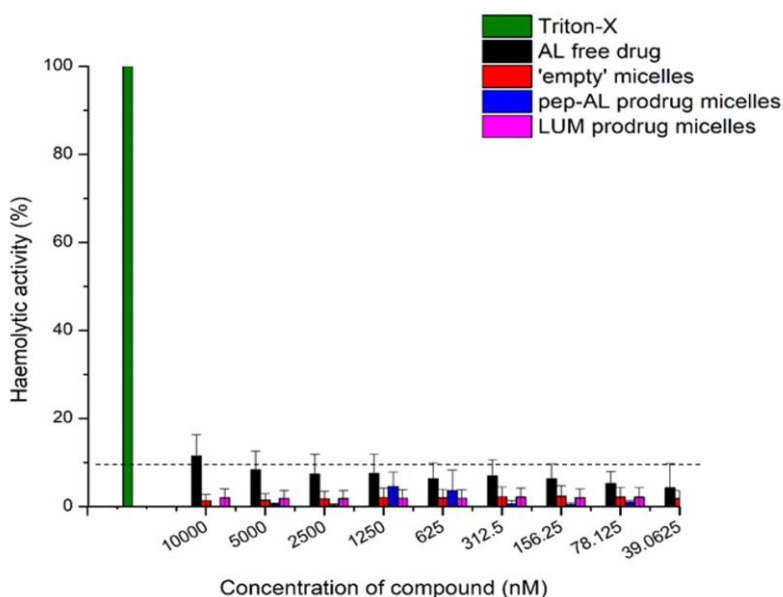
Figure 5.14 In vitro haemolysis of compounds incubated with healthy red blood cells with at decreasing concentrations by a factor of 2 (n = 3 independent biological repeats with technical triplicates).

The haemolytic toxicity of these compounds is shown in Figure 5.14, where negligible haemolysis (<10%) was incurred by the compounds over the concentrations tested. At the highest concentration (10 µM) of the pep-AL prodrug micelles incubated with RBCs, a >20-fold decrease in the haemolytic toxicity compared to the free drug was found. For the LUM prodrug micelles tested at their highest concentration, a <4-fold decrease in the haemolytic toxicity compared to the free drug resulted.

Following the haemolytic toxicity assay, the cytotoxicity was analysed using a Caucasian human hepatoma cell line (HepG2). The HepG2 cells used are liver carcinoma and liver cells, which are responsible for metabolising toxic compounds into non-toxic compounds to be excreted from the body.[79] A drug that elicits *in vitro* cytotoxicity will also likely result in *in vivo* toxicity. Lactate dehydrogenase (LDH) is a hydrogen transfer enzyme found in the cytoplasm of every living cell. LDH is released from the cell into the culture media only once the integrity of the cell has been lost, in this way providing a means to analyse the cytotoxic effect of various compounds.[80] The cytotoxicity determination and HepG2 cell culture methods were followed according to Verlinden *et al.* using standard protocols.[81] The cytotoxicity results for the 'empty' micelles and the pep-AL prodrug micelles relative to the AL free drug are shown in Table 5.2. Negligible cytotoxicity resulted from the 'empty' micelles and the pep-AL prodrug micelles when concentrations of 2 and 10 µM were used. At the high concentration of 10 µM, the prodrug micelles remained non-cytotoxic. The values highlighted in blue indicate a 10-fold decrease in the cytotoxicity of the prodrug micelles compared to the free drug combination.

Table 5.2 In vitro cytotoxicity against mammalian cells. The values highlighted in blue indicate a 10-fold difference in cytotoxicity compared to the free drug

Concentration	free drug *vs.* compound tested		
	free drug *vs.* 'empty' micelles	free drug *vs.* LUM prodrug micelles	free drug *vs.* pep-AL prodrug micelles
2 µM	-	1.00	1.00
10 µM	2.11	>10	>10

The *in vitro* toxicity results of the pep-AL prodrug micelles against healthy RBCs and HepG2 cells are promising and indicate that for all analyses, negligible toxicity levels were detected. These results indicate that the various synthetic processes did not cause the micelles to become harmful to cells and that it would likely not cause significant harm to organs and tissues once applied *in vivo* as a drug delivery system. Likewise, the loading of the artemether and the covalent conjugation of lumefantrine to PVP-*b*-PAVL did not cause significant haemolysis to RBCs or cytotoxicity to HepG2 cells. These results support the kinetic stability studies conducted (Section 5.2.3) prior to the biological assays which indicated that the drug payload was relatively protected within the core of the micelles during the initial stages of being dispersed in a simulated physiological environment of PBS-FBS. Furthermore, the cytotoxicity to HepG2 cells was similar for the peptide-conjugated prodrug and the prodrug *sans* peptide, indicating that the peptide did not significantly increase the cytotoxic effects of the micelles.

b) Activity

The *in vitro* growth inhibition of the synthesised prodrug micelles was determined against a hydroxychloroquine-sensitive strain of asexual, ring-stage *P. falciparum* parasites, NF54. This was achieved using the malaria SYBR green I-based fluorescence (SYBR green) assay following standardised protocol based on literature.[82–84] SYBR Green I is a DNA intercalating dye which binds to the minor groove of double-stranded DNA. Mature RBCs do not have DNA or RNA so the binding of this dye is specific for malarial DNA in any blood stage of *P. falciparum* development. The binding of the dye causes fluorescence which is directly proportional to parasitic proliferation levels.[83,85]

The evaluation of the compounds occurred against blood stages of *P. falciparum* over a 96 h developmental period (two life cycles of the parasite). The half-maximal inhibitory concentration (IC$_{50}$) indicates the amount of a specific pharmacologic agent that is needed to inhibit a particular biological activity, *i.e.* the parasitic population, by half.[86] This measure was determined using dose-response assays and are presented in Table 5.3 along with standard error of the mean (SE) values. The stage-specific dose response curves of the AL free drug compared with the pep-AL prodrug micelles against *P. falciparum* NF54 are shown in Figure 5.15.

Table 5.3 In vitro antimalarial activity of the AL free drug, 'empty' PVP-b-PAVL micelles, LUM prodrug micelles and pep-AL prodrug micelles against a NF54 P. falciparum parasites. Results are representative of one independent biological replicate, n = 3, each performed as technical triplicates, ± SE.

Compound	Antimalarial activity against *P. falciparum* NF54	
	IC$_{50}$ (nM)	SE [a]
Free drug	0.86	0.21
'Empty' micelles	No activity	-
LUM prodrug micelles	1025.0	58.17
Pep-AL prodrug micelles	1021.8	270.9

[a] Results are representative of three independent biological triplicates, n = 3, each performed as a technical triplicate, ± SE.
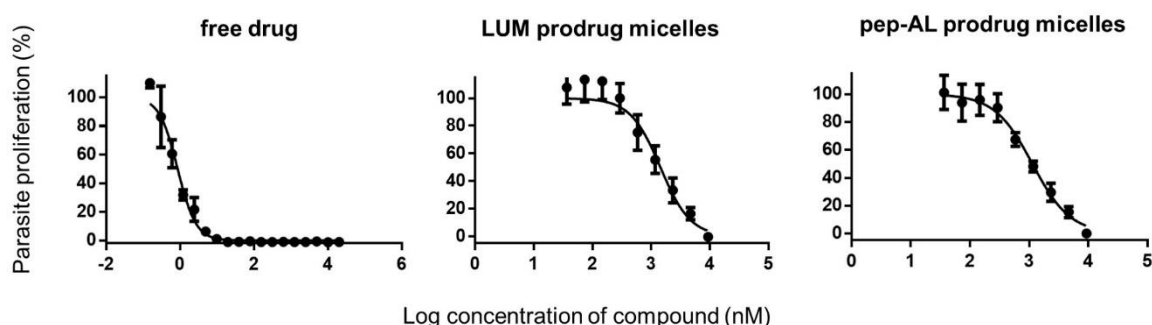

Figure 5.15 Stage-specific dose response curves of the AL free drug compared with the LUM prodrug micelles and the pep-AL prodrug micelles against NF54 parasites. The curves represent three independent biological repeats (n = 3) and error bars indicate the SE. Error bars not shown fall within the area of the symbol.

Several types of classifications have been proposed for considering a compound to be active against malaria and one such that is commonly applied is shown in Table 5.4.[87,88] A compound is considered highly active against *P. falciparum* parasites and especially interesting as an antimalarial if the IC_{50} is below 1000 nM. For the pep-AL prodrug micelles, an IC_{50} of 1021.8 ± 270.9 nM was obtained which is much higher than that of the AL free drug combination (0.86 ± 0.21 nM) and also has a much larger SE. The AL free drug can therefore be classified as a potent antimalarial against NF54 *P. falciparum* parasites. Using the classification criteria shown in Table 5.3, the pep-AL prodrug micelles and LUM prodrug micelles can be classified as antimalarials having good activity towards *P. falciparum* growth inhibition, where similar IC_{50} values were obtained.

Table 5.4 Classification criteria of the IC_{50} values of compounds related to their activity as antimalarial agents

IC_{50}	Classification
greater than 200 000 nM	no activity
between 200 000 to 100 000 nM	low activity
between 100 000 to 20 000 nM	moderate activity
between 20 000 to 1000 nM	good activity
less than 1000 nM	excellent / potent activity

The decreased activity of the prodrug micelles compared with the free drug combination could be associated with the mechanism of the drug delivery vehicle. The drug release trigger of lumefantrine is an acid-sensitive acetal linker which would be susceptible to cleavage only in the slightly acidic parasitic food vacuole compartment within the iRBC. Two plausible events that could have taken place to retard the growth inhibition of the parasites are that (i) the drug was not released within the iRBCs once the pep-AL prodrug was taken up and (ii) the pep-AL prodrug micelles were not effectively taken up by the iRBCs due to ineffective binding by the targeting ligand.

The LUM prodrug micelles have shown good antimalarial activity which means that at least a portion of lumefantrine was released by cleavage of the acetal bond. This would imply that it was possible for this cleavage to occur, which is supported by the drug release study conducted in Section 5.2.4. Event (ii) seems more likely as the targeting ligand binding is less of an 'all-or-nothing' outcome and NPPs to the iRBC allow for non-selective targeting primarily through size effects (passive targeting). It is likely that the targeting ligand was not able to bind to iRBCs effectively, therefore causing the low pH drug-triggering event not to take place over an adequate time-frame (<96 h test period).

Moreover, few therapeutic agents have been developed by taking advantage of the membrane changes of iRBCs compared with RBCs. The selection of small peptide targeting ligands by Eda, Eda and Sherman was based on their ability to differentiate between the surfaces of iRBCs and uninfected RBCs.[25] The 'GSRSKGT' peptide was previously identified due to its hydrophilic nature, ease of bioconjugation and low molecular weight.[73] The differentiation of iRBCs to RBCs was based on the surface perturbations on the iRBCs as a result of the parasitic invasion. Although the more hydrophilic

peptide 'GSRSKGT' was identified after the sixth panning of the phage display peptide library (PDL) on the surface of iRBCs, it was subsequently not found to be highly effective during *in vitro* binding to iRBCs. This supports the notion that event (ii) had likely taken place. It was further asserted that the highly effective peptide and its clones contained sequences of three to four amino acids with aliphatic side chains and lacked polar groups. It was therefore postulated that a minimum degree of hydrophobicity is necessary to target iRBCs through these membrane distinctions.[25,89]

Future work should focus on the exploration of specific protein-protein interactions of targeting ligands to the parasite proteins that are trafficked within the iRBC. For example, the major adhesion ligand on the iRBC surface is *P. falciparum* erythrocyte membrane protein 1 (PfEMP1), which could bind to a number of receptors expressed on vascular endothelial cells. Knob-associated histidine-rich protein (KAHRP), mature parasite-infected erythrocyte surface antigen (MESA), and PfEMP3 are also localised on the cytosolic side of the iRBC membrane.[90] Heparin and other glycosamine glycans have also been highly effective in selectively binding to iRBCs.[91–93] The high molar masses of these macromolecules pose challenges related to the self-assembly of the resultant prodrug. This, along with conjugation strategies, should be accounted for in the design of these systems.

The developed prodrug system likely caused appreciable antimalarial action through passive targeting events or micelle destabilisation which would occur over longer periods of time compared to actively targeting compounds. Furthermore, the possibility of obtaining long circulation times of the prodrug micelles and low toxicities holds great potential for further development with AL therapy. It also holds potential for the adaptation of other hydrophobic drugs, as it was recently shown by Hussein and Youssry using drug solubilisation studies, that PVL outperformed PCL and four other common biodegradable polymers in drug-polymer compatibility studies through determination of the Flory-Huggins interaction parameters with five hydrophobic drugs.[12] In practice, this was confirmed in di-block copolymer systems composed using PVL as the core-forming block instead of PCL, that higher DLCs of paclitaxel and campothecin (anticancer drugs) were obtained indicating greater polymer-drug compatibility for those drugs.[94,95]

5.3 Conclusions

In a series of simple steps, the polymeric carrier which was developed as described in Chapters 3 and 4, was used to incorporate the antimalarial drug combination of artemether-lumefantrine. PVP-*b*-PAVL was carboxylated, functionalised with EGVE and conjugated to hydroxy-functional lumefantrine via an acid degradable acetal linkage. Artemether was physically entrapped within the core of the LUM prodrug micelles using the cosolvent technique which yielded micelles of diameter 114 nm from DLS. After drug incorporation, the stability of the AL prodrug micelles was investigated and found to be sufficient for intravenous administration into the body, where extreme dilution effects and degradation by opsonin proteins would take place. The periphery of the AL prodrug micelles was tethered with a targeting ligand using disulfide exchange, which was made possible by modifying the peptide to bear thiol groups.

The pep-AL prodrug system is highly tuneable and can be easily modified and adapted by using a variety of drugs and targeting ligands. It is not cytotoxic or haemolytic at the highest concentrations tested with, and without highly potent drugs residing in the core of its self-assembled micelles. The artemether-lumefantrine drug combination was found to have excellent activity in inhibiting the growth of *P. falciparum* but in comparison, the AL prodrug micelles exhibited a pronounced decrease in activity. It is likely that the targeting ligand was not successful in binding to iRBCs and that the appreciable activity measured for the AL prodrug micelles was due to passive targeting via NPPs to reach the low pH food vacuole needed to trigger the drug release, or eventual micelle destabilisation. Cellular internalisation studies and the analysis of the targeting ability of these prodrug micelles tethered to a library of ligands with different ligand densities would be beneficial in understanding the biological response to the polymeric prodrug system. In this way, it is promising that more potent prodrug micelles can be developed. The drug delivery system developed for this combination therapy is novel, and lays the basis for future systems by detailing simple techniques to achieve the incorporation of potent drug combinations.

5.4 Experimental

5.4.1 General details

18-Crown-6 (≥99.0%, Sigma-Aldrich), ethylene glycol vinyl ether (97%, Sigma-Aldrich), 4-dimethylaminopyridine (≥99%, Sigma-Aldrich), *N*,*N*'-dicyclohexylcarbodiimide (99%, Sigma-Aldrich), *N*-succinimidyl 3-(2-pyridyldithio)propionate (≥95%, Sigma-Aldrich), pyrene (≥99.0%, Sigma-Aldrich), 1,4-dithiothreitol (≥97%, Roche), *p*-toluenesulfonic acid (≥98.5%, Sigma-Aldrich), peptide sequence 'GSRSKGT' (≥98%, GL Shanghai), PBS tablets (pH 7.4, Sigma-Aldrich), ethylenediaminetetraacetic acid trisodium salt (≥95%, Alfa Aesar), potassium permanganate (≥99.0%, Merck), sodium bisulfite (ACS reagent, Sigma-Aldrich), sodium bicarbonate (≥99.7%, Sigma-Aldrich), anhydrous magnesium sulfate (≥99.5%, Sigma-Aldrich), hydrochloric acid (37%, Sigma-Aldrich), sodium hydroxide (≥97.0%, Sigma-Aldrich) and artemether (AM, ≥98%, Sigma-Aldrich) were used as received. Lumefantrine (LUM) was kindly gifted by CSIR Material Science & Manufacturing. PBS-EDTA was made by adding EDTA (0.02%) to PBS buffer at pH 8. Acetate buffer was made up with sodium acetate anhydrous (≥99%, Sigma-Aldrich) and acetic acid glacial (≥99.85%, Sigma-Aldrich) to a pH of 5. The block copolymer PVP-*b*-PAVL (M$_{n,theoretical}$ = 7800 g·mol^{-1}, M$_{n,SEC}$ = 9300 g·mol^{-1}, Đ = 1.2) was synthesised and characterised as detailed in Chapter 4. Snakeskin™ (Thermo Scientific™) and Float-A-Lyzer™ G2 dialysis tubes (Spectrum™) were used as specified. Reaction grade, anhydrous THF, DMF and 1,4-dioxane were purchased from Sigma-Aldrich and were used as received. Dichloromethane was distilled and stored over activated 3 Å molecular sieves when needed. Acetone was stirred over anhydrous calcium sulfate (CaSO$_4$) (25 g·L^{-1}) before distilling prior to use. Other solvents such as hexane and diethyl ether were purchased from Kimix and used as supplied. Distilled, deionised water was obtained from a Millipore Milli-Q purification system and all buffers were thoroughly degassed before use. CDCl$_3$ (99.9%, Aldrich) was used as the NMR solvent.

The Malaria Parasite Molecular Laboratory (M^{2}PL), where the *in vitro* biological assays were conducted, holds ethical clearance from the Faculty of Natural and Agricultural Sciences Ethics Committee of the University of Pretoria (EC 120821-077) for the cultivation of parasites and the use of human red blood cells (RBCs). *P. falciparum* parasites were cultured at M^{2}PL which has a certified P2 facility. Human whole blood (blood type dependant on availability) was collected in an anticoagulated blood bag (Adcock Ingram) from consenting donors. Caucasian hepatocellular carcinoma cells (HepG2) were kindly gifted by Duncan Cromarty, University of Pretoria. Dulbecco's Modified Eagle's Medium (DMEM) (HyClone, Fischer Scientific), fetal bovine serum (FBS) (Sigma-Aldrich), penicillin/streptomycin (10 000 units penicillin and 10 mg streptomycin·mL^{-1}, Sigma-Aldrich), Trypan-Blue (Gibco™, Fischer Scientific), Trypsin-EDTA (HyClone, Fischer Scientific), CytoSelect™ LDH Cytotoxicity Assay Kit (Cell Biolabs Inc., CBA-241)*,* complete culture medium RPMI 1640 medium (Sigma-Aldrich), HEPES (≥99.5%, Sigma-Aldrich), D-glucose (≥99.5%, Sigma-Aldrich), hypoxanthine (≥99.0%, Sigma-Aldrich), gentamycin (50 mg·mL^{-1} in deionized water, Sigma-Aldrich), AlbuMAX™ II Lipid-Rich BSA (Gibco™, Fischer Scientific), complete RPMI media supplemented with L-glutamine and U.S. origin FBS (10%, Sigma-Aldrich), SYBR® Green I nucleic acid gel stain 10 000 × in DMSO (Sigma-Aldrich)**,** saponin (Sigma-Aldrich) and Triton X-100 (Sigma-Aldrich) were used as received. The free drug was artemether-lumefantrine (AL) mixed in a ratio of 1:6.

^{1}H and ^{13}C NMR spectra were obtained with a Varian VXR-Unity spectrometer (400 mHz unless stated otherwise) with samples dissolved in deuterated solvents with tetramethylsilane (TMS) as internal reference. MestreNova 11.0.4 software was used to process the spectra. LC-MS was conducted using a Waters Synapt G2 quadrupole time-of-flight mass spectrometer with electron spray ionisation in the positive mode fitted with a Waters UPLC and photo diode array detector. Separation was achieved using a Waters BEH C18 column of dimensions 50 × 2.1 mm. A gradient was applied using ammonium acetate (5 mM, solvent A) and methanol containing ammonium acetate (5 mM) and ammonium hydroxide 0.5% (solvent B). The gradient began with solvent A (60% solvent, 0.3 min) and changed to solvent B (100 %, 3 min) linearly. Re-equilibration was achieved by reverting back to the initial conditions of solvent A (60%, 2 min). The flow rate was 0.3 mL·min^{-1} and the column was kept at 45 °C. The injection volume was 1 µL. Data were acquired in MS^E mode which consisted of a low collision energy scan (6 V) from *m/z* 100 to 1500 and a high collision energy scan from *m/z* 40 to 1500. The high collision energy scan was done using a collision energy ramp of 30 – 60 V. The MS was optimised for the best sensitivity with a cone voltage of 15 V. The desolvation gas was nitrogen at 650 L·h^{-1} and the desolvation temperature was 275 °C. The identities of the drug compounds were confirmed by matching the retention times, accurate masses and fragment ions for the samples compared with the standards. The concentrations of the drugs used to construct the calibration curves ranged from 0.1 – 100 µg·mL. Acceptable linearity (coefficients of variation >0.995), method precision (RSDs of repeat injections of standards, (n = 6, < 2%) and sensitivity was achieved. Since all peaks were well resolved, selectivity was adequate for the analysis. MassLynx software was used to process the data. SEC data were obtained from a Shimadzu LC-10AT isocratic pump, a Waters 717+ autosampler, a column system fitted with a PSS guard column (50 × 8 mm) in series with three PSS GRAM columns (300 × 8 mm, 10 μm, 2 × 3000 Å and 1 × 100 Å) kept at 40 °C, a Waters 2487 dual wavelength UV

detector and a Waters 2414 differential refractive index (DRI) detector. DMF was used as eluent, stabilised with 0.05% 2,6-di-*tert*-butyl-4-methylphenol (BHT) and 0.03% LiCl (w/v) at a flow rate of 1 mL·min^{-1}. The calculated molar masses were relative to poly(methyl methacrylate) (PMMA) calibration standards (Polymer Laboratories) ranging from 690 to 1.2×10^6 g·mol^{-1}. Data acquisition was performed using Millennium software version 4. DLS was conducted to determine the particle size and particle size distribution of the polymeric prodrug micelles using a Malvern Instrument ZetaSizer Nano ZS90 equipped with a 4 mW He-Ne laser, operating at a wavelength of 633 nm. The scattered light was detected at a scattering angle of 90° at 25 °C or 37 °C. The final particle size and size distribution were obtained from three measurements, each comprising 10 – 15 sub-runs, and calculated via the Malvern Zetasizer software. DSC measurements were recorded on a TA Instruments Q100 DSC. The instrument was calibrated using indium standards with a standard cooling and heating rate of 10 °C·min^{-1} over a temperature range of 25 – 120 °C where three cycles of data were acquired and the second cycle was used. Samples of 3 mg were prepared for analysis in aluminium pans and the data were analysed using the TA Universal Analysis program. TEM analysis was conducted to observe the morphology of the self-assembled prodrug micelles. The samples were imaged using the Tecnai 20 transmission electron microscope (Thermo Fisher) fitted with a LaB$_6$ emitter and operating at 200 kV and a Gatan Tridiem 863 UHS (Gatan). The images were collected using the embedded Gatan CCD camera (2048 $\times$ 2048 pixels). A drop of the sample solution was deposited onto a copper grid and dried at room temperature. The samples were negatively stained with uranyl acetate. ImageJ software was used for nanomorphology measurements where 100 micelles were measured to record the average and standard deviation. The fluorescence excitation spectra of pyrene were measured at varying block copolymer concentrations using a Perkin Elmer Luminescence LS50B spectrometer using FL Winlab version 4.0 for data processing. A Perkin Elmer Lambda 20 photodiode array spectrophotometer was used to measure the UV-Vis spectra. It consisted of a holographic monochromator, pre-aligned deuterium and halogen lamps and a photodiode array detector. UV Winlab (version 2.0) software was used for data acquisition and processing.

5.4.2 Synthetic procedures

5.4.2.1 Synthesis of carboxylic-acid functionalised PVP-*b*-PAVL

In a 50 mL round-bottom flask equipped with a magnetic stir bar, PVP-*b*-PAVL (200 mg, 2.2×10^{-5} mol) was dissolved in DCM (10 mL) and acetic acid (1.8 mL, 0.03 mol). 18-Crown-6 (100 mg, 3.8×10^{-4} mol) was added and the mixture was stirred vigorously at 0 °C in an ice bath. KMnO$_4$ (95 mg, 6×10^{-3} mol) was then added and the reaction was observed to turn violet, and then became brown within minutes as the manganese oxide was produced. The suspension was stirred for 18 h, after which water (10 mL) was added followed by enough saturated NaHSO$_3$ to reduce any oxidant species until the suspension became colourless. The organic layer was washed twice with water, dried over MgSO$_4$ and concentrated under reduced pressure. The carboxylated polymer was precipitated twice from hexane/diethyl ether. Yield: 184 mg, quantitative conversion. ^{1}H NMR (600 MHz, CDCl$_3$) δ (ppm) 8.0 – 7.1 (aromatic), 4.4 – 3.5 ((CH$_3$-C**H**-), (-O-C**H$_2$**-), (-CH$_2$-C**H$_2$**-O-), PVL (-C**H$_2$**-OH), PVP (-S-C**H**-)), 4.1

PVL (-C**H₂**-O-), 3.4 – 3.1 PVP (-N-C**H₂**-), 2.5 – 2.4 PVL (C=OC**H**-), PVL (-CH-C**H₂**-), 2.4 – 1.7 PVP (-C=OC**H₂**-), PVP (-CH₂-C**H₂**-), 1.6 PVL (-C**H₂**- ×2), 1.6 – 1.2 PVP (-CH-C**H₂**-), (-CH-C**H₃**). ¹³C NMR (600 MHz, CDCl₃) δ (ppm) 175.2, 174.4, 173.3, 136.0, 128.7, 126.9, 125.3, 64.0, 47.0, 44.9, 37.7, 36.5, 33.6, 31.6, 29.3, 28.2, 26.5, 21.6, 21.1, 18.5, 14.2. $M_{n,SEC}$ = 9800 g·mol⁻¹, Đ = 1.2

5.4.2.2 Synthesis of vinyl ether-functionalised PVP-*b*-PAVL

Under argon gas flow, to a 50 mL round-bottom flask equipped with a magnetic stir bar were added the carboxylated PVP-VL block copolymer (150 mg, 1.53×10^{-5} mol), DMAP (42.7 mg, 3.5×10^{-4} mol), DCC (431.7 mg, 2.1×10^{-3} mol), and 1,4-dioxane (10 mL). The flask was sealed and the reaction was allowed to proceed with stirring for 10 h at 25 °C. Degassed EGVE (308.4 mg, 3.5×10^{-3} mol) in 1,4-dioxane (0.2 mL) was then added to the flask and the reaction was allowed to proceed for 24 h at 25 °C. The opaque solution was filtered and the filtrate was precipitated in cold diethyl ether. The product was collected and dried under vacuum. Yield: 128 mg, %f,NMR (EGVE : polymer) = ~70 mol%. ¹H NMR (400 MHz, CDCl₃) δ (ppm) 8.0 – 7.1 (aromatic), 6.5 EGVE (-C**H**=CH₂), 4.4 – 3.5 ((CH₃-C**H**-), (-O-C**H₂**-), (-CH₂-C**H₂**-O-), PVL (-C**H₂**-OH), PVP (-S-C**H**-)), 4.2 – 4.0 EGVE (-CH=C**H₂**), 4.1 PVL (-C**H₂**-O-), 3.5 EGVE (-O-C**H₂**- ×2), 3.4 – 3.1 PVP (-N-C**H₂**-), 2.5 – 2.4 PVL (C=OC**H**-), PVL (-CH-C**H₂**-), 2.4 – 1.7 PVP (-C=OC**H₂**-), PVP (-CH₂-C**H₂**-), 1.6 PVL (-C**H₂**- ×2), 1.6 – 1.2 PVP (-CH-C**H₂**-), (-CH-C**H₃**). $M_{n,SEC}$ = 11 300 g·mol⁻¹, Đ = 1.2.

### 5.4.2.3 Synthesis of the acetal-linked lumefantrine prodrug

Under argon gas flow, to a 25 mL Schlenk flask equipped with a magnetic stir bar, were added EGVE-functionalised PVP-PVL block copolymer (100 mg, 8.8×10^{-6} mol), LUM (47 mg, 8.8×10^{-5} mol), *p*-TSA (0.32 mg, 1.86×10^{-6} mol), activated 4 Å molecular sieves (1 g) and DMF (10 mL). The flask was sealed and the reaction was left to stir at 50 °C for 4 days. The resulting mixture was filtered to remove the molecular sieves and the filtrate was dialysed against 250 mL DMF for 24 h, then against water for 24 h changing the solvent periodically to remove unreacted LUM (MWCO 3500 g·mol⁻¹). The prodrug was lyophilised for 24 h until dry. Yield: 78 mg, %f,NMR (LUM : polymer) = 22 mol%. $M_{n,SEC}$ = 15 600 g·mol⁻¹, Đ = 1.4.

5.4.2.4 Targeting ligand conjugation

a) Modification of the peptide

The peptide with sequence 'GSRSKGT' (25 mg, 3.6×10^{-5} mol) was dissolved in degassed DMF (0.15 mL) and the pH was adjusted to 9 by addition of 1 M Na₂CO₃. SPDP (6 mg, 1.9×10^{-5} mol) was then added to the solution and the reaction was stirred at 4 °C for 2 h. The pH was monitored and maintained at approximately 8.5 during the course of the reaction. The modified peptide was dialysed using a Float-a-lyzer™ dialysis tube (MWCO 3500 g·mol⁻¹) against PBS-EDTA (pH 8) for 24 h to remove any unreacted SPDP. The SPDP-modified peptide was stored in the PDS-protected state until further use. Prior to the bioconjugation reaction, DTT was used *in situ* as a reducing agent to render the free thiols necessary for the peptide conjugation. The peptide modification was quantified by monitoring the

displacement pyridine-2-thione during the course of the conjugation reaction using UV-Vis spectrophotometry following protocol.
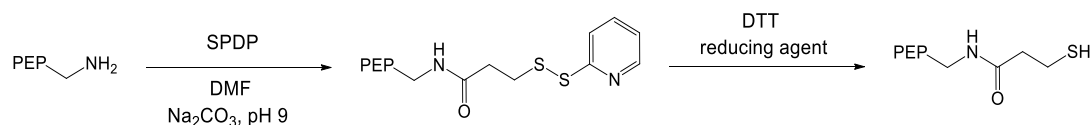
Scheme 5.3. Modification of peptide with SPDP and subsequent reduction to render a thiol-terminated peptide.

b) Polymer-peptide bioconjugation

Under argon gas flow, the SPDP-modified peptide (2.5 mg, 2.8 × 10^{-6} mol) was reconstituted in PBS (1 mL, pH 7) and treated with DTT (3.2 mg, 2.1 × 10^{-5} mol) for 1 h to generate the thiol-terminated peptide and excess DTT was removed by dialysing the deprotected peptide in PBS for 6 h. After this time, the SH-peptide and the PDS-modified prodrug (420 mg, 2.8 × 10^{-5} mol, quantitative PDS functionality by ^{1}H NMR) were dissolved in PBS (10 mL, pH 7) and the mixture was stirred for 4 h at 25 °C. The peptide-conjugated prodrug was dialysed using a Float-a-lyzer™ dialysis tube (MWCO 3500 g·mol^{-1}) against PBS (pH 7) for 18 h. The peptide conjugation was quantified by monitoring the displacement pyridine-2-thione during the course of the conjugation reaction using UV-Vis spectrophotometry following DTT assay protocol.
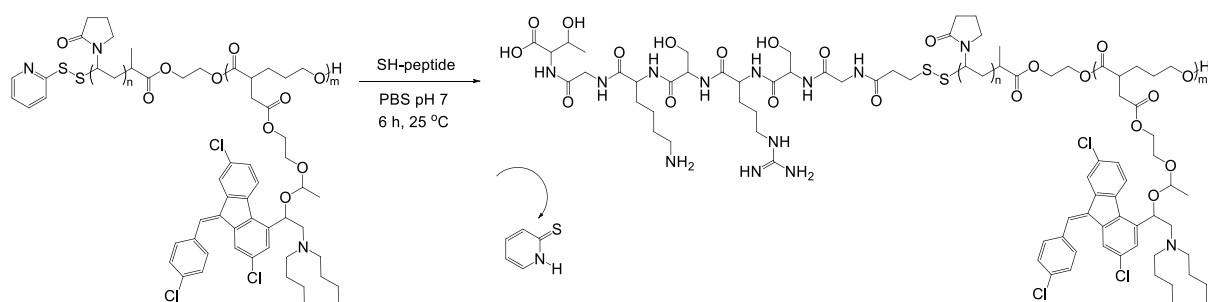
Scheme 5.4 LUM prodrug and thiol-terminated peptide bioconjugation.

5.4.3 General procedures

a) Protocol for DTT assay

An accurately recorded mass of the modified compound (peptide or polymeric prodrug) was dissolved in PBS-EDTA (1 mL, pH 7.4) and the absorbance was measured at 343 nm in relation to the PBS-EDTA blank, in triplicate. Following this, DTT (10 μL, 15 mg·mL^{-1} in water) was added directly to the cuvette containing the modified compound and this solution was agitated for 10 s until combined. After exactly 15 min, the absorbance at 343 nm was recorded in the same manner as before the reduction had taken place. The change in absorbance can be calculated by ΔA_{343} = (average A_{343} after DTT) – (average A_{343} before DTT). The number of moles of pyridine-2-thione released is equivalent to the number of moles of PDS groups that were originally attached to the PDS-conjugated compound before the reduction with DTT. The molar ratio of PDS groups relative to the peptide or polymer can then be

calculated using Equation 5.3, where the value 8080 is the molar extinction coefficient of pyridine-2-thione at 343 nm, 8080 $M^{-1} \cdot cm^{-1}$.

$$\text{PDS molar ratio} = \frac{\Delta A}{8080} \times \frac{\text{MW of peptide or polymer}}{[\text{peptide or polymer}]} \qquad \text{Equation 5.3}$$

b) Self-assembly and simultaneous entrapment of artemether into its hydrophobic core

Artemether was entrapped within the core of PVP-*b*-PAVL micelles using the cosolvent technique. In a typical procedure, the prodrug (10 mg, 6.67×10^{-7} mol) and AM (5 mg, 1.67×10^{-5} mol) were completely dissolved in THF or acetone (5 mL) by stirring in a scintillation vial equipped with a screw-top lid at 25 °C for 2 h. Following this, water (0.4 mL) was added via syringe using a metered flow pump at a slow rate (0.015 mL·min^{-1}). The AL prodrug micelles were purified using dialysis with a Snakeskin™ dialysis tube (MWCO 3500 g·mol^{-1}), against THF or acetone/water (1:1) for 12 h and then against water for 24 h, changing the solvent periodically to remove free artemether.

c) Determination of the entrapment efficiency and drug loading content

The entrapment efficiency (EE) and the drug loading content (DLC) were determined by dissolving a known amount of the prodrug micelles in the extraction solvent (1:1 MeOH/DMSO). The solution obtained after extraction was filtered using a 0.4 μm size filter. The filtrate was appropriately diluted with MeOH/DMSO (1:1) and the amount of drug contained within the micelle was estimated using the LC-MS method with standard protocols. Equations 5.1 and 5.2 are reiterated below which were used to determine the EE and DLC.

$$\text{EE \%} = \frac{\text{amount of drug entrapped}}{\text{drug initially used in formulation}} \times 100 \qquad \text{Equation 5.1}$$

$$\text{DLC \%} = \frac{\text{amount of drug in micelles}}{\text{amount of micelles recovered}} \times 100 \qquad \text{Equation 5.2}$$

d) Thermodynamic stability

The critical micelle concentration (CMC) of the block copolymers were determined using pyrene as the probe, based on protocol described in literature.[96] First, a dilution series of each conjugate was prepared in PBS at concentrations ranging from 0.0001 – 1 mg·mL^{-1}, each made up to a final volume of 4.5 mL. Following this, a stock solution of pyrene dissolved in acetone (36.4 mg·mL^{-1}, 1.8×10^{-4} M) was prepared and stored over ice to prevent solvent evaporation which could lead to concentration fluctuations. From this solution, 15 µL was pipetted into each conjugate dilution to make up a final pyrene concentration of 6.0×10^{-7} M. The conjugate dilutions containing pyrene were left for 24 h at 25 °C in the dark to equilibrate the partitioning of pyrene into the hydrophobic domain of the polymer. The fluorescence excitation spectra were recorded from 300 to 360 nm with the emission wavelength at 390 nm. The spectra were recorded at a scan rate of 250 nm·min^{-1} and the intensity ratio of I_{337}/I_{333} was plotted against the logarithm of the conjugate concentration to determine the CMC.

e) Kinetic stability

The kinetic stability of the micelles was assessed by DLS. This was investigated in systems mimicking biological fluids (PBS, pH 7.4) and PBS containing 10 % fetal bovine serum (PBS-FBS). The solutions were incubated at 37 °C and DLS measurements were recorded periodically at 37 °C. The particle sizes were measured as a function of time at a concentration of 0.5 mg·mL^{-1}.

f) Drug release

In vitro drug release was conducted in acidic media and in neutral media using an acetate buffer (pH 5.0) and PBS (pH 7.4), respectively. The prodrug micelles were dispersed in 5 mL PBS in a Float-a-lyzer™ dialysis membrane with a MWCO of 8000, preceding their submergence in their respective buffers (50 mL). The system was sealed and maintained at 37 °C in an incubation oven. At time intervals of 0, 2, 4, 6, 12, 24, 48 and 72 h, samples (2 mL) were withdrawn and replaced with an equivalent volume of buffer to maintain sink conditions. The drug concentration was determined using LC-MS and 100% release was determined by analysing a sample that had been incubated for one week, where the pH was adjusted to 2 using HCl (0.1 M) 24 h prior to the sample removal.

5.4.4 Biological analysis

a) Haemolysis

Human whole blood was collected and washed thrice with PBS (1×, pH 7.4) and centrifuged at 3000 ×g to remove serum and the buffy coat. Fresh RBCs in haematocrit (4%) were exposed to varying concentrations of the compounds to be tested in 96-well plates in PBS pH 7.4 for 48 h at 37 °C. For comparison, adequate amounts of the prodrug micelles were used relative to the free drug. Untreated RBCs and RBCs treated with Triton X-100 served as the negative control (0% haemolysis) and positive control (100% haemolysis), respectively. After incubation, RBC suspensions were centrifuged at 3000 ×g for 3 min. Thereafter, the supernatant (30 μL) in PBS (70 μL) was transferred to new 96-well plates. The amount of released haemoglobin in the supernatant is indicative of cell lysis and this was measured by measuring the absorbance at 540 nm using a UV-Vis spectrophotometer. Equation 5.4 was used to determine the haemolysis where OD is the absorbance, T is the treated RBCs, P is the positive control and N is the negative control. Experiments were performed in technical triplicate for three biological replicates (n = 3).

$$\text{Haemolysis (\%)} = \frac{(OD_T - OD_N)}{(OD_P - OD_N)} \times 100 \qquad \text{Equation 5.4}$$

b) Cytotoxicity

Caucasian hepatocellular carcinoma cells (HepG2) were grown in DMEM with FBS (5%) and penicillin/streptomycin (1%) at 37 °C (CO_2 (5%), 90% humidity). The media was changed every 2 days as needed depending on the cell confluency, which was monitored using a phase contrast microscope (400× magnification). Cells were passaged at 70 – 80% monolayer confluency. The cell viability was

monitored microscopically with Trypan-Blue (0.2%) and the cells were trypsinised with Trypsin-EDTA ($1\times$). Approximately 100 000 cells were plated in 96-well plates and the cells were grown for 24 h at 37 °C. After this time, the cells were treated with each compound (10 and 2 µM) for 48 h at 37 °C (CO_2 (5%)). PBS (40 µL) was used to dilute the supernatant (60 µL) which was added to new 96-well plates. The cytotoxicity was determined using the CytoSelect™ LDH Cytotoxicity Assay Kit. DMEM complete culture media was used as the background control. Untreated viable cells and cells treated with Triton-X 100 (dead cells) were used as the negative and positive control for cytotoxicity, respectively. Equation 5.5 was used to calculate the cytotoxicity where OD is the absorbance at 450 nm determined using a UV-Vis spectrometer, T is drug treated RBCs, P is the positive control and N is the negative control. Experiments were performed in technical triplicate for a three biological repeats (n = 3).

$$\text{Cytotoxicity } (\%) = \frac{(OD_T - OD_N)}{(OD_P - OD_N)} \times 100 \qquad \text{Equation 5.5}$$

c) Activity

P. falciparum parasites were maintained at 37 °C in human RBCs suspended in complete culture RPMI 1640 medium supplemented with HEPES (25 nM), D-glucose (20 mM), hypoxanthine (200 µM), sodium bicarbonate (0.2%), gentamycin (24 µg·mL), and AlbuMAX II (0.5%) in a gaseous environment of N_2 (90%), O_2 (5%), and CO_2 (5%) (hypoxic gas conditions). Incubation was on a rotary platform (60 rpm) and parasite viability was monitored daily on fixed Giemsa stained thin blood smears using a light microscope ($1000\times$ magnification). Parasitaemia were maintained at 4 – 6% rings and 2 – 3% trophozoites. *In vitro* ring-stage intra-erythrocytic *P. falciparum* NF54 (drug sensitive) parasite cultures (200 µL, haematocrit (1%) and parasitaemia (1%)) were treated with serially diluted concentrations of the compounds for dose-response evaluation followed by a 48 h stationary incubation period at 37 °C under hypoxic gas conditions. The positive controls for these assays included artemether/lumefantrine (1:6) (1 µM) for IC_{50} determination. Complete RPMI 1640 media was used as the negative control for all of the assays and were grown in 96-well plates for 96 h at 37 °C in hypoxic gas conditions. At the conclusion of the 96 h growth period, equal volumes (100 µL) of each *P. falciparum* parasite culture and SYBR Green I lysis buffer were combined. The samples were incubated at 37 °C for 1 h after which the fluorescence was measured using a GloMax®-Explorer Detection System with Instinct® Software (excitation at 485 nm and emission at 538 nm). The 'background' fluorescence (*i.e.* the fluorescence measured from artemether-lumefantrine treated *Plasmodium*-infected RBCs samples in which parasite proliferation was completely inhibited) was subtracted from the total fluorescence measured for each sample to provide a measure of the parasite proliferation. Sigmoidal dose-response curves were plotted using GraphPad 6.0. Experiments were performed in technical triplicate for a three biological repeats (n = 3).

5.5 References

(1)   *World Malaria Report*; World Health Organization: Geneva, 2018.

(2)   Sinclair, D.; Zani, B.; Donegan, S.; Olliaro, P.; Garner, P. *Cochrane Database Syst. Rev.* **2009**, *3* (1), 1.

(3)   Nosten, F.; White, N. J. *Am. J. Trop. Med. Hyg.* **2007**, *77* (6), 181.

(4)   Warhurst, D. C.; Adagu, I. S.; Beck, H. P.; Duraisingh, M. T.; Kirby, G. C.; Von Seidlein, L.; Wright, C. W. *SE Asian J. Trop. Med.* **2001**, *32* (1), 4.

(5)   Price, R.; Nosten, F.; Simpson, J. A.; Luxemburger, C.; Phaipun, L.; Kuile, F. Ter; Van Vugt, M.; Chongsuphajaisiddhi, T.; White, N. J. *Am. J. Trop. Med. Hyg.* **1999**, *60* (6), 1019.

(6)   White, N. J.; Van Vugt, M.; Ezzet, F. *Clin. Pharmacokinet.* **1999**, *37* (2), 105.

(7)   Makanga, M.; Krudsood, S. *Malar. J.* **2009**, *8* (1), 5.

(8)   Ezzet, F.; Van Vugt, M.; Nosten, F.; Looareesuwan, S.; White, N. J. *Antimicrob. Agents Chemother.* **2000**, *44* (3), 697.

(9)   Warhurst, D. C. *Biochem. Pharmacol.* **1981**, *30* (24), 3323.

(10)   Djimdé, A.; Lefèvre, G. *Malar. J.* **2009**, *8* (1), 4.

(11)   Bhandari, S.; Rana, V.; Tiwary, A. K. *Ther. Deliv.* **2017**, *8* (4), 201.

(12)   Hussein, Y. H. A.; Youssry, M. *Materials* **2018**, *11* (5), 688.

(13)   Kerns, E. H. *J. Pharm. Sci.* **2001**, *90* (11), 1838.

(14)   Huh, K. M.; Min, H. S.; Lee, S. C.; Lee, H. J.; Kim, S.; Park, K. *J. Control. Release* **2008**, *126* (2), 122.

(15)   Moo Huh, K.; Cheon Lee, S.; Woo Cho, Y.; Lee, J.; Hyun Jeong, J.; Park, K. *J. Control. Release* **2004**, *101* (1), 59.

(16)   Gaucher, G.; Dufresne, M. H.; Sant, V. P.; Kang, N.; Maysinger, D.; Leroux, J. C. *J. Control. Release* **2005**, *109* (1), 169.

(17)   Kataoka, K.; Harada, A.; Nagasaki, Y. *Adv. Drug Deliv. Rev.* **2012**, *64* (1), 37.

(18)   Richter, A.; Olbrich, C.; Krause, M.; Kissel, T. *Int. J. Pharm.* **2010**, *389* (1), 244.

(19)   Nishiyama, N.; Kataoka, K. *Nanostructured Devices Based on Block Copolymer Assemblies for Drug Delivery: Designing Structures for Enhanced Drug Function*; Springer: Berlin, 2006.

(20)   Chithrani, B. D.; Chan, W. C. W. *Nano Lett.* **2007**, *7* (6), 1542.

(21)   Chang, T.; Lord, M. S.; Bergmann, B.; MacMillan, A.; Stenzel, M. H. *J. Mater. Chem. B* **2014**, *2*

(19), 2883.

(22)   Mitragotri, S.; Lahann, J. *Nat. Mater.* **2009**, *8* (1), 15.

(23)   Biagini, G. A.; Ward, S. A.; Bray, P. G. *Trends Parasitol.* **2005**, *21* (7), 299.

(24)   Goodyer, I. D.; Pouvelle, B.; Schneider, T. G.; Trelka, D. P.; Taraschi, T. F. *Mol. Biochem. Parasitol.* **1997**, *87* (1), 13.

(25)   Eda, K.; Eda, S.; Sherman, I. W. *Am. J. Trop. Med. Hyg.* **2004**, *71* (2), 190.

(26)   Kurth, N.; Brachet, F.; Robic, D.; Bourbouze, R.; Renard, E.; Guerin, P. *Polymer* **2001**, *43* (4), 1095.

(27)   Lee, D. G.; Chang, V. S. *J. Org. Chem.* **1978**, *43* (8), 1532.

(28)   Pedersen, C. J. *J. Am. Chem. Soc.* **1967**, *89* (26), 7017.

(29)   Sam, D. J.; Simmons, H. E. *J. Am. Chem. Soc.*, **1972**, *94* (11), 4024.

(30)   Neises, B.; Steglich, W. *Angew. Chem.* **1978**, *17* (7), 522.

(31)   Mangold, C.; Dingels, C.; Obermeier, B.; Frey, H.; Wurm, F. *Macromolecules* **2011**, *44* (16), 6326.

(32)   Gu, Y.; Zhong, Y.; Meng, F.; Cheng, R.; Deng, C.; Zhong, Z. *Biomacromolecules* **2013**, *14* (8), 2772.

(33)   Li, M.; Gao, M.; Fu, Y.; Chen, C.; Meng, X.; Fan, A.; Kong, D.; Wang, Z.; Zhao, Y. *Colloids Surf. B* **2016**, *140* (1), 11.

(34)   Haynes, R. *Curr. Top. Med. Chem.* **2006**, *6* (5), 509.

(35)   Christian, J.; Shah, P.; Patel, M.; Patel, K.; Gandhi, T. *J. Taibah Sci.* **2016**, *11* (5), 729.

(36)   Roggan, A.; Friebel, M.; Dörschel, K.; Hahn, A.; Müller, G. *J. Biomed. Opt.* **1999**, *4* (1), 36.

(37)   Shuai, X.; Ai, H.; Nasongkla, N.; Kim, S.; Gao, J. *J. Control. Release* **2004**, *98* (3), 415.

(38)   Kuntworbe, N.; Acquah, F. A.; Johnson, R.; Ofori-Kwakye, K. *J. Pharm. Pharmacogn. Res.* **2018**, *6* (3), 167.

(39)   Menczel, J. D.; Prime, R. B. *Thermal analysis of polymers*; Wiley: Hoboken, 2009.

(40)   Fule, R. A.; Meer, T. S.; Sav, A. R.; Amin, P. D. *J. Pharm.* **2013**, *1* (1), 3.

(41)   Knopp, M. M.; Olesen, N. E.; Holm, P.; Langguth, P.; Holm, R.; Rades, T. *J. Pharm. Sci.* **2015**, *104* (9), 2905.

(42)   Cao, C.; Zhao, J.; Lu, M.; Garvey, C. J.; Stenzel, M. H. *Biomacromolecules* **2019**, *20* (4), 1545.

(43)   Amin, N. C.; Fabre, H.; Blanchin, M. D.; Montels, J.; Aké, M. *Malar. J.* **2013**, *12* (1), 202.

(44)   Huang, L.; Cai, M.; Xie, X.; Chen, Y.; Luo, X. *J. Mater. Chem. B* **2014**, *25* (13), 1407.

(45)   Mohanty, C.; Acharya, S.; Mohanty, A. K.; Dilnawaz, F.; Sahoo, S. K. *Nanomedicine* **2010**, *5* (3), 433.

(46)   Owen, S. C.; Chan, D. P. Y.; Shoichet, M. S. *Nano Today* **2012**, *7* (1), 53.

(47)   Huh, K. M.; Lee, S. C.; Cho, Y. W.; Lee, J.; Jeong, J. H.; Park, K. *J. Control. Release* **2005**, *101* (1), 59.

(48)   Torchilin, V. P. *Pharm. Res.* **2006**, *24* (1), 1.

(49)   Lu, Y.; Park, K. *Int. J. Pharm.* **2013**, *453* (1), 198.

(50)   Prazeres, T. J. V.; Beija, M.; Fernandes, F. V.; Marcelino, P. G. A.; Farinha, J. P. S.; Martinho, J. M. G. *Inorganica Chim. Acta* **2012**, *381* (15), 181.

(51)   Torchilin, V. P. *J. Control. Release.* **2001**, *73* (2), 137.

(52)   Torchilin, V. P.; Levchenko, T. S.; Whiteman, K. R.; Yaroslavov, A. A; Tsatsakis, A. M.; Rizos, A. K.; Michailova, E. V.; Shtilman, M. I. *Biomaterials* **2001**, *22* (22), 3035.

(53)   Ma, C.; Pan, P.; Shan, G.; Bao, Y.; Fujita, M.; Maeda, M. *Langmuir* **2015**, *31* (4), 1527.

(54)   Letchford, K.; Liggins, R.; Burt, H. *J. Pharm. Sci.* **2008**. *97* (3), 1179.

(55)   Ahmad, Z.; Shah, A.; Siddiq, M.; Kraatz, H. B. *RSC Adv.* **2014**, *4* (33), 17028.

(56)   Zhang, Y.; Huo, M.; Zhou, J.; Yu, D.; Wu, Y. *Carbohydr. Polym.* **2009**, *77* (2), 231.

(57)   Liang, K.; Chung, J. E.; Gao, S. J.; Yongvongsoontorn, N.; Kurisawa, M. *Adv. Mater.* **2018**, *30* (14), 1706963.

(58)   Nie, S. *Nanomedicine* **2010**, *5* (4), 523.

(59)   Roser, M.; Fischer, D.; Kissel, T. *Eur. J. Pharm. Biopharm.* **1998**, *46* (3), 255.

(60)   Li, S. D.; Huang, L. *Biochim. Biophys. Acta.* **2009**, *1788* (10), 2259.

(61)   Vangeyte, P.; Leyh, B.; Auvray, L.; Grandjean, J.; Misselyn-Bauduin, A. M.; Jérôme, R. *Langmuir* **2004**, *20* (21), 9019.

(62)   Liu, J.; Istvan, E. S.; Gluzman, I. Y.; Gross, J.; Goldberg, D. E. *Proc. Natl. Acad. Sci.* **2006**, *103* (23), 8840.

(63)   Lew, V. L.; Tiffert, T.; Ginsburg, H. *Blood* **2003**, *101* (10), 4189.

(64)   Goldberg, D. E. *Hemoglobin Degradation*; Springer: Berlin, 2005.

(65)   Dorn, A.; Vippagunta, S. R.; Matile, H.; Jaquet, C.; Vennerstrom, J. L.; Ridley, R. G. *Biochem. Pharmacol.* **1998**, *55* (6), 727.

(66)   Kuhn, Y.; Rohrbach, P.; Lanzer, M. *Cell. Microbiol.* **2007**, *9* (4), 1004.

(67)   Santos-Magalhães, N. S.; Mosqueira, V. C. F. *Adv. Drug Deliv. Rev.* **2010**, *62* (4), 560.

(68)   Becker, K.; Kirk, K. *Trends Parasitol.* **2004**, *20* (12), 590.

(69)   Yayon, A.; Cabantchik, Z. I.; Ginsburg, H. *EMBO J.* **1984**, *3* (11), 2695.

(70)   Zhang, Y.; Huang, C.; Kim, S.; Golkaram, M.; Dixon, M. W. A.; Tilley, L.; Li, J.; Zhang, S.; Suresh, S. *Proc. Natl. Acad. Sci.* **2015**, *112* (19), 6068.

(71)   Moxon, C. A.; Grau, G. E.; Craig, A. G. *Br. J. Haematol.* **2011**, *154* (6), 670.

(72)   Elias, D. R.; Poloukhtine, A.; Popik, V.; Tsourkas, A. *Nanomedicine* **2013**, *9* (2), 194.

(73)   Reader, P. *Anti-malarial polymer-polypeptide conjugates [PhD Thesis];* Stellenbosch University, 2014.

(74)   Sélo, I.; Négroni, L.; Créminon, C.; Grassi, J.; Wal, J. M. *J. Immunol. Methods* **1996**, *199* (2), 127.

(75)   Freed, J. K.; Smith, J. R.; Li, P.; Greene, A. S. *Proteomics* **2007**, *7* (14), 2371.

(76)   Kavimandan, N. J.; Losi, E.; Wilson, J. J.; Brodbelt, J. S.; Peppas, N. A. *Bioconjug. Chem.* **2006**, *17* (6), 1376.

(77)   Aditya, N. P.; Patankar, S.; Madhusudhan, B.; Murthy, R. S. R.; Souto, E. B. *Eur. J. Pharm. Sci.* **2010**, *40* (5), 448.

(78)   Rautenbach, M.; Vlok, N. M.; Stander, M.; Hoppe, H. C. *Biochim. Biophys. Acta.* **2007**, *1768* (6), 1488.

(79)   Beckwitt, C. H.; Clark, A. M.; Wheeler, S.; Taylor, D. L.; Stolz, D. B.; Griffith, L.; Wells, A. *Exp. Cell Res.* **2018**, *363* (1), 15.

(80)   Parhamifar, L.; Andersen, H.; Moghimi, S. M. *Methods Mol. Biol.* **2019**, *1* (1), 291.

(81)   Verlinden, B. K.; Niemand, J.; Snyman, J.; Sharma, S. K.; Beattie, R. J.; Woster, P. M.; Birkholtz, L. M. *J. Med. Chem.* **2011**, *54* (19), 6624.

(82)   Bacon, D. J.; Latour, C.; Lucas, C.; Colina, O.; Ringwald, P.; Picot, S. *Antimicrob. Agents Chemother.* **2007**, *51* (4), 1172.

(83)   Johnson, J. D.; Dennull, R. A.; Gerena, L.; Lopez-Sanchez, M.; Roncal, N. E.; Waters, N. C. *Antimicrob. Agents Chemother.* **2007**, *51* (6), 1926.

(84)   Smilkstein, M.; Sriwilaijaroen, N.; Kelly, J. X.; Wilairat, P.; Riscoe, M. *Antimicrob. Agents Chemother.* **2004**, *48* (5), 1803.

(85)   Bennett, T. N.; Paguio, M.; Gligorijevic, B.; Seudieu, C.; Kosar, A. D.; Davidson, E.; Roepe, P.

D. *Antimicrob. Agents Chemother.* **2004**, *48* (5), 1807.

(86)   Aykul, S.; Martinez-Hackert, E. *Anal. Biochem.* **2016**, *508* (1), 97.

(87)   Nogueira, C. R.; Lopes, L. M. X. *Molecules* **2011**, *16* (3), 2146.

(88)   Batista, R.; De Jesus Silva Júnior, A.; De Oliveira, A. B. *Molecules* **2009**, *14* (8), 3037.

(89)   Sherman, I. W.; Eda, S.; Winograd, E. *J. Infect.* **2003**, *5* (10), 897.

(90)   Glenister, F. K.; Fernandez, K. M.; Kats, L. M.; Hanssen, E.; Mohandas, N.; Coppel, R. L.; Cooke, B. M. *Blood* **2009**, *113* (4), 919.

(91)   Marques, J.; Moles, E.; Urbán, P.; Prohens, R.; Busquets, M. A.; Sevrin, C.; Grandfils, C.; Fernàndez-Busquets, X. *Nanomedicine* **2014**, *10* (8), 1719.

(92)   Valle-Delgado, J. J.; Urbán, P.; Fernàndez-Busquets, X. *Nanoscale* **2013**, *5* (9), 3673.

(93)   Boyle, M. J.; Skidmore, M.; Dickerman, B.; Cooper, L.; Devlin, A.; Yates, E.; Horrocks, P.; Freeman, C.; Chai, W.; Beeson, J. G. *Antimicrob. Agents Chemother.* **2017**, *61* (11), 17.

(94)   Chang, Y. C.; Chu, I. M. *Eur. Polym. J.* **2008**, *44* (12), 3922.

(95)   Lee, H.; Zeng, F.; Dunne, M.; Allen, C. *Biomacromolecules* **2005**, *6* (6), 3119.

(96)   Giacomelli, F. C.; Stepánek, P.; Giacomelli, C.; Schmidt, V.; Jäger, E.; Jäger, A.; Ulbrich, K. *Soft Matter* **2011**, *7* (19), 9316.

Chapter Six

Epilogue

The work presented in this dissertation focused on the design and development of a novel drug delivery system for the antimalarial drug combination of artemether and lumefantrine. This combination is currently advocated by the WHO for the treatment of uncomplicated malaria, but suffers from rapid degradation in gastric fluid as well as erratic absorption and low aqueous solubility.[1,2] Drug resistance is also a major issue for the longevity of this combination therapy. Polymer nanotechnology applied to malaria therapy has provided a means of overcoming these challenges. The path leading to the final assembly of the drug delivery vehicle will be outlined, as well as the analysis of the system for implementation *in vivo*.[3] Recommendations for further studies will be also made.

6.1 General conclusions

In Chapter 2, historical and theoretical information regarding malaria, drug resistance and the current tools needed to aid in its eradication were discussed. The developing field of polymer nanotechnology was explored as applied to malaria therapy and strategies were considered to curtail drug resistance. The development of a polymeric prodrug and its components were discussed as related to Ringsdorf's rational model.[4] Important outcomes of self-assembled polymeric prodrug micelles were also assessed such as drug release, stimuli-responsiveness, cellular uptake, targeting and stability.

The acid-degradable nature of various linkages was explored in Chapter 3 as it was ascertained that the low pH found in the parasitophorous food vacuole (approximately pH 5) can act as the stimulus to release the drug from the polymeric carrier. Blood serum has a neutral pH of 7.4, so the acid-degradable linker should be relatively stable at this pH so as to protect the drug payload from releasing prematurely. Poly(*N*-vinylpyrrolidone) (PVP)-based model drug compounds were synthesised using RAFT polymerisation, and two key methods of incorporating different acid-degradable linkers were highlighted. The hydrolysis kinetics of seven polymer-model drug compounds were conducted: P1 (PVP conjugated to phenyl acrylate), P2 (PVP conjugated to *N*-phenylacrylamide), P3 (PVP conjugated to *N*-phenylmaleimide), P4 (PVP conjugated to benzyl acrylate), P5 (PVP conjugated to *N*-benzylacrylamide), P6 (PVP conjugated to *N*-benzylmaleimide) and P7 (PVP conjugated to phenyl vinyl ether). Of the polymer-model drug conjugates with a β-thiopropionate linkage, the ester-based polymers, P1 and P4, were unique in exhibiting acid-lability at pH 5. Under neutral pH conditions, P4 exhibited higher selectivity compared with P1. The acetal-bound polymer-model drug conjugate (P7) was stable at neutral pH, indicating higher selectivity compared with P1 and P4. Based on selectivity, hydrolysis rate, synthesis route and degradation products, the acetal linkage showed the most promise for its implementation in the antimalarial polymeric prodrug.

In Chapter 4, the amphiphilic block copolymer carrier, PVP-*block*-(α-allylvalerolactone) (PVP-*b*-PAVL) was synthesised after optimising the conditions for the synthesis of the parent block copolymer, PVP-

block-(δ-valerolactone) (PVP-*b*-PVL), with special focus on the type of organocatalyst relevant for the system. Triazabicyclodecene (TBD) was chosen as the succeeding organocatalyst over diazabicycloundecene and thiourea (DBU + TU) because of the greater certainty over the end-group fidelity, as well as faster polymerisation kinetics, *i.e.* quantitative monomer conversions in less than one minute. A pyridyl-disulfide protected thiol terminated hydroxy-functional PVP (PDS-PVP-OH) was synthesised and used as the macroinitiator during the ring-opening polymerisations of α-allylvalerolactone and δ-valerolactone. The crystallisation-driven self-assembly (CDSA) of PVP-*b*-PVL was investigated because this system holds potential for a variety of applications and because the CDSA behaviour has not yet been reported in literature. Using THF as the non-selective solvent and water as the selective solvent for the hydrophobic block, PVL, a range of nanomorphologies, including spherical micelles, cylindrical micelles and lamellae micelles, were observed using TEM. The ageing time of the micelles in water was integral to the adopted morphology as crystallisation was confirmed to take place upon ageing. External stimuli were also explored in order to fragment micelle morphologies, where the processes of freeze-thawing as well as hydrogen bonding were found to be the most successful in controlling the final self-assembled structure. The novel freeze-thaw process is a simple, reproducible and beneficial method to effect morphological transitions from lamellae micelles to cylindrical micelles. Ongoing work is focused on understanding the mechanism of this process and controlling the lengths of the cylindrical micelles.

In Chapter 5, the components described in the preceding chapters were applied in the complete antimalarial polymeric prodrug for the combination therapy of artemether and lumefantrine. To achieve this, PVP-*b*-PAVL's allyl functional groups were converted into carboxylic acid groups quantitatively, and the resulting polymer was functionalised with ethylene glycol vinyl ether (70 mol% relative to the polymeric carrier). Lumefantrine was then covalently conjugated to the block copolymer (22 mol%) through a 'click'-type reaction, simultaneously rendering the acetal acid-degradable linkage. Artemether was entrapped within the hydrophobic core of spherical micelles self-assembled from the lumefantrine polymeric prodrug (114 nm from DLS measurements) using the cosolvent technique (THF: non-selective solvent; water: selective solvent), where it was found that artemether existed within the self-assembled micelles in the amorphous state. The PDS functionality terminating the antimalarial polymeric prodrug were used to a thiol-terminated targeting ligand using disulfide exchange. The targeting ligand was a low molecular weight peptide of sequence 'GSRSKGT' which had been modified quantitatively with SPDP. The targeting ligands were tethered to self-assembled prodrug micelles at a ligand density of 12 ± 3 mol%. The antimalarial polymeric prodrug micelles were found to be sufficiently stable for exposure *in vivo* by assessing the thermodynamic stability (CMC of 2.0 mg·mL^{-1}) and the kinetic stability against physiologically-mimicking serum (stable for four days).

The prodrug micelles were found to be have negligible toxicity to healthy red blood cells and were non-cytotoxic to liver carcinoma cells at the highest concentration tested. The prodrug micelles exhibited good antimalarial activity against hydroxychloroquine-sensitive *P. falciparum* parasites, though showed decreased activity compared with the free drug. The drug delivery system that was developed for this antimalarial combination therapy is novel, and shows great potential for further development in

addressing the therapeutic challenges that are associated with current life-threatening diseases such as malaria.

6.2 Recommendations for future work

The results presented in this dissertation indicate the potential of using the developed polymeric prodrug for the delivery of a range of hydrophobic drugs, where the hydrolysis rate can be effectively tuned by applying specific acid-degradable linkages. In this regard, substituent effects in the near-vicinity of the acid-degradable linkage should be considered as this was shown to affect the hydrolysis potential.

Future studies could focus on the parent block copolymer, PVP-*b*-PVL, which could be self-assembled and ultimately modulated using various external stimuli and ageing times to create a range of tailored nanomorphologies. The PDS moiety terminating PVP-*b*-PVL can be used to bioconjugate thiol or maleimide-terminated biological compounds of interest to the block copolymer. Cylindrical and lamellae micelles, for instance, are especially sought-after due to their high aspect ratios. It would therefore be worthwhile to investigate the conditions necessary to specifically tailor the diameters, shapes and lengths of these morphologies. Special focus could be placed on the use of low temperatures to control the lengths of cylindrical micelles, as this was found to be a novel, inexpensive and additive-free method of micelle fragmentation through CDSA.

Concerning the antimalarial polymeric prodrug, active targeting should be improved by conjugating a library of possible targeting ligands to the prodrug micelles based on their ability to discern between healthy- and *P. falciparum* infected red blood cells. It would also be beneficial to design for a range of targeting ligand densities as well as varying diameters of prodrug micelles, so that a clear correlation can be drawn between these important parameters. Regarding micelle size, non-tethered and tethered targeting ligand micelles should be tested for their activity towards *P. falciparum* parasites so as to explore the limitations of passive targeting through the 'new permeation pathways' (NPPs), which form in infected red blood cells.

6.3 References

(1)   *World Malaria Report*; World Health Organization: Geneva, 2017.

(2)   Nosten, F.; White, N, J. *Am. J. Trop. Med. Hyg.* **2007**, *77* (1), 181.

(3)   Rohini, N. A.; Anupam, J.; Alok, M. *J. Antivir. Antiretrovir.* **2013**, *15* (1), 12.

(4)   Ringsdorf, H. *J. Polym. Sci. Polym. Symp.* **2007**, *51* (1), 135.

Addenda

Addendum A
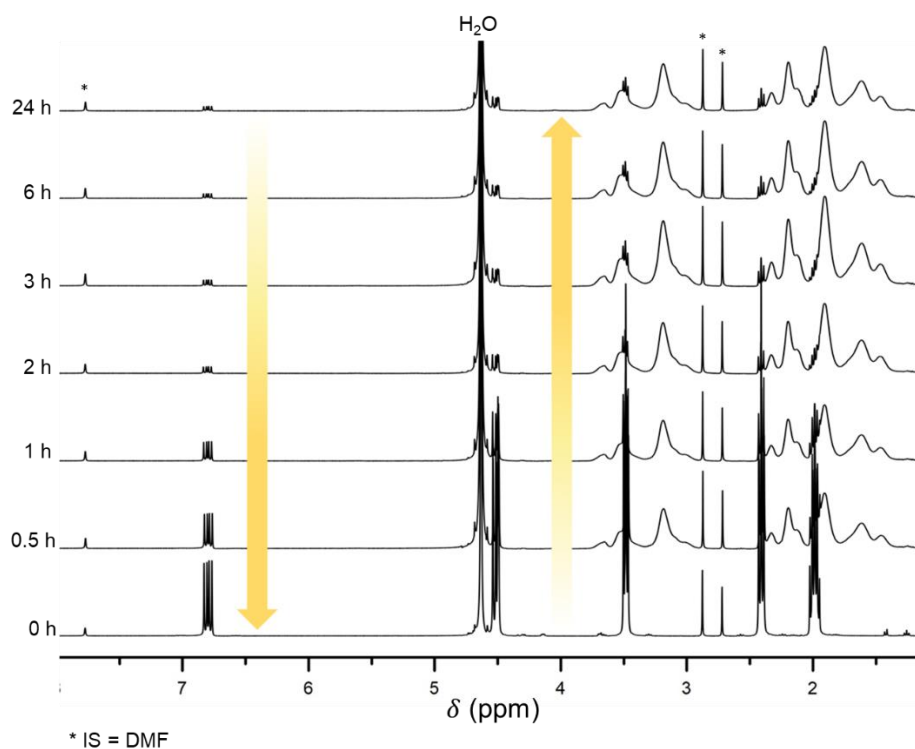
Conversion of NVP to PVP-X2 using RAFT-X2 in aqueous media

Figure A1 ^{1}H NMR stacked spectra of NVP polymerisation to render PVP-X2.

Addendum B

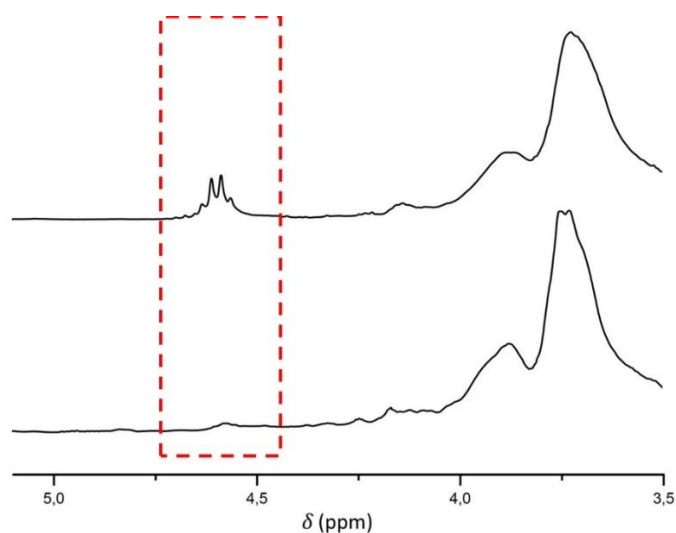Xanthate group removal or reduction via thermolysis of PVP

Figure A2 ^{1}H NMR spectra of PVP-X2 (above) and thermolysed PVP-X2 (below) between 5 – 3.5 ppm.

Addendum C

Correlation coefficients for P1, P4 and P7 and exemplified zero order and first order kinetic models of P1 pH 5.0

Table A1 Correlation coefficients for the kinetic models zero order and first order for P1, P4 and P7 at pH 5.0 and pH 7.4

	P1 pH 5.0	P1 pH 7.4	P4 pH 5.0	P4 pH 7.4	P7 pH 5.0	P7 pH 7.4
zero order	0.928	0.970	0.950	0.972	0.977	-
first order	0.990	0.972	0.989	0.973	0.979	-
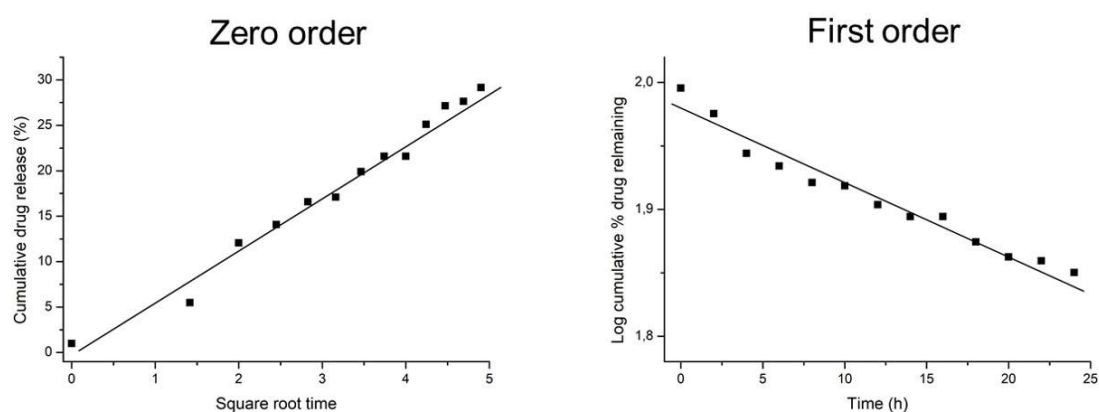
Figure A3 Representative zero-order and first-order model drug release kinetic models for P1 at pH 5.

Addendum D

^{1}H NMR spectrum of α-allylvalerolactone (AVL) monomer (CDCl$_3$, 400 MHz).
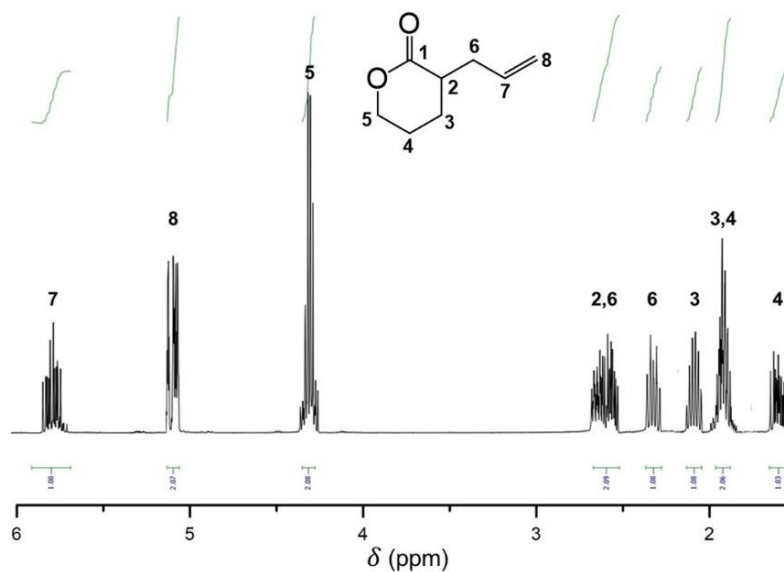
Figure A4 ^{1}H NMR spectrum of α-allylvalerolactone.

Addendum E

Reaction conditions used to synthesise pyridyl disulfide (PDS)-terminated PVP.

Table A2 Reaction conditions of PDS-PVP-OH

Run [a]	Reaction time	2,2'dipyridyl disulfide:PVP	Method	PDS functionality
	h	Moles		%
1	3	10 : 1	Bubbling	15
2	6	10 : 1	Freeze-pump-thaw	90
3	6	15 : 1	Freeze-pump-thaw	quantitative

[a] In all instances, ethanolamine (10 molar excess to PVP), solvent (acetonitrile) and temperature (25 °C) were kept constant.

Addendum F

The molar mass distribution curves of a DBU + TU-catalysed crude and purified PVP-PVL block copolymer.
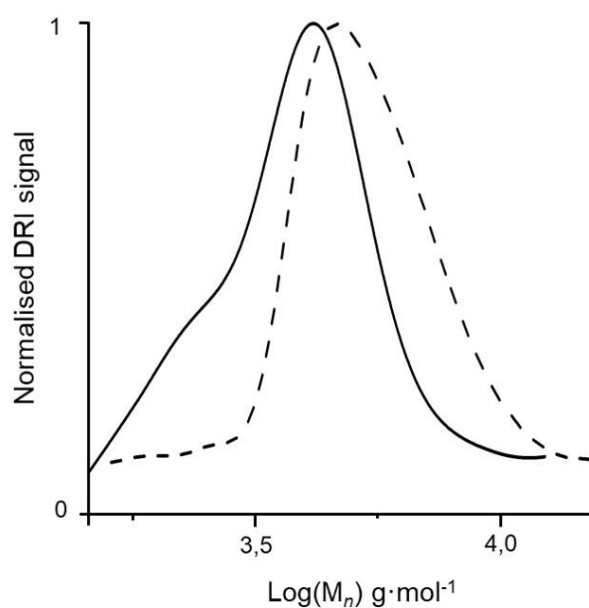
Figure A5 Molar mass distribution curves from SEC of a crude (solid curve) and purified (dashed curve) PVP-b-PVL.

Addendum G

The SEC molar mass distribution curve of PVP-*b*-PAVL.
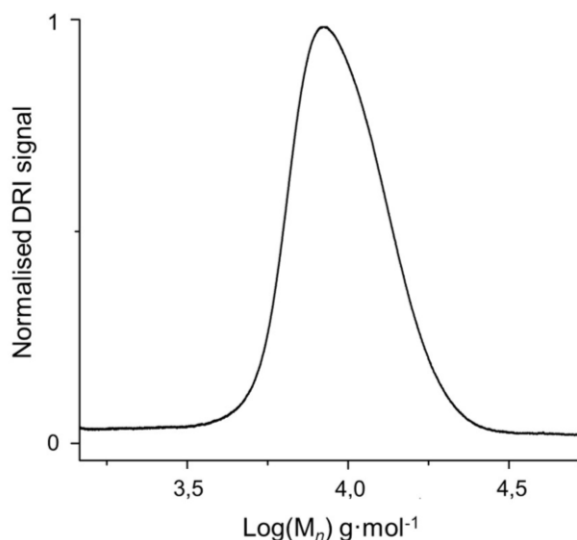
Figure A6 The molar mass distribution curve from SEC of PVP-b-PAVL ($M_{n,theoretical}$ = 7800 g·mol^{-1}, $M_{n,SEC}$ = 9300 g·mol^{-1}, Đ = 1.2).

Addendum H

The aqueous self-assembly of PVP-*b*-PVL of different block ratios using acetone or THF as the good solvent for the block copolymers and water as the selective solvent for PVL.
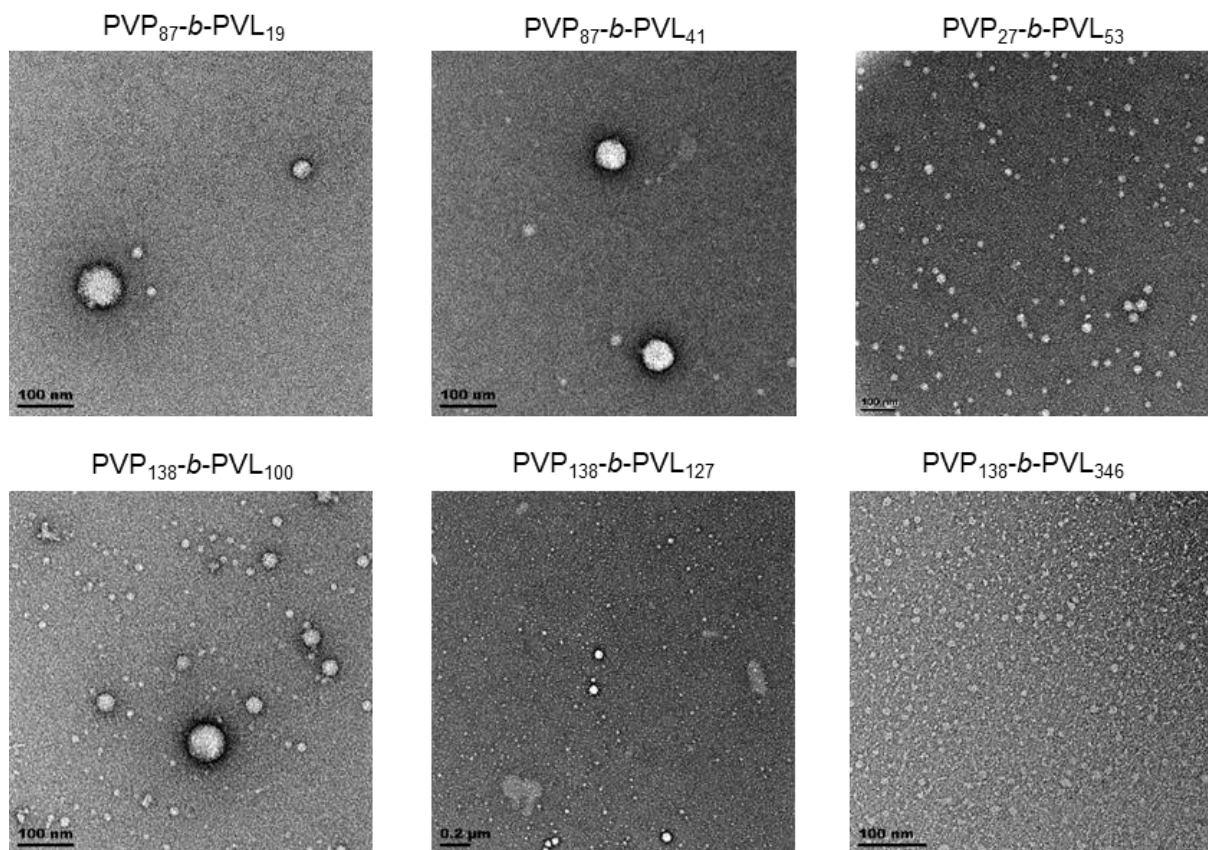

Figure A7 TEM images of micelles self-assembled from PVP-b-PVLs using acetone as the good solvent and water as the selective solvent. One drop of each unfiltered aqueous micelle dispersion was dropped onto a carbon coated TEM grid and dried under ambient conditions after being stained with uranyl acetate (20 wt.% in water).
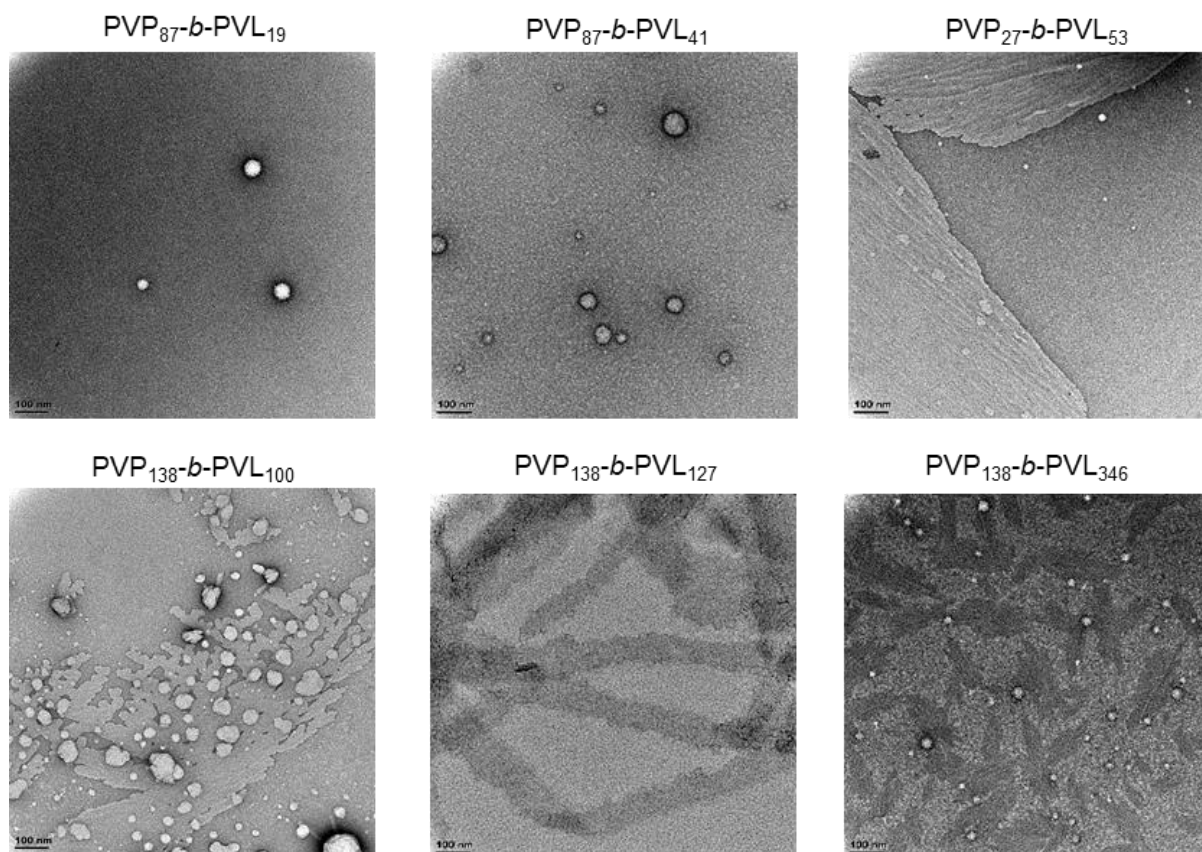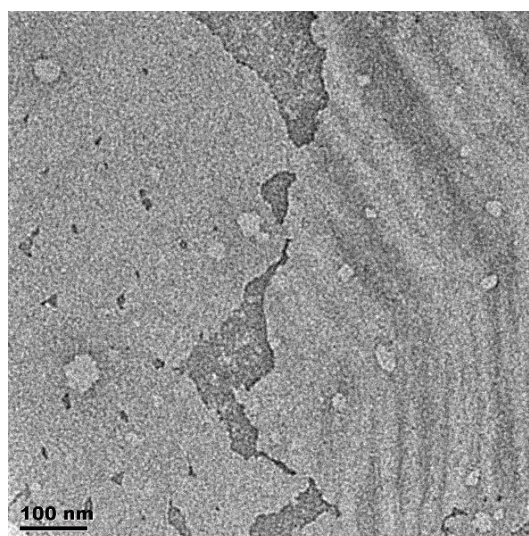
Figure A8 TEM images of micelles self-assembled from PVP-b-PVLs using THF as the good solvent and water as the selective solvent. One drop of each unfiltered aqueous micelle dispersion was dropped onto a carbon coated TEM grid and dried under ambient conditions after being stained with uranyl acetate (20 wt.% in water).

Addendum I

The aqueous self-assembly of PVP_{27}-*b*-PVL_{53} into micelles that were aged for one month at room temperature led to the observation of lamellae structures. No cylindrical micelles were observed.

Figure A9 TEM image of micelles self-assembled from PVP27-b-PVL53 using THF as the good solvent and water as the selective solvent. The sample was aged for one month at room temperature. One drop of the unfiltered aqueous micelle dispersion was dropped onto a carbon coated TEM grid and dried under ambient conditions after being stained with uranyl acetate (20 wt.% in water).

Addendum J

TEM images of micelles self-assembled from PVP_{138}-*b*-PVL_{100} by annealing in ethanol and ageing for four days. After this time the sample was dialysed against water, lyophilised and reconstituted in water.
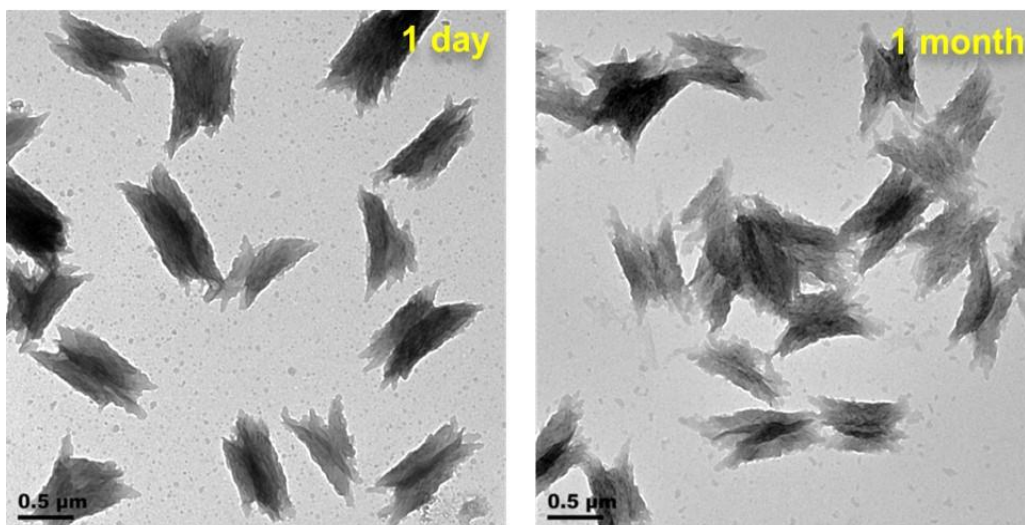

Figure A10 TEM images showing PVP_{138}-b-PVL_{100} self-assembled micelles in ethanol after four days which were reconstituted in water and stored for the indicated periods of time.

Addendum K

^{1}H NMR spectra of PVP-*b*-PAVL before and after undergoing oxidation to transform the allyl functional groups into carboxylic acid groups (Figure A11) and the ^{1}H NMR spectrum of EGVE-terminated PVP-*b*-PVL (Figure A12).
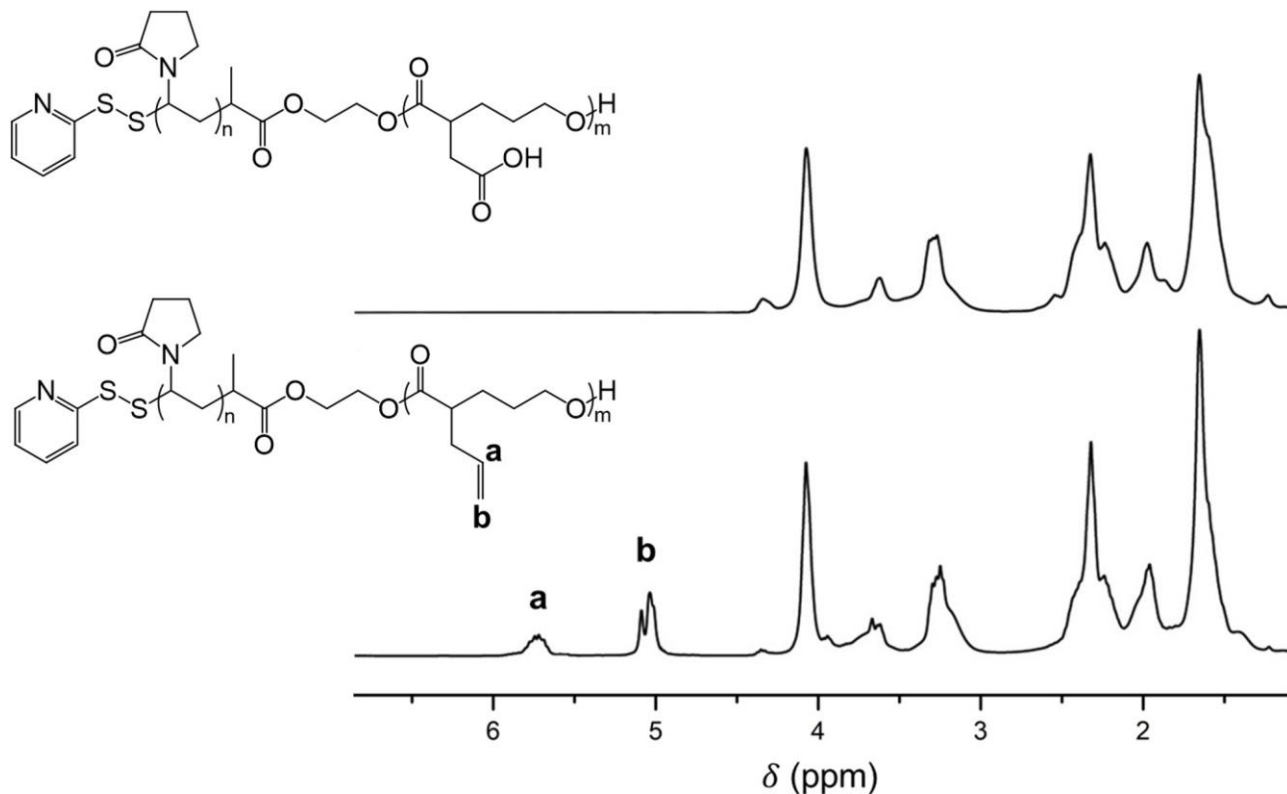

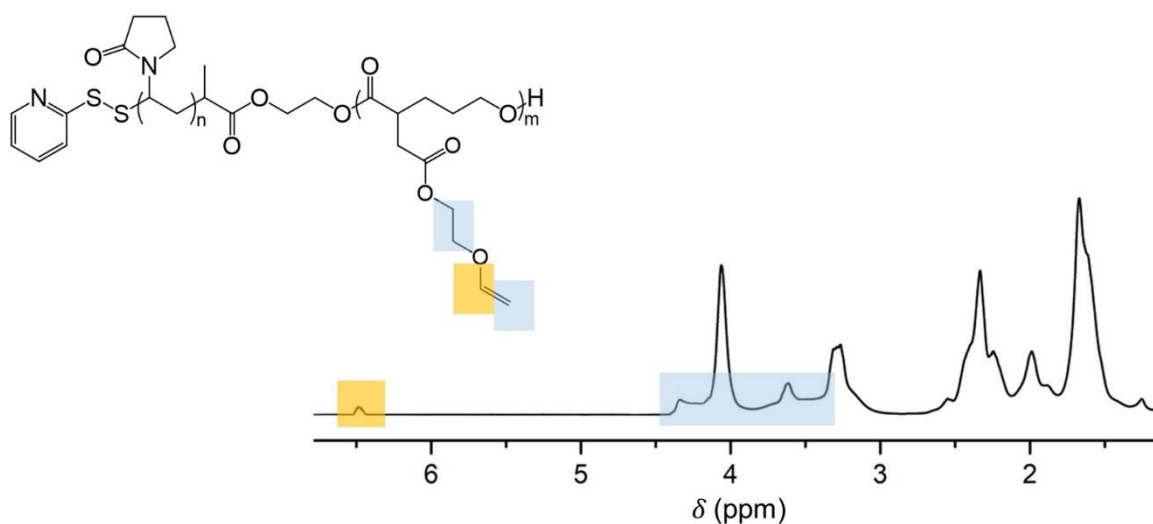*Figure A11 ^{1}H NMR spectra of carboxylated PVP-b-PVL (above) and PVP-b-PAVL (below).*

Figure A12 Colour coded ^{1}H NMR spectra of EGVE-terminated PVP-b-PVL.

Addendum L

Artemether (a) and lumefantrine (b) have retention times of Rt = 3.33 and 4.67 min, respectively. The molar mass ion peak at *m/z* 530 belongs to that of lumefantrine (528.94 g·mol^{-1}) and *m/z* 316 [M+NH$_4$]$^+$ to that of artemether (298.37 g·mol^{-1}).
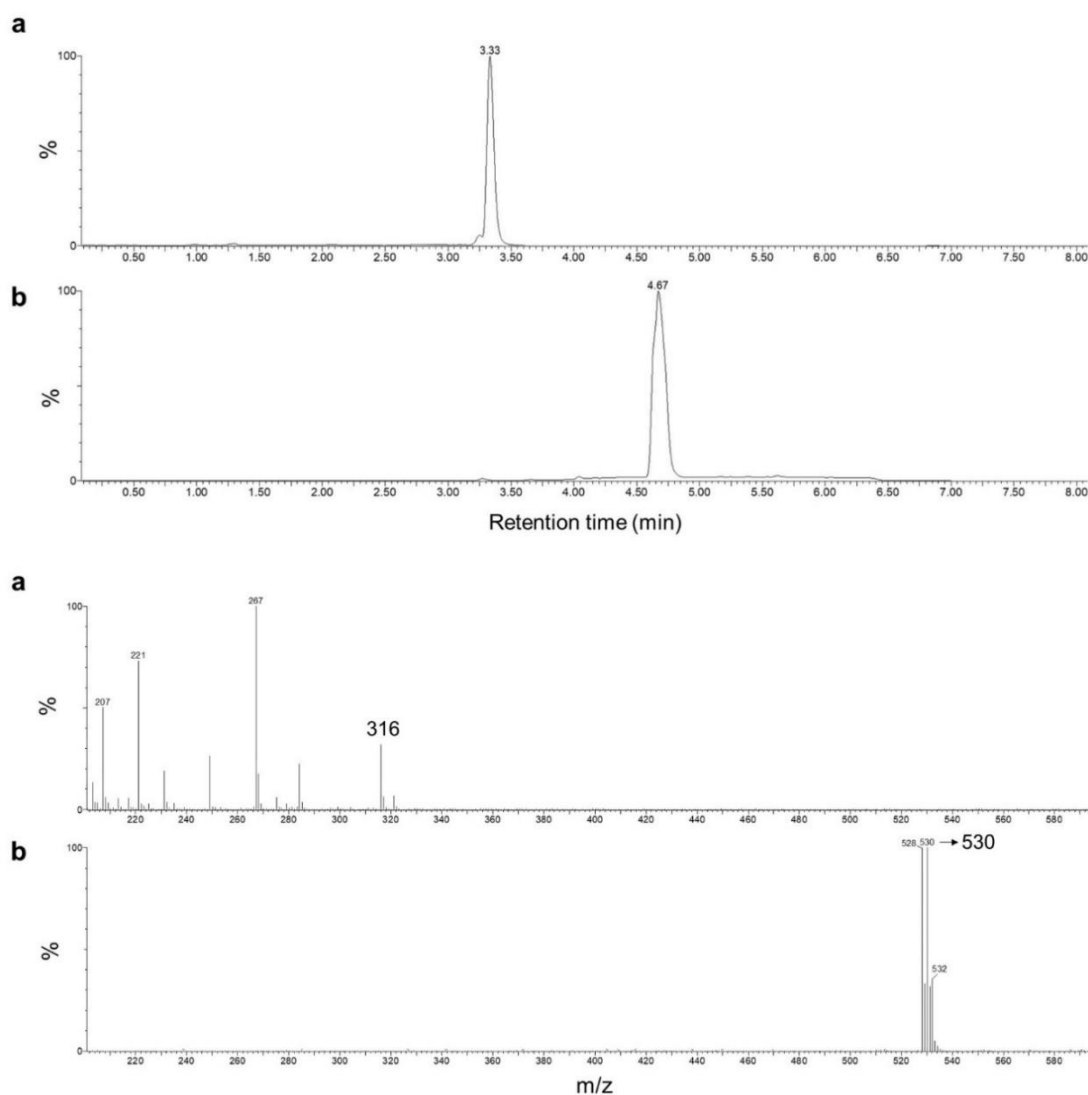

Figure A13 LC-MS spectra for a) artemether (Rt = 3.33 min, m/z = 316) and b) lumefantrine (Rt = 4.67 min, m/z = 530).